
Synthesis, Characterization and
Postsynthetic Modification of a Novel
Two-Dimensional Zr-based Metal-Organic
Framework

Von der Naturwissenschaftlichen Fakultät der
Gottfried Wilhelm Leibniz Universität Hannover

zur Erlangung des Grades
Doktor der Naturwissenschaften (Dr. rer. nat.)

genehmigte Dissertation
von

Alexander Mohmeyer, M. Sc.

2019

Referent: Prof. Dr. rer. nat. Peter Behrens
Korreferent: Prof. Dr. rer. nat. Jürgen Caro
Tag der Promotion: 15.11.2019

Danksagung

An dieser Stelle möchte ich einigen Personen danken, die mich während meiner Studienzeit an der Leibniz Universität Hannover unterstützt, gefördert und begleitet haben.

Mein Dank gilt zunächst Herrn Prof. Dr. Peter Behrens, der mir in seiner Arbeitsgruppe nach Bachelor- und Masterarbeit auch während der Promotion interessante, vielfältige und interdisziplinäre Themen zu bearbeiten gab.

Prof. Dr. Jürgen Caro danke ich für die Übernahme des Korreferats und Prof. Dr. Franz Renz für die Übernahme des Prüfungsvorsitzes.

An dieser Stelle möchte ich Dr. Andreas Schaate danken, der während der Masterarbeit und Doktorarbeit immer ein offenes Ohr für mich hatte und mit dem ich immer konstruktive Gespräche führen konnte.

Mein Dank gilt auch Dr. Andreas M. Schneider, der während des gesamten Studiums viel ermöglicht hat und man ihn immer um Rat fragen konnte.

Ebenfalls möchte ich Herrn Dr. Michael Wiebcke danken, der bei Fragen rund um das Thema Röntgenbeugung immer eine passende Antwort oder Idee bereithielt.

Meinen Kooperationspartnern aus den Arbeitsgruppen um Prof. Rolf J. Haug vom Institut für Festkörperphysik und Dr. Athanasia Warnecke von der Medizinischen Hochschule Hannover danke ich für den wissenschaftlichen Austausch und die schöne und produktive Zusammenarbeit in verschiedenen Projekten.

Der gesamten Arbeitsgruppe Behrens danke ich herzlich für die gemeinsame Zeit, viele angenehme Gespräche auf sowohl fachlicher als auch weniger fachlicher Basis. Vor allem auch vielen Dank für die Unterstützung in Hinsicht auf die Veröffentlichungen und das Korrekturlesen der Arbeit, dabei besonders zu erwähnen sind Hendrik A. Schulze und Tim J. Strauß, die mich seit Anbeginn des Studiums begleitet haben.

Ein besonderer Dank geht an die MOF-Gruppe und an die Bio-Gruppe für den stets spannenden wissenschaftlichen Austausch, die kritischen Anmerkungen und die immer unterhaltsamen Dienstreisen, die uns ermöglicht wurden.

Zudem möchte ich mich recht herzlich bei Merle Feldt und Birgit Zekoll bedanken, die stets hilfsbereit waren und bei auch kleinsten Problemen immer ein offenes Ohr hatten und viel ermöglichten.

Katharina Nolte danke ich für die vielen thermogravimetrische Analysen.

Für die zahlreichen elektronenmikroskopischen Aufnahmen danke ich Dr. Bastian Hoppe, Dr. Dennes Nettelroth, Hendrik A. Schulze, Inga Wille, Thea Heinemeyer und Dawid P. Warwas.

Danke auch an Malte Schäfer für die vielen Simulationen und theoretischen Berechnungen.

Ein ganz besonderer Dank gilt meiner gesamten Familie, die immer an mich glauben und ohne die ich das niemals erreicht hätte.

Und danke Nadja, dafür dass es dich gibt, du mich immer unterstützt hast und mir Rückhalt gibst und mich in meinen Vorhaben stärkst!

Abstract

The focus in many fields of research is the generation of materials with adjustable properties for specific applications. Among porous materials, metal-organic frameworks (MOFs) have developed over the past 20 years to a material class with enormous potential. Due to the modular design of MOFs from metal cations and organic linkers, it is possible to tailor the properties of the resulting extended frameworks by selecting individual components for the needs of specific applications. Careful selection of metal ions and organic molecules with functional groups makes it possible to adjust and influence the pore system, the type of linkage and the physical and chemical properties of the framework.

In the present work, the main aspect was the preparation of a novel MOF with high adjustability of its properties, based on light-induced postsynthetic reactions on the organic linker molecules. The framework is composed of Zr^{4+} ion-based oxo clusters and benzophenone-4,4'-dicarboxylate anions (*bzpd*²⁻) as linker molecules. The benzophenone unit is able to react with any molecule that contains C–H bonds after excitation with photons, resulting in a covalent bond. This reaction opens the possibility of changing the properties of the framework post-synthetically. The novel *Zr-bzpd* MOF is chemically and thermally stable and has a two-dimensional structure, which opens up the possibility of obtaining nanometer-thin layers through delamination methods. Further studies have shown that the adaptation of the surface chemistry by the linkage of molecules has a huge impact on the dispersibility in polar and nonpolar solvents. Furthermore, the direct polymerization of a conductive polymer, starting from the surface of the MOF, yields electrically conductive composite materials. Interestingly, in the course of this study it was found that the unmodified MOF is also electrically conductive. Furthermore, a systematic study concerned with the postsynthetic modification of *Zr-bzpd*-MOF with alkanes and alcohols of different chain lengths was undertaken. This showed that small hydrophilic molecules react with all linker molecules throughout the crystal, whereas molecules with longer chain lengths and thus more hydrophobic properties only modify the surface of the MOF crystals.

The so far largely unaccessed approach to employ specific photochemical modification reactions on the linker molecule the modification of MOFs has been developed here to upgrade the novel *Zr-bzpd*-MOF to an unexpectedly versatile compound which is further augmented by the possibility to obtain nanosheets of this substance. Various pathways to adapt this material to specific applications have thus been opened up.

Keywords: metal-organic framework, Zr-based MOF, benzophenone, photochemistry, postsynthetic modification, delamination

Kurzfassung

In vielen Bereichen der Forschung liegt der Fokus auf der Erzeugung von Materialien mit einstellbaren Eigenschaften für spezifische Anwendungsgebiete. Unter den porösen Materialien haben sich in den letzten 20 Jahren Metall-organische Gerüstverbindungen (*metal-organic frameworks*: MOFs) zu einer Materialklasse mit enormem Potenzial entwickelt. Aufgrund des modularen Aufbaus von MOFs aus Metallkationen und organischen verbrückenden Molekülen ist es möglich, ihre Eigenschaften anzupassen, indem einzelne Komponenten für den Aufbau der resultierenden Netzwerke gemäß den Anforderungen spezifischer Anwendungen ausgewählt werden. Die gezielte Auswahl von Metallionen und organischen Molekülen mit funktionellen Gruppen ermöglicht es, das Porensystem, die Art der Verknüpfung und die physikalischen und chemischen Eigenschaften des Gerüsts anzupassen und zu beeinflussen.

In der vorliegenden Arbeit lag der Hauptaspekt auf der Herstellung eines neuartigen MOFs mit variabel einstellbaren Eigenschaften, basierend auf lichtinduzierten Reaktionen an den organischen Linkermolekülen. Das Gerüst besteht aus Zr^{4+} -basierten Oxo-Clustern und Benzophenon-4,4'-dicarboxylat-Anionen (*bzpd*²⁻) als Linkermolekülen. Die Benzophenoneinheit kann nach Anregung mit Photonen mit jedem Molekül unter Ausbildung einer kovalenten Bindung reagieren, das C–H-Bindungen enthält. Diese Reaktion eröffnet die Möglichkeit, die Eigenschaften des Gerüsts postsynthetisch zu verändern. Der neuartige *Zr-bzpd*-MOF ist chemisch und thermisch stabil und weist eine zweidimensionale Struktur auf, die die Möglichkeit eröffnet, nanometerdünne Schichten durch Delaminierungsverfahren zu gewinnen. Weitere Studien haben gezeigt, dass die Anpassung der Oberflächenchemie durch die Anbindung von unterschiedlichen Molekülen einen großen Einfluss auf die Dispergierbarkeit in polaren und unpolaren Lösungsmitteln hat. Weiterhin kann durch direkte Polymerisation eines leitfähigen Polymers von der Oberfläche des MOF aus ein elektrisch leitfähiges Kompositmaterial erhalten werden. Interessanterweise wurde im Verlauf dieser Untersuchungen bemerkt, dass auch der unmodifizierte *Zr-bzpd*-MOF elektrisch leitfähig ist. Darüber hinaus hat eine systematische Studie der postsynthetischen Modifizierung des *Zr-bzpd*-MOF mit Alkanen und Alkoholen verschiedener Kettenlängen gezeigt, dass kleine, hydrophile Moleküle mit allen Linkermolekülen im gesamten Kristall reagieren, während Moleküle mit längeren Kettenlängen und stärker hydrophoben Eigenschaften nur die Oberflächen der MOF-Kristalle modifizieren.

Der bisher kaum beschrittene Weg, spezifische photochemische Reaktionen des Linkers zur Modifizierung von MOFs zu nutzen, wurde hier so weit ausgebaut, dass der neue *Zr-bzpd*-MOF zu einer unerwartet vielseitigen Verbindung veredelt werden konnte, was durch die Möglichkeit zur Herstellung von nanometerdünnen Schichten noch verstärkt wird. In diesem Sinne wurden verschiedene Wege aufgezeigt, dieses Material für unterschiedliche Applikationen anzupassen.

Stichwörter: Metall-organisches Gerüst, Zr-basiert, Benzophenon, Photochemie, Postsynthetische Modifizierung, Delaminierung

Table of contents

List of abbreviations.....	VII
1 Introduction.....	1
2 General background.....	4
2.1 Metal-organic frameworks.....	4
2.1.1 General principles.....	4
2.1.2 Electrically conductive MOFs.....	16
2.1.3 Modulated synthesis.....	19
2.2 Zirconium-based metal-organic frameworks.....	21
2.3 Postsynthetic modification.....	27
2.3.1 General strategies.....	27
2.3.2 PSM of Zr-based MOF.....	30
2.3.3 Photoreactivity in MOFs.....	31
2.4 Benzophenone.....	33
2.4.1 Photochemistry of benzophenone.....	33
2.4.2 Photoinduced reactions of benzophenone.....	35
2.5 References.....	37
3 Results and discussion.....	50
3.1 Delamination and Photochemical Modification of a Novel Two-Dimensional Zr-Based Metal-Organic Framework.....	50
3.2 Direct grafting-from of PEDOT from a photoreactive Zr-based MOF – A novel route to electrically conductive composite materials.....	72
3.3 Inside/Outside: Postsynthetic Modification of the Zr- <i>benzophenonedicarboxylate</i> -MOF.....	85
4 Conclusion and outlook.....	113
5 Supplementary Information.....	118
5.1 Delamination and Photochemical Modification of a Novel Two-Dimensional Zr-Based Metal–Organic Framework.....	118
5.2 Direct grafting-from of PEDOT from a photoreactive Zr-based MOF – A novel route to electrically conductive composite materials.....	137

5.3	Inside/Outside: Postsynthetic Modification of the Zr- <i>benzophenonedicarboxylate</i> -MOF.....	161
6	List of publications.....	186
7	Curriculum vitae.....	189

List of abbreviations

2PP	Two-photon polymerization
AFM	Atomic force microscopy
ATRP	Atom Transfer Radical Polymerization
BET	Brunauer-Emmett-Teller
CAU	<i>Christian-Albrechts University</i>
CNT	Carbon nanotube
CPO	Coordination Polymer of Oslo
DH6T	α,ω -Dihexylsexithiophene
DMF	N,N-Dimethylformamide
DMSO	Dimethyl sulfoxide
<i>dsbdc</i>	2,5-Disulfidobenzene-1,4-dicarboxylate
DUT	<i>Dresden University of Technology</i>
e.g.	For example
EDOT	3,4-Ethylenedioxythiophene
EDXS	Energy-dispersive X-ray spectroscopy
FA	Formic acid
<i>H₂bzpd</i>	Benzophenone-4,4'-dicarboxylic acid
<i>H₂tpdc</i>	Triphenyldicarboxylic acid
<i>H₃tp</i>	Tris(4-carboxyphenyl) phosphine
hcp	Hexagonal close-packing
<i>hhtp</i>	2,3,6,7,10,11-Hexahydroxytriphenylene
<i>hitp</i>	2,3,6,7,10,11-Hexaaminotriphenylene
HKUST	<i>Hong Kong University of Science and Technology</i>
IBU	Inorganic building unit
IR	Infrared spectroscopy
IRMOF	Isorecticular metal-organic framework
LDW	Laser direct writing
MIL	<i>Materials Institute Lavoisier</i>
MMA	Methyl methacrylate
MOF	Metal-organic framework
MOP	Metal-organic polyhedron
NMR	Nuclear magnetic resonance
NU	<i>Northwestern University</i>
PANI	Polyaniline
PCBM	[6,6]-Phenyl-C ₆₁ -butyric acid methyl ester

PCN	Porous coordination network
PCP	Porous coordination polymer
pcu	Primitive cubic
PEDOT	Poly(3,4-ethylenedioxythiophene)
PEDOT:PSS	Poly(3,4-ethylenedioxythiophene)-poly(styrenesulfonate)
PIZOF	Porous Interpenetrated Zirconium–organic Frameworks
PMMA	Poly(methyl methacrylate)
PSM	Postsynthetic modification
PXRD	Powder X-ray diffraction
SALE	Solvent-assisted ligand exchange
SALI	Solvent-assisted ligand incorporation
SBU	Secondary building unit
SEM	Scanning electron microscopy
TEM	Transmission electron microscopy
TGA	Thermogravimetric analysis
UiO	<i>Universitet i Oslo</i>
UPG	<i>University of Perugia</i>
XRD	X-ray diffraction

1 Introduction

In materials science, the design of (multi)-functional and advanced materials has been one of the main tasks for the last years, with challenging current and future requirements on functional materials for specific applications, e.g. industrial usage or environmental issues. One of the main goals is to combine required functions and properties in a novel material with enhanced performances.

However, many classes of materials possess only a limited customizability and a restricted amenability to further chemical optimization procedures for specific applications. A class of materials with the potential to overcome this lack is the class of metal-organic frameworks (MOFs). MOFs have been one of the most investigated and discussed materials class for the last two decades. Since the first publication of a coordination polymer with a three-dimensional framework in 1990 by Hoskins and Robson^[1] and later, in 1999, the published structure of a porous zinc terephthalate framework, the nowadays well-known and widely investigated MOF-5, by Yaghi and co-workers, many MOFs with targeted properties and diverse structures and compositions could be generated.^[2]

Metal-organic frameworks consist of metal ions or metal oxo clusters which are coordinated to organic molecules via functional groups like carboxylates resulting in one- to three-dimensional frameworks. The modular construction of MOFs opens nearly unlimited possible combinations of metal centers and organic molecules to adjust the pore shape and dimensions as well as the functionalities. Larger organic molecules can lead to expanded pore dimensions and additional functional groups like halide-, amino-, hydroxy- or carboxy-groups to facilitate the equipment of the framework with specific functionalities. In spite of the various possibilities to adapt the properties of MOFs, near-term prospects for commercial applications still remain limited. Major challenges for further applications lie in the limited choice of organic ligands with sensitive yet desirable functionalities which are not stable under synthesis conditions of MOFs and also tailoring properties like thermal and chemical stability of the framework in an appropriate way for specific applications as well as aspects like shaping.

Some strategies have been developed to alleviate the restrictions of the integration of specific functionalities. The most intensively investigated one is to modify and functionalize MOFs via postsynthetic modification (PSM) reactions at functionalities of the already formed framework. Nowadays, PSM implies different approaches like linker exchange, postsynthetic metalation or organic reactions at the linker molecules, whereby the reaction at linker molecules can facilitate a good combination of processability and versatility.

The first prerequisite for a permanent and robust adjustment of properties would be a covalent attachment of molecules to the framework through the linker molecules. In this work, the linker molecule benzophenone-4,4'-dicarboxylate (*bzpd*²⁻) was chosen because of the possibility of postsynthetic modifications at the keto group of the benzophenone moiety. After excitation with light this linker reacts with practically any compound containing a C–H bond. Few metal-organic frameworks containing benzophenone-4,4'-dicarboxylate as linker molecule are already reported, based on copper, zinc and cadmium and lanthanides.^[3–7] Also Al(III)-based frameworks, CAU-8 and CAU-21 (CAU: *Christian-Albrechts-University*), are reported and investigated by Stock and co-workers.^[8,9] Further investigations of CAU-8 indicated a possible postsynthetic modification of the framework performed on the keto group of the linker molecule. Based on the crystal structure, these reactions always occur throughout the whole pore system.^[10]

A prerequisite for a reliable postsynthetic modification at the keto groups of benzophenone-4,4'-dicarboxylate linker molecules is a high chemical and thermal stability of the resulting framework. Zr-based MOFs are well-known for their high chemical and thermal stability making them an appropriate prospect for the processability in specific postsynthetic modification reactions at the linker molecule while largely retaining the structural properties, especially the topology, of the pristine framework. Therefore, in parallel to the work of the group from Kiel we studied the synthesis system containing Zr⁴⁺ ions and the H₂*bzpd* linker.

Accordingly, this work focusses on the preparation, characterization and postsynthetic modification of a novel two-dimensional zirconium-based metal-organic framework with the photoreactive linker molecule benzophenone-4,4'-dicarboxylate. A novel Zr-*benzophenonedicarboxylate*-MOF, short Zr-*bzpd*-MOF, has been successfully synthesized using the synthesis control offered by the modulation approach, inspired by Kitagawa and co-workers and further developed in our group,^[11,12] and resulting in a crystalline material with crystals suitable for the proposal of a structure model based on single-crystal X-ray diffraction. The resulting two-dimensional framework crystallizes in an orthorhombic system as rhombic shaped crystals.

A prominent feature of this novel MOF is based on the two-dimensional structure, which facilitates delamination of the microcrystals by an ultrasonication approach to produce sheets with thicknesses of a few nanometers. The accessibility of those sheets could be interesting for various applications like membranes,^[13,14] dielectrics^[15] or as heterostructures^[16] for further applications. The main interesting feature of this MOF is based on the already mentioned photoreactivity of the linker molecule and the possibility to form covalent C–C bonds by reactions of C–H bond containing molecules with photo-excited keto groups. The photoreactive keto groups

of the benzophenone moieties are exposed at the surface of the largest faces of the rhombic crystals, facilitating postsynthetic photochemical modifications to regulate the surface properties.

In several studies it was possible to regulate the hydrophilicity or hydrophobicity of the framework by postsynthetic modification with simple hydrophilic and hydrophobic molecules. The direct polymerization reaction of an electrically conductive polymer at the outer surface resulted in an electrically conductive hybrid material. A systematic consideration of molecules with different chain lengths and different polarities gave an insight into preferred postsynthetic modifications at the outer surface or through the whole crystals. The consequences for the framework are discussed, building a helpful basis for the handling of other molecules for targeted adjustments of the properties of the MOF.

The novel Zr-*bzpd*c-MOF, on the one hand, showed some promising features for shaping MOFs, like the delamination approaches and the adjustment of the surface properties; on the other hand it opens the way to a wide range of different postsynthetic modification reactions with the reported generation of an electrically conductive composite material and also a facilitating guideline for selective PSM reactions.

2 General background

The following chapters deal with an introduction into metal-organic frameworks (MOFs), their modular composition, properties and peculiarities. Subsequently Zr-based MOFs are described, followed by an overview of different strategies of postsynthetic modification reactions and a deeper insight into the photochemical reactivity of the benzophenone group, which is used as linker basis for the linker molecule of the novel MOF described in this work.

2.1 Metal-organic frameworks

2.1.1 General principles

Metal-organic frameworks (MOFs), also called porous coordination polymers (PCPs), are one of the most investigated class of materials in the last decades since O. Yaghi and co-workers introduced the concept of permanent porous metal-organic frameworks constructed of organic molecules and metal ions in 1995.^[17] Two years later, Kitagawa and co-workers synthesized porous three-dimensional coordination polymers as methane storage materials and named them porous coordination polymers.^[18] Yaghi and co-workers published in 1999 the first so-called MOF synthesis and the structure of MOF-5, a porous framework consisting of zinc oxo clusters coordinated by terephthalate molecules as organic linker molecules.^[2]

In general, metal-organic frameworks consist of metal ions or metal oxo clusters coordinated by organic linker molecules with two or more coordinating groups which can connect at least two metal units resulting in one-, two- or three-dimensionally infinite frameworks. MOFs are well known for their high surface areas and tunable pore sizes. Besides of these outstanding properties, the hallmark of MOFs is their structural diversity and the possibility to tailor properties by designing a target structure with specific metal nodes and linker molecules. That provides endless possibilities in combinations and captivates the imagination of materials with perfectly adjusted properties for specific applications^[19,20] including gas storage and separation,^[21–24] catalysis,^[22,25] biomedicine^[26–29] and sensing.^[30–33] In the last years, first commercial attempts^[34] for the application of metal-organic frameworks started indicating the growth to market-ready class of materials. The main drawback of MOFs compared to other porous materials, which also hinders the commercial viability is the lower stability under mechanical, chemical and thermal stress, making them unusable for some applications. Normally, high stabilities are required but in

specific cases a precise or continuous degradation can also be an advantage, like in biomedical applications.

One of the most intensively investigated metal-organic frameworks is MOF-5, a Zn-terephthalate-MOF, and therefore a suitable example to explain several aspects on the description and definition of MOFs. The so-called inorganic building unit (IBU) consists of a central oxygen atom coordinated tetrahedrally by four zinc atoms, which are also coordinated tetrahedrally by the oxygen atoms of six carboxylate groups of the terephthalate molecules (Figure 1a). Two IBUs are connected with a terephthalate molecule through the carboxylates (Figure 1b). The six points of extension of the IBUs in combination with the linear linker molecule lead to a three-dimensional framework with a primitive cubic (**pcu**) topology (Figure 1c). It should be mentioned that due to the alternating orientation of the linker molecules the resulting structure of MOF-5 is less symmetrical than this idealized topology. This results in two types of pores with different dimensions.

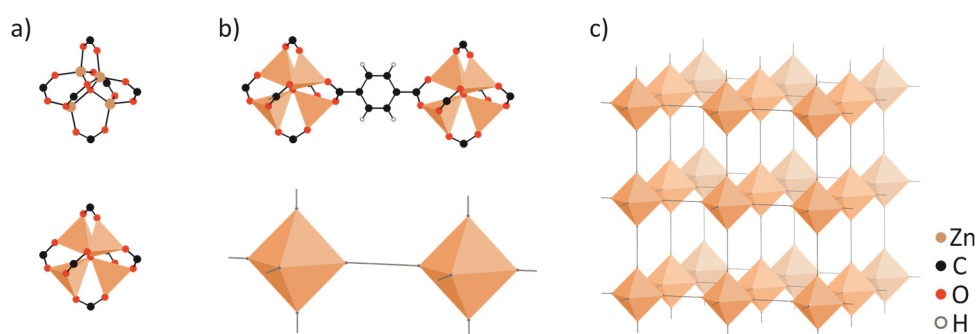


Figure 1. Schematic representation of the construction of a metal-organic framework, here shown by the example of MOF-5, starting with a) a zinc-oxo-cluster capped by the oxygen atoms of the carboxylates of the linker (IBU). b) The bridging of two IBUs with a terephthalate molecule (and a simplified version). c) Illustration of the primitive cubic topology, **pcu**-net, with simplified polyhedra (orange) representing the octahedral coordination pattern of the IBU and a straight line representing the terephthalate molecules.

The term inorganic building unit describes the metal-oxo-cluster including the oxygen atoms of the carboxylates of the linker molecules and overcomes the inconsistent terminology of the term secondary building unit (SBU), which was transferred from zeolites; there, it describes the basic building units with which the whole zeolite framework can be described. Its use in context of MOF structures does not take into consideration the majority of the linker molecules, and therefore it should not be applied to describe the framework of MOFs. To show the diversity of possible IBUs built up of different metal ions, Figure 2 illustrates some IBUs of well-investigated MOFs. The geometry of the polyhedra of the different metal-oxo clusters is generated by taking the metal ions as central atom and the surrounding oxygen atoms as edges of the polyhedra. For the copper based MOF HKUST-1 (HKUST: *Hong Kong University of Science and Technology*) with the tritopic linker

1,3,5-benzenetricarboxylate, this results in two square pyramids of two copper atoms coordinated by four carboxylates of the linker molecule and two water molecules.^[35] For the already mentioned MOF-5, the IBU consists of four corner-connected tetrahedra resulting in a Zn_4O basic building unit capped with six carboxylates of the linker molecules. In case of the zirconium-based MOF UiO-66 (UiO: *Universitetet i Oslo*; linker: terephthalate), six edge-connected antiprisms of $Zr_6O_4(OH)_4$ basic building units are capped with twelve carboxylates of the linker molecules.^[36] Besides these examples, many other metal nodes are in focus of research based on different metals like chromium, aluminum, iron and several other transition metals or other geometries of the IBUs with different numbers of points of extensions.^[37]

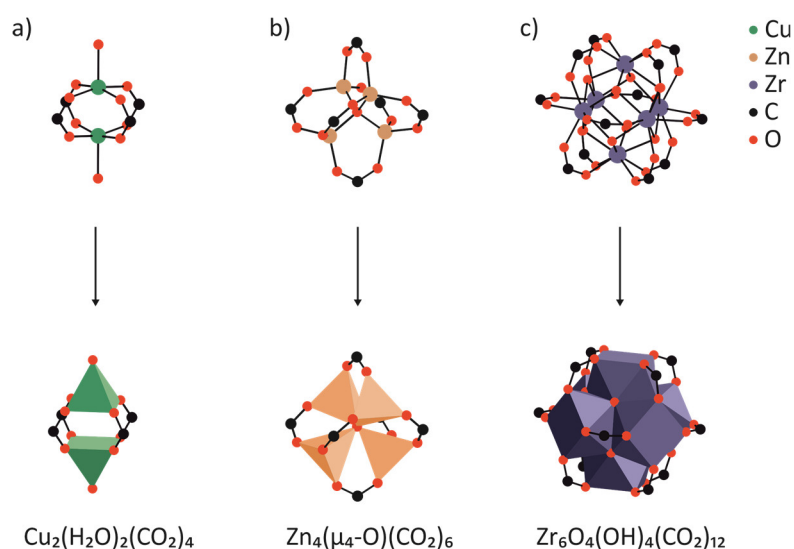


Figure 2. Scheme of three different IBUs: a) In case of HKUST-1^[35] two copper ions are capped by four carboxylates of the linker molecules and two water molecules resulting in an IBU consisting of two square pyramids (green); b) The already mentioned Zn-based IBU, consisting of a $Zn_4(\mu_4-O)$ cluster (orange) and the oxygen atoms of the carboxylates of the linker molecules; c) the Zr-based IBU present in MOFs like UiO-66^[36] or the Zr-*fumarate*-MOF,^[38] with six octahedrally arranged zirconium ions (violet). Hydrogen atoms are not shown for the sake of clarity.

The examples of IBUs based on different metals shown in Figure 2 explains on part of the diversity of metal-organic frameworks. The other feature ensuring diversity, the coordination and bridging of these building units by multitopic ligands, further defines the structural topology by the number of orientation coordination topology of the linkers and influences the pore metrics as determined by the length of the linkers. The combination of different IBUs and different linkers result in a large variety of different frameworks, with their properties depending on both, the IBUs and the organic ligand.

Reticular chemistry

One of the main challenges is the construction of crystalline porous frameworks from molecular building blocks. To facilitate the description of the structural diversity of MOFs, Yaghi and O’Keeffe extended the original work of Robson and co-workers^[1] to a rational methodology, the so-called reticular chemistry, which is based on the “node and spacer” approach of Wells and co-workers from 1977,^[39] used for zeolite structures. Metal ions serve as nodes and organic ligands as linear spacers for the unrestricted construction of infinite frameworks. Reticular chemistry is a methodology to systematically generate series of MOFs with varying pore metrics, predetermined structures, compositions and properties of the framework by varying the molecular building blocks.

To describe and organize structures of MOFs, they can be abstracted and simplified by underlying nets and therefore they can be categorized in different topologies.^[40,41] The inorganic building units are abstracted as triangles, squares, tetrahedra and octahedra and therefore can be linked by the linkers into periodic structures. The most prominent series of this approach is the already mentioned MOF-5 and the other members of the **pcu**-net MOFs. MOF-5 has a **pcu**-net as an underlying topology, a primitive cubic topology (illustrated in Figure 1c).^[41] The topology and then the resulting structure depend on the symmetry of the IBU and the number of points of extensions as well as on the number of connecting sites of the organic linker molecule.

A deliberate variation of linker molecules, especially their molecular lengths, to adjust the pore dimensions with regard to the desired application, in combination with the Zn₄O based IBU of MOF-5 results in the same topology, so called isorecticular metal-organic frameworks (IRMOFs).^[42] Many examples of IRMOFs have been formulated and published in the last decades in which each member shares the same primitive cubic topology like MOF-5. The first series of sixteen metal organic frameworks sharing the same cubic topology as MOF-5 (IRMOF-1) were synthesized and published by Yaghi and co-workers in 2002.^[42] This concept was applied to several other MOFs to obtain, for example, isorecticular frameworks of HKUST-1 and UiO-66, respectively. For each of the IBUs (Zn-, Cu- and Zr-based) two isorecticular MOFs are depicted in Figure 3.

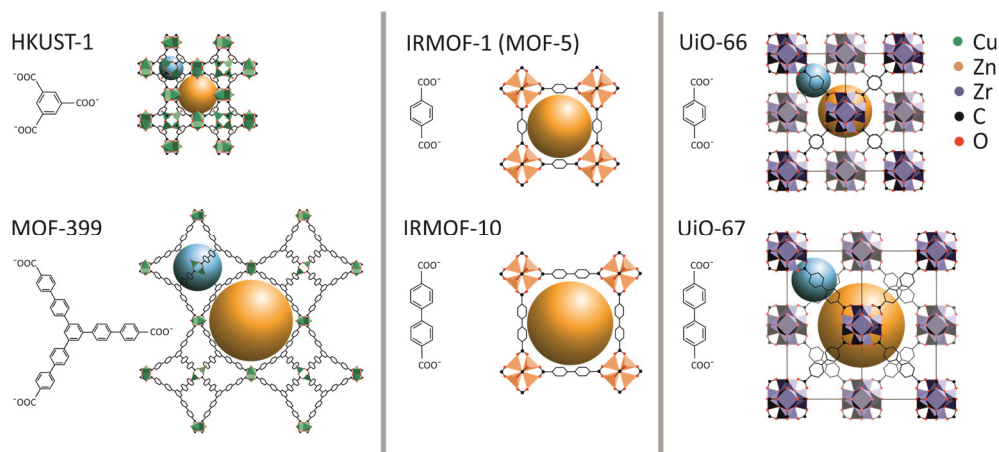


Figure 3. Scheme of three different examples of reticular chemistry with different pore dimensions indicated as orange and blue balls. Left: Cu-based IBUs (green polyhedra) coordinated by benzene-1,3,5-tricarboxylates resulting in HKUST-1^[35] and by elongating each of the three points of extension with biphenyl units results in an isoreticular MOF, MOF-399, sharing the underlying **tbo**-net. Middle: The well-known MOF-5 (IRMOF-1), built up of Zn-based IBUs (orange polyhedra) coordinated by terephthalate molecules resulting in a **pcu**-net. Elongation of the linker results in IRMOF-10 with larger pores but the same topology. Right: The 12-fold connecting Zr-based IBU (purple polyhedra) with terephthalate molecules acting as linker results in UiO-66 with an underlying **fcu**-net. By using biphenyl dicarboxylate as linker molecule, UiO-67 results, a MOF with larger pores but the same topology.

In the first case, HKUST-1 and the isoreticular MOF-399 are depicted, which results by expanding each of the three points of extension of the linker molecule of HKUST-1 with biphenyl units, sharing the same underlying **tbo**-net but with a ten times smaller crystallographic density of 0.13 g cm^{-3} .^[43]

As derivatives of MOF-5, isoreticular MOFs with the underlying **pcu**-net but larger pore dimensions were achieved by using other rigid, linear carboxylates like biphenyl- or terphenyl-dicarboxylate. Therefore, it is possible to increase the pore dimensions of the resulting frameworks to 24.8 \AA (IRMOF-10, Figure 3) and 28.8 \AA (IRMOF-16) compared to 12.8 \AA for MOF-5 (IRMOF-1).^[42] It is also possible to generate an isoreticular MOF with a shorter linker molecule and smaller pore dimensions, when the linker molecules are exchanged for acetylene-dicarboxylates resulting in the same cubic topology (IRMOF-0).^[44] In this case, a doubly interpenetrating structure occurs, originating from the slim rod-like nature of the linker.

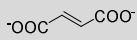
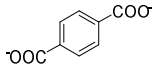
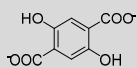
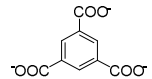
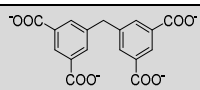
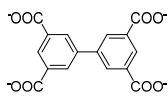
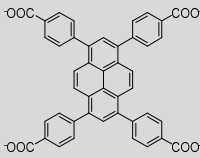
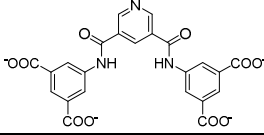
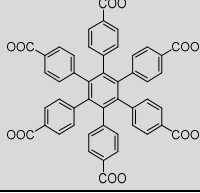
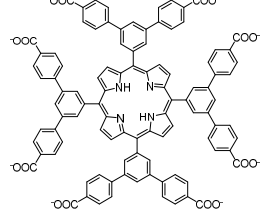
The Zr-based MOF UiO-66 also consists of terephthalic acid as linker molecule but instead of the 6-fold connecting paddle-wheel Zn-IBUs, 12-fold connecting Zr-IBUs are coordinated by the ligands. This results in a MOF with a higher density compared to MOF-5, an increased stability based on the high number of strong zirconium-oxygen bonds and a different topology; in case of UiO-66, a **fcu**-net. The elongation of the linker molecule to a biphenyl dicarboxylate leads to the isoreticular MOF UiO-67 (Figure 3) with larger pore dimensions with retention of the underlying **fcu**-

net. A further elongation of the linker molecule by using unsubstituted terphenylene-dicarboxylates resulting in a UiO-68 was apparently predicted by Lillerud but derivatives with further functionalities, which are also increasing the normally low solubility of the terphenylene-dicarboxylate, were successfully synthesized with retention of the **fcu**-net.¹²

The generation of isorecticular MOFs with enlarged pore dimensions by the use of rod-like or very long linkers can result in interpenetrating frameworks. By utilization of rod-like linker molecules consisting of alternating phenylene (P) and ethylene (E) units Schaate and co-workers^[45] introduced a novel series of isorecticular MOFs, the PIZOF series (porous interpenetrated zirconium-organic framework), which shows two interpenetrating independent networks, each isorecticular to the UiO topology. Due to the linker molecules and pore dimensions PIZOFs have the potential of a high chemical versatility and the opportunity of tuning the properties by postsynthetic modifications at the linker molecules. Compared to the UiO series, the PEPEP linker molecules of the PIZOFs are considerably longer (UiO-66: 6.8 Å; PIZOF-2: 20.4 Å). Also, a variety of different functionalities can be introduced into the framework at the phenylene rings of the linker molecule. Lippke and co-workers^[46] extended the investigations concerning PIZOFs and have shown that reducing the linker length to a PEEP motif results in a UiO-type framework with no interpenetration. Compared to the elongation of the linker molecules by retaining the same topology, it is also possible to use higher functionalized linker molecules. Isorecticular functionalization of the framework is possible by using linker molecules with further functionalities like hydroxy-, amino- or nitro-groups resulting in, for UiO-66 as an example, a series of isorecticular MOFs with a variety of functionalized pores. On the other hand it is possible to change the topology and pore size of MOFs by using linker molecules with different functionalities like in case of the Zr-based MOF NU-903, NU-904 and NU-1008 (NU: *Northwestern University*), which are based on the tetatopic linker molecule 1,2,4,5-tetrakis(4-carboxyphenyl)benzene and two derivatives with additional functional groups on the central phenylene ring.^[47]

Ditopic (e.g. terephthalate), tritopic (e.g. 1,3,5-benzenetricarboxylate) or tetatopic linkers (e.g. biphenyl-3,3',5,5'-tetracarboxylate) with a rigid structure are often used as linker molecules for MOF syntheses. An extended concept to synthesize MOFs was demonstrated by Cohen and co-workers, where the organic ligand is not a typical small, rigid molecule for MOF synthesis but is based on flexible polymer chains with aromatic dicarboxylates in the backbone.^[48] A short overview of some of the most prominent linker molecules with diverse points of extension (topicity) and examples of the successfully synthesized crystalline metal-organic frameworks is shown in Table 1.

Table 1. Overview of a selection of multitopic ligands for MOF syntheses and resulting crystalline MOF examples.

Topicity	Ligand examples	MOFs	References
Ditopic		MIL-88A (Fe ^{III})	[49]
		Ca-/Al- <i>fum</i> (Ca ^{II} , Al ^{III})	[50,51]
		Zr- <i>fum</i> (Zr ^{IV})	[38]
		MIL-47 (V ^{IV})	[52]
		MIL-53 (Al ^{III} , Fe ^{III} , Cr ^{III} , Sc ^{III})	[53–55]
		MIL-101 (Cr ^{III})	[56]
		MOF-5 (Zn ^{II})	[2]
UiO-66 (Zr ^{IV})	[36,57]		
		MOF-74 (Mg ^{II} , Co ^{II} , Mn ^{II} , etc.)	[58–60]
Tritopic		HKUST-1 (Cu ^{II})	[35]
		MIL-100 (Fe ^{III} , Cr ^{III})	[61,62]
		Zn- <i>btc</i> (Zn ^{II})	[63]
Tetratopic		MIP-200 (Zr ^{IV})	[64]
		CPF-1 (Mg ^{II})	[65]
		MOF-505 (Cu ^{II})	[66]
		NOTT-100 (Cu ^{II})	[67]
		NU-1000 (Zr ^{IV})	[68]
Pentatopic		PCN-124 (Cu ^{II})	[69]
		PMOF-3 (Cu ^{II})	[70]
Hexatopic		MOF-892 (Zr ^{IV})	[71]
		MOF-893 (Zr ^{IV})	
		MOF-894 (In ^{III})	
Octatopic		MMPF-10 (Cu ^{II})	[72]

The examples of combinations of IBUs and organic multitopic ligands give a hint to the nearly infinite possibilities of MOF structures modifications to generate a material with specific properties.

Defective MOFs

In recent years, one important field of research was the targeted creation of defects in MOFs to introduce new properties to the framework like enhanced catalytical activity or conductivity.^[73–75] It is possible to distinguish between two methods to prepare MOFs with defective sites. The first one is the so-called “*de novo*” synthesis, also known as modulation approach, originating from the reduction of the crystallization rate of MOFs to obtain MOFs with higher crystallinity by impacting the equilibrium of the formation of the framework. The modulation approach is described in detail in section 2.1.3.

It is possible to introduce defective sites into MOFs by using higher concentrations of modulating molecules like monocarboxylic acids. Some studies use this approach, one example given by Ravon and co-workers^[76] in 2010, by adding 2-methyl-toluic acid as modulator to the synthesis of MOF-5. Also the work of Vermoortele and co-workers^[77] in 2013, the synthesis of a highly defective UiO-66 using trifluoric acid as modulator, is based on the same approach. In a next step it was possible to remove the modulator molecules by thermal treatment to generate Lewis acidic unsaturated sites. A systematical study of the defect generation in UiO-66 by several monocarboxylic acids is given by Shearer and co-workers in 2016,^[78] which showed that the Brønsted acidity of the modulator is correlating with the defect concentration.

The second approach to generate defective MOFs is based on postsynthetic treatment methods, introducing defective sites after the synthesis of the MOF. Several approaches are based on a treatment of the framework with modified linker molecules or acids like Vermoortele and co-workers used trifluoric acid and perchloric acid to modify MIL-100 (Fe) to generate additional Brønsted acid sites.^[79] The modification of MOFs by replacing or incorporating linker with modified linker molecules with other functional groups, catalytical active sites or longer linker molecules is the so-called “solvent-assisted ligand exchange” (SALE)^[80–82] or by incorporating new linker molecules is the so-called “solvent-assisted ligand incorporation” (SALI).^[83] SALE is more promising in the modification of stable MOFs like UiO-66 and SALI is a method appropriate for MOFs with open metal sites for the postsynthetic coordination of the linker molecules. Other postsynthetic treatments to generate defects are extensive washing or activation procedures at high temperatures or ball milling approaches by breaking of a fraction of metal–ligand bonds.^[84–86]

Mixed metal/ mixed linker MOFs

An important field of MOF research in recent years is the combination of not only one metal source and one linker molecule to construct a metal-organic framework. Furthermore, approaches that basing on multicomponent systems consisting of mixed-metal or mixed-linker MOFs to increase the selectivity and activity of MOFs for specific applications are in focus. Mixed-metal approaches are predominantly interesting in the field of heterogeneous catalysis especially for cascade or tandem reactions.^[87,88] For a successful preparation of mixed-metal MOFs the use of metals with same coulombic charge and ionic radius to increase the chance for a homogeneous distribution of the metals in the resulting framework. Several mixed-metal approaches show promising results as heterogeneous catalysts, e.g. STU-2 with zinc and copper^[89] and CPO-27 with manganese and cobalt^[90] for cyanosilylation of aldehydes or MOF-74 with nickel and cobalt for the oxidation of cyclohexene.^[91] Another example is the already mentioned Zr-based MOF UiO-66.^[36] A mixed metal UiO-66 with varying ratios of Ce⁴⁺ and Zr⁴⁺ is given by Lammert and co-workers^[92] resulting in enhanced thermal and chemical stability.

Another strategy is the formation of a framework with different linker molecules with diverse functionalities. One of the first series of mixed-linker MOFs was reported by Yaghi and co-workers in 2010, where they reported a series of multivariate MOF-5 type structures with terephthalate molecules with different functionalities like -NH₂, -NO₂, -Br, -Cl₂, -(CH₃)₂, -C₄H₄, -(OC₃H₅)₂ and -(OC₇H₇)₂.^[93] That methodology of the use of linkers with different functionalities resulting in the same topology is also described for UiO-66 by several research groups.^[94,95] These approaches are based on derivatives of the originated linker molecule but it is also possible to use structurally distinct linkers. One aim is the generation of a well-defined compartment by arranging specific functionalities of different linker molecules. Telfer and co-workers have shown several MOFs with mixed multitopic ligands which are geometrically distinct,^[96-98] e.g. demonstrated an example of mixed-linker MOF, the MUF-7 (MUF: *Massey University Framework*) series,^[99] with three topologically distinct linkers resulting in eight isorecticular frameworks by variation of the functional groups of the different linkers. The first one, MUF-7a, is shown in Figure 4.

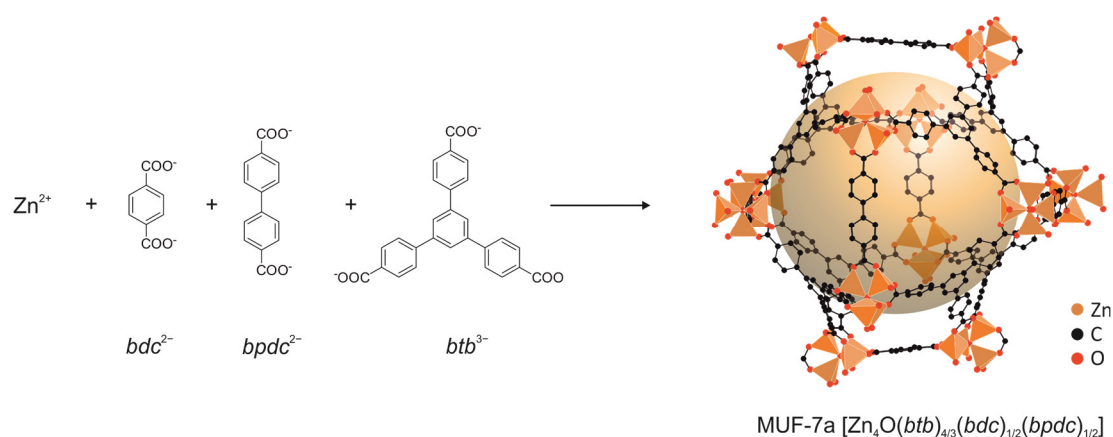


Figure 4. MUF-7a, a multivariate Zn-based MOF with three different linker molecules, terephthalate (bdc^{2-}), biphenyl-4,4'-dicarboxylate (bpdc^{2-}) and benzene-1,3,5-tribenzoate (btb^{3-}). The illustration of the structure highlights the octahedral pore.^[99]

One major drawback of one-pot syntheses, often used to build up multivariate MOFs, is the prerequisite precise adjustment of the synthesis conditions of solvothermal approaches. Another approach that overcomes this restriction is based on postsynthetic modifications of MOFs, which is discussed in detail in section 2.3.

MOF composites

For the generation of MOFs with designed properties for specific applications, one recent topic is the combination of the properties of MOFs with other functional materials, which results in multifunctional composites/hybrid materials with superior properties compared to the individual components.^[100,101]

MOF/polymer composites

One of the most investigated class of MOF composites is the integration of MOFs with polymers for several potential fields of application, above all, for mixed-matrix membranes^[102–105], also for conductive materials,^[106,107] gas storage and separation,^[108,109] bio-imaging^[110,111] and as electrodes in dye-sensitized solar cells (DSSCs).^[112] Beside mixing a MOF with a polymer there are two other major strategies, the first one is to generate MOF/polymer composites by crystallizing a MOF onto a polymer (MOF@polymer), which has major interest in the field of biomedicine.^[110,113] The second strategy for MOF/polymer composites is the growth or incorporation of a polymer^[114,115] inside or on the surface of a MOF (polymer@MOF), e.g. for the preparation of electrically conductive materials.^[106,116–118] The direct polymerization initiating on functionalities on the MOF surface, so-called “grafting-from” approaches, should lead to higher polymer densities on the MOFs compared to the “grafting-on”^[119] approach, the attachment of fully formed polymers onto the MOF.^[120–122] Recent examples of MOF/polymer composites are, e.g., the decoration of a MOF with thermoresponsive polymers for a

switchable controlled drug release,^[123] superhydrophilic/superoleophilic MOF composites for oil/water separation^[124] or nylon-MOF composites for the breakdown of chemical warfare simulants^[125] which indicates the high diversity of possible applications. Another possibility to use metal-organic frameworks in combination with polymers is a templating-approach, where the framework acts as a template and polymers are synthesized in the pore system to generate ordered polymer structures.^[126,127]

MOFs based on polymeric linker molecules are so-called polyMOFs. They represent highly crystalline hybrid materials constructed from a soft, flexible and nonporous organic polymer carrying functionalities acting as linker moieties for the synthesis of a crystalline metal-organic framework (schematically shown in Figure 5).^[48,128–131]

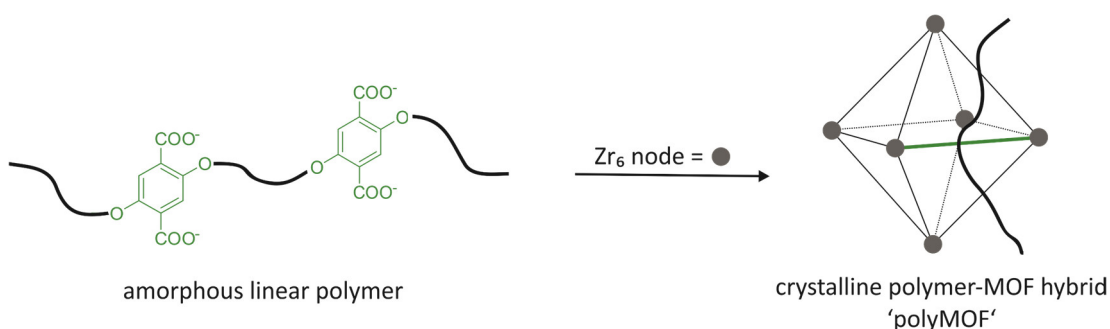


Figure 5. Schematic representation of the synthesis of polyMOFs, polymer-MOF hybrid materials, based on amorphous linear polymers with dicarboxylate moieties acting as linker, here shown for an UiO-66 polyMOF (adapted from ref. 128).^[128]

MOF/nanoparticle composites

Beside composite materials of MOFs containing polymers, the combination with nanoparticles is a large field of research. First attempts dealt with nanoparticle growth on MOF surfaces and vice versa. For purposeful adjustments of particle sizes, morphology and properties, two strategies were developed. On the one hand the encapsulation of pre-synthesized nanoparticles followed by the growth of the MOF around the nanoparticle, like core-shell gold nanorods overgrown with a Zr-based MOF^[132] and on the other hand the growth of nanoparticles within the pores of a pre-formed MOF.^[133] Another approach, which benefits from the ordered framework of MOFs, is a templating method to synthesize ordered metallic structures like nanowires within a MOF acting as the template.^[134] In general, several different approaches are suitable to generate MOF/nanoparticle composites like solid grinding^[135,136] (e.g. Au@Al-MIL-53),^[135] liquid impregnation^[137,138] (e.g. Ni@MOF-5),^[139] chemical vapor deposition (e.g. Au/Pd/Cu@MOF-5)^[140] or double solvent methods^[141,142] (e.g. Pt@MIL-101)^[141] as well as different encapsulation approaches.^[143,144] With these different concepts, several types of nanoparticles can be used to form MOF/nanoparticle composites, like different metal or metal oxide

nanoparticles,^[145,146] quantum dots, polyoxometalates and non-metal-based nanoparticles like carbon nanotubes, graphene, fullerenes or silica.^[94,147]

Beside these major material combinations containing MOFs also other composite materials are in focus of research, like the fabrication of different metal-organic framework combinations resulting in core-shell systems. This is an appropriate way to combine different functionalities of MOFs without affecting the pristine properties of MOFs itself.^[148] Two different strategies have emerged as the most promising, first, the encapsulation of a MOF crystal seed with another MOF with different metal centers and/or linker molecules in separated regions of the particle. The second strategy is a postsynthetic treatment by selectively replacing the metal ions or linker molecules.^[149] In recent years it has been shown that MOFs, compared to other materials like silica, also are an appropriate class of materials to immobilize and stabilize enzymes without affecting the enzymatic activity. Several different strategies have been shown to be suitable for the generation of MOF/enzyme composite materials like encapsulation, surface attachment or covalent linkage and co-precipitation.^[150] Also other functional molecules^[151,152] have been used for the fabrication of MOF composites like organic dyes,^[153,154] organometallic compounds^[155] and biomolecules.^[156,157] That variety of different strategies and combinations are appropriate for several applications like catalysis,^[158] gas storage,^[159] drug-delivery systems^[27,49,157] and adsorbent materials.^[160,161]

2.1.2 Electrically conductive MOFs

Electrical conductivity, the capacity of a material to transport charges, is a desirable property in metal-organic frameworks for several applications like sensing, energy storage or electronics. Naturally, the porous structure of MOFs – generally their main hallmark – is per se detrimental to electrical conductivity. The general mechanism of electron or hole transport requires strong and extended overlap between the valence orbitals; geometric restrictions – as they are observed in nano-objects, but to which porosity also belongs – reduce this overlap and leads to localized states. Most MOFs are built of metal centers and ligands with low or zero concentration of free charge carriers, and the electronic states of both types of building units are isolated and highly localized.^[162] Furthermore, if there are charge carriers, their mobility is low, with the contact between the two basic building units often being a further obstacle to charge transport due to non-fitting orbital energies. An overview of the different strategies to overcome these obstacles and to develop electrically conductive MOFs is shown in Figure 6. Some of these strategies are further described below.

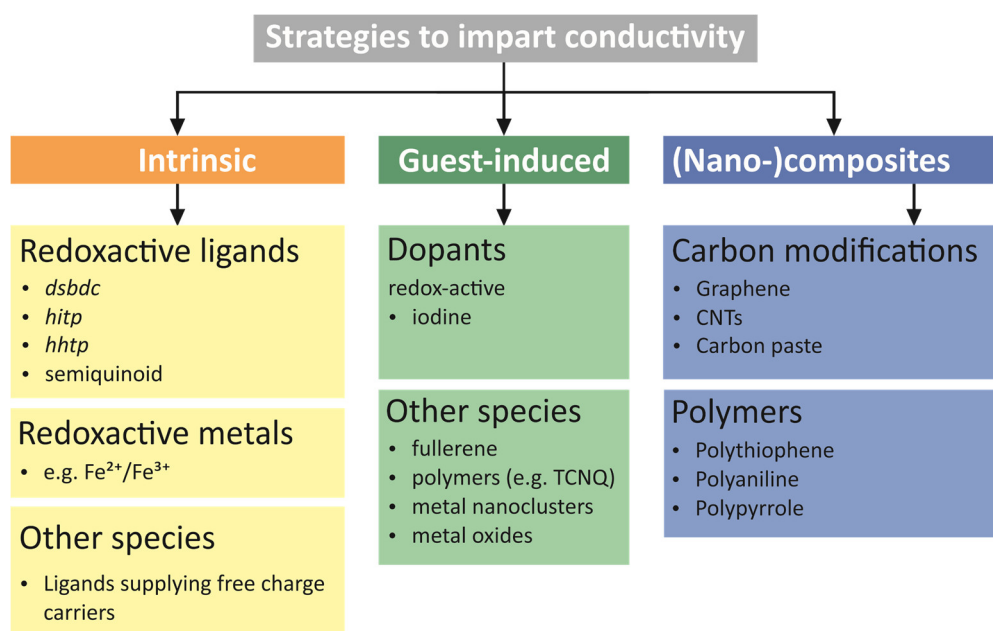


Figure 6. Different strategies to introduce electrical conductivity into MOFs.^[163]

Intrinsic electrical conductivity

In recent years, different possibilities to introduce electrical conductivity to metal-organic frameworks were in focus of research as appropriate candidates for applications in electronics, in sensing of molecules (hydroquinone, catechol, glucose, etc.), for photovoltaics and catalysis.^[163]

The most obvious approach is the synthesis of intrinsic conductive frameworks by redox-active metal ions which can provide charge carriers; by redox-active linkers doing the same; and by delocalized π -electrons in conjugated organic linker molecules allowing for charge transport, also between them through π -stacked aromatic ligands.^[162] Also, adapting the orbital energies between the IBUs and the linkers can allow for further delocalization of charge carriers or for simplifying electron/hole hopping processes. The resulting conductivity may – usually in accordance with the dimensionality of the structure – occur in one, two or three dimensions; examples being stacked square-planar complexes with suitable linkers building up a linear coordination polymer,^[164] 2D graphene-like MOFs or diverse three-dimensional frameworks (see below).

In the literature, some examples of MOFs based on metal-ions providing mobile charge carriers are known. One of the first examples of a 3D conducting MOF was presented by Kitagawa and coworkers in 2009, the cubic Cu-based MOF Cu[Cu(2,3-pyrazinedithiolate)₂] with an electrical conductivity of about 6×10^{-4} S/cm at room temperature; mixed-valent Cu centers can supply electrons which can be delocalized over the conjugated linker molecules due to the choice of nitrogen donor functions (instead of the usual dicarboxylate ones).^[165] Other MOFs based on the Fe^{II}/Fe^{III} ions also led to intrinsic electrically conductive frameworks, e.g. Fe(1,2,3-triazolate)₂ with an electrical conductivity of about 7.7×10^{-5} S/cm,^[166] [(Bu₄N)₂Fe^{III}₂(2,5-dihydroxybenzoquinone)₃] with a conductivity of 0.16 S/cm^[167] or Fe₂(2,5-dihydroxybenzene-1,4-dicarboxylate) and Fe₂(2,5-disulfhydrylbenzene-1,4-dicarboxylate) with conductivities of 3.2×10^{-7} and 3.9×10^{-6} S/cm at room temperature.^[168]

In recent years, 2D graphene-like MOFs have shown the highest values of intrinsic electrical conductivities of MOFs in combination with a moderate porosity.^[169] These MOFs are based on trigonal linker molecules with phenylene^[170,171] or triphenylene^[170,172–176] backbones equipped with hexahydroxy-,^[172,174] hexamino-^[172,175,176] and hexathiol-moieties,^[170,171,173] resulting in linker structures which can exhibit redox activity in analogy to the well-known quinone/hydroquinone redox pair. Combined with square-planar metal ions (e.g. Cu²⁺, Co²⁺, Ni²⁺, Pt²⁺) hexagonal layers could be generated; by stacking the individual layers a one-dimensional pore system can be formed. The resulting graphene like metal-organic frameworks exhibit electrical conductivities at room temperature in the range from 2×10^{-3} S/cm up to

59 S/cm^[172,177] as pressed pellets and up to 1580 S/cm in case of thin films of Cu₃(benzenhexathiolate)₃.^[171] Graphene-like MOFs show appropriate properties for several applications and were already tested as electrodes for sensing, energy storage in supercapacitors or hydrogen generation.^[172,178]

Guest-induced electrical conductivity

The doping of MOFs with guest molecules that can inject charge carriers or enable charge delocalization through the framework could also lead to electrically conductive MOF materials. Many examples seem to be appropriate to guest-induced electrical conductivity into MOFs, like redox-active molecules, fullerenes, carbon nanotubes or conductive polymers.^[163]

One approach to introduce electrical conductivity to insulating frameworks is the infiltration of iodine or tetracyano-quinodimethane (TCNQ). Reported by Zeng and co-workers in 2010, the doping of the [Zn₃(lactate)₂(4-pyridinebenzoate)₂] framework with iodine resulted in an electrically conductive material with values of about 1.7×10^{-4} S/cm up to 3.4×10^{-3} S/cm. Compared to the inherent conductivity of iodine (7.7×10^{-6} S/cm) the increase indicates highly ordered iodine molecules in the pore channels of the framework, which corresponds to guest-induced conductivity.^[179] Another example, where iodine acts as a dopant and was used to oxidize the network, was shown by Allendorf and co-workers who doped the framework Cu[Ni(pyrazine2,3-dithiolate)₂] with iodine, which led to a partial oxidation of the Ni centers enhancing the conductivity to a value of about 1×10^{-4} S/cm, compared to the intrinsic conductive framework Cu[Cu(pyrazine2,3-dithiolate)₂] with a conductivity of about 1×10^{-8} S/cm.^[180] In case of the redox-active TCNQ, the coordinated cross-linking of redox-active metal clusters in HKUST-1 is appropriate to induce electrical conductivity, as developed by Allendorf and co-workers in 2014, when they doped the insulating MOF HKUST-1 (conductivity of about 10^{-8} S/cm at room temperature) with TCNQ. The unsaturated Cu-paddlewheel nodes were coordinated by TCNQ molecules, which cross-linked the Cu-nodes and enabled a through-bond charge transport with an electrical conductivity of about 0.07 S/cm.^[181] Also studies, which dealt with the incorporation of fullerene into the pores of MOFs, resulted in an increased conductivity, e.g. in case of the Zr-based MOF NU-901 with an increased conductivity from immeasurably low to 10^{-3} S/cm.^[182] Another promising strategy to induce guest-based electrical conductivity in MOFs is to incorporate conductive polymers into the pore system like in case of polypyrrole@Cd(2,6-naphthalenedicarboxylate)_{0.5}(4-pyridinecarboxylate)] (1×10^{-3} S/cm compared to 1×10^{-12} S/cm)^[183] or poly(3,4-ethylenedioxythiophene)@Cr-MIL-101 (1.1×10^{-3} S/cm compared to 1×10^{-9} S/cm).^[118]

Another approach to combine metal-organic frameworks with conductive polymers is the coating of MOF crystals with polymers. One study showed a successful

preparation of a composite by coating crystals of the metal-organic framework UiO-66-NH₂ with the electrically conductive polymer polyaniline (PANI).^[184] On the other way round, it is also possible to crystallize the MOF on electrically conductive polymer films. One example is the generation of highly conductive films of poly(3,4-ethylenedioxythiophene)-poly(styrenesulfonate) (PEDOT:PSS) threaded HKUST-1 with electrical conductivity of up to 13 S/cm and a high permanent porosity.^[185] Beside polymers, different carbon modifications like graphene or carbon nanotubes could also end up in semiconducting materials which are appropriate candidates for sensing applications. One study by the group of Alkordi, focusses on an approach to produce a monolithic composite of graphene and the Cu-based MOF HKUST-1. The crystallization of HKUST-1 crystals on the graphene flakes resulted in a composite material with a high permanent porosity and an electrical conductivity in the range of 10⁻⁸ S/cm up to 10⁻³ S/cm, correlating with the amount of graphene. Another promising approach was developed by Hendrik A. Schulze from our group, with a composite material consisting of UiO-66 nanoparticles, that were grown onto the surface carbon nanotubes, resulting in a highly integrated nanocomposite with strong intergrowth between the CNT and the MOF nanoparticles. These composites show a wide range of electrical conductivity, depending on the amount of CNTs added to the reaction solution, between 10⁻⁶ S/cm (3% CNT) up to 10⁰ S/cm (30% CNT).^[186]

In case of the *Zr-bzpd*c-MOF, the compound on which this thesis is based, it was possible to directly polymerize 3,4-ethylenedioxythiophene at the MOF surface resulting in a hybrid material with an increased electrical conductivity of about 1×10⁻³ S/cm, three orders of magnitude higher compared to the pristine MOF.^[187] Noteworthy is the fact that the pristine *Zr-bzpd*c-MOF was detected here as another of the few frameworks which exhibit intrinsic electrical conductivity.

2.1.3 Modulated synthesis

The theoretical combinations of metal centers and organic linker molecules is nearly infinite, the limiting factor is often the experimental synthesis of crystalline frameworks – many attempts to combine metal ions with linker molecules just lead to amorphous materials. One decisive step to overcome this lack was achieved by Kitagawa and co-workers in 2009 by the addition of monocarboxylic acids like acetic acid and benzoic acid to the synthesis solution. This approach led to a competition between a monocarboxylic molecule and the linker molecule in coordination processes at the IBUs. With this attempt it was possible to synthesize crystalline MOF nanoparticles with defined shape and size with a solvothermal synthesis approach, where normally bulk material with just moderate porosity was obtained.^[11] In their

work, they used acetic acid to compete with the linker molecule resulting in an anisotropic growth of the framework with a prismatic habitus.

The so-called coordination modulation approach leads to a more controlled crystal growth due to the competing coordination processes of monocarboxylic modulator molecules and the linker molecules at the coordination sites of the IBU (Figure 7).

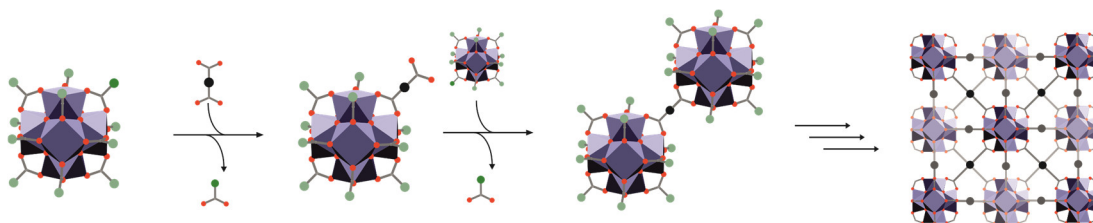


Figure 7. Schematic representation of modulated synthesis approach. The metal oxo cluster (here visualized by a Zr_6 node) is ideally saturated with monocarboxylic modulator molecules and undergoes a ligand exchange with a linker molecule. This enables the connection between two clusters by ligand exchange and in a controlled and slow way the formation of a crystalline framework. Ideally all modulator molecules are exchanged by linker molecules.

Schaate and co-workers adapted the modulation approach to Zr-based MOFs and introduced a sophisticated way to achieve crystalline materials by adding monocarboxylic acids like acetic acid or benzoic acid to the reaction solution.^[12] With this approach it was possible to synthesize several highly crystalline Zr-based metal organic frameworks with distinct particle size and morphology. Also, single crystals of the Zr-based MOF UiO-68-NH₂ with 2'-amino-1,1':4',1''-terphenyl-4,4''-dicarboxylate as linker molecule could be obtained. In recent years, many other examples are described, where it was possible to synthesize single crystals with the modulation approach.^[45,188,189] Also, first approaches have shown a correlation between molar ratios of modulator to ligand and the impact of the pK_a values of modulator and ligand and the synthesis of UiO-type Zr/Hf-MOFs.^[190]

On the one hand it is possible to generate well-ordered frameworks with usually less defects or on the other hand defects and cavities can be introduced into the MOF to enhance the surface area and e.g. the catalytic activity. Wu and co-workers demonstrated a generation of linker vacancies of UiO-66 by variation of acetic acid as modulating agent resulting in adjustable Brunauer-Emmett-Teller (BET) areas of 1000 to 1600 $\text{cm}^3 \cdot \text{g}^{-1}$.^[191] Another approach is demonstrated by Vermoortele and co-workers using trifluoric acid and hydrochloric acid as modulators resulting in UiO-66 with defects and open Zr sites.^[77] Hydrochloric acid is in this case an example for a second modulation beside the coordination modulation approach with competing molecules. It is also possible to affect the synthesis of MOFs by a modulation based on protonation and deprotonation of the linker molecules to regulate the coordination with IBUs. The modulator is not directly competing the coordination

sites but affecting the protolysis equilibrium and therefore regulates the solubility and the ability to coordinate on the IBUs of the linker molecule.^[192]

In the present study, the modulation approach using formic acid as modulator was by far the only way to obtain a crystalline and porous metal-organic framework, the *Zr-bzpd*c-MOF.^[193] In this case, the modulator does not just act as a competitor to the linker molecule but also is a component of the framework by partially saturating the IBU with two formate molecules per IBU and eight-fold connected by linker molecules. The different repercussions of several modulators and modulator concentrations on the synthesis of *Zr-bzpd*c-MOF are shown in section 3.1.

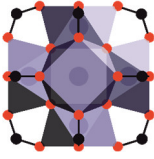
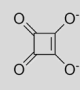
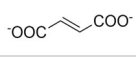
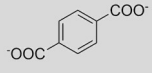
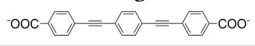
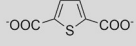
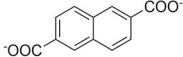
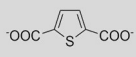
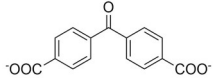
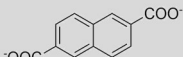
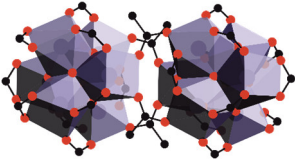
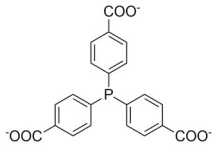
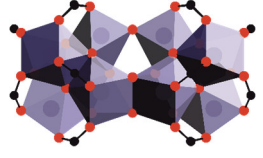
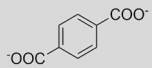
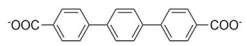
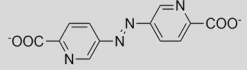
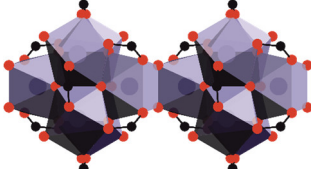
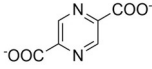
2.2 Zirconium-based metal-organic frameworks

In this chapter zirconium-based metal-organic frameworks, their structural characteristics and their appropriate properties for several applications are further described. The advantage of Zr-based MOFs compared to many other MOFs lies in the high chemical and thermal stability based on the high oxidation state of Zr(IV) ions with high charge density and bond polarization, which results in a strong affinity between Zr(IV) ions and carboxylate ligands. Combined with the high degree of interconnection between the IBUs and linker molecules by the strong zirconium-oxygen bonds, most Zr-based MOFs are stable in water, under acidic conditions and in many organic solvents. The comparatively low stability in basic aqueous media is based on stronger bond formation between hydroxide and Zr(IV) ions compared to carboxylates resulting in a decomposition of the framework.^[194–196]

IBUs based on Zr_6O_8 cores

So far, most of Zr-based MOFs are based on the already mentioned $Zr_6O_4(OH)_4$ cluster, firstly described in UiO-66,^[36] with different connectivities ranging from 12-fold down to 6-fold; but in the last years also other Zr-oxo clusters could be observed in MOFs which are derived from the Zr_6 core. An overview of the IBUs of several observed Zr-based MOFs is given in Table 2, with a selection of typical linker molecules and their resulting frameworks.

Table 2. Overview of Zr-based MOFs based on the $Zr_6O_4(OH)_4$ cluster and its variants with selected examples of corresponding linker molecules.

IBU	Connectivity	Linker	MOF	Ref.
 $Zr_6O_4(OH)_4$	12-fold		Zr-squarate-MOF	[197]
			Zr-fumarate-MOF	[38]
			UiO-66	[36]
	10-fold	e.g. 	PIZOFs	[45,46]
			DUT-69	[189]
	8-fold		DUT-53	[198]
			DUT-67	[189]
		Zr-bzpd-MOF	[193]	
6-fold		DUT-84	[198]	
 $\{[Zr_6O_4(OH)_4]_2 (CH_3COO)_4\}$	6-fold	 H_3tpp	$[Zr_{12}O_8(OH)_8 (CH_3COO)_{18}(tpp)] \cdot 4CH_3COOH \cdot nsolvent$	[199]
 $Zr_{12}O_8(OH)_{14}$	18-fold		hcp UiO-66	[200]
	18-fold	 H_2tpdc	Zr ₁₂ -tpdc	[201]
	12-fold		CAU-39	[202]
 $\{Zr_6O_4(OH)_4(\mu-OH)_2\}$ chain	6-fold		CAU-22	[203]

In case of the most investigated Zr-based IBU $Zr_6O_4(OH)_4$ (Table 2), the six Zr(IV) centers are octahedrally arranged and capped by four μ_3 -O and four μ_3 -OH groups resulting in a square-antiprismatic coordination of the Zr(IV) centers by oxygen

atoms. In UiO-66, this IBU is connected 12-fold by terephthalate molecules resulting in a **fcu**-topology. The same IBU is observed in many other Zr-based MOFs isorecticular to UiO-66, like *Zr-fumarate*-MOF, UiO-67, UiO-68, DUT-52 (DUT: *Dresden University of Technology*),^[198] *Zr-squarate*-MOF,^[197] or PIZOFs (with twofold interpenetration of two identical isorecticular frameworks),^[45,46] as well as in frameworks with different topologies and connectivities. With various multitopic linker molecules and points of extension of six to twelve, the Zr_6 node can build up in completely different structures and topologies. One approach, that facilitates Zr-MOFs with decreased coordination numbers is the modulated synthesis where monocarboxylic acids are added to the synthesis mixture which compete for the coordination sites at the IBU. The group of Kaskel published several Zr-based metal-organic frameworks (designated as DUT-*n*) where the $Zr_6O_4(OH)_4$ IBU does not exert its highest possible number of connections but instead partly carries deprotonated monocarboxylate ligands of the modulating agent.^[198] In one case, naphthalenedicarboxylate was used as linker molecule and the synthesis was modulated with acetic acid causing different connectivities of the IBUs achieved only by adjusting the amount of the modulator:^[198] DUT 52 with the maximum 12-fold connection, DUT-53 (8-fold connected) and DUT-84 (6-fold connected). Other examples of MOFs with the hexanuclear IBU and decreased connection numbers are DUT-69^[189] with ten-fold connected IBUs as well as DUT-67,^[189] NU-1000,^[68] PCN-222^[204] and *Zr-bzpd*-MOF,^[193] all with eight-fold connected IBUs; MOF-808^[188] and *Zr-calixarene*-MOF^[33] can serve as further examples with a six-fold connected IBU.

One example of the topological diversity of Zr-based MOFs is the synthesis of three different MOFs, namely NU-903, NU-904 and NU-1008, with linkers based on the tetratopic molecule 1,2,4,5-tetrakis(4-carboxyphenyl)benzene; all these MOFs feature 8-fold connected $Zr_6O_4(OH)_4$ IBUs. With two different derivatives of the linker molecule (bearing additional functional groups on the central phenylene ring), three different MOFs with varying topologies are obtained.^[47]

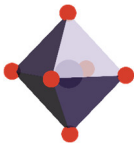
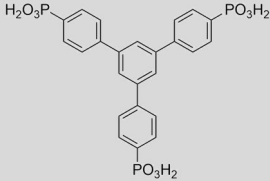
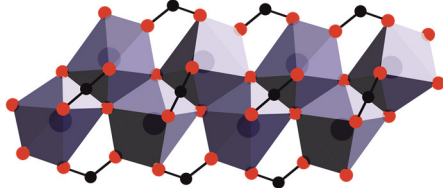
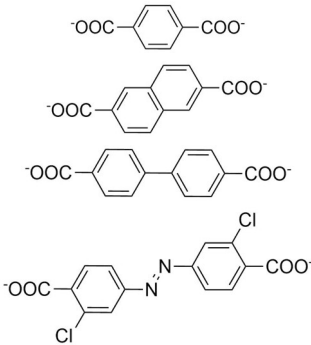
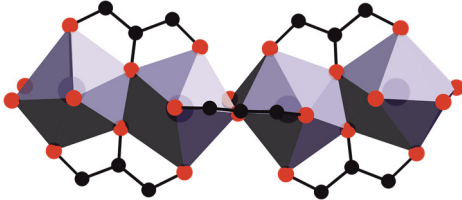
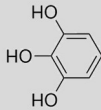
Derived from the Zr_6O_4 core, other Zr-oxo clusters in MOFs were described in recent years by the groups of Stock^[202,203] and Dietzel.^[199] In 2016, a novel one-dimensional Zr-based IBU, consisting of μ -OH bridged $Zr_6O_4(OH)_4$ clusters, was observed in a MOF obtained from a water-based synthesis. Every unit is coordinated by six 2,5-pyrazinedicarboxylates resulting in the three-dimensional framework CAU-22. Residual coordination sites are capped by two formate molecules (formic acid was used as modulator) and H_2O/OH^- .^[203] In 2017, the first Zr-based dodecanuclear cluster $Zr_{12}O_8(OH)_{14}$ was reported in the MOF *Zr₁₂-tpdc* based on triphenyldicarboxylate (*tpdc*²⁻) as linker.^[201] It is the first Zr-based IBU where two Zr_6 cores are bridged by six hydroxide groups. In 2018, CAU-39 with the same dodecanuclear IBU was reported, based on the linker 4,4'-azopyridine-dicarboxylate. The IBU of CAU-39 is

coordinated by twelve linker molecules resulting in a two-dimensional structure.^[202] A similar dodecanuclear core was published in a metal-organic framework, based on a dimeric $(Zr_6)_2$ core bridged by four acetate molecules resulting in the formula $\{[Zr_6O_4(OH)_4]_2(CH_3COO)_4\}$. For the synthesis of a metal-organic framework the cluster $\{[Zr_6O_4(OH)_4]_2(CH_3COO)_{24}\}$ was used in combination with the tritopic linker tris(4-carboxyphenyl) phosphine (H_3tpp), and it was possible to exchange several acetate molecules with the linker molecule resulting in a two-dimensional framework with the formula $[Zr_{12}O_8(OH)_8(CH_3COO)_{18}(tpp)_2] \cdot 4 CH_3COOH \cdot n$ solvent.^[199] Such Zr-based clusters, bridged by carboxylates, have been investigated and described before as molecular compounds with several monocarboxylates like acetates, propionates or methacrylates.^[205]

Various other Zr-based IBUs

In recent years, MOFs with other Zr-oxo clusters, besides those based on the Zr_6 core, have been obtained. The different IBUs are shown in Table 3 with examples of some corresponding MOFs.

Table 3. Overview of Zr-based MOFs based on other clusters than the $Zr_6O_4(OH)_4$ with selected examples of corresponding linker molecules.

IBU	Linker	MOF	Ref.
 <p>Zr₆ core</p>		Zr- <i>btbp</i> -MOF	[206]
 <p>1D ZrO₇ core</p>		MIL-140(A-D)	[207]
 <p>1D ZrO₈ core</p>		MIL-153	[208]

The simplest Zr-based IBU is an octahedral ZrO_6 core. This IBU was observed in Zr-phosphonate MOFs with various phosphonate linker molecules like 1,3,5-tris(4-phosphonophenyl)benzene resulting in a honeycomblike layered structure with large pores but no permanent porosity. The structure consist of a central ZrO_6 core connected with two equivalent terminal ZrO_6 cores via twelve bidentate and monodentate PO_3C tetrahedra.^[206] With the linker molecule 2,4,6-tris(4-(phosphonomethyl)phenyl)-1,3,5-triazine, the microcrystalline MOF UPG-1 (UPG: *University of Perugia*) was synthesized, containing a one-dimensional chain of ZrO_6 polyhedra coordinated by six PO_3C groups, one bidentate and four monodentate.^[209] A MOF called PCN-221 with the formula $Zr_8(\mu_4-O)_6(OH)_8(\text{tetrakis}(4\text{-carboxyphenyl)porphyrin})_3$ has been reported by the group of Zhou. Its structure was assumed to contain a novel Zr_8O_6 cluster. In other MOFs, this IBU could not be observed so far. The structure refinement resulted in rather high R_1/wR_2 values (0.192/0.436); it could not be reproduced in our group and the existence of this IBU appears doubtful.^[210]

Besides of the Zr_6O_4 core, a popular example of Zr-based IBUs is the one-dimensional $Zr(\mu_3-O)_3O_4$ chain, observed in the MIL-140 (MIL: *Materials Institut Lavoisiers*) MOF series, firstly reported 2012. In the 1D chains, the Zr ions are coordinated by three μ_3 -oxo groups and four carboxylate oxygen atoms from the linker molecules. Each one-dimensional chain is interlinked with six other chains via dicarboxylate linker molecules. The MIL-140 MOF series starts with the corresponding terephthalate MOF (MIL-140A) and proceeds via 2,6-naphthalenedicarboxylate (MIL-140B) and 4,4'-biphenyldicarboxylate (MIL-140C) up to 3,3'-dichloro-4,4'-azobenzene-dicarboxylate (MIL-140D).^[207]

Zr-based MOFs with IBUs based on ZrO_8 coordination geometry showing one-dimensional structures and were reported by Devic and co-workers. The first example, MIL-153, is based on pyrogallate as linker molecule which is coordinating two Zr atoms resulting in edge-sharing ZrO_8 polyhedra. In case of MIL-154, based on gallate and salicylate linker molecules, zirconium is coordination by three gallate ligands via five oxygen atoms, two carboxylates of salicylate and one solvent molecule.^[208] Another example for this one-dimensional IBU composed of ZrO_8 cores is MIL-163 containing a bis-1,2,3-trioxobenzene ligand.^[211]

Two-dimensional Zr-based MOFs

The first Zr-based MOF with a two-dimensional structure was DUT-84, obtained using linear 2,6-naphthalenedicarboxylate as linker molecule and high amounts of acetic acid as modulator (compared to DUT-53 and DUT-54 which were produced with lower modulator concentration and exhibit three-dimensional structures), features a double-layer structure where the Zr_6O_8 cores are coordinated by six linker molecules.^[198] Another 2D Zr-based MOF was reported by Matzger and co-workers. UMCM-309a

was obtained with 1,3,5-tris(4-carboxyphenyl)benzene as linker molecule and HCl as modulating agent. It consists of $Zr_6O_4(OH)_4$ IBUs coordinated by six linker molecules resulting in a 2D-layered framework.^[212] D'Alessandro and co-workers firstly reported a two-dimensional Zr-based MOF based on monocarboxylates as linker molecules. The edges of the $Zr_6O_4(OH)_4$ IBU are capped by eight formate molecules and the resulting clusters are bridged via the residual open sites by eight formate molecules resulting in 2D layers, which are further stacked to a 3D structure.

Zr-*bzpd*c-MOF:

Inspired by the high chemical and thermal stability of UiO-type MOFs and other Zr-based MOFs, we constructed a two-dimensional Zr-based MOF with separated photoreactive benzophenone moieties in a rigid and stable framework which provides a good accessibility of guest molecules to the reactive keto groups. Photochemical PSM reactions therefore allow a good adjustment of its properties.^[193] The structure consists of $Zr_6O_4(OH)_4$ IBUs coordinated by eight benzophenone-4,4'-dicarboxylate (*bzpd*c²⁻) molecules as bridging ligands and is partially saturated by two formate molecules, formic acid was used as modulating agent. A structure model of the resulting framework is shown in Figure 7.

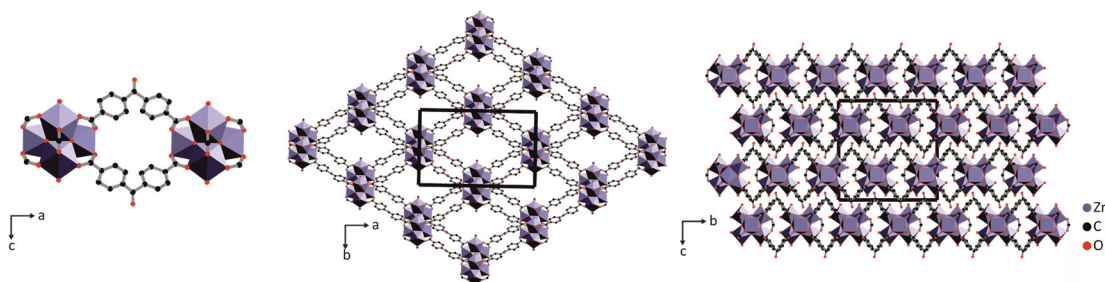


Figure 7. Model for the crystal structure of the Zr-*bzpd*c-MOF. Two $Zr_6O_4(OH)_4$ IBUs are bridged by two linker molecules (left); this leads to a structure with rhombic shaped pore entrances to the one-dimensional pores (pore diameter of about 6.5 Å), as seen along the c-axis (middle); the view along the a axis shows the AB stacking of the layers (right).

The amenability to generate delaminated nanosheets of Zr-*bzpd*c-MOF has been described by us.^[193] The photochemical reactivity of the benzophenone groups has been studied in great detail. It opens the road for a variety of modifications with which this MOF can be adapted to the envisaged application. Further details regarding the synthesis, properties and postsynthetic treatments are described in the main part of this thesis in sections 3.1 – 3.3 and in the corresponding Supporting Information (see sections 5.1 – 5.3).

In recent years, two-dimensional MOF nanosheets as they can also be obtained from the Zr-*bzpd*c-MOF, are in focus of many research groups with regard to their properties like large surface areas combined with small particle thickness, which make them appropriate candidates for several applications (e.g. sensing, catalysis, sensors, electronics or

biomedicine). Strategies to generate nanosheets are based on two main approaches – the bottom-up (interfacial synthesis, three-layer synthesis, surfactant-assisted synthesis, modulated synthesis, and sonication synthesis) and top-down methods (sonication, mechanical exfoliation, as well as intercalation and chemical exfoliation).^[213]

2.3 Postsynthetic modification

The hybrid nature of metal-organic frameworks offers special opportunities for the further adaptation of their properties to intended applications, much more so than with other solid materials. Especially the organic part opens a wide range of strategies for tailoring the properties in ways not feasible for purely inorganic materials. In principle, the whole arsenal of organic reactions can be applied to the linkers of the framework once it has formed, i.e. post-synthetically, provided the backbone is stable under the reaction conditions.

Each year, many novel MOFs are described and MOF structures are discovered. However, the preparation of highly functionalized MOFs with labile or sophisticated organic linker molecules, which may, for example, not be thermally or chemically stable enough to withstand the MOF synthesis conditions or are not soluble in the required solvent for MOF syntheses; also, such linkers may contain functional groups that are liable to coordinate to metal ions and could thus interfere with the MOF formation process. Such restrictions can be overcome by postsynthetic modification (PSM) reactions, for which different strategies are described further in the following section. PSM reactions have become an important and active field of study and represent promising tools for the preparation and derivatization of metal-organic frameworks; in this way, they add a diverse range of functionalities to MOFs to enhance their physical and chemical properties.^[149,214]

2.3.1 General strategies

Different approaches have been elaborated to generate highly functionalized MOFs. The most obvious approach is of course a presynthetic treatment by modifying organic linker molecules with required functionalities and to prepare the metal-organic framework afterwards. This presynthetic modification is often not appropriate due to limited stability of functional groups or insufficient solubility of highly functionalized organic molecules, or due to reactions with solvents under the synthetic conditions for MOFs. Nevertheless, this presynthetic modification could lead to functionalized MOFs by incorporating simple functionalities like $-\text{Br}$, $-\text{NH}_2$,

-CH₃ and other functionalities in many MOFs like IRMOFs or MIL-53(Fe) series.^[42,215,216]

Various strategies have been described to modify MOFs in a postsynthetic manner in order to overcome these restrictions imposed upon the direct synthesis and to reliably alter chemical and physical properties. Also, the modification of a framework which has already been prepared and characterized may be a more clever approach as compared to an odyssey of experiments in search for the synthetic access to a material containing an elaborate linker. Postsynthetic modification reactions can affect both, the metal ions and the organic components, of MOFs, by maintaining the stability and topology of the framework and introducing highly labile and sophisticated functionalities to the framework.

The modification strategies concerning the linker molecules in a postsynthetic manner are postsynthetic reactions at reactive moieties at the linker molecules as well as linker exchange, linker insertion or deprotection of functionalities. A more recent strategy, the postsynthetic polymerization at MOF moieties, opens further methods to equip metal-organic frameworks with valuable functionalities (Figure 8).

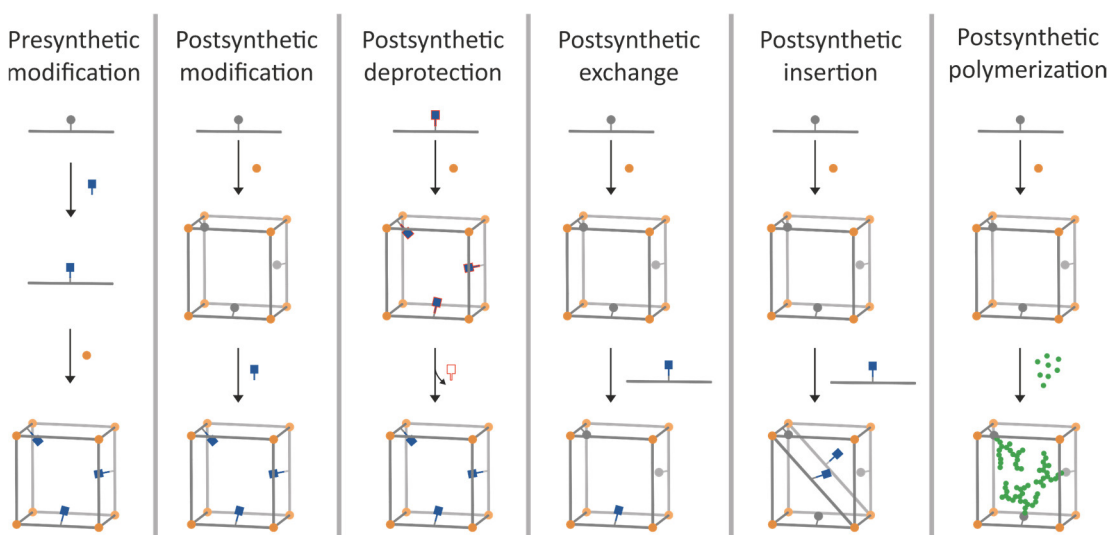


Figure 8. Schematic description of different postsynthetic strategies, compared to a presynthetic modification, to introduce environmental changes in the framework. IBUs are simplified as orange spheres, ligand struds as grey rods and novel functionalities as blue squares or green strands (adapted from ref. 141).^[149]

The concept of postsynthetic modification was first predicted in 1990 by Robson and co-workers^[1] with following formulation:

“Relatively unimpeded migration of species throughout the lattice may allow chemical functionalization of the rods subsequent to the construction of the framework.”^[1]

It took nearly 10 years to convert the concept to experimental studies, which were made by Kim and co-workers in 1999,^[217] where they have shown alkylation

reactions in MOFs. First descriptions of postsynthetic modifications in a manner with focus on the chemical alteration of MOFs were shown by Wang and Cohen in 2007 with the reaction of IRMOF-3 with acetic anhydride. IRMOF-3 consist of a derivative of the terephthalate, the 2-aminoterephthalate as linker molecule which enables the reaction with acetic anhydride and anhydrides with longer alkyl chains resulting in a progressing decrease in porosity with increasing chain length.^[218] An overview of possible postsynthetic modifications and deprotections at a single MOF was reported in 2016 by Yaghi and co-workers at an isorecticular derivative of the well-known MOF-74 with *tert*-butyloxycarbonyl-protected (*Boc* group) amines performing seven separate postsynthetic reactions like deprotection of *Boc*-protected amines and peptide couplings without affecting the crystallinity of the framework.^[219] In recent years many research groups, like Hupp,^[220] Long,^[221] Yaghi^[222] and Cohen^[223,224] focused on postsynthetic modification reactions to add diverse functionalities to the framework ending up in highly functionalized materials.^[149,214] Also, many studies of postsynthetic exchange or insertion of linker molecules are described in literature adding a wide range of functionalities to MOFs.

Postsynthetic exchange and insertion

Postsynthetic exchange (Figure 8) is one of the most explored field of postsynthetic reactions based on the kinetics of metal-linker bonds.^[225] Under certain conditions the completely formed MOF undergoes either an exchange of metal ions at the IBUs or at additional binding sites at the linker, an early example reported by Kim and co-workers^[226] and mechanistic studies reported by Dincă and co-workers.^[227,228] The exchange of linker molecules, also known as the already mentioned solvent-assisted linker exchange (SALE),^[81] was reported by Choe and co-workers in 2011.^[229] Farha and co-workers reported a combination of metal- and linker-exchange reactions in the same MOF, that shows the high potential of this method to introduce novel functionalities to already formed MOFs.^[230] Compared to the linker exchange, the insertion of novel linker molecules to the framework by coordinating to vacant sites at the IBUs is known as the so-called solvent-assisted linker insertion (SALI).^[83] Due to this opportunity, it is possible to build-up three-dimensional frameworks out of two-dimensional ones.^[231,232]

Postsynthetic polymerization

A recent method to transform MOFs into MOF-polymer composites or polymer materials is based on postsynthetic polymerization. The MOF can be used as template to crosslink a MOF lattice resulting in a polymer monolith based on click chemistry of azide groups at the linker molecules and alkynes resulting in a highly crosslinked MOF lattice, as reported by Sada and co-workers.^[233] A study by Queen and co-workers showed the possibility to enhance the stability of diverse MOFs (HKUST-1,

UiO-66, Mg-MOF-74, MIL-100) in aqueous media under acidic and basic conditions by modifying the MOFs with dopamine followed by a Michael addition with hydrophobic molecules.^[234] The first report regarding postsynthetic polymerization of metal-organic polyhedras (MOPs) was shown by Choe and co-workers in 2017 by crosslinking MOPs via condensation reactions with flexible organic molecules resulting in a series of crystalline and porous cross-linked MOPs.^[235]

Another promising approach to generate highly functionalized MOFs with polymers by polymerization techniques is to start from active sites on the MOF. One of the first examples of those so-called grafting-from reactions at MOFs was shown by Matzger and co-workers in 2015,^[120] where they encapsulated a MOF crystal (core-shell system IRMOF-3@MOF-5) within a polymer by atom transfer radical polymerization (ATRP) within a poly(methyl methacrylate) (PMMA) polymer coating. In a comparable manner, Wang and co-workers presented the modification of UiO-66-NH₂ crystals with methacrylic anhydride and a subsequent photopolymerization of the terminal olefin groups of the MOF with butyl methacrylate and a photoinitiator resulting in a polymer film to produce a flexible membrane.^[122] Cohen and co-workers generated a nylon-MOF composite by covalently incorporating UiO-66-NH₂ into the growing polymer nylon-6,6, resulting in a material appropriate for the breakdown of a chemical warfare simulant.^[125] Postsynthetic polymerizations and especially grafting-from approaches are combining the crystalline and amorphous materials with covalent bonds and may find the way into applicable materials with unique properties.

2.3.2 PSM of Zr-based MOF

Zr-based MOFs gained attention due to their high chemical and thermal stability^[194–196] and therefore the opportunity of different postsynthetic modification reactions to introduce various functional moieties. These properties make Zr-based MOFs appropriate candidates for applications like gas or liquid storage and separation, catalysis, sensing or biomedical applications. In particular, plenty of studies are described for postsynthetic modification of Zr-based MOFs with various emphases. The majority of postsynthetic modifications at Zr-based MOFs are based so far on functional groups at the linker molecules like amino-groups in UiO-66-NH₂ and e.g. catalyst-free aza-Michael addition reactions.^[80,236] One of the most investigated strategies of PSM reactions in general, the linker exchange, were also examined for Zr-based MOFs, firstly described by Cohen and co-workers. They demonstrated the exchange of linker molecules in UiO-66^[237] and in further studies the incorporation of a molecular proton reduction catalyst by linker exchange into UiO-66^[238] or a urethane formation in UiO-68 with 2-hydroxymethyl groups at the linker molecules,^[239] just to mention some approaches of linker exchange reactions

at Zr-based MOFs.^[240] So far, ligand exchange was focused on the exchange of the linker molecules of the MOF but can also be performed on vacant sites of defective MOFs. It is possible to exchange monocarboxylates with other monocarboxylates,^[241] phosphonates,^[83] phosphinates^[242] or sulfates^[243] or the compensation of missing metal clusters.^[244] Beside the classical PSM approaches that affect the whole framework several studies focused on the surface functionalization. One approach deals with a PEGylation of Zr-*fumarate*-MOF as drug delivery system with a biocompatible shell of polyethylene glycol, loaded with dichloroacetate, which is a promising material for selective cancer cytotoxicity.^[245,246]

2.3.3 Photoreactivity in MOFs

In recent years, many examples of MOFs, which are responsive to irradiation, are described.^[247] Some studies focused on different energy transfer pathways in MOFs like ligand-to-ligand (fulleretic MOFs containing fullerene-^[248] or corannulene^[249] -based linkers), metal-to-metal (4,4'-bipyridine-based MOF doped with Eu³⁺ and Tb³⁺),^[250] ligand-to-metal (Eu- or Tb-based MOFs)^[251] and guest-to-MOF transfers (incorporation of α,ω -dihexylsexithiophene (DH6T) and [6,6]phenyl-C₆₁-butyric acid methyl ester (PCBM) into MOF-177).^[252] Other fields of research deal with photocatalytically active MOFs like several Ti-based MOFs (e.g. MIL-125 for alcohol oxidation)^[253,254] or Fe-based MOFs (MIL-100 and MIL-68 as photocatalysts for selective benzene hydroxylation),^[255] metalloligands in Ru- and Ir-MOFs^[256] or metallated porphyrins in In- and Sn-MOFs.^[257,258] In 2016, Cohen and co-workers reported a postsynthetic modification strategy based on photocatalysis of 2,2,2-trifluoro-ethylation of styrenes by Ir(III) polypyridyl complexes into UiO-67.^[259] A broad field of application for photocatalytically active MOFs is the purification of water.^[260]

Another approach to generate photoresponsive MOFs is to incorporate photochromic compounds into the MOF, as a guest molecule, as backbone of the MOF or as a side group of the linker molecule. Many approaches are based on spiropyran-, diarylethene- and azobenzene-based compounds. These compounds are able to switch between two states and, in consequence, affecting the properties of the MOF by, e.g. selectively control of the adsorption behavior,^[261] the controlled release of molecules^[262-264] or a photo-induced degradation of the framework combined with a drug release.^[265] Beside photocatalytical reactions and photo-switchable molecules, a recent topic is the use of photoreactive groups at the linker molecule of MOFs. One example is a reversible solid-state 2+2 cycloaddition of well-aligned linker molecules, 1,4-bis[2-(4'-pyridyl)ethenyl]benzene, in a double-pillared MOF.^[266,267]

Another strategy to equip MOFs with further functionalities based on photochemical processes is the already mentioned grafting-from method, the direct polymerization of polymer chains initiated at the MOF surface. A first example of photoinduced postsynthetic polymerization reactions at MOFs was described by Wang and co-workers by using nanosized UiO-66-NH₂, functionalized with polymerizable methacrylic anhydride and a subsequent polymerization with butyl methacrylate^[122] or a study by Dong and co-workers also based on UiO-66-NH₂ and polymerizations of methyl methacrylate (MMA), styrene or 2-isopropenyl-2-oxazoline at the MOF surface.^[268]

Another concept, which can be adapted to MOFs, is based on C-H bond transformation reactions and hydrogen abstractions by aryl ketones. Common molecules to undergo those reactions are shown in Figure 9.^[269]

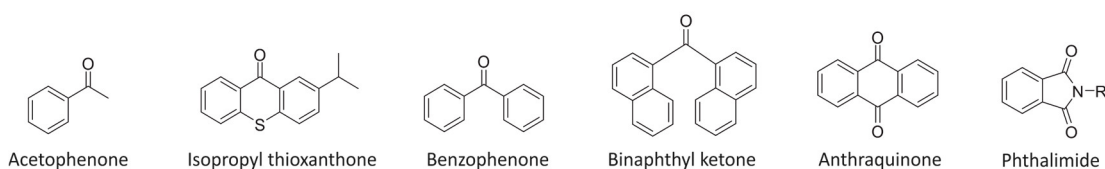


Figure 9. Several aryl ketones used for C-H bond transformation reactions.

The Al-based MOF CAU-8,^[8] based on benzophenone-4,4'-dicarboxylate as linker molecule, showed promising results in photochemical reactivity and indicated a possible postsynthetic modification of the framework performed on the keto groups of the linker molecule.^[10] Based on the crystal structure, these reactions can occur within the pore system. A PSM in a similar way should be possible in case of CAU-21,^[9] another three-dimensional Al-based MOF with the same linker molecule but with a different crystal structure compared to CAU-8, but also with the keto groups pointing in the pore system.

The 2D Zr-*bzpd*c-MOF, discussed in this work, opens, with the photoreactive benzophenone moieties, the possibility of postsynthetic modification reactions and adaption of properties. First studies have shown promising results by adjusting properties like dispersibility in nonpolar solvents^[193] or the generation of a conductive material by polymerizing a conductive polymer^[187] from the surface of the MOF through photochemical reactions on the linker molecules by maintaining the porosity. These are two promising approaches to adapt the properties for further applications.

2.4 Benzophenone

Photochemical excitation to generate radicals is based on the absorption of photons. The excitation of a molecule and a thereto relating promotion of an electron is possible when the difference in energy between the excited state and ground state corresponds to the energy of the photon. In general, photochemistry are chemical effects and reactions due to the absorption of photons from UV-, visible or IR-radiation. There are several effects of photons on matter, in this context, the work concentrates on the photochemical generation of radicals.

Photochemically based reactions provide several advantages compared to thermally activated processes. Variations of intensity, location and duration of the irradiation can control the reactions. One of the most prominent examples for photochemically reactive substances is benzophenone, which has been widely used in photopolymerization reactions and photoinduced hydrogen atom transfer, prerequisite for free-radical related processes like radical polymerization or radical coupling-based molecular conjugation.^[270]

2.4.1 Photochemistry of benzophenone

The photochemical properties of benzophenone are well known for several decades through many studies.^[271-277] By inducing photons to benzophenone and its derivatives, the keto group promotes to a singlet diradicaloid leading to a formation of a triplet biradical and by hydrogen abstraction in presence of a molecule containing C-H bonds the formation of a ketyl radical. Hydrogen abstraction by triplet carbonyl compounds has been extensively studied for bimolecular and intramolecular mechanisms. The reaction mechanisms in case of benzophenone are shown in Figure 10.

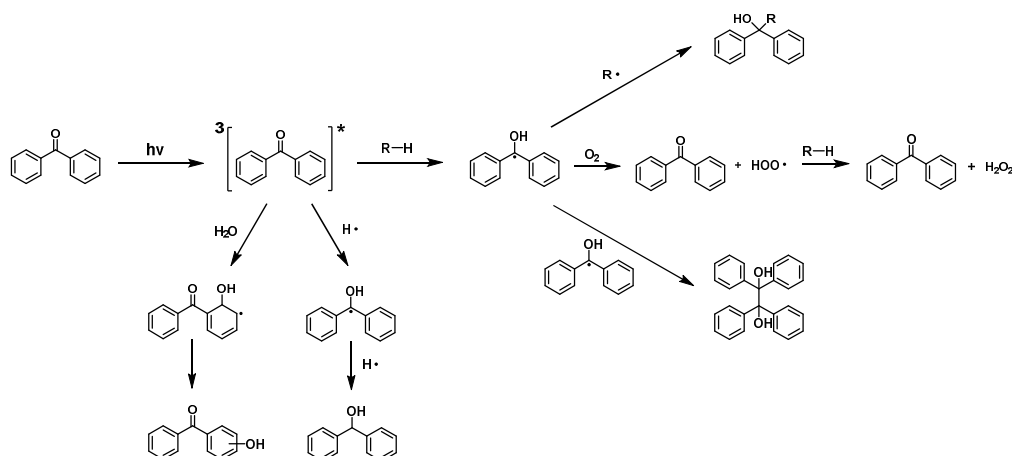


Figure 10. Photoexcitation of benzophenone and subsequently reactions with C-H bond containing molecules, water, oxygen and recombination to benzpinacol.

The hydrogen abstraction leads to a stabilized ketyl radical through completing the half-filled orbital of the ketyl oxygen. The resulting ketyl radical can react with other radical species like hydrogen atom donors or dimerize with a second ketyl radical resulting in a benzpinacol. The reaction with oxygen could lead to the formation of hyperoxide radicals and hydrogen peroxide reclaiming benzophenone, which shows that the reactivity in presence of oxygen is given.^[271] In presence of water the photoexcited benzophenone, so far formulated for the ketyl radical cation, can react with OH⁻ ions resulting in a hydroxylation and an OH adduct formation at the benzene rings.^[274,275]

Molecules containing carbonyl groups like formaldehyde or acetone show $\pi-\pi^*$ absorption at about 180 nm wavelength (absorption maxima of $\pi-\pi^*$ transition predictable for α,β -unsaturated carbonyl compounds with Woodward's rules)^[278] and a weaker $n-\pi^*$ absorption at 300 nm. The absorption is increased and shifts to higher wavelengths by conjugation with π -electrons from double bonds or benzene rings, e.g. in case of aryl ketones like benzophenone.^[279,280]

Absorption of UV irradiation ($\lambda \approx 365$ nm) to benzophenone leads to an electronic transition from the nonbonding n -orbital of oxygen to the antibonding π^* -orbital of the carbonyl group which is separated from the $\pi-\pi^*$ transition. The resulting triplet state, starting from the singlet state, is responsible for hydrogen abstraction from C-H bonds. The corresponding Jablonski diagram is shown in Figure 11.

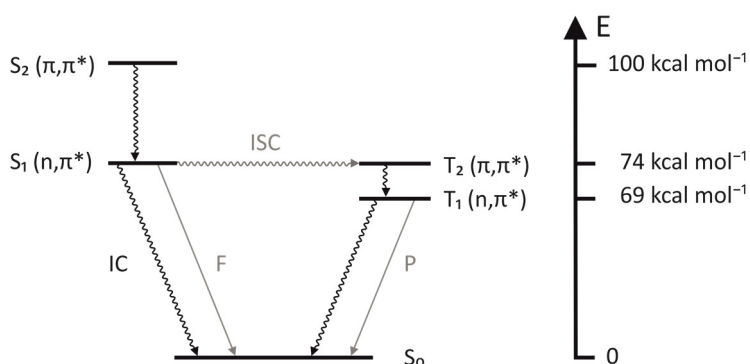


Figure 11. Jablonski diagram of benzophenone^[281] with electronic states (S_1 , S_2 , T_1 , T_2) and transitions with internal conversion (IC), intersystem crossing (ISC), fluorescence (F) and phosphorescence (P).

The irradiation of benzophenone with wavelengths of about 365 nm causes an excitement of ground state (S_0) to a singlet state (S_1) that undergoes intersystem crossing (ISC) to the triplet state T_2 , in accordance to El Sayed's rule,^[282] in a much higher rate than fluorescence (F).^[281] The triplet lifetime of benzophenone is about 7.7×10^{-3} s.^[283] Under continuous irradiation, the formation of biradicaloid molecules in triplet state $n-\pi^*$ (T_1) occurs. The biradical is able to abstract a hydrogen atom from C-H bond containing molecules like aliphatic compounds resulting in the formation of the ketyl radical (see Figure 10). In case of benzophenone, the solvent

polarity has no influence on the rate constant for hydrogen abstraction. It is also possible to induce the transition from the bonding π -orbital to the antibonding π^* -orbital of the carbonyl group with a wavelength of about 250 nm (S_2). The weaker $n-\pi^*$ absorption is based on the poor overlap of the p-orbital with the π^* orbital.^[284] The possible triplet states are shown in Figure 12.

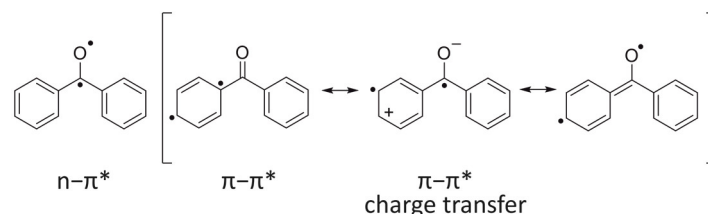


Figure 12. Triplet states for benzophenone with the most reactive $n-\pi^*$ state and the $\pi-\pi^*$ states with the charge transfer state, which is poorly reactive.^[285]

The photochemical reactivity of benzophenone is depending on substituents and the solvent. The $\pi-\pi^*$ triplet state with a higher energy level (Figure 11, T_2) can be inverted in energy by substituents with electron donating functionalities like amino-^[286] or hydroxy-groups^[285] resulting in the more preferable lower energy state. That would lead to a stabilization of the charge transfer state shown in Figure 12 and a less electrophilic and reactive compound. In case of ortho-substituted benzophenone derivatives, the reactivity is lowered by intramolecular hydrogen abstraction.^[287,288]

The solvent plays a significant role for the photochemical reactivity of benzophenone derivatives, like in case of *p*-aminobenzophenone^[288] with different reactivities in 2-propanol and cyclohexane. The polarity of 2-propanol causes an inversion in energy of the $\pi-\pi^*$ triplet state preventing reactions of *p*-aminobenzophenone. In cyclohexane the $n-\pi^*$ triplet state is more favored, resulting in a reactive *p*-aminobenzophenone.^[288]

2.4.2 Photoinduced reactions of benzophenone

In general, benzophenone shows high photochemical reactivity and is extensively used for different photoinduced reactions. The properties of benzophenone open different photoinduced reactions to generate covalent bonds.

In the field of biochemistry, benzophenone could be used to label photoaffinity probes with the advantage that the low excitation energy for benzophenone ($\lambda \approx 365$ nm) does not damage sensitive molecules like proteins.^[289] In polymer systems, benzophenone can act both as photo-initiator and for photo-grafting reactions. Based on the biradicaloid character of the $n-\pi^*$ triplet state,

photopolymerization of vinyl monomers or acrylates (with a co-initiator) are accessible.^[269]

Prucker and co-workers introduced a covalent modification of surfaces with polymer thin layers and monolayers by functionalizing them with benzophenone groups acting as anchor groups for several polymers.^[273,290] It is also possible that the radical formation in polymers, initiated by benzophenone, could lead to chain-scission and a resulting photodegradation.^[269] Polymers containing benzophenone moieties are also appropriate candidates to generate surface attached films, hydrogels and biomedical coatings,^[291] or micro-devices^[292] and also as photo-initiator to induce cross-linking of polymers.^[293]

The photochemical properties of the keto group of benzophenone derivatives are making the benzophenone moiety to an appropriate system for the usage as a linker molecule in metal-organic frameworks, to postsynthetically modify the MOF and adjust properties for specific applications. The wide range of postsynthetically applicable molecules and strategies shows the high potential of this construction. The first Al-based MOF CAU-8 based on benzophenone-4,4'-dicarboxylate as linker, showed promising results concerning postsynthetic modifications of the MOF based on the benzophenone moieties of the linker, but, based on the three dimensional crystal structure and the keto groups pointing into the pore system, these reactions always occur within the pore system and also could lead to a loss of porosity.^[10] The wide range of postsynthetically applicable molecules to covalently bind to the benzophenone group and strategies shows the high potential of this construction. The novel Zr-*bzpd*c-MOF with the two-dimensional structure opens the generation of thin sheets with thicknesses in nm-range. In case of Zr-*bzpd*c-MOF, the keto groups pointing out at the largest surface of the rhombic shaped crystals should be directly accessible, which opens a wide range of different postsynthetic modifications of the surface or the whole crystal depending on the molecule. The separate studies concerning synthesis, characterization, delamination and several postsynthetic modification reactions are depicted in the next sections.

2.5 References

- 1 B. F. Hoskins, R. Robson, *J. Am. Chem. Soc.* **1990**, *112*, 1546.
- 2 H. Li, M. Eddaoudi, M. O'Keeffe, O. M. Yaghi, *Nature* **1999**, *402*, 276.
- 3 H. Furukawa, J. Kim, N. W. Ockwig, M. O'Keeffe, O. M. Yaghi, *J. Am. Chem. Soc.* **2008**, *130*, 11650.
- 4 H. J. Park, M P. Su, *Chem. Eur. J.* **2008**, *14*, 8812.
- 5 H. J. Park, M P. Su, *Chem. Commun.* **2010**, *46*, 610.
- 6 L. Qin, L. Yu, X.-Z. Yan, W.-N. Zhao, L. Han, *Inorg. Chim. Acta* **2014**, *409*, 233.
- 7 J. D. Einkauf, J. M. Clark, A. Paulive, G. P. Tanner, D. T. de Lill, *Inorg. Chem.* **2017**, *56*, 5544.
- 8 H. Reinsch, M. Krüger, J. Marrot, N. Stock, *Inorg. Chem.* **2013**, *52*, 1854.
- 9 M. Krüger, A. K. Inge, H. Reinsch, Y.-H. Li, M. Wahiduzzaman, C.-H. Lin, S.-L. Wang, G. Maurin, N. Stock, *Inorg. Chem.* **2017**, *56*, 5851.
- 10 H. G. Baldovi, M. Krüger, H. Reinsch, M. Alvaro, N. Stock, H. Garcia, *J. Mater. Chem. C* **2015**, *3*, 3607.
- 11 T. Tsuruoka, S. Furukawa, Y. Takashima, K. Yoshida, S. Isoda, S. Kitagawa, *Angew. Chem. Int. Ed.* **2009**, *48*, 4739.
- 12 A. Schaate, P. Roy, A. Godt, J. Lippke, F. Waltz, M. Wiebcke, P. Behrens, *Chem. Eur. J.* **2011**, *17*, 6643.
- 13 Y. Peng, Y. Li, Y. Ban, W. Yang, *Angew. Chem. Int. Ed.* **2017**, *56*, 9757.
- 14 C. R. P. Fulong, J. Liu, V. J. Pastore, H. Lin, T. R. Cook, *Dalton Trans.* **2018**, *47*, 7905.
- 15 W.-J. Li, J. Liu, Z.-H. Sun, T.-F. Liu, J. Lü, S.-Y. Gao, C. He, R. Cao, J.-H. Luo, *Nat. Commun.* **2016**, *7*, 11830.
- 16 R. Rajak, M. Saraf, S. M. Mobin, *J. Mater. Chem. A* **2019**, *7*, 1725.
- 17 O. M. Yaghi, G. Li, H. Li, *Nature* **1995**, *378*, 703.
- 18 M. Kondo, T. Yoshitomi, H. Matsuzaka, S. Kitagawa, K. Seki, *Angew. Chem. Int. Ed.* **1997**, *36*, 1725.
- 19 C. Pettinari, F. Marchetti, N. Mosca, G. Tosi, A. Drozdov, *Polym. Int.* **2017**, *66*, 731.
- 20 H. Furukawa, K. E. Cordova, M. O'Keeffe, O. M. Yaghi, *Science* **2013**, *341*, 1230444.
- 21 B. Li, H.-M. Wen, W. Zhou, B. Chen, *J. Phys. Chem. Lett.* **2014**, *5*, 3468.
- 22 M. Schröder, M. Banerjee, *Functional metal-organic frameworks: gas storage, separation and catalysis*, Springer, Berlin **2010**.
- 23 H. Li, K. Wang, Y. Sun, C. T. Lollar, J. Li, H.-C. Zhou, *Mater. Today* **2018**, *21*, 108.
- 24 S. Ma, H.-C. Zhou, *Chem. Commun.* **2010**, *46*, 44.
- 25 A. Dhakshinamoorthy, Z. Li, H. Garcia, *Chem. Soc. Rev.* **2018**, *47*, 8134.
- 26 W. Chen, C. Wu, *Dalton Trans.* **2018**, *47*, 2114.

- 27 P. Horcajada, R. Gref, T. Baati, P. K. Allan, G. Maurin, P. Couvreur, G. Férey, R. E. Morris, C. Serre, *Chem. Rev.* **2012**, *112*, 1232.
- 28 C. Orellana-Tavra, R. J. Marshall, E. F. Baxter, I. A. Lázaro, A. Tao, A. K. Cheetham, R. S. Forgan, D. Fairen-Jimenez, *J. Mater. Chem. B* **2016**, *4*, 7697.
- 29 C. Orellana-Tavra, E. F. Baxter, T. Tian, T. D. Bennett, N. K. H. Slater, A. K. Cheetham, D. Fairen-Jimenez, *Chem. Commun.* **2015**, *51*, 13878.
- 30 P. Kumar, A. Deep, K.-H. Kim, *Trends Anal. Chem.* **2015**, *73*, 39.
- 31 X. Fang, B. Zong, S. Mao, *Nano-micro Lett.* **2018**, *10*, 64.
- 32 L. E. Kreno, K. Leong, O. K. Farha, M. Allendorf, R. P. van Duyne, J. T. Hupp, *Chem. Rev.* **2012**, *112*, 1105.
- 33 M. Schulz, A. Gehl, J. Schlenkrich, H. A. Schulze, S. Zimmermann, A. Schaate, *Angew. Chem. Int. Ed.* **2018**, *57*, 12961.
- 34 *Nat. Chem.* **2016**, *8*, 987.
- 35 S. S. Chui, *Science* **1999**, *283*, 1148.
- 36 J. H. Cavka, S. Jakobsen, U. Olsbye, N. Guillou, C. Lamberti, S. Bordiga, K. P. Lillerud, *J. Am. Chem. Soc.* **2008**, *130*, 13850.
- 37 A. Schoedel, M. Li, D. Li, M. O'Keeffe, O. M. Yaghi, *Chem. Rev.* **2016**, *116*, 12466.
- 38 G. Wißmann, A. Schaate, S. Lilienthal, I. Bremer, A. M. Schneider, P. Behrens, *Microporous Mesoporous Mater.* **2012**, *152*, 64.
- 39 A. F. Wells, *Three-dimensional nets and polyhedra*, Wiley, New York **1977**.
- 40 O. Delgado-Friedrichs, M. O'Keeffe, *J. Solid State Chem.* **2005**, *178*, 2480.
- 41 M. Li, D. Li, M. O'Keeffe, O. M. Yaghi, *Chem. Rev.* **2014**, *114*, 1343.
- 42 M. Eddaoudi, J. Kim, N. Rosi, D. Vodak, J. Wachter, M. O'Keeffe, O. M. Yaghi, *Science* **2002**, *295*, 469.
- 43 H. Furukawa, Y. B. Go, N. Ko, Y. K. Park, F. J. Uribe-Romo, J. Kim, M. O'Keeffe, O. M. Yaghi, *Inorg. Chem.* **2011**, *50*, 9147.
- 44 D. J. Tranchemontagne, J. R. Hunt, O. M. Yaghi, *Tetrahedron* **2008**, *64*, 8553.
- 45 A. Schaate, P. Roy, T. Preusse, S. J. Lohmeier, A. Godt, P. Behrens, *Chem. Eur. J.* **2011**, *17*, 9320.
- 46 J. Lippke, B. Brosent, T. von Zons, E. Virmani, S. Lilienthal, T. Preuße, M. Hülsmann, A. M. Schneider, S. Wuttke, P. Behrens, A. Godt, *Inorg. Chem.* **2017**, *56*, 748.
- 47 J. Lyu, X. Zhang, K.-i. Otake, X. Wang, P. Li, Z. Li, Z. Chen, Y. Zhang, M. C. Wasson, Y. Yang, P. Bai, X. Guo, T. Islamoglu, O. K. Farha, *Chem. Sci.* **2019**, *10*, 1186.
- 48 Z. Zhang, H. T. H. Nguyen, S. A. Miller, S. M. Cohen, *Angew. Chem. Int. Ed.* **2015**, *54*, 6152.
- 49 P. Horcajada, T. Chalati, C. Serre, B. Gillet, C. Sebrie, T. Baati, J. F. Eubank, D. Heurtaux, P. Clayette, C. Kreuz, J.-S. Chang, Y. K. Hwang, V. Marsaud, P.-N. Bories, L. Cynober, S. Gil, G. Férey, P. Couvreur, R. Gref, *Nat. Mater.* **2010**, *9*, 172.

- 50 F. Ke, C. Peng, T. Zhang, M. Zhang, C. Zhou, H. Cai, J. Zhu, X. Wan, *Sci. Rep.* **2018**, *8*, 939.
- 51 S. Karmakar, J. Dechnik, C. Janiak, S. De, *J. Hazard. Mater.* **2016**, *303*, 10.
- 52 K. Barthelet, J. Marrot, D. Riou, G. Férey, *Angew. Chem. Int. Ed.* **2002**, *41*, 281.
- 53 C. Serre, F. Millange, C. Thouvenot, M. Noguès, G. Marsolier, D. Louër, G. Férey, *J. Am. Chem. Soc.* **2002**, *124*, 13519.
- 54 T. Loiseau, C. Serre, C. Huguenard, G. Fink, F. Taulelle, M. Henry, T. Bataille, G. Férey, *Chem. Eur. J.* **2004**, *10*, 1373.
- 55 F. Millange, N. Guillou, R. I. Walton, J.-M. Grenèche, I. Margiolaki, G. Férey, *Chem. Commun.* **2008**, *39*, 4732.
- 56 J. Yang, Q. Zhao, J. Li, J. Dong, *Microporous Mesoporous Mater.* **2010**, *130*, 174.
- 57 M. J. Katz, Z. J. Brown, Y. J. Colón, P. W. Siu, K. A. Scheidt, R. Q. Snurr, J. T. Hupp, O. K. Farha, *Chem. Commun.* **2013**, *49*, 9449.
- 58 N. L. Rosi, J. Kim, M. Eddaoudi, B. Chen, M. O'Keeffe, O. M. Yaghi, *J. Am. Chem. Soc.* **2005**, *127*, 1504.
- 59 M. Díaz-García, Á. Mayoral, I. Díaz, M. Sánchez-Sánchez, *Cryst. Growth Des.* **2014**, *14*, 2479.
- 60 L. J. Wang, H. Deng, H. Furukawa, F. Gándara, K. E. Cordova, D. Peri, O. M. Yaghi, *Inorg. Chem.* **2014**, *53*, 5881.
- 61 P. Horcajada, S. Surblé, C. Serre, D.-Y. Hong, Y.-K. Seo, J.-S. Chang, J.-M. Grenèche, I. Margiolaki, G. Férey, *Chem. Commun.* **2007**, *27*, 2820.
- 62 G. Férey, C. Serre, C. Mellot-Draznieks, F. Millange, S. Surblé, J. Dutour, I. Margiolaki, *Angew. Chem. Int. Ed.* **2004**, *43*, 6296.
- 63 X. Huang, Y. Chen, Z. Lin, X. Ren, Y. Song, Z. Xu, X. Dong, X. Li, C. Hu, B. Wang, *Chem. Commun.* **2014**, *50*, 2624.
- 64 S. Wang, J. S. Lee, M. Wahiduzzaman, J. Park, M. Muschi, C. Martineau-Corcos, A. Tissot, K. H. Cho, J. Marrot, W. Shepard, G. Maurin, J.-S. Chang, C. Serre, *Nat. Energy* **2018**, *3*, 985.
- 65 Q. Lin, T. Wu, S.-T. Zheng, X. Bu, P. Feng, *Chem. Commun.* **2011**, *47*, 11852.
- 66 B. Chen, N. W. Ockwig, A. R. Millward, D. S. Contreras, O. M. Yaghi, *Angew. Chem. Int. Ed.* **2005**, *44*, 4745.
- 67 X. Lin, I. Telepeni, A. J. Blake, A. Dailly, C. M. Brown, J. M. Simmons, M. Zoppi, G. S. Walker, K. M. Thomas, T. J. Mays, P. Hubberstey, N. R. Champness, M. Schröder, *J. Am. Chem. Soc.* **2009**, *131*, 2159.
- 68 J. E. Mondloch, W. Bury, D. Fairen-Jimenez, S. Kwon, E. J. DeMarco, M. H. Weston, A. A. Sarjeant, S. T. Nguyen, P. C. Stair, R. Q. Snurr, O. K. Farha, J. T. Hupp, *J. Am. Chem. Soc.* **2013**, *135*, 10294.
- 69 P. Zhang, B. Li, Y. Zhao, X. Meng, T. Zhang, *Chem. Commun.* **2011**, *47*, 7722.
- 70 J. Park, J.-R. Li, Y.-P. Chen, J. Yu, A. A. Yakovenko, Z. U. Wang, L.-B. Sun, P. B. Balbuena, H.-C. Zhou, *Chem. Commun.* **2012**, *48*, 9995.

- 71 P. T. K. Nguyen, H. T. D. Nguyen, H. N. Nguyen, C. A. Trickett, Q. T. Ton, E. Gutiérrez-Puebla, M. A. Monge, K. E. Cordova, F. Gándara, *ACS Appl. Mater. Interfaces* **2018**, *10*, 733.
- 72 X. Wang, W.-Y. Gao, Z. Niu, L. Wojtas, J. A. Perman, Y.-S. Chen, Z. Li, B. Aguila, S. Ma, *Chem. Commun.* **2018**, *54*, 1170.
- 73 A. K. Cheetham, T. D. Bennett, F.-X. Coudert, A. L. Goodwin, *Dalton Trans.* **2016**, *45*, 4113.
- 74 S. Dissegna, K. Epp, W. R. Heinz, G. Kieslich, R. A. Fischer, *Adv. Mater.* **2018**, *30*, e1704501.
- 75 J. Canivet, M. Vandichel, D. Farrusseng, *Dalton Trans.* **2016**, *45*, 4090.
- 76 U. Ravon, M. Savonnet, S. Aguado, M. E. Domine, E. Janneau, D. Farrusseng, *Microporous Mesoporous Mater.* **2010**, *129*, 319.
- 77 F. Vermoortele, B. Bueken, G. Le Bars, B. van de Voorde, M. Vandichel, K. Houthoofd, A. Vimont, M. Daturi, M. Waroquier, V. van Speybroeck, C. Kirschhock, D. E. de Vos, *J. Am. Chem. Soc.* **2013**, *135*, 11465.
- 78 G. C. Shearer, S. Chavan, S. Bordiga, S. Svelle, U. Olsbye, K. P. Lillerud, *Chem. Mater.* **2016**, *28*, 3749.
- 79 F. Vermoortele, R. Ameloot, L. Alaerts, R. Matthessen, B. Carlier, E. V. R. Fernandez, J. Gascon, F. Kapteijn, D. E. de Vos, *J. Mater. Chem.* **2012**, *22*, 10313.
- 80 R. J. Marshall, R. S. Forgan, *Eur. J. Inorg. Chem.* **2016**, *2016*, 4310.
- 81 O. Karagiari, W. Bury, J. E. Mondloch, J. T. Hupp, O. K. Farha, *Angew. Chem. Int. Ed.* **2014**, *53*, 4530.
- 82 O. Karagiari, M. B. Lalonde, W. Bury, A. A. Sarjeant, O. K. Farha, J. T. Hupp, *J. Am. Chem. Soc.* **2012**, *134*, 18790.
- 83 P. Deria, W. Bury, I. Hod, C.-W. Kung, O. Karagiari, J. T. Hupp, O. K. Farha, *Inorg. Chem.* **2015**, *54*, 2185.
- 84 T. D. Bennett, T. K. Todorova, E. F. Baxter, D. G. Reid, C. Gervais, B. Bueken, B. van de Voorde, D. de Vos, D. A. Keen, C. Mellot-Draznieks, *Phys. Chem. Chem. Phys.* **2016**, *18*, 2192.
- 85 G. C. Shearer, S. Chavan, J. Ethiraj, J. G. Vitillo, S. Svelle, U. Olsbye, C. Lamberti, S. Bordiga, K. P. Lillerud, *Chem. Mater.* **2014**, *26*, 4068.
- 86 S. Gadipelli, Z. Guo, *Chem. Mater.* **2014**, *26*, 6333.
- 87 A. Dhakshinamoorthy, A. M. Asiri, H. Garcia, *Catal. Sci. Technol.* **2016**, *6*, 5238.
- 88 A. Dhakshinamoorthy, H. Garcia, *ChemSusChem* **2014**, *7*, 2392.
- 89 J.-J. Du, X. Zhang, X.-P. Zhou, D. Li, *Inorg. Chem. Front.* **2018**, *5*, 2772.
- 90 H.-F. Yao, Y. Yang, H. Liu, F.-G. Xi, E.-Q. Gao, *J. Mol. Catal. A-Chem.* **2014**, *394*, 57.
- 91 D. Sun, F. Sun, X. Deng, Z. Li, *Inorg. Chem.* **2015**, *54*, 8639.
- 92 M. Lammert, C. Glißmann, N. Stock, *Dalton Trans.* **2017**, *46*, 2425.
- 93 H. Deng, C. J. Doonan, H. Furukawa, R. B. Ferreira, J. Towne, C. B. Knobler, B. Wang, O. M. Yaghi, *Science* **2010**, *327*, 846.

- 94 M. Taddei, D. Tiana, N. Casati, J. A. van Bokhoven, B. Smit, M. Ranocchiari, *Phys. Chem. Chem. Phys.* **2017**, *19*, 1551.
- 95 Z. H. Rada, H. R. Abid, H. Sun, J. Shang, J. Li, Y. He, S. Liu, S. Wang, *Prog. Nat. Sci.: Mater. Int.* **2018**, *28*, 160.
- 96 S. J. Lee, C. Doussot, A. Baux, L. Liu, G. B. Jameson, C. Richardson, J. J. Pak, F. Trouselet, F.-X. Coudert, S. G. Telfer, *Chem. Mater.* **2016**, *28*, 368.
- 97 A. Alkaş, J. Cornelio, S. G. Telfer, *Chem. Asian J.* **2018**, *14*, 1167.
- 98 S. J. Lee, C. Doussot, S. G. Telfer, *Cryst. Growth Des.* **2017**, *17*, 3185.
- 99 L. Liu, K. Konstas, M. R. Hill, S. G. Telfer, *J. Am. Chem. Soc.* **2013**, *135*, 17731.
- 100 S. Li, F. Huo, *Nanoscale* **2015**, *7*, 7482.
- 101 Q.-L. Zhu, Q. Xu, *Chem. Soc. Rev.* **2014**, *43*, 5468.
- 102 R. Lin, B. Villacorta Hernandez, L. Ge, Z. Zhu, *J. Mater. Chem. A* **2018**, *6*, 293.
- 103 H. B. Tanh Jeazet, C. Staudt, C. Janiak, *Dalton Trans.* **2012**, *41*, 14003.
- 104 S. Friebe, L. Diestel, A. Knebel, A. Wollbrink, J. Caro, *Chem. Ing. Tech.* **2016**, *88*, 1788.
- 105 B. Seoane, J. Coronas, I. Gascon, M. Etxeberria Benavides, O. Karvan, J. Caro, F. Kapteijn, J. Gascon, *Chem. Soc. Rev.* **2015**, *44*, 2421.
- 106 L. Wang, X. Feng, L. Ren, Q. Piao, J. Zhong, Y. Wang, H. Li, Y. Chen, B. Wang, *J. Am. Chem. Soc.* **2015**, *137*, 4920.
- 107 H.-B. Luo, M. Wang, S.-X. Liu, C. Xue, Z.-F. Tian, Y. Zou, X.-M. Ren, *Inorg. Chem.* **2017**, *56*, 4169.
- 108 G. Chen, W. J. Koros, C. W. Jones, *ACS Appl. Mater. Interfaces* **2016**, *8*, 9700.
- 109 I. Ahmed, S. H. Jhung, *Mater. Today* **2014**, *17*, 136.
- 110 L. Wang, W. Wang, X. Zheng, Z. Li, Z. Xie, *Chem. Eur. J.* **2017**, *23*, 1379.
- 111 Z. Neisi, Z. Ansari-Asl, S. Jafarinejad-Farsangi, M. E. Tarzi, T. Sedaghat, V. Nobakht, *Colloids Surf. B Biointerfaces* **2019**, *178*, 365.
- 112 C.-C. Chueh, C.-I. Chen, Y.-A. Su, H. Konnerth, Y.-J. Gu, C.-W. Kung, K. C.-W. Wu, *J. Mater. Chem. A* **2019**, *7*, 17079.
- 113 M. Giménez-Marqués, E. Bellido, T. Berthelot, T. Simón-Yarza, T. Hidalgo, R. Simón-Vázquez, Á. González-Fernández, J. Avila, M. C. Asensio, R. Gref, P. Couvreur, C. Serre, P. Horcajada, *Small* **2018**, *14*, e1801900.
- 114 T. Uemura, N. Yanai, S. Kitagawa, *Chem. Soc. Rev.* **2009**, *38*, 1228.
- 115 G. Distefano, H. Suzuki, M. Tsujimoto, S. Isoda, S. Bracco, A. Comotti, P. Sozzani, T. Uemura, S. Kitagawa, *Nat. Chem.* **2013**, *5*, 335.
- 116 R. Haldar, B. Sen, S. Hurrle, T. Kitao, R. Sankhla, B. Köhl, A. Welle, S. Heissler, G. Brenner-Weiß, P. Thissen, T. Uemura, H. Gliemann, C. Barner-Kowollik, C. Wöll, *Eur. Polym. J.* **2018**, *109*, 162.
- 117 T. C. Wang, I. Hod, C. O. Audu, N. A. Vermeulen, S. T. Nguyen, O. K. Farha, J. T. Hupp, *ACS Appl. Mater. Interfaces* **2017**, *9*, 12584.
- 118 B. Le Ouay, M. Boudot, T. Kitao, T. Yanagida, S. Kitagawa, T. Uemura, *J. Am. Chem. Soc.* **2016**, *138*, 10088.

- 119 C. Chen, J. Kim, D.-W. Park, W.-S. Ahn, *Mater. Lett.* **2013**, *106*, 344.
- 120 K. A. McDonald, J. I. Feldblyum, K. Koh, A. G. Wong-Foy, A. J. Matzger, *Chem. Commun.* **2015**, *51*, 11994.
- 121 H. Liu, H. Zhu, S. Zhu, *Macromol. Mater. Eng.* **2015**, *300*, 191.
- 122 Y. Zhang, X. Feng, H. Li, Y. Chen, J. Zhao, S. Wang, L. Wang, B. Wang, *Angew. Chem. Int. Ed.* **2015**, *54*, 4259.
- 123 S. Nagata, K. Kokado, K. Sada, *Chem. Commun.* **2015**, *51*, 8614.
- 124 M.-L. Gao, S.-Y. Zhao, Z.-Y. Chen, L. Liu, Z.-B. Han, *Inorg. Chem.* **2019**, *58*, 2261.
- 125 M. Kalaj, M. S. Denny, K. C. Bentz, J. M. Palomba, S. M. Cohen, *Angew. Chem. Int. Ed.* **2019**, *58*, 2336.
- 126 C. Lu, T. Ben, S. Xu, S. Qiu, *Angew. Chem. Int. Ed.* **2014**, *53*, 6454.
- 127 T. Wang, M. Farajollahi, S. Henke, T. Zhu, S. R. Bajpe, S. Sun, J. S. Barnard, J. S. Lee, J. D. W. Madden, A. K. Cheetham, S. K. Smoukov, *Mater. Horiz.* **2017**, *4*, 64.
- 128 S. Ayala, Z. Zhang, S. M. Cohen, *Chem. Commun.* **2017**, *53*, 3058.
- 129 Z. Zhang, H. T. H. Nguyen, S. A. Miller, A. M. Ploskonka, J. B. DeCoste, S. M. Cohen, *J. Am. Chem. Soc.* **2016**, *138*, 920.
- 130 M. J. MacLeod, J. A. Johnson, *Polym. Chem.* **2017**, *8*, 4488.
- 131 S. Ayala, K. C. Bentz, S. M. Cohen, *Chem. Sci.* **2019**, *10*, 1746.
- 132 J. W. M. Osterrieth, D. Wright, H. Noh, C.-W. Kung, D. Vulpe, A. Li, J. E. Park, R. P. van Duyne, P. Z. Moghadam, J. J. Baumberg, O. K. Farha, D. Fairen-Jimenez, *J. Am. Chem. Soc.* **2019**, *141*, 3893.
- 133 J. Yu, C. Mu, B. Yan, X. Qin, C. Shen, H. Xue, H. Pang, *Mater. Horiz.* **2017**, *4*, 557.
- 134 B. Voloskiy, K. Niwa, Y. Chen, Z. Zhao, N. O. Weiss, X. Zhong, M. Ding, C. Lee, Y. Huang, X. Duan, *ACS Nano* **2015**, *9*, 3044.
- 135 T. Ishida, M. Nagaoka, T. Akita, M. Haruta, *Chem. Eur. J.* **2008**, *14*, 8456.
- 136 H.-L. Jiang, B. Liu, T. Akita, M. Haruta, H. Sakurai, Q. Xu, *J. Am. Chem. Soc.* **2009**, *131*, 11302.
- 137 C. Zlotea, R. Campesi, F. Cuevas, E. Leroy, P. Dibandjo, C. Volkringer, T. Loiseau, G. Férey, M. Latroche, *J. Am. Chem. Soc.* **2010**, *132*, 2991.
- 138 Y. K. Hwang, D.-Y. Hong, J.-S. Chang, S. H. Jhung, Y.-K. Seo, J. Kim, A. Vimont, M. Daturi, C. Serre, G. Férey, *Angew. Chem. Int. Ed.* **2008**, *47*, 4144.
- 139 H. Zhao, H. Song, L. Chou, *Inorg. Chem. Commun.* **2012**, *15*, 261.
- 140 S. Hermes, M.-K. Schröter, R. Schmid, L. Khodeir, M. Muhler, A. Tissler, R. W. Fischer, R. A. Fischer, *Angew. Chem. Int. Ed.* **2005**, *44*, 6237.
- 141 A. Aijaz, A. Karkamkar, Y. J. Choi, N. Tsumori, E. Rönnebro, T. Autrey, H. Shioyama, Q. Xu, *J. Am. Chem. Soc.* **2012**, *134*, 13926.
- 142 M. Imperor-Clerc, D. Bazin, M.-D. Appay, P. Beaunier, A. Davidson, *Chem. Mater.* **2004**, *16*, 1813.

- 143 G. Lu, S. Li, Z. Guo, O. K. Farha, B. G. Hauser, X. Qi, Y. Wang, X. Wang, S. Han, X. Liu, J. S. DuChene, H. Zhang, Q. Zhang, X. Chen, J. Ma, S. C. J. Loo, W. D. Wei, Y. Yang, J. T. Hupp, F. Huo, *Nat. Chem.* **2012**, *4*, 310.
- 144 C.-H. Kuo, Y. Tang, L.-Y. Chou, B. T. Sneed, C. N. Brodsky, Z. Zhao, C.-K. Tsung, *J. Am. Chem. Soc.* **2012**, *134*, 14345.
- 145 Y. Li, Y. Xu, W. Yang, W. Shen, H. Xue, H. Pang, *Small* **2018**, *14*, e1704435.
- 146 H. Lu, L. Zhang, B. Wang, Y. Long, M. Zhang, J. Ma, A. Khan, S. P. Chowdhury, X. Zhou, Y. Ni, *Cellulose* **2019**, *12*, 7353.
- 147 J. Pokhrel, N. Bhorla, C. Wu, K. S. K. Reddy, H. Margetis, S. Anastasiou, G. George, V. Mittal, G. Romanos, D. Karonis, G. N. Karanikolos, *J. Solid State Chem.* **2018**, *266*, 233.
- 148 S. Furukawa, K. Hirai, K. Nakagawa, Y. Takashima, R. Matsuda, T. Tsuruoka, M. Kondo, R. Haruki, D. Tanaka, H. Sakamoto, S. Shimomura, O. Sakata, S. Kitagawa, *Angew. Chem. Int. Ed.* **2009**, *48*, 1766.
- 149 S. M. Cohen, *J. Am. Chem. Soc.* **2017**, *139*, 2855.
- 150 X. Lian, Y. Fang, E. Joseph, Q. Wang, J. Li, S. Banerjee, C. Lollar, X. Wang, H.-C. Zhou, *Chem. Soc. Rev.* **2017**, *46*, 3386.
- 151 A. Knebel, L. Sundermann, A. Mohmeyer, I. Strauß, S. Friebe, P. Behrens, J. Caro, *Chem. Mater.* **2017**, *29*, 3111.
- 152 D. Hermann, H. Emerich, R. Lepski, D. Schaniel, U. Ruschewitz, *Inorg. Chem.* **2013**, *52*, 2744.
- 153 Q. Li, Z.-L. Fan, D.-X. Xue, Y.-F. Zhang, Z.-H. Zhang, Q. Wang, H.-M. Sun, Z. Gao, J. Bai, *J. Mater. Chem. A* **2018**, *6*, 2148.
- 154 W. Chen, Y. Zhuang, Le Wang, Y. Lv, J. Liu, T.-L. Zhou, R.-J. Xie, *ACS Appl. Mater. Interfaces* **2018**, *10*, 18910.
- 155 T. Zhou, Y. Du, A. Borgna, J. Hong, Y. Wang, J. Han, W. Zhang, R. Xu, *Energy Environ. Sci.* **2013**, *6*, 3229.
- 156 D. Cunha, C. Gaudin, I. Colinet, P. Horcajada, G. Maurin, C. Serre, *J. Mater. Chem. B* **2013**, *1*, 1101.
- 157 K. Jiang, L. Zhang, Q. Hu, X. Zhang, J. Zhang, Y. Cui, Y. Yang, B. Li, G. Qian, *Microporous Mesoporous Mater.* **2019**, *275*, 229.
- 158 W. Xiang, Y. Zhang, H. Lin, C.-J. Liu, *Molecules* **2017**, *22*, e2103.
- 159 D.-W. Lim, J. W. Yoon, K. Y. Ryu, M. P. Suh, *Angew. Chem. Int. Ed.* **2012**, *51*, 9814.
- 160 C. Petit, B. Levasseur, B. Mendoza, T. J. Bandoz, *Microporous Mesoporous Mater.* **2012**, *154*, 107.
- 161 X. Zhao, S. Liu, Z. Tang, H. Niu, Y. Cai, W. Meng, F. Wu, J. P. Giesy, *Sci. Rep.* **2015**, *5*, 11849.
- 162 N. Nidamanuri, K. Maity, S. Saha, *Elaboration and applications of metal-organic frameworks*, World Scientific, New Jersey **2018**, 655.

- 163 S. Takaishi, M. Hosoda, T. Kajiwara, H. Miyasaka, M. Yamashita, Y. Nakanishi, Y. Kitagawa, K. Yamaguchi, A. Kobayashi, H. Kitagawa, *Inorg. Chem.* **2009**, *48*, 9048.
- 164 C.-T. Chen, K. S. Suslick, *Coord. Chem. Rev.* **1993**, *128*, 293.
- 165 F. Gándara, F. J. Uribe-Romo, D. K. Britt, H. Furukawa, L. Lei, R. Cheng, X. Duan, M. O'Keeffe, O. M. Yaghi, *Chem. Eur. J.* **2012**, *18*, 10595.
- 166 L. E. Darago, M. L. Aubrey, C. J. Yu, M. I. Gonzalez, J. R. Long, *J. Am. Chem. Soc.* **2015**, *137*, 15703.
- 167 L. Sun, C. H. Hendon, M. A. Minier, A. Walsh, M. Dincă, *J. Am. Chem. Soc.* **2015**, *137*, 6164.
- 168 C. F. Leong, P. M. Usov, D. M. D'Alessandro, *MRS Bull.* **2016**, *41*, 858.
- 169 A. J. Clough, J. W. Yoo, M. H. Mecklenburg, S. C. Marinescu, *J. Am. Chem. Soc.* **2015**, *137*, 118.
- 170 X. Huang, P. Sheng, Z. Tu, F. Zhang, J. Wang, H. Geng, Y. Zou, C.-A. Di, Y. Yi, Y. Sun, W. Xu, D. Zhu, *Nat. Commun.* **2015**, *6*, 7408.
- 171 M. G. Campbell, S. F. Liu, T. M. Swager, M. Dincă, *J. Am. Chem. Soc.* **2015**, *137*, 13780.
- 172 R. Sakamoto, T. Kambe, S. Tsukada, K. Takada, K. Hoshiko, Y. Kitagawa, M. Okumura, H. Nishihara, *Inorg. Chem.* **2013**, *52*, 7411.
- 173 M. Hmadeh, Z. Lu, Z. Liu, F. Gándara, H. Furukawa, S. Wan, V. Augustyn, R. Chang, L. Liao, F. Zhou, E. Perre, V. Ozolins, K. Suenaga, X. Duan, B. Dunn, Y. Yamamoto, O. Terasaki, O. M. Yaghi, *Chem. Mater.* **2012**, *24*, 3511.
- 174 D. Sheberla, L. Sun, M. A. Blood-Forsythe, S. Er, C. R. Wade, C. K. Brozek, A. Aspuru-Guzik, M. Dincă, *J. Am. Chem. Soc.* **2014**, *136*, 8859.
- 175 D. Sheberla, J. C. Bachman, J. S. Elias, C.-J. Sun, Y. Shao-Horn, M. Dincă, *Nat. Mater.* **2017**, *16*, 220.
- 176 L. Sun, C. H. Hendon, M. Dincă, *Dalton Trans.* **2018**, *47*, 11739.
- 177 B. Hoppe, K. D. J. Hindricks, D. P. Warwas, H. A. Schulze, A. Mohmeyer, T. J. Pinkvos, S. Zailskas, M. R. Krey, C. Belke, S. König, M. Fröba, R. J. Haug, P. Behrens, *CrystEngComm* **2018**, *20*, 6458.
- 178 S. K. Bhardwaj, N. Bhardwaj, R. Kaur, J. Mehta, A. L. Sharma, K.-H. Kim, A. Deep, *J. Mater. Chem. A* **2018**, *6*, 14992.
- 179 M.-H. Zeng, Q.-X. Wang, Y.-X. Tan, S. Hu, H.-X. Zhao, L.-S. Long, M. Kurmoo, *J. Am. Chem. Soc.* **2010**, *132*, 2561.
- 180 Y. Kobayashi, B. Jacobs, M. d. Allendorf, J. R. Long, *Chem. Mater.* **2010**, *22*, 4120.
- 181 A. A. Talin, A. Centrone, A. C. Ford, M. E. Foster, V. Stavila, P. Haney, R. A. Kinney, V. Szalai, F. El Gabaly, H. P. Yoon, F. Léonard, M. d. Allendorf, *Science* **2014**, *343*, 66.
- 182 S. Goswami, D. Ray, K.-i. Otake, C.-W. Kung, S. J. Garibay, T. Islamoglu, A. Atilgan, Y. Cui, C. J. Cramer, O. K. Farha, J. T. Hupp, *Chem. Sci.* **2018**, *9*, 4477.

- 183 B. Dhara, S. S. Nagarkar, J. Kumar, V. Kumar, P. K. Jha, S. K. Ghosh, S. Nair, N. Ballav, *J. Phys. Chem. Lett.* **2016**, *7*, 2945.
- 184 Y. Wang, L. Wang, W. Huang, T. Zhang, X. Hu, J. A. Perman, S. Ma, *J. Mater. Chem. A* **2017**, *5*, 8385.
- 185 Z. Li, Y. Guo, X. Wang, W. Ying, D. Chen, X. Ma, X. Zhao, X. Peng, *Chem. Commun.* **2018**, *54*, 13865.
- 186 H. A. Schulze, B. Hoppe, M. Schäfer, D. P. Warwas, P. Behrens, *ChemNanoMat* **2019**.
- 187 A. Mohmeyer, A. Schaate, B. Hoppe, H. A. Schulze, T. Heinemeyer, P. Behrens, *Chem. Commun.* **2019**, *55*, 3367.
- 188 H. Furukawa, F. Gándara, Y.-B. Zhang, J. Jiang, W. L. Queen, M. R. Hudson, O. M. Yaghi, *J. Am. Chem. Soc.* **2014**, *136*, 4369.
- 189 V. Bon, I. Senkowska, I. A. Baburin, S. Kaskel, *Cryst. Growth Des.* **2013**, *13*, 1231.
- 190 Z. Hu, I. Castano, S. Wang, Y. Wang, Y. Peng, Y. Qian, C. Chi, X. Wang, D. Zhao, *Cryst. Growth Des.* **2016**, *16*, 2295.
- 191 H. Wu, Y. S. Chua, V. Krungleviciute, M. Tyagi, P. Chen, T. Yildirim, W. Zhou, *J. Am. Chem. Soc.* **2013**, *135*, 10525.
- 192 J. Cravillon, R. Nayuk, S. Springer, A. Feldhoff, K. Huber, M. Wiebcke, *Chem. Mater.* **2011**, *23*, 2130.
- 193 A. Mohmeyer, A. Schaate, B. Brechtken, J. C. Rode, D. P. Warwas, G. Zahn, R. J. Haug, P. Behrens, *Chem. Eur. J.* **2018**, *24*, 12848.
- 194 J. B. DeCoste, G. W. Peterson, H. Jasuja, T. G. Glover, Y.-g. Huang, K. S. Walton, *J. Mater. Chem. A* **2013**, *1*, 5642.
- 195 J. E. Mondloch, M. J. Katz, N. Planas, D. Semrouni, L. Gagliardi, J. T. Hupp, O. K. Farha, *Chem. Commun.* **2014**, *50*, 8944.
- 196 C. G. Piscopo, A. Polyzoidis, M. Schwarzer, S. Loebbecke, *Microporous Mesoporous Mater.* **2015**, *208*, 30.
- 197 B. Bueken, H. Reinsch, N. Reimer, I. Stassen, F. Vermoortele, R. Ameloot, N. Stock, C. E. A. Kirschhock, D. de Vos, *Chem. Commun.* **2014**, *50*, 10055.
- 198 V. Bon, I. Senkowska, M. S. Weiss, S. Kaskel, *CrystEngComm* **2013**, *15*, 9572.
- 199 A. A. Bezrukov, K. W. Törnroos, E. Le Roux, P. D. C. Dietzel, *Chem. Commun.* **2018**, *54*, 2735.
- 200 M. Ermer, J. Mehler, M. Kriesten, Y. S. Avadhut, P. S. Schulz, M. Hartmann, *Dalton Trans.* **2018**, *47*, 14426.
- 201 P. Ji, K. Manna, Z. Lin, X. Feng, A. Urban, Y. Song, W. Lin, *J. Am. Chem. Soc.* **2017**, *139*, 7004.
- 202 S. Waitschat, H. Reinsch, M. Arpacioğlu, N. Stock, *CrystEngComm* **2018**, *20*, 5108.
- 203 S. Waitschat, H. Reinsch, N. Stock, *Chem. Commun.* **2016**, *52*, 12698.
- 204 D. Feng, Z.-Y. Gu, J.-R. Li, H.-L. Jiang, Z. Wei, H.-C. Zhou, *Angew. Chem. Int. Ed.* **2012**, *51*, 10307.

- 205 M. Puchberger, F. R. Kogler, M. Jupa, S. Gross, H. Fric, G. Kickelbick, U. Schubert, *Eur. J. Inorg. Chem.* **2006**, 2006, 3283.
- 206 M. Taddei, F. Costantino, R. Vivani, S. Sabatini, S.-H. Lim, S. M. Cohen, *Chem. Commun.* **2014**, 50, 5737.
- 207 V. Guillerme, F. Ragon, M. Dan-Hardi, T. Devic, M. Vishnuvarthan, B. Campo, A. Vimont, G. Clet, Q. Yang, G. Maurin, G. Férey, A. Vittadini, S. Gross, C. Serre, *Angew. Chem. Int. Ed.* **2012**, 51, 9267.
- 208 L. Cooper, N. Guillou, C. Martineau, E. Elkaim, F. Taulelle, C. Serre, T. Devic, *Eur. J. Inorg. Chem.* **2014**, 2014, 6281.
- 209 M. Taddei, F. Costantino, F. Marmottini, A. Comotti, P. Sozzani, R. Vivani, *Chem. Commun.* **2014**, 50, 14831.
- 210 D. Feng, H.-L. Jiang, Y.-P. Chen, Z.-Y. Gu, Z. Wei, H.-C. Zhou, *Inorg. Chem.* **2013**, 52, 12661.
- 211 G. Mouchaham, L. Cooper, N. Guillou, C. Martineau, E. Elkaim, S. Bourrelly, P. L. Llewellyn, C. Allain, G. Clavier, C. Serre, T. Devic, *Angew. Chem. Int. Ed.* **2015**, 54, 13297.
- 212 J. Ma, A. G. Wong-Foy, A. J. Matzger, *Inorg. Chem.* **2015**, 54, 4591.
- 213 M. Zhao, Y. Huang, Y. Peng, Z. Huang, Q. Ma, H. Zhang, *Chem. Soc. Rev.* **2018**, 47, 6267.
- 214 S. M. Cohen, *Chem. Rev.* **2012**, 112, 970.
- 215 K. K. Tanabe, S. M. Cohen, *Chem. Soc. Rev.* **2011**, 40, 498.
- 216 T. Devic, P. Horcajada, C. Serre, F. Salles, G. Maurin, B. Moulin, D. Heurtaux, G. Clet, A. Vimont, J.-M. Grenèche, B. Le Ouay, F. Moreau, E. Magnier, Y. Filinchuk, J. Marrot, J.-C. Lavalley, M. Daturi, G. Férey, *J. Am. Chem. Soc.* **2010**, 132, 1127.
- 217 J. S. Seo, D. Whang, H. Lee, S. I. Jun, J. Oh, Y. J. Jeon, K. Kim, *Nature* **2000**, 404, 982.
- 218 Z. Wang, S. M. Cohen, *J. Am. Chem. Soc.* **2007**, 129, 12368.
- 219 A. M. Fracaroli, P. Siman, D. A. Nagib, M. Suzuki, H. Furukawa, F. D. Toste, O. M. Yaghi, *J. Am. Chem. Soc.* **2016**, 138, 8352.
- 220 T. Gadzikwa, G. Lu, C. L. Stern, S. R. Wilson, J. T. Hupp, S. T. Nguyen, *Chem. Commun.* **2008**, 43, 5493.
- 221 S. S. Kaye, J. R. Long, *J. Am. Chem. Soc.* **2008**, 130, 806.
- 222 W. Morris, C. J. Doonan, H. Furukawa, R. Banerjee, O. M. Yaghi, *J. Am. Chem. Soc.* **2008**, 130, 12626.
- 223 S. J. Garibay, Z. Wang, K. K. Tanabe, S. M. Cohen, *Inorg. Chem.* **2009**, 48, 7341.
- 224 M. S. Denny, S. M. Cohen, *Angew. Chem. Int. Ed.* **2015**, 54, 9029.
- 225 M. Lalonde, W. Bury, O. Karagiari, Z. Brown, J. T. Hupp, O. K. Farha, *J. Mater. Chem. A* **2013**, 1, 5453.
- 226 S. Das, H. Kim, K. Kim, *J. Am. Chem. Soc.* **2009**, 131, 3814.
- 227 C. K. Brozek, M. Dincă, *Chem. Commun.* **2015**, 51, 11780.

- 228 C. K. Brozek, V. K. Michaelis, T.-C. Ong, L. Bellarosa, N. López, R. G. Griffin, M. Dincă, *ACS Cent. Sci.* **2015**, *1*, 252.
- 229 B. J. Burnett, P. M. Barron, C. Hu, W. Choe, *J. Am. Chem. Soc.* **2011**, *133*, 9984.
- 230 Y. Xu, N. A. Vermeulen, Y. Liu, J. T. Hupp, O. K. Farha, *Eur. J. Inorg. Chem.* **2016**, *2016*, 4345.
- 231 R. Kitaura, F. Iwahori, R. Matsuda, S. Kitagawa, Y. Kubota, M. Takata, T. C. Kobayashi, *Inorg. Chem.* **2004**, *43*, 6522.
- 232 Z. Chen, S. Xiang, D. Zhao, B. Chen, *Cryst. Growth Des.* **2009**, *9*, 5293.
- 233 T. Ishiwata, Y. Furukawa, K. Sugikawa, K. Kokado, K. Sada, *J. Am. Chem. Soc.* **2013**, *135*, 5427.
- 234 S. Yang, L. Peng, D. T. Sun, M. Asgari, E. Oveisi, O. Trukhina, S. Bulut, A. Jamali, W. L. Queen, *Chem. Sci.* **2019**, *10*, 4542.
- 235 D. Nam, J. Huh, J. Lee, J. H. Kwak, H. Y. Jeong, K. Choi, W. Choe, *Chem. Sci.* **2017**, *8*, 7765.
- 236 H. Amer Hamzah, T. S. Crickmore, D. Rixson, A. D. Burrows, *Dalton Trans.* **2018**, *47*, 14491.
- 237 M. Kim, J. F. Cahill, Y. Su, K. A. Prather, S. M. Cohen, *Chem. Sci.* **2012**, *3*, 126.
- 238 S. Pullen, H. Fei, A. Orthaber, S. M. Cohen, S. Ott, *J. Am. Chem. Soc.* **2013**, *135*, 16997.
- 239 M. Taddei, R. J. Wakeham, A. Koutsianos, E. Andreoli, A. R. Barron, *Angew. Chem. Int. Ed.* **2018**, *57*, 11706.
- 240 S. Anan, K. Kokado, K. Sada, *Chem. Lett.* **2019**, *48*, 285.
- 241 O. V. Gutov, S. Molina, E. C. Escudero-Adán, A. Shafir, *Chem. Eur. J.* **2016**, *22*, 13582.
- 242 J. Hýnek, S. Ondrušová, D. Bůžek, P. Kovář, J. Rathouský, J. Demel, *Chem. Commun.* **2017**, *53*, 8557.
- 243 J. Jiang, F. Gándara, Y.-B. Zhang, K. Na, O. M. Yaghi, W. G. Klemperer, *J. Am. Chem. Soc.* **2014**, *136*, 12844.
- 244 M. J. Cliffe, W. Wan, X. Zou, P. A. Chater, A. K. Kleppe, M. G. Tucker, H. Wilhelm, N. P. Funnell, F.-X. Coudert, A. L. Goodwin, *Nat. Commun.* **2014**, *5*, 4176.
- 245 I. Abánades Lázaro, S. Haddad, J. M. Rodrigo-Muñoz, R. J. Marshall, B. Sastre, V. Del Pozo, D. Fairen-Jimenez, R. S. Forgan, *ACS Appl. Mater. Interfaces* **2018**, *10*, 31146.
- 246 I. Abánades Lázaro, S. Haddad, J. M. Rodrigo-Muñoz, C. Orellana-Tavra, V. Del Pozo, D. Fairen-Jimenez, R. S. Forgan, *ACS Appl. Mater. Interfaces* **2018**, *10*, 5255.
- 247 C. L. Jones, A. J. Tansell, T. L. Easun, *J. Mater. Chem. A* **2016**, *4*, 6714.
- 248 D. E. Williams, E. A. Dolgoplova, D. C. Godfrey, E. D. Ermolaeva, P. J. Pellechia, A. B. Greytak, M. D. Smith, S. M. Avdoshenko, A. A. Popov, N. B. Shustova, *Angew. Chem. Int. Ed.* **2016**, *55*, 9070.

- 249 A. M. Rice, W. B. Fellows, E. A. Dolgoplova, A. B. Greytak, A. K. Vannucci, M. D. Smith, S. G. Karakalos, J. A. Krause, S. M. Avdoshenko, A. A. Popov, N. B. Shustova, *Angew. Chem. Int. Ed.* **2017**, *56*, 4525.
- 250 X. Rao, T. Song, J. Gao, Y. Cui, Y. Yang, C. Wu, B. Chen, G. Qian, *J. Am. Chem. Soc.* **2013**, *135*, 15559.
- 251 L.-N. Jia, L. Hou, L. Wei, X.-J. Jing, B. Liu, Y.-Y. Wang, Q.-Z. Shi, *Cryst. Growth Des.* **2013**, *13*, 1570.
- 252 K. Leong, M. E. Foster, B. M. Wong, E. d. Spoerke, D. van Gough, J. C. Deaton, M. d. Allendorf, *J. Mater. Chem. A* **2014**, *2*, 3389.
- 253 M. Dan-Hardi, C. Serre, T. Frot, L. Rozes, G. Maurin, C. Sanchez, G. Férey, *J. Am. Chem. Soc.* **2009**, *131*, 10857.
- 254 M. A. Nasalevich, M. G. Goesten, T. J. Savenije, F. Kapteijn, J. Gascon, *Chem. Commun.* **2013**, *49*, 10575.
- 255 D. Wang, M. Wang, Z. Li, *ACS Catal.* **2015**, *5*, 6852.
- 256 C. Wang, Z. Xie, K. E. DeKrafft, W. Lin, *J. Am. Chem. Soc.* **2011**, *133*, 13445.
- 257 J. A. Johnson, X. Zhang, T. C. Reeson, Y.-S. Chen, J. Zhang, *J. Am. Chem. Soc.* **2014**, *136*, 15881.
- 258 J. A. Johnson, J. Luo, X. Zhang, Y.-S. Chen, M. D. Morton, E. Echeverri´a, F. E. Torres, J. Zhang, *ACS Catal.* **2015**, *5*, 5283.
- 259 X. Yu, L. Wang, S. M. Cohen, *J. Am. Chem. Soc.* **2016**, *138*, 12320.
- 260 J. Bedia, V. Muelas-Ramos, M. Peñas-Garzón, A. Gómez-Avilés, J. J. Rodríguez, C. Berver, *Catalysts* **2019**, *9*, 52.
- 261 C. B. Fan, Z. Q. Liu, L. Le Gong, A. M. Zheng, Le Zhang, C. S. Yan, H. Q. Wu, X. F. Feng, F. Luo, *Chem. Commun.* **2017**, *53*, 763.
- 262 J. Park, D. Yuan, K. T. Pham, J.-R. Li, A. Yakovenko, H.-C. Zhou, *J. Am. Chem. Soc.* **2012**, *134*, 99.
- 263 X. Meng, B. Gui, D. Yuan, M. Zeller, C. Wang, *Sci. Adv.* **2016**, *2*, e1600480.
- 264 J. W. Brown, B. L. Henderson, M. d. Kiesz, A. C. Whalley, W. Morris, S. Grunder, H. Deng, H. Furukawa, J. I. Zink, J. F. Stoddart, O. M. Yaghi, *Chem. Sci.* **2013**, *4*, 2858.
- 265 C. C. Epley, K. L. Roth, S. Lin, S. R. Ahrenholtz, T. Z. Grove, A. J. Morris, *Dalton Trans.* **2017**, *46*, 4917.
- 266 I.-H. Park, R. Medishetty, H.-H. Lee, C. E. Mulijanto, H. S. Quah, S. S. Lee, J. J. Vittal, *Angew. Chem. Int. Ed.* **2015**, *127*, 7421.
- 267 I.-H. Park, A. Chanthapally, Z. Zhang, S. S. Lee, M. J. Zaworotko, J. J. Vittal, *Angew. Chem. Int. Ed.* **2014**, *126*, 424.
- 268 L. Hou, L. Wang, N. Zhang, Z. Xie, D. Dong, *Polym. Chem.* **2016**, *7*, 5828.
- 269 P. Yang, W. Yang, *Chem. Rev.* **2013**, *113*, 5547.
- 270 J. C. Morris, L. A. Walsh, B. A. Gomes, D. Gimes, K. E. Fairfull-Smith, S. E. Bottle, J. P. Blinco, *RSC Adv.* **2015**, *5*, 95598.

- 271 J. N. Pitts, R. L. Letsinger, R. P. Taylor, J. M. Patterson, G. Recktenwald, R. B. Martin, *J. Am. Chem. Soc.* **1959**, *81*, 1068.
- 272 X. Zhang, J. Ma, D. L. Phillips, *J. Phys. Chem. Lett.* **2016**, *7*, 4860.
- 273 M. S. Churio, M. A. Grela, *J. Chem. Educ.* **1997**, *74*, 436.
- 274 A. Demeter, K. Horváth, K. Böör, L. Molnár, T. Soós, G. Lendvay, *J. Phys. Chem. A* **2013**, *117*, 10196.
- 275 O. Prucker, C. A. Naumann, J. Rühle, W. Knoll, C. W. Frank, *J. Am. Chem. Soc.* **1999**, *121*, 8766.
- 276 J. Säuberlich, O. Brede, d. Beckert, *J. Phys. Chem.* **1996**, *100*, 18101.
- 277 L. F. Vieira Ferreira, I. Ferreira Machado, J. P. Da Silva, T. J. F. Branco, *Photochem. Photobiol. Sci.* **2006**, *5*, 665.
- 278 R. B. Woodward, *J. Am. Chem. Soc.* **1941**, *63*, 1123.
- 279 J. d. Coyle, H. A. J. Carless, *Chem. Soc. Rev.* **1972**, *1*, 465.
- 280 P. J. Wagner, *Triplet states III*, Vol. 66, Springer-Verlag, Berlin, New York **1976**.
- 281 N. J. Turro, *Modern molecular photochemistry*, Univ. Science Books, Sausalito **1991**.
- 282 M. Nič, J. Jirát, B. Košata, A. Jenkins, A. McNaught, *IUPAC Compendium of Chemical Terminology*, IUPAC, Research Triangle Park, NC **2009**.
- 283 E. H. Gilmore, G. E. Gibson, D. S. McClure, *J. Chem. Phys.* **1955**, *23*, 399.
- 284 L. Giering, M. Berger, C. Steel, *J. Am. Chem. Soc.* **1974**, *96*, 953.
- 285 A. C. Bhasikuttan, A. K. Singh, D. K. Palit, A. v. Sapre, J. P. Mittal, *J. Phys. Chem. A* **1998**, *102*, 3470.
- 286 N. Ghoneim, A. Monbelli, D. Pilloud, P. Suppan, *J. Photochem. Photobiol. A* **1996**, *94*, 145.
- 287 H. Morawetz, *J. Polym. Sci. B Polym. Lett. Ed.* **1988**, *26*, 276.
- 288 G. Porter, P. Suppan, *Trans. Faraday Soc.* **1965**, *61*, 1664.
- 289 G. d. Prestwich, G. Dormán, J. T. Elliott, D. M. Marecak, A. Chaudhary, *Photochem. Photobiol.* **1997**, *65*, 222.
- 290 H. Murata, B.-J. Chang, O. Prucker, M. Dahm, J. Rühle, *Surf. Sci.* **2004**, *570*, 111.
- 291 V. B. Schwartz, F. Thétiot, S. Ritz, S. Pütz, L. Choritz, A. Lappas, R. Förch, K. Landfester, U. Jonas, *Adv. Funct. Mater.* **2012**, *22*, 2376.
- 292 S. Zakharchenko, N. Puretskiy, G. Stoychev, M. Stamm, L. Ionov, *Soft Matter* **2010**, *6*, 2633.
- 293 N. d. Carbone, M. Ene, J. R. Lancaster, J. T. Koberstein, *Macromolecules* **2013**, *46*, 5434.

3 Results and discussion

3.1 Delamination and Photochemical Modification of a Novel Two-Dimensional Zr-Based Metal-Organic Framework

Authors:

Alexander Mohmeyer,^a Andreas Schaate,^a Benedikt Brechtken,^b Johannes C. Rode,^b Dawid P. Warwas,^{a,c} Gesa Zahn,^a Rolf J. Haug^{b,c} and Peter Behrens^{*a,c}

Chem. Eur. J. **2018**, *24*, 12848–12855

DOI: 10.1002/chem.201802189

Cover feature:

Chem. Eur. J. **2018**, *24*, 12737–12737

DOI: 10.1002/chem.201804056

Postal Addresses:

^aInstitute for Inorganic Chemistry, Leibniz University Hannover, D-30167 Hannover, Germany

^bInstitute for Solid State Physics, Leibniz University Hannover, D-30167 Hannover, Germany

^cLaboratory for Nano- and Quantum-engineering, Leibniz University Hannover, D-30167 Hannover, Germany

*Corresponding author: peter.behrens@acb.uni-hannover.de
phone: +49 (0)511 762-3697

Preface

In this study, the synthesis and characterization of a novel two-dimensional Zr-based metal-organic framework, which offers the possibility for postsynthetic photochemical modification at the linker molecule benzophenone-4,4'-dicarboxylic acid (H_2bzpdc), is presented. The material had once been obtained by Dr. Gesa Zahn from our group but was not investigated in detail. Its synthesis, including the preparation of single crystals, and thorough characterization were investigated in depth by the author. The crystal structure model established by Dr. Andreas Schaate shows that the *Zr-bzpdc*-MOF is built up from 2D-layers; therefore, the delamination of the crystals for the preparation of thin sheets was investigated using a variety of methods. Finally, first studies on the photochemistry of the *Zr-bzpdc*-MOF were carried out.

The synthetic requirements for the generation of the *Zr-bzpdc*-MOF were studied using the modulation approach, with variation of amount and type of modulator (formic acid, acetic acid, propionic acid), precursor equivalents, temperature and reaction duration. The only way to successfully synthesize a crystalline and porous material consisting of Zr-based IBUs and *bzpdc* ligands was the modulated synthesis with formic acid, which also acts as a coordinating molecule partially saturating the IBUs of the final framework. Single crystals of the *Zr-bzpdc*-MOF were modified postsynthetically based on the intrinsic photochemical reactivity of the benzophenone moiety with C-H bond containing molecules. In this way, the surface properties of the MOF crystals (e.g. dispersibility in different solvents) can be changed drastically. *Zr-bzpdc*-MOF crystals were dispersed in polyethylene glycol 300 and decane and irradiated under inert conditions resulting in yellowish products indicating a successful reaction. The MOF itself as well as the sample modified with PEG show hydrophilic characteristics. However, the sample modified with decane leads to a hydrophobic material.

Based on the 2D layered structure, the *Zr-bzpdc*-MOF also offers the possibility of delamination which leads to thin sheets of the material of only few nanometers thicknesses. The *Zr-bzpdc*-MOF sheets obtained by delamination have thicknesses of 2-10 nm, measured with atomic force microscopy by Benedict Brechtken and Johannes C. Rode under supervision of Prof. Dr. Rolf. J. Haug from the Institute for Solid State Physics of the Leibniz University Hannover. Delamination and adaptation of the surface chemistry open up novel ways for shaping MOFs, e.g. for the incorporation into polymer composites, and pave the way for various applications.

The electron microscopic images were obtained by Dawid P. Warwas (TEM), Hendrik A. Schulze and Dr. Bastian Hoppe (SEM). Dr. Michael Wiebcke performed the X-ray diffraction measurements. NMR spectra were supplied from the service unit of the Institute for Organic Chemistry of the Leibniz University Hannover.

Prof. Dr. Peter Behrens and Dr. Andreas Schaate guided this study. The author of this thesis wrote the initial manuscript which was refined in cooperation with Prof. Dr. Peter Behrens.

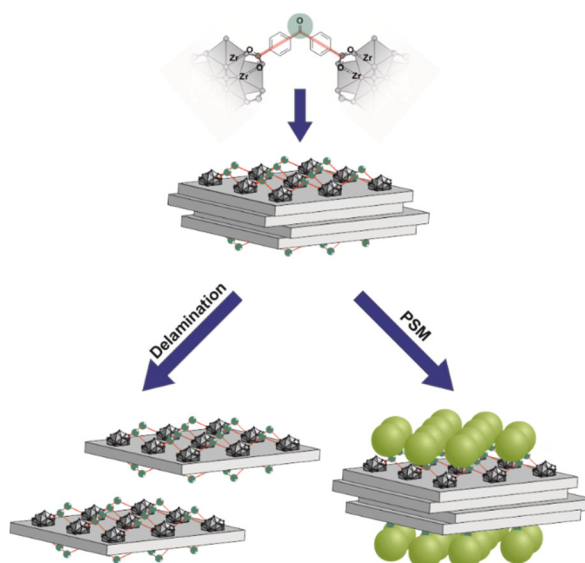
Delamination and Photochemical Modification of a Novel Two-Dimensional Zr-Based Metal-Organic Framework

Alexander Mohmeyer, Andreas Schaate, Benedikt Brechtken, Johannes C. Rode, Dawid P. Warwas, Gesa Zahn, Rolf J. Haug and Peter Behrens

Abstract

In this contribution we present a novel two-dimensional Zr-based metal-organic framework which offers the possibility for delamination and postsynthetic photochemical modification at the linker molecule derived from benzophenone-4,4'-dicarboxylic acid (H_2bzpdc). The new Zr-*bzpdc*-MOF crystallizes in the orthorhombic system as crystals with rhombic shape. The structure was determined from single-crystal diffraction data. The MOF is stable up

to 300 °C in air and exhibits a moderate BET surface area of 650 m² g⁻¹. The material can be obtained as thin sheets of a few nanometer thickness. Single crystals were modified postsynthetically exploiting the intrinsic reactivity of the benzophenone group with C-H bond containing molecules. In this way, the surface properties of the MOF crystals (e.g. dispersibility in different solvents) can be changed drastically. Delamination and adaptation of the surface chemistry open up novel ways for shaping MOFs, e.g. for the incorporation into polymer composites, and pave the way for various applications.



Introduction

Metal-organic frameworks (MOFs), also known as porous coordination polymers, have been extensively studied during the last two decades as one of the most promising porous materials. Especially the possibility to combine different metal cations as nodes with organic molecules as linkers to tailor properties like surface area, pore size, pore dimensions, but also thermal stability, chemical stability and functionality, is a great advantage in comparison to other materials.^[1-3] This variety

of properties enables a wide range of possible applications^[4] like catalysis,^[5] sensing,^[4] gas storage and separation,^[5] drug delivery systems^[6] or imaging.^[6,7] The properties of MOFs can further be modified by postsynthetic modification. This is usually performed on specific functionalities of the organic linker molecules like amino, alkyne, azide or halide groups, by click chemistry or directly at the inorganic building unit.^[8,9]

In spite of the various possibilities to adapt the properties of MOFs, near-term prospects for commercial applications remain limited. Only a few MOFs are already commercially available and have been integrated in applications.^[10] Major blocks on the road to further applications lie in the lacking processability of typical MOF substances, consisting of powders of brittle microcrystals. Ways to circumvent this issue have been summarized under the term “shaping”, which involves the processing into various forms or constructions which are suitable for applications.^[11] One prerequisite for many of these shaping procedures is the availability of well-defined (nano-)crystals of uniform size and shape. For some MOFs, the modulation approach has proven as an effective means to provide these features.^[12–14] Another prerequisite for efficient processing, e.g. for designed dispersibility in different solvents, for control of aggregation properties or for tailored interactions with polymers, is the adaptation of the surface chemistry of MOFs, including properties like polarity, hydrophobicity/hydrophilicity or surface charge.^[15] Surface modification has, for example, been achieved by the adsorption of polymers which, however, may detach from the surface. A covalent attachment of molecules to surface-standing linker molecules would be more reliable.

In this study the linker benzophenone-4,4'-dicarboxylic acid (H_2bzpdc) (Figure 1) was chosen due to the possibility for postsynthetic modification at the photoreactive keto group. The first metal-organic framework reported in the literature containing this linker molecule is CAU-8 with Al^{3+} as metal cation.^[16,17] Further investigations indicated a possible postsynthetic modification of the framework performed on the keto group of the linker molecule.^[16]

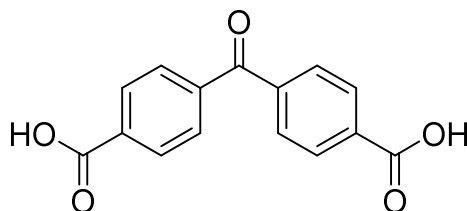


Figure 1. Benzophenone-4,4'-dicarboxylic acid used as linker molecule for the synthesis of Zr-*bzpdc*-MOF.

In this contribution we report the synthesis of the new metal-organic framework ($Zr_6O_4(OH)_6(HCO_2)_2(bzpdc)_4$) at gram scale-and introduce two interesting features of

this material which are of relevance for further processing. The choice of zirconium for the metal centres is caused by the high thermal and chemical stability of many Zr-based MOFs, which is a basic requirement for many applications.^[18] The approach we used to synthesize the metal-organic framework was the modulated synthesis procedure, consisting in adding monocarboxylic acids like formic acid or benzoic acid to the synthesis solution, in many cases the only way to reliably obtain crystalline Zr-based metal-organic frameworks.^[12,13,19] The first feature of interest is based on the two-dimensional structure and the resulting possibility to delaminate microcrystals of the material into extended sheets with a thickness of only few nanometers down to monolayers. The accessibility of such sheets could lead to interesting properties for applications like membranes,^[20] dielectrics^[21] or two-dimensional heterostructures.^[22] The second feature is related to the benzophenone keto group of the linker molecule, which can form a biradical when exposed to UV light. This reactive form of the linker is able to react with any molecule containing C–H bonds, resulting in the formation of stable covalent C–C bonds.^[23,24] According to the structure of the *Zr-bzpd*c-MOF, these keto groups are exposed at the surface of the largest faces of the crystals, thus allowing for efficient and stable postsynthetic photochemical modification for regulating the surface properties.

Results and Discussion

Synthesis

The modulation approach,^[12] here employing formic acid as modulator, was used to generate crystalline *Zr-bzpd*c-MOF. The MOF was obtained in the $\text{Zr}^{4+}/\text{H}_2\text{bzpd}$ c/formic acid/DMF/ H_2O system by systematic parameter variation of reactant molar ratios, concentration, temperature and duration of synthesis (Supporting Information). As shown exemplarily in Figure 2, the parameter space for the formation of this MOF is quite restricted, affording concentrations of the modulator between 100 and 200 eq and reaction times longer than 24 h. Another porous unknown phase was obtained when a combination of formic acid and sodium formate is used as modulator (Supporting Information). Noteworthy, experiments with other modulators like acetic acid, propionic acid and benzoic acid were carried out but did not lead to a crystalline material (Supporting Information). In addition to the concentration of the modulator formic acid, the reaction temperature and the reaction time are important parameters in the synthesis of the novel *Zr-bzpd*c-MOF.

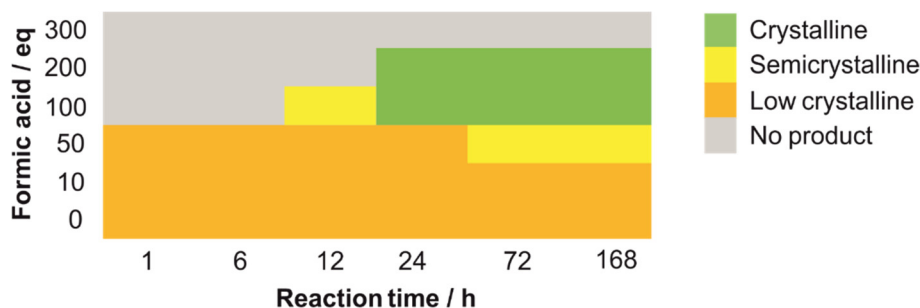


Figure 2. Variation of the synthesis parameters concentration of modulator formic acid and reaction time (reaction temperature $T = 120\text{ }^{\circ}\text{C}$). Highly crystalline Zr-*bzpdC*-MOF was obtained in the green region.

The PXRD patterns assembled in Figure 3 display the structural evolution of the Zr-*bzpdC*-MOF with increasing amount of formic acid. As is often observed,^[12,13] small amounts of modulator lead to non-crystalline products or samples with low crystallinity. Only for products obtained with formic acid concentrations larger than 100 eq, distinct reflections on a low scattering background can be observed. Figure 3 also displays the theoretical reflections which were calculated on the basis of the crystal structure determination. Noteworthy, the PXRD of the sample prepared with 100 eq FA shows only one (weak) reflection at ca. 7° whereas for samples prepared with higher modulator concentrations, two peaks are observed in this region of the diffractogram. This may indicate the presence of a minor impurity in those samples or to slight variations in the structure of samples which were prepared with different amounts of modulator.

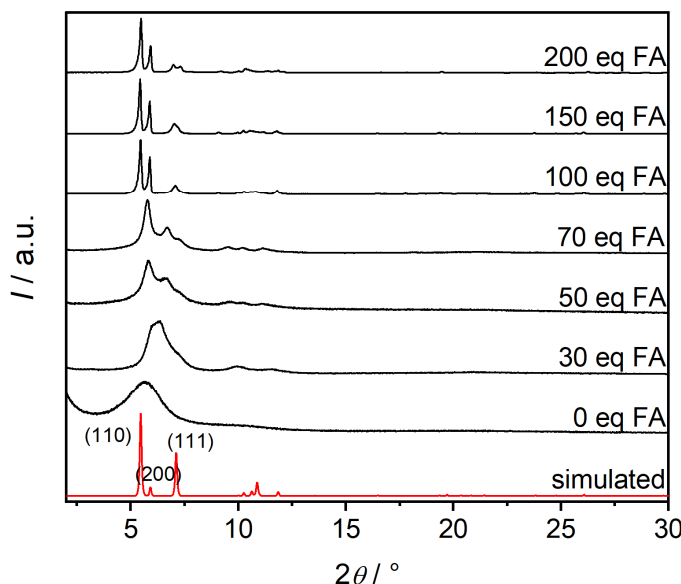


Figure 3. Influence of modulator concentration on reaction product. PXRD patterns of synthesis products prepared with different amounts of formic acid added to the synthesis solution (synthesis temperature: $120\text{ }^{\circ}\text{C}$, synthesis duration: 24 h); simulated XRD pattern based on crystal structural data are given in red.

Scanning electron microscopy corroborates the distinction between the sample prepared with 100 eq of FA and samples prepared with higher modulator concentrations, as morphological differences between the crystals formed can be observed. The sample synthesized with 100 eq formic acid consists of rhombic crystals which exhibit a platelet morphology (Figure 4, left), in agreement with the layered structure of the *Zr-bzpd*c-MOF (see below). The synthesis with 200 eq of formic acid leads to more isometric crystals with a clearly distinct morphology (Figure 4, right). All results described below therefore refer to samples synthesized with a modulator amount of 100 eq, except for the crystal structure determination.

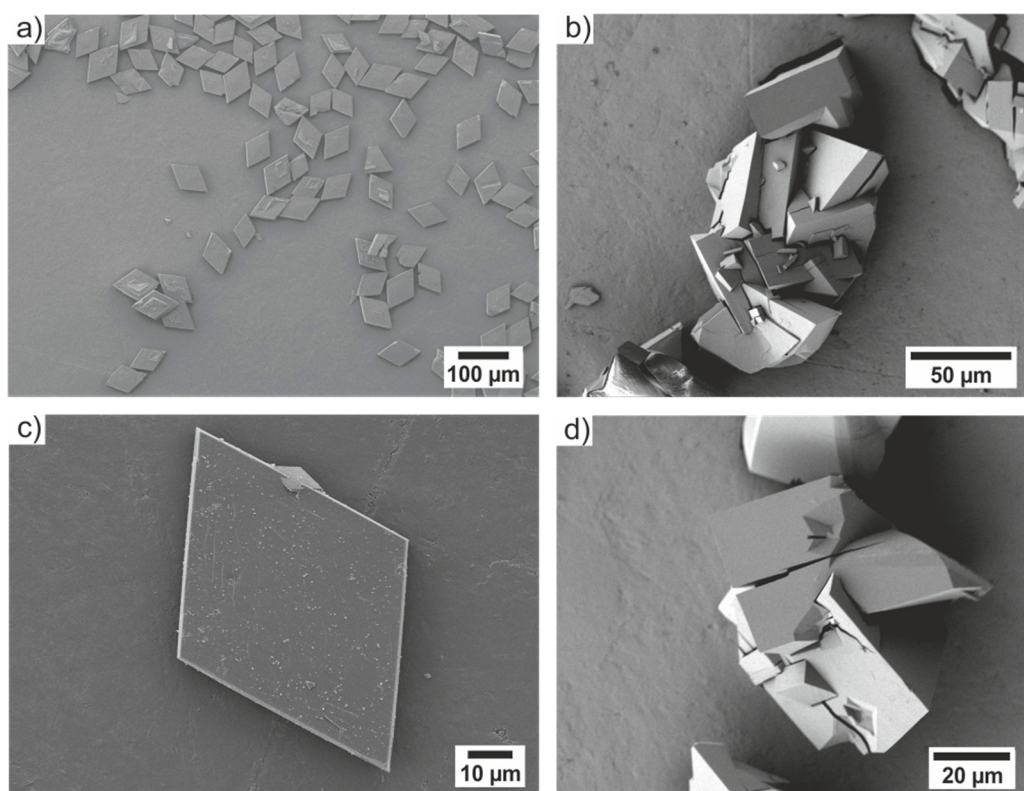


Figure 4. SEM micrographs of the products of syntheses of *Zr-bzpd*c-MOF carried out in the presence of (a,c) 100 eq and (b,d) 200 eq of modulator formic acid. Note the different morphologies of the crystals. A single crystal like the one shown in c) was used for single crystal structure determination.

Crystal structure model

Several suitable single crystals (Figure 4a) were selected from syntheses with 100 eq formic acid (FA) as modulator and were measured on the single-crystal diffractometer. The structure determination was difficult due to the small thickness of the rhombic shaped crystals of about 5-10 μm . Further information about the crystal structure investigation and evaluation is presented in the Supporting Information.

Despite of the difficulties, it was possible to derive a reasonable crystal structure model of the Zr-*bzpd*c-MOF in an orthorhombic crystal system with the space group *Cmcm* and lattice parameters of $a=29.86$ Å, $b=19.25$ Å, $c=19.40$ Å. Several views of the crystal structure are shown in Figure 5.

The structure consists of $Zr_6O_4(OH)_4$ octahedra which are typical of many structures of Zr-based MOFs and can be up to twelvefold coordinated. Here, these inorganic building units (IBUs) are eightfold coordinated by linker molecules. IBUs and linkers span a two-dimensional rhombic structure. The proposed structure and further data (TGA, NMR, see below) indicate that of the eight remaining coordination sites, six are capped with hydroxyl groups and two sites are coordinated by formate molecules. The basic motif of the structure is a building block within which two IBUs are bridged through two linker molecules via their carboxylate groups. The periodic connection in the *ab*-plane results in a two-dimensional rhombic grid. The distance between two IBUs in the basis rhombus is ca. 18 Å, the internal angle of the rhombus is 114.4°. Such rhombic layers are stacked along the *c* direction. The layers are interlocked with each other so that the keto groups point into hollow regions of the next layer. The AB stacking of the rhombic layers generates one-dimensional pore channels with rhombic shape with a diameter of about 8 Å. There are no linker molecules interconnecting the IBUs of different layers with each other. Note that the internal angle of the basic rhombus (114.4°) fits very well with the angle observed on the rhombic-shaped microcrystals of around 115° (Figure 5). In high-resolution TEM images, lattice planes are observable. Their distance of about 15 Å matches half of the lattice constant *b* with about 14.93 Å (Figure 5); also, lattice planes producing an angle of 114.8° can be observed. These observations further corroborate the correctness of the crystal structure model. In the structure described, each IBU is coordinated by eight linker molecules. The IBU, however, offers twelve ligand sites. The structure investigation does not allow any conclusions to be drawn about the situation at the remaining four ligand sites. However, additional investigations described below yield a reasonably complete view of the structure.

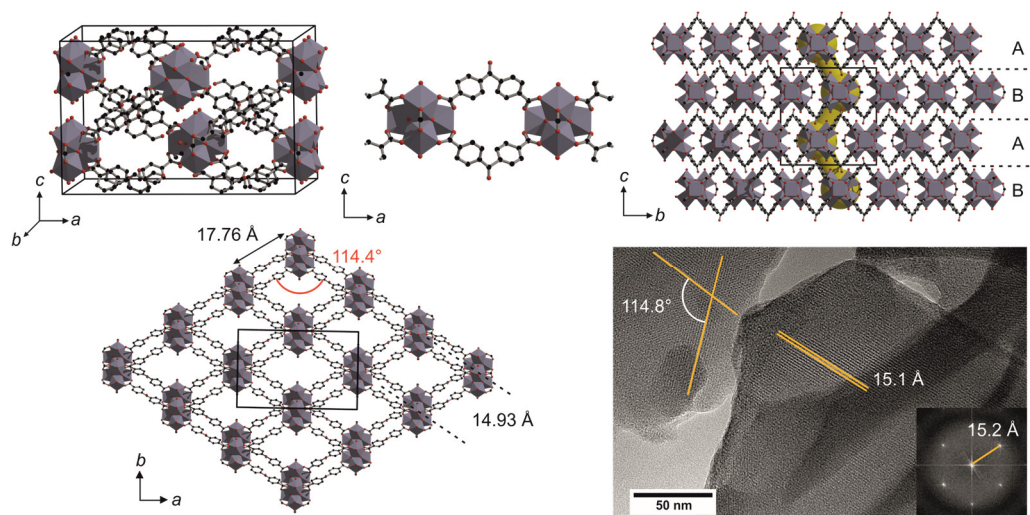


Figure 5. Crystal structure model of the Zr-*bzpdC*-MOF. Top left: unit cell. Top centre: two IBUs and their interconnection. Top right: view of the crystal structure along the *a* axis; the stacking of the two-dimensional layers and the shape of a pore along the *c* axis are indicated (yellow channel). Bottom left: view of the crystal structure along the *c* axis showing an A and a B layer which span a rhombic substructure, characteristic dimensions of which are given; the elliptical shape of the pores in the *a*-*b*-plane can be seen. Bottom right: the TEM image with the corresponding diffraction pattern as inset reveals distances characteristic of the rhombic layer substructure.

Chemical stability, thermal properties and composition

The Zr-*bzpdC*-MOF is hydrolytically stable in acidic and basic media. Only under harsh conditions ($\text{pH} < 3$ or $\text{pH} > 11$), structural collapse occurs (further information is given in Supporting Information).

The thermal behaviour of the Zr-*bzpdC*-MOF was investigated via TGA/DTA (Figure 6, left) and temperature-dependent X-ray diffraction (TD-XRD, Figure 6, right). The TD-XRD shows a decrease of crystallinity at 300 °C whereas the thermogravimetric measurement shows a major mass loss only above a temperature of ca. 400 °C, indicating that the framework of the Zr-*bzpdC*-MOF collapses before its components are combusted. Assuming that the first mass loss of 21.8% up to 400 °C is due to the removal of guest molecules, the decomposition of the framework delivers a mass loss of 62.5% and an inorganic residue (ZrO_2) of 37.5%. This does not agree with a formula $\text{Zr}_6\text{O}_4(\text{OH})_8(\text{bzpdC})_4$ (calculated contents: linker: 60.8%; residue: 39.2%), but very well with the composition $\text{Zr}_6\text{O}_4(\text{OH})_6(\text{HCO}_2)_2(\text{bzpdC})_4$ (linker: 62.8%; residue: 37.2%), which contains formate ligands.

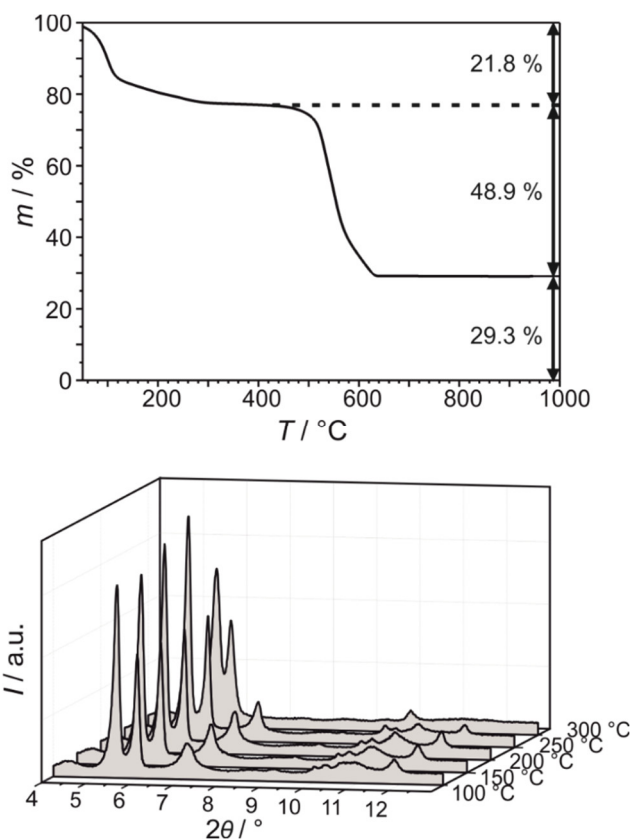


Figure 6. top: Thermogravimetric analysis of Zr-*bzpdC*-MOF; bottom: temperature-dependent powder X-ray diffraction.

To further confirm the presence of formate anions in the crystal structure of the Zr-*bzpdC*-MOF, a sample of the MOF was dissolved and ^1H NMR spectra were recorded on the solution. The signal of the H-COOH proton of formic acid could be clearly observed (Supporting Information). Quantitative evaluation agrees with a molar ratio of 2:1 of linker molecules related to formic acid. Based on these results, the coordination of two formate molecules per IBU in the framework appears very likely. This incorporation of formate molecules into the framework necessitates the modulation of the synthesis with formic acid, and can explain the finding that in the presence of other modulators, like the often-used acetic acid or benzoic acid, the crystallization of the Zr-*bzpdC*-MOF could not be observed. Closer inspection of the crystal structure reveals that the space where the formate molecules are located is limited and does not offer enough space for larger ligands. Combining the results from X-ray crystallography, thermogravimetry and ^1H NMR spectroscopy, the idealized chemical composition of the Zr-*bzpdC*-MOF is formulated as $\text{Zr}_6\text{O}_4(\text{OH})_6(\text{HCO}_2)_2(\text{bzpdC})_4$.

In the TD-XRD experiment, no loss of crystallinity and no structural changes are observed below 250 °C. At 300 °C, the 111 reflection disappears and the first two reflections (110, 200) shift slightly to larger angles (see Supporting Information).

These observations indicate the loss of defined interlayer relations and of three-dimensional order at elevated temperatures; also, a slight relaxation of the in-plane structure of the two-dimensional layers can be discerned.

Physisorption properties

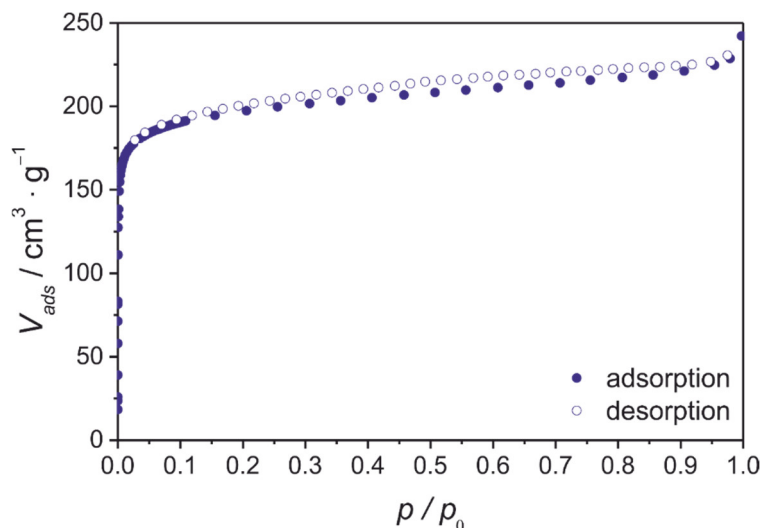


Figure 7. Physisorption isotherm measured with Ar at 87 K.

A physisorption measurement at 87 K with argon as adsorbate (Figure 7) shows a type I(a) isotherm, typical for microporous materials with relatively small amount of external surface and mainly narrow micropores (<1 nm). The MOF exhibits a moderate porosity with a BET area of about $650 \text{ m}^2 \cdot \text{g}^{-1}$. The pore volume is about $0.5 \text{ cm}^3 \cdot \text{g}^{-1}$. Analysis of the pore size distribution (Supporting Information) gives an indication of micropores <1 nm but at such small pore sizes, no meaningful results for the pore size distribution can be derived from Ar sorption.

Delamination

The pronounced layered nature of the structure of *Zr-bzpd*c-MOF and the observation that the interactions between the layers can be partly overcome by increasing the temperature indicate that it might be possible to delaminate *Zr-bzpd*c-MOFs into individual layers or very thin platelets and to generate dispersions of the resulting nanoobjects which would be very interesting with regard to shaping MOFs for specific applications. Therefore, we carried out attempts to delaminate the *Zr-bzpd*c-MOF. The best result was obtained by ultrasonication of the MOF first directly in the mother liquor and subsequently in 2-propanol for several hours. SEM and TEM images of the delaminated *Zr-bzpd*c-MOF are shown in Figure 8.

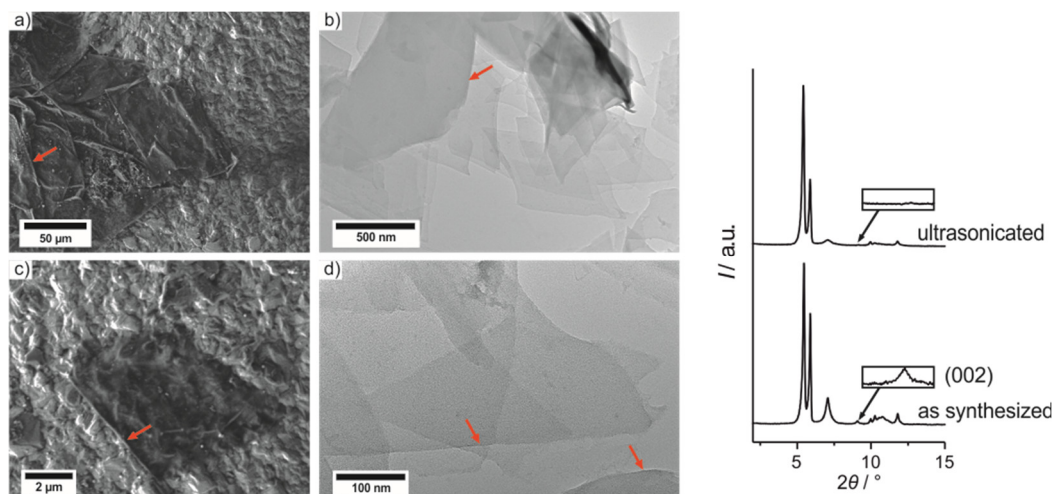


Figure 8. a,c) SEM images of delaminated sheets of Zr-*bzpd*-MOF on a Cu grid; b,d) TEM images of the same sample. Right: PXRD patterns of Zr-*bzpd*-MOF as-synthesized compared with a delaminated sample; inset: region of the 002 reflection (enlarged TEM and SEM images in Supporting Information).

Thin rhombic shaped crystals with diameters of about 5 to 50 μm could be observed in the SEM images. The rough copper surface of the carrier material is visible through the particles, which indicates a thickness of maximally a few layers of the MOF. TEM images also show single sheets with diameters in the μm range and, globally, rhombic shape. Note that the platelets often do not show sharp edges, but exhibit corrugations. In some cases, it appears that the edges have rolled up (arrows). The regular difference in contrast observed on superimposed sheets (numbered as 1, 2, 3, 4 in Figure 8d) indicates that layers with identical thickness have stacked on top of each other, suggesting that in fact Zr-*bzpd*-MOF monolayers (or AB-stacked bilayers) are present. However, it was not possible to extract height information from these data. PXRD patterns still show many reflections resembling those of the three-dimensional crystalline Zr-*bzpd*-MOF, proving that basic structural motifs are still present. However, the 002 reflection is not visible anymore after delamination, suggesting the loss of crystallinity in the third dimension, i.e. the stacking of the layers. This together with the observations in the SEM and TEM images indicates the successful delamination of the Zr-*bzpd*-MOF into thin sheets or even monolayers.

In order to determine the thickness of the sheets we conducted AFM measurements on samples which were prepared by dip-coating silica-terminated Si-wafers from the isopropanolic suspension of the delaminated Zr-*bzpd*-MOF (Figure 9). The particles which were found by AFM have thicknesses of 2-10 nm and thus consist of two to a few monolayers. Larger particles present steps on their facets (Figure 9) with heights of ca. 0.9 nm, in good agreement with the thickness of an individual layer as observed in the crystal structure of the Zr-*bzpd*-MOF. Also, isolated particles with a thickness

of 2 nm are observable. This corresponds to particles consisting of bilayers, i.e. two monolayers.

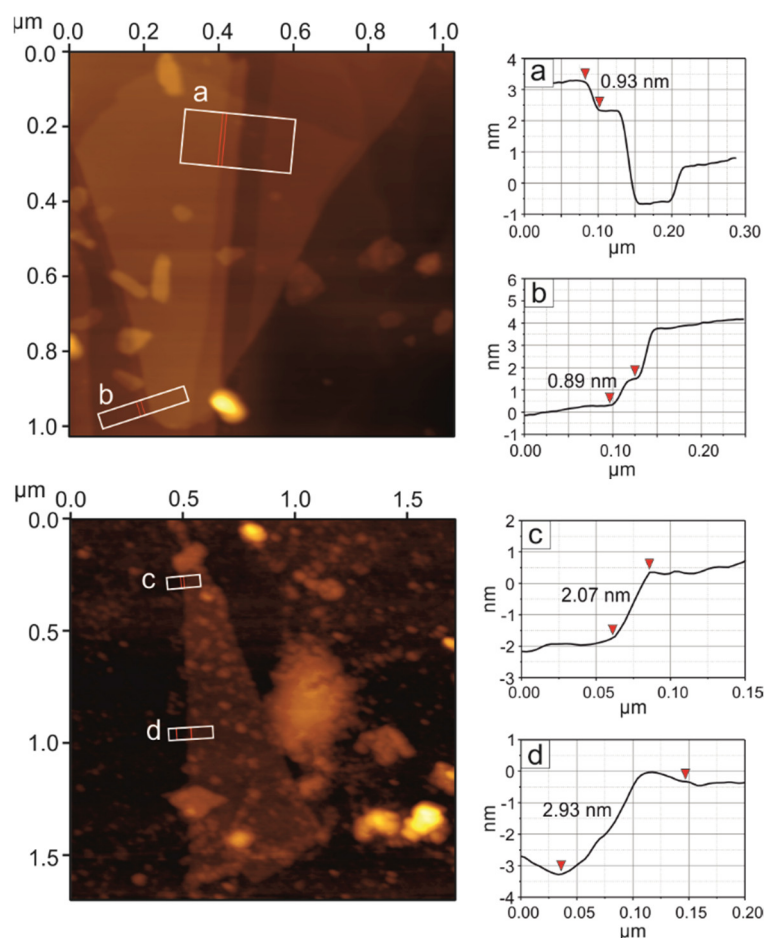


Figure 9. AFM measurements of Zr-*bzpdC*-MOF. Top: thin particle with stepped faces at the edges; height determinations are provided for two different facets. Bottom: Isolated thin sheet with height determination at two different positions.

In summary, the delamination of Zr-*bzpdC*-MOF by ultrasonication in isopropanol leads to thin sheets made up of one to a few (ca. <10) Zr-*bzpdC*-MOF layers and with diameters of several μm .

Postsynthetic modification

The photoreactive keto group of benzophenone-4,4'-dicarboxylate is able to form covalent bonds upon irradiation with UV light with any substance containing a C-H bond.^[23,24] The mechanism is schematically shown in Figure 10. For the intended post-synthetic modification of the Zr-*bzpdC*-MOF at the photoreactive keto groups of the linker molecules, accessibility and low steric hindrance of these groups is a prerequisite. In the crystal structure, the keto groups are directed orthogonally to the *ab*-plane and thus are available for photochemical reactions at the outer surface of

the particles (Figure 10). For monolayers, all keto groups should be accessible for postsynthetic modifications (PSMs).

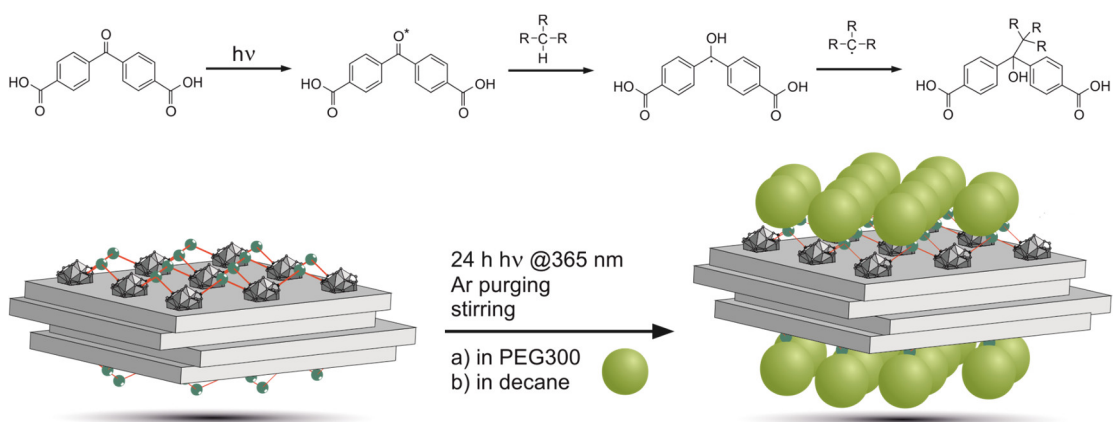


Figure 10. Top: Schematic mechanism for the photoreaction of the keto group of H_2bzpdC : formation of a ketyl radical and, subsequently, of a covalent bond with any substance containing a C-H bond.^[23] Bottom: Scheme depicting the photochemical postsynthetic modification of the outer surfaces of Zr- $bzpdC$ -MOF crystals.

Baldovi *et al.*^[16] had already shown the photochemical reactivity of the keto group in CAU-8 with acetonitrile and ethanol. In the present study, PEG300 and decane were chosen as reactants for model reactions to demonstrate the accessibility of the keto groups at the outer surface for large molecules and the possible postsynthetic modification of the surface. Surface functionalization with PEG300 should lend the crystals a hydrophilic character, whereas decane should lead to hydrophobisation of the particle surface.

Suspensions of the MOF in the neat polymer or alkane were irradiated with UV light. During the reaction, the mixtures were purged with argon, because oxygen molecules present could otherwise quench the ketyl radicals, thus preventing the reaction with the C-H bonds of the reactant. The photochemically treated sample was dried under reduced pressure and analyzed with infrared spectroscopy and physisorption measurements. As a control, the MOF and the reactants were treated for the same time under equivalent conditions, but without UV irradiation. Upon starting the irradiation of the MOF suspensions, the colour of the suspensions changed from slightly yellow to green-bluish, which is an indication for ketyl radical formation. After 24 hours irradiation the colour of the suspension and of the resulting solid changed to yellow. IR spectra and physisorption measurements indicate a successful covalent attachment of PEG300 and decane at the Zr- $bzpdC$ -MOF particles (Figure 11). In addition, the properties imparted by the surface modification were visualized by the distribution of the particles in hydrophilic and hydrophobic solvents (Figure 11).

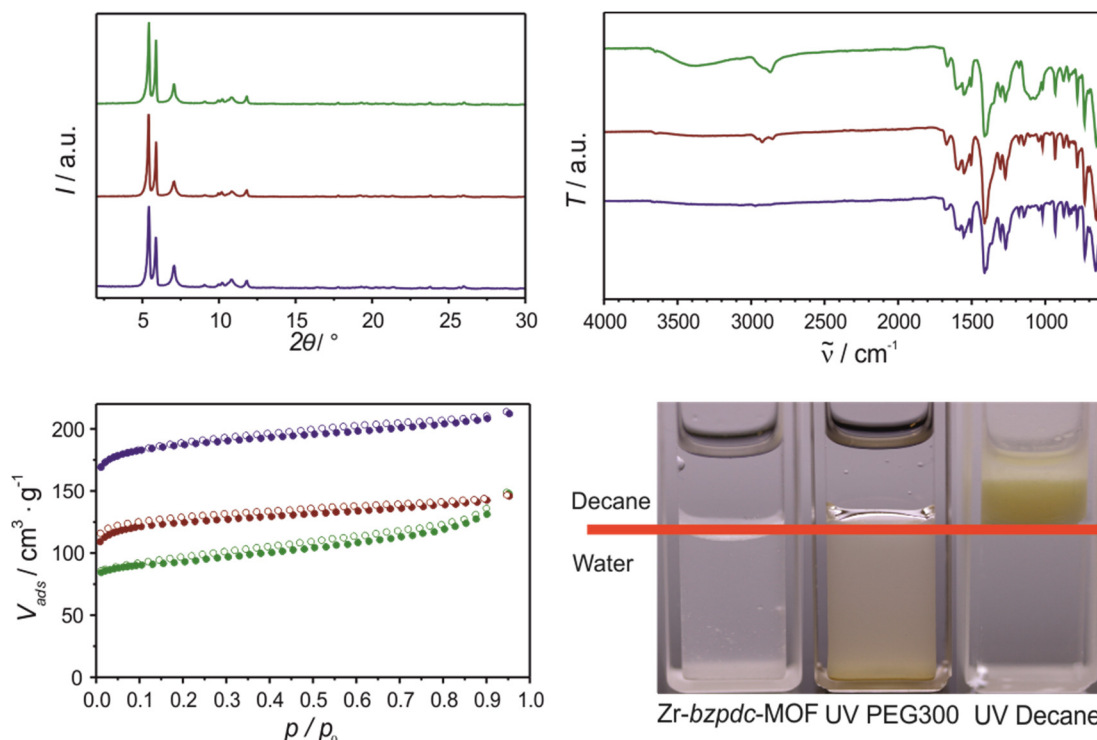


Figure 11. Characterisation of Zr-*bzpdC*-MOF (blue) and postsynthetically modified samples, with decane (red) and PEG300 (green). Top left: PXRD patterns show no differences in crystallinity. Top right: IR spectra of the postsynthetically treated samples show characteristic C–H valence vibration bands in the region between 2800–3000 cm^{-1} . Bottom left: Nitrogen physisorption measurements show that a moderate porosity is still accessible after PSM. Bottom right: The Zr-*bzpdC*-MOF and its postsynthetically modified derivatives exposed to a water/decane two-phase system; Zr-*bzpdC*-MOF and its PEG derivative collect in the water phase and sediment on the bottom of the container; in contrast, the decane-reacted MOF collects in the decane phase, showing a drastic change in the surface properties of the MOF.

The photochemical reaction does not incur any changes in the PXRD patterns, showing first of all that the MOF is basically stable under the reaction conditions. In case of the UV-treated sample, the IR spectra show vibrational bands of C–H groups in the region between 2800–3000 cm^{-1} which can clearly be assigned to the presence of PEG or decane residues. As the photochemical reaction is accompanied by a change in hybridization of the keto- sp^2 -C to a sp^3 -C atom, structural changes should occur in the MOF layer structures. The fact that no differences are observed in the PXRD patterns (Figure 11 bottom left) indicates that the reaction has occurred only at the surface of the MOF particles. Probably, the large PEG300 and decane molecules cannot enter the pore system. This is in line with the results of the physisorption measurements. The BET areas decrease from about 650 $\text{m}^2\cdot\text{g}^{-1}$ to 250–350 $\text{m}^2\cdot\text{g}^{-1}$ after PSM and the accessible pore volume is decreased to nearly half. Thus, a total blocking of the pores by immobilized reactants is avoided, resulting in a still moderate porosity of the MOF after PSM which can be used for further applications.

The successful attachment and immobilization of PEG300 residues at the surface was further substantiated by results from ^1H and ^{13}C NMR spectra which were measured on a dissolved sample (see Supporting Information). After PSM, alkylic carbon atoms and protons are observable. Also, the coupling of the protons of the aromatic ring ($\delta\sim 7.5\text{-}8.5$ ppm) shows some differences compared to the untreated sample, although only a small amount of surface-standing molecules were postsynthetically modified. To visualize the consequences of the surface-limited PSM reaction, Figure 11 (bottom right) shows the distribution of particles of the *Zr-bzpd*c-MOF and its postsynthetically modified derivatives between a polar and a nonpolar solvent, i.e. between water and decane. Due to their hydrophilic surfaces, the *Zr-bzpd*c-MOF and the PEG300-modified sample show a good dispersibility in water, whereas the particles modified with decane prefer to disperse in the nonpolar organic phase. The used PSM thus allows for a phase transfer of the particles. Together with the general applicability of the used photochemical reaction, these results show that the postsynthetic photoreaction can be used to tailor the surface properties.

Conclusions

We present a new Zr-based metal-organic framework containing a V-shaped linker molecule featuring a photoreactive keto group. The new *Zr-bzpd*c-MOF is one of a few examples for a two-dimensional porous metal-organic framework and shows interesting properties. Specifically, the *Zr-bzpd*c-MOF can be delaminated into thin sheets and the MOF surface can be selectively modified using the benzophenone-based photoreaction. Noteworthy, the benzophenone photoaddition is universally applicable to organic compounds containing a C-H bond, thus allowing for nearly any desired surface modification; also, benzophenone moieties can act as photoinitiators, offering the prospect of grafting-from radical polymerization reactions. Both features – the possibility to prepare thin sheets and the adaptation of the surface chemistry – are helpful in the shaping of MOFs. Furthermore, the MOF features a high thermal and chemical stability and provides moderate specific surface area even after modification of its surface.

Experimental Section

Materials. Zirconium(IV) oxychloride octahydrate, formic acid, acetic acid, propionic acid, benzoic acid, decane, polyethylene glycol 300 (PEG300) and *N,N*-dimethylformamide (DMF) were purchased from Sigma Aldrich. 2-Propanol and ethanol were purchased from Roth and benzophenone-4,4'-dicarboxylic acid from abcr Chemicals. All chemicals were used without further purification.

Instrumentation. X-ray powder diffraction measurements were performed at room temperature using a STOE STADI-P transmission diffractometers equipped with curved Ge(111) monochromators with $\text{CuK}\alpha_1$ radiation ($\lambda = 1.540594 \text{ \AA}$) and a linear position-sensitive detector. The samples were fixed between X-ray amorphous foils or in thin-walled glass capillaries for temperature-dependent measurements.

Single crystal X-ray diffraction data were obtained on a BRUKER KAPPA Apex II diffractometer at 233 K. The procedure is in detail described in the Supporting Information.

Scanning electron microscopy was carried out with a JEOL JSM-6700F (2 kV). For transmission electron microscopy, a FEI Tecnai G2 F20 TMP was used in bright field mode (200 kV). For sample preparation, the Zr-*bzpd*c-MOF was dispersed in 2-propanol via ultrasonication and the resulting dispersions were dropped on a 400-mesh carbon coated Cu-grid and dried under reduced pressure. Liquid-phase ^1H and ^{13}C NMR spectra were measured on a BRUKER instrument at 400 MHz and were analyzed with ACD NMR Processor 12. Sorption isotherms were measured at an Autosorb 1 (Ar@87 K) and an Autosorb 3 (N₂@77 K) instrument by Quantachrome and were evaluated with the software ASiQwin 2.0 by Quantachrome. BET surface areas of the microcrystalline products were calculated via the BET assistant of the ASiQwin software in a range of $p/p_0 = 0.005 - 0.03$ for nitrogen physisorption measurement at the Autosorb 3 instrument and in a range of $p/p_0 = 0.0005 - 0.03$ for argon physisorption measurement at the Autosorb 1 instrument, respectively. For the determination of the pore size distribution, the Kernel “Ar at 87 K_zeolites/silica (cylinder. Pores, NLDFT equ.)” of the ASiQwin 2.0 software was used. FT-IR data were recorded in transmission mode on a BRUKER Tensor 27 instrument. TGA data were obtained at a NETZSCH STA 409PC/PG instrument with a heating rate of $10 \text{ K}\cdot\text{min}^{-1}$ with a gas flow of 80% argon and 20% oxygen. Sonication of dispersions was performed with a BANDELIN Sonotex Digirec ultrasonic bath at room temperature with a peak output of 1200 watt. Atomic force microscopy investigations were performed with a BRUKER Multimode II with a J-type scanner under ambient conditions.

Synthesis of $(\text{Zr}_6\text{O}_4(\text{OH})_6(\text{HCO}_2)_2(\text{bzpd})_4)$. Solvothermal syntheses were carried out in Teflon-sealed screw cap glass vessels. The synthesis of the Zr-*bzpd*c-MOF was investigated by varying reaction parameters like temperature, reaction time, modulator, concentration and the molar ratio of the precursors (Supporting Information). Favourable conditions are as follows: 0.165 g (0.517 mmol) $\text{ZrOCl}_2\cdot 8 \text{ H}_2\text{O}$ were dissolved in 20 mL DMF. After adding between 1.95 mL up to 3.90 mL formic acid (100 up to 200 molar equivalents (eq) based on the amount of Zr^{4+}) and 0.279 g (0.517 mmol) H_2bzpd , the clear solution was transferred to a 100 mL Teflon-sealed glass vessel and was kept at $120 \text{ }^\circ\text{C}$ for 72 h in a circulating air

oven. After the reaction, the glass vessel was cooled down to room temperature. The resulting solid was centrifuged and washed once with 20 mL of DMF and twice with 20 mL ethanol.

For further investigations, part of the product was further purified via Soxhlet-extraction with ethanol for 24 hours. The white powder was kept under reduced pressure. When applying the delamination procedure, the whole synthesis solution was used without any further treatment.

Delamination procedure. For delamination, the crystalline *Zr-bzpd*-MOF was treated with ultrasonication for 1 hour in the synthesis solution. Afterwards the product was washed three times with 2-propanol. The centrifuged solid was dispersed in 20 mL of 2-propanol and ultrasonicated for 6 hours. The dispersion was left standing for 16 hours to let larger particles sediment. Finally, the supernatant was decanted off from the sedimented slurry and used for further investigations.

Postsynthetic modification. Postsynthetic modification was carried out with polyethylene glycol 300 (PEG300) and decane. For the photochemical modification a mixture of 5 mL of the solvent and 50 mg of the bulk material was sonicated in an ultrasonic bath for 10 minutes at room temperature. After transferring the suspension into a quartz glass cuvette, it was purged with argon for the whole irradiation period. The stirred suspension was treated under UV light at 365 nm wavelength (UV-LED: epiSPOT UV 365 nm by epi-light, radiance ca. 100 mW cm⁻²) for 24 hours. The resulting yellow solid was centrifuged and Soxhlet-extracted with ethanol for 24 hours to remove unbound molecules. Afterwards the product was dried under reduced pressure at room temperature for 24 hours for further investigations.

Acknowledgements

We thank Hendrik A. Schulze and Dr. Bastian Hoppe, for preparing the electron microscopic images, and Dr. Michael Wiebcke for X-ray diffraction measurements and expertise. Also, we thank the Institut für Organische Chemie at the Leibniz Universität Hannover for performing NMR spectroscopy measurements.

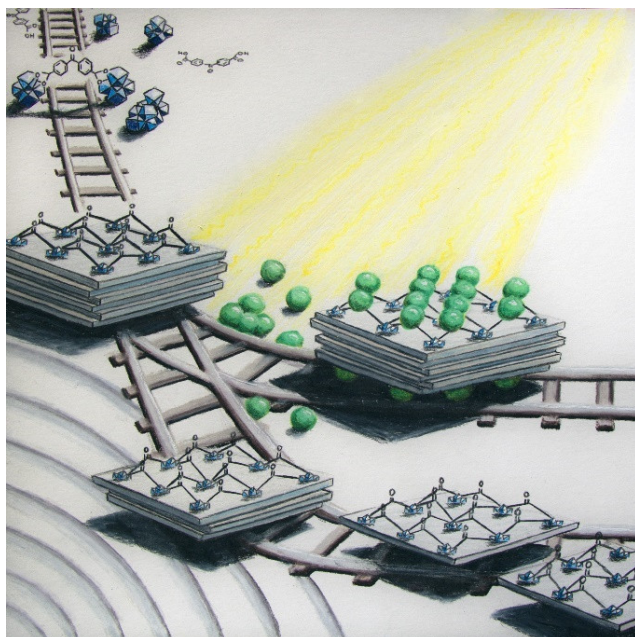
Keywords: Zr-based MOF, modulation, postsynthetic modification, delamination, benzophenone

References

- 1 S. Kitagawa, R. Kitaura, S.-i. Noro, *Angew. Chem. Int. Ed.* **2004**, *43*, 2334; *Angew. Chem.* **2004**, *116*, 2388; b) O. M. Yaghi, M. O'Keeffe, N. W. Ockwig, H. K. Chae, M. Eddaoudi, J. Kim, *Nature* **2003**, *423*, 705; c) O. M. Yaghi, G. Li, H. Li, *Nature* **1995**, *378*, 703; d) G. Férey, *J. Solid State Chem.* **2000**, *152*, 37.
- 2 H. Furukawa, K. E. Cordova, M. O'Keeffe, O. M. Yaghi, *Science* **2013**, *341*, 1230444.
- 3 a) D. Farrusseng, S. Aguado, C. Pinel, *Angew. Chem. Int. Ed.* **2009**, *48*, 7502; *Angew. Chem.* **2009**, *121*, 7638; b) J. Lee, O. K. Farha, J. Roberts, K. A. Scheidt, S. T. Nguyen, J. T. Hupp, *Chem. Soc. Rev.* **2009**, *38*, 1450.
- 4 L. E. Kreno, K. Leong, O. K. Farha, M. Allendorf, R. P. van Duyne, J. T. Hupp, *Chem. Rev.* **2012**, *112*, 1105.
- 5 a) Z. R. Herm, E. D. Bloch, J. R. Long, *Chem. Mater.* **2014**, *26*, 323; b) A. R. Millward, O. M. Yaghi, *J. Am. Chem. Soc.* **2005**, *127*, 17998; c) M. P. Suh, H. J. Park, T. K. Prasad, D.-W. Lim, *Chem. Rev.* **2012**, *112*, 782; d) J.-R. Li, J. Sculley, H.-C. Zhou, *Chem. Rev.* **2012**, *112*, 869.
- 6 P. Horcajada, C. Serre, M. Vallet-Regi, M. Sebban, F. Taulelle, G. Férey, *Angew. Chem. Int. Ed.* **2006**, *45*, 5974; *Angew. Chem.* **2006**, *118*, 6120.
- 7 a) Y. Chen, C. Tan, H. Zhang, L. Wang, *Chem. Soc. Rev.* **2015**, *44*, 2681; b) P. Horcajada, T. Chalati, C. Serre, B. Gillet, C. Sebrie, T. Baati, J. F. Eubank, D. Heurtaux, P. Clayette, C. Kreuz, J. S. Chang, Y. K. Wang, V. Marsaud, P. N. Bories, L. Cynober, S. Gil, G. Férey, P. Couvreur, R. Gref, *Nat. Mater.* **2010**, *9*, 172.
- 8 a) P. Deria, J. E. Mondloch, O. Karagiari, W. Bury, J. T. Hupp, O. K. Farha, *Chem. Soc. Rev.* **2014**, *43*, 5896; b) K. K. Tanabe, S. M. Cohen, *Chem. Soc. Rev.* **2011**, *40*, 498; c) S. M. Cohen, *Chem. Rev.* **2012**, *112*, 970; d) S. M. Cohen, *J. Am. Chem. Soc.* **2017**, *139*, 2855; e) W. Morris, C. J. Doonan, O. M. Yaghi, *Inorg. Chem.* **2011**, *50*, 6853; f) R. J. Marshall, R. S. Forgan, *Eur. J. Inorg. Chem.* **2016**, *2016*, 4310; g) F.-G. Xi, H. Liu, N.-N. Yang, E.-Q. Gao, *Inorg. Chem.* **2016**, *55*, 4701; h) B. Li, B. Gui, G. Hu, D. Yuan, C. Wang, *Inorg. Chem.* **2015**, *54* (11), 5139; i) Y. Zhang, B. Gui, R. Chen, G. Hu, Y. Meng, D. Yuan, M. Zeller, C. Wang, *Inorg. Chem.* **2018**, *57* (4), 2288.
- 9 a) P. Roy, A. Schaate, P. Behrens, A. Godt, *Chem. Eur. J.* **2012**, *18*, 6979; T. von Zons, L. Brokmann, J. Lippke, T. Preuße, M. Hülsmann, A. Schaate, P. Behrens, A. Godt, *Inorg. Chem.* **2018**, *57* (6), 3348.
- 10 a) U. Mueller, M. Schubert, F. Teich, H. Puetter, K. Schierle-Arndt, J. Pastré, *J. Mater. Chem.* **2006**, *16*, 626; b) M. Jacoby, *Chem. Eng. News* **2008**, *86*, 13.
- 11 a) B. Bueken, N. van Velthoven, T. Willhammar, T. Stassin, I. Stassen, D. A. Keen, G. V. Baron, J. F. M. Denayer, R. Ameloot, S. Bals, D. De Vos, T. D. Bennett, *Chem. sci.* **2017**, *8*, 3939; b) S. Furukawa, J. Reboul, S. Diring, K. Sumida, S. Kitagawa, *Chem. Soc. Rev.* **2014**, *43*, 5700; c) Y. Chen, X. Huang, S. Zhang, S. Li, S. Cao, X.

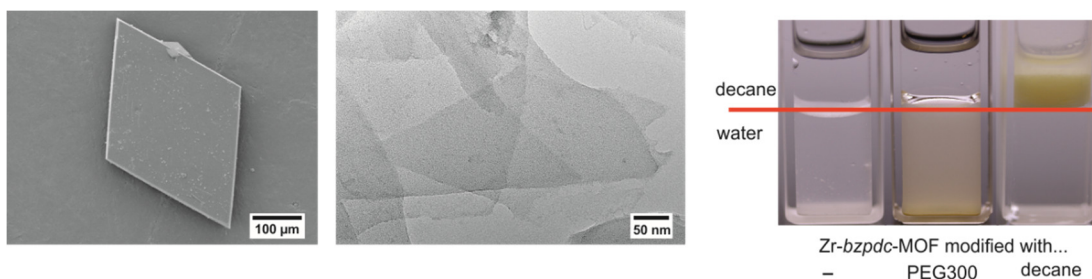
- Pei, J. Zhou, X. Feng, B. Wang, *J. Am. Chem. Soc.* **2016**, *138*, 10810; d) A. I. Spjelkavik, Aarti, S. Divekar, T. Didriksen, R. Blom, *Chem. Eur. J.* **2014**, *20*, 8973.
- 12 A. Schaate, P. Roy, A. Godt, J. Lippke, F. Waltz, M. Wiebcke, P. Behrens, *Chem. Eur. J.* **2011**, *17*, 6643.
- 13 G. Wißmann, A. Schaate, S. Lilienthal, I. Bremer, A. M. Schneider, P. Behrens, *Microporous Mesoporous Mater.* **2012**, *152*, 64.
- 14 M. Bosch, X. Sun, S. Yuan, Y.-P. Chen, Q. Wang, X. Wang, H.-C. Zhou, *Eur. J. Inorg. Chem.* **2016**, *2016*, 4368.
- 15 C. V. McGuire, R. S. Forgan, *Chem. Commun.* **2015**, *51*, 5199.
- 16 H. G. Baldovi, M. Krüger, H. Reinsch, M. Alvaro, N. Stock, H. Garcia, *J. Mater. Chem. C* **2015**, *3*, 3607.
- 17 H. Reinsch, M. Krüger, J. Marrot, N. Stock, *Inorg. Chem.* **2013**, *52*, 1854.
- 18 a) J. H. Cavka, S. Jakobsen, U. Olsbye, N. Guillou, C. Lamberti, S. Bordiga, K. P. Lillerud, *J. Am. Chem. Soc.* **2008**, *130*, 13850; b) B. Wang, X.-L. Lv, D. Feng, L.-H. Xie, J. Zhang, M. Li, Y. Xie, J.-R. Li, H.-C. Zhou, *J. Am. Chem. Soc.* **2016**, *138*, 6204; c) Y. Bai, Y. Dou, L.-H. Xie, W. Rutledge, J.-R. Li, H.-C. Zhou, *Chem. Soc. Rev.* **2016**, *45*, 2327.
- 19 a) T. Tsuruoka, S. Furukawa, Y. Takashima, K. Yoshida, S. Isoda, S. Kitagawa, *Angew. Chem. Int. Ed.* **2009**, *48*, 4739; *Angew. Chem.* **2009**, *121*, 4833; b) S. Diring, S. Furukawa, Y. Takashima, T. Tsuruoka, S. Kitagawa, *Chem. Mater.* **2010**, *22*, 4531; c) A. Schaate, S. Dühren, G. Platz, S. Lilienthal, A. M. Schneider, P. Behrens, *Eur. J. Inorg. Chem.* **2012**, *2012*, 790.
- 20 a) Y. Peng, Y. Li, Y. Ban, W. Yang, *Angew. Chem. Int. Ed.* **2017**, *56*, 9757; *Angew. Chem.* **2017**, *129*, 9889; b) M. S. Denny, J. C. Moreton, L. Benz, S. M. Cohen, *Nat. Rev. Mater.* **2016**, *1*, 16078.
- 21 a) S. Eslava, L. Zhang, S. Esconjauregui, J. Yang, K. Vanstreels, M. R. Baklanov, E. Saiz, *Chem. Mater.* **2013**, *25*, 27; b) W.-J. Li, J. Liu, Z.-H. Sun, T.-F. Liu, J. Lü, S.-Y. Gao, C. He, R. Cao, J.-H. Luo, *Nat. Commun.* **2016**, *7*, 11830; c) M. Usman, S. Mendiratta, K.-L. Lu, *ChemElectroChem* **2015**, *2*, 786.
- 22 a) R. Koitz, M. Iannuzzi, J. Hutter, *J. Phys. Chem. C* **2015**, *119*, 4023; b) X. Huang, B. Zheng, Z. Liu, C. Tan, J. Liu, B. Chen, H. Li, J. Chen, X. Zhang, Z. Fan, W. Zhang, Z. Guo, F. Huo, Y. Yang, L.-H. Xie, W. Huang, H. Zhang, *ACS nano* **2014**, *8*, 8695.
- 23 O. Prucker, C. A. Naumann, J. Rühle, W. Knoll, C. W. Frank, *J. Am. Chem. Soc.* **1999**, *121*, 8766.
- 24 a) A. J. Turgeon, B. A. Harley, R. C. Bailey, *Methods Cell Biol.* **2014**, *121*, 231; b) D. Karaca Balta, Ö. Karahan, D. Avci, N. Arsu, *Prog. Org. Coat.* **2015**, *78*, 200.

Cover feature



A Zr-based metal-organic framework based on the photoreactive linker molecule benzophenone-4,4'-dicarboxylic acid has a two-dimensional layered structure with rhombic-shaped crystals. The *Zr-bzpd*c-MOF features two interesting pathways for post-synthetic treatments. The first route makes use of exposed photoreactive keto groups and allows for versatile surface functionalization of the MOF crystals. On the second route, delamination produces ultrathin sheets. These features are excellent prerequisites for shaping MOFs for applications.

Table of content



The novel two-dimensional Zr-based MOF with the photochemically active linker benzophenone-dicarboxylic acid and its delamination and surface chemistry at the linker molecules open up novel ways for shaping MOFs and pave the way for various applications.

3.2 Direct grafting-from of PEDOT from a photoreactive Zr-based MOF – A novel route to electrically conductive composite materials

Authors:

Alexander Mohmeyer,^{a,b} Andreas Schaate,^a Bastian Hoppe,^a
Hendrik A. Schulze,^a Thea Heinemeyer^a and Peter Behrens^{*a,b}

Chem. Commun. **2019**, 55, 3367-3370

DOI: 10.1039/C8CC10298H

Postal Addresses:

^aInstitute for Inorganic Chemistry, Leibniz University Hannover, D-30167
Hannover, Germany

^bCluster of Excellence Hearing4all, Institute for Inorganic Chemistry, Leibniz
University Hannover, D-30167 Hannover, Germany

*Corresponding author: peter.behrens@acb.uni-hannover.de
phone: +49 (0)511 762-3697

Preface

This study describes a grafting-from polymerization approach based on the photochemical reactivity of Zr-*bzpd*c-MOF. The radical-induced polymerization of 3,4-ethylenedioxythiophene (EDOT) to the electrically conductive polymer poly(3,4-ethylenedioxythiophene) (PEDOT), starting from the surface of the MOF crystals, yielded an electrically conducting and porous composite. For this purpose, the MOF was irradiated in neat EDOT. The composite material, consisting of MOF crystals carrying with covalently attached PEDOT chains, shows an electrical conductivity which is about three orders of magnitude higher than that of the original MOF while largely preserving the inner porosity of the nanoporous material. So far, all of the polymerization procedures leading from EDOT to conductive PEDOT which have been described in the literature make use of an additional oxidant. Therefore, the authors assume a possible reaction mechanism where further benzophenone groups (possibly from the interior of the MOF crystals) act as oxidants facilitating the polymerization of EDOT at the MOF surface. Noteworthy, in the course of this study it was realized that the pristine Zr-*bzpd*c-MOF is electrically conductive, making it one of the few frameworks which exhibit intrinsic electrical conductivity.

The composite materials resulting from different irradiation times of the Zr-*bzpd*c-MOF in EDOT were basically characterized by the author. Conductivity measurements were performed in collaboration with Dr. Bastian Hoppe and Hendrik A. Schulze, employing a van der Pauw setup working under inert atmosphere in the dark constructed by Dr. Bastian Hoppe. The samples were pressed as pellets and showed an electrical conductivity in the range of $10^{-3} \text{ S}\cdot\text{cm}^{-1}$ for the composite material. X-ray powder diffraction investigations show no changes in the PXRD patterns compared to the pristine MOF, showing that the MOF does not undergo any structural transformations during postsynthetic treatment and thus does become modified only on the outer surface. Nitrogen physisorption measurements revealed a maintained permanent porosity after PSM showing the successful merging of both material properties – the electrical conductivity of PEDOT and the permanent porosity of Zr-*bzpd*c-MOF. These composite materials therefore represent a promising material for various applications, e.g. sensing.

To probe the presence of PEDOT chains on the MOF surface, energy-dispersive X-ray spectroscopy (EDX) measurements were performed by Thea Heinemeyer. The results show a sulfur signal associated with the rhombic-shaped MOF crystals after postsynthetic modification with PEDOT. To quantify the amount of EDOT attached on the MOF surface, thermogravimetric analysis was performed by Katharina Nolte and elemental (carbon and sulfur, C-S) analysis was performed by Claudia Schulze. To determine the degree of conversion of keto groups in the composite material, NMR spectroscopy measurements were performed in collaboration with the service

unit of the Institute for Organic Chemistry at the Leibniz University Hannover, showing that the majority of the keto groups was not affected by the PSM, giving further proof that the modification took place only at the outer surface.

Prof. Dr. Peter Behrens conceived and guided this study. The author of this thesis wrote the manuscript and it was refined in cooperation with Prof. Dr. Peter Behrens.

Direct grafting-from of PEDOT from a photoreactive Zr-based MOF – A novel route to electrically conductive composite materials

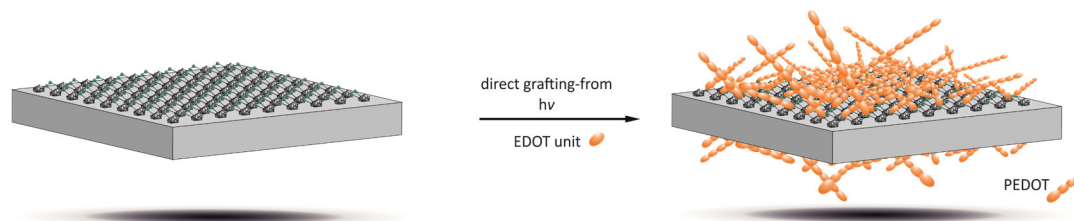
Alexander Mohmeyer, Andreas Schaate, Bastian Hoppe,
Hendrik A. Schulze, Thea Heinemeyer and Peter Behrens

The postsynthetic potential of the two-dimensional metal-organic framework Zr-*bzpd*c-MOF which is based on the photoreactive molecule benzophenone-4,4'-dicarboxylic acid (H_2bzpd c) is used here to selectively functionalize the MOF surface. We report the direct radical-induced oxidative grafting-from polymerization of the precursor EDOT on Zr-*bzpd*c-MOF, leading to an electrically conductive composite material and opening the road to a variety of applications.

Metal-organic frameworks (MOFs) feature an ordered structure with permanent porosity which is suitable for a variety of possible applications¹ like catalysis,^{2,3} gas separation and storage,^{4,5} sensing,^{6,7} in biomedicine^{8,9} or in energy-storage devices.¹⁰ However, the direct synthesis of materials with desired yet sensitive functionalities is limited due to the synthesis conditions of MOFs. Postsynthetic modification (PSM) is a strategy to alleviate such problems. PSM summarizes different approaches like linker exchange, postsynthetic metalation or organic reactions at the linker molecules.^{11–15}

The synthetic possibilities of organic reactions at linker molecules are in principle limitless.¹⁶ Usually, grafting procedures^{17–20} are carried out as grafting-to reactions. Especially for the modification of crystal surfaces with polymers this approach may be problematic as the first grafted-to polymer strands may hinder further access to the reactive functionalities at the surface, resulting in a low degree of functionalization. Grafting-from reactions, where polymer chains grow in a simultaneous and parallel fashion from surface-standing polymerization-initiating entities are usually more effective. Only few grafting-from MOF polymerization reactions have been described in the literature. These usually involve additional preparatory steps as fixing polymerization-initiating groups on the surface^{21,22} or adding a reactive MOF shell to an innocent MOF core.²² Here, we describe grafting-from polymerizations from the surface of MOF particles directly as they are obtained after synthesis and purification. We photochemically initiated a polymerization of 3,4-ethylenedioxythiophene (EDOT) to the electrically conductive polythiophene

derivative poly-ethylenedioxythiophene (PEDOT), in this way directly synthesizing an electrically conductive MOF-polymer composite (illustrated in Scheme 1).



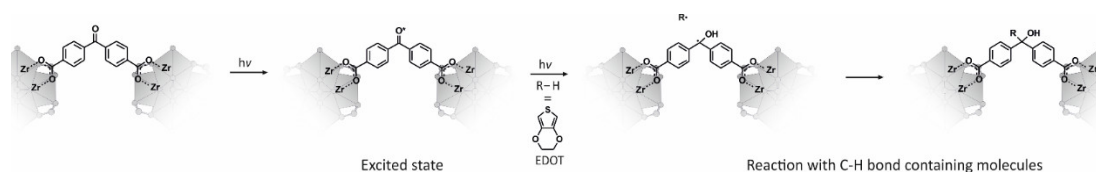
Scheme 1. Schematic illustration of the direct grafting-from approach of PEDOT (orange chain) from photochemically reactive sites at the surface of a *Zr-bzpdC*-MOF crystal, starting from EDOT monomer units (orange dot).

Electrical conductivity is currently a much sought-after property in metal-organic frameworks for applications like sensing, energy storage or electronics.^{23–29} Also applications in coatings of neuronal electrodes could be of interest, as they would allow electrical stimulation of nerve cells/registration of neuronal signals combined with drug delivery from the pores of the MOF. However, only very few MOFs exhibit intrinsic electrical conductivity. The rare examples rely on the formation of π -stacked pathways through three-dimensional MOFs^{30,31}, delocalization in two-dimensional coordination polymers^{32–36} or via sulfur-based linker molecules³⁷ as well as the special properties of iron-based MOFs.^{38–40}

Alternatively, the introduction of guest molecules like tetracyanoquinodimethane,⁴¹ fullerene,⁴² polyaniline and polythiophene derivatives,^{40,43–49} as well as the formation of composites with conducting carbon modifications^{42,50–54} or conducting polymers^{55,56} can lead to conductive MOF-based materials. Generally, the introduction of guests into the pore space can compromise porosity; on the contrary, polymerization of EDOT in the pore system of MIL-101(Cr) leads to a conductive material with only slightly reduced porosity.⁵⁵

Especially for Zr-based MOFs there have been only a few studies to impart electrical conductivity on these compounds,^{42,46,57} although this family has been in the spotlight of research during the last years due to a controlled synthetic access using the modulation method,^{58,59} to their chemical and topological versatility and to their high chemical and thermal stability, as compared to other MOFs.^{60,61} Recently, we have described the *Zr-bzpdC*-MOF, which contains linkers derived from benzophenone-4,4'-dicarboxylic acid (*H₂bzpdC*).⁶² This MOF has a two-dimensional structure, a moderate porosity of about $650 \text{ m}^2 \cdot \text{g}^{-1}$, and can be delaminated into very thin sheets. The most striking feature of the *Zr-bzpdC*-MOF, however, is the possibility to use the photoreactive keto groups of the linker molecules for PSM reactions. Upon excitation with light, benzophenone moieties react with practically any compound containing a C–H bond,^{63–65} according to Scheme 2. We have

exemplarily shown that such reactions can also proceed when the *bzpd*c linker is part of a MOF by grafting-to reactions of the *Zr-bzpd*c-MOF with decane and polyethylene glycol.⁶² Meanwhile, we have extended these grafting-to reactions to other organic molecules and have described that molecules with more than four carbon atoms react pre-dominantly at the outer surface of the crystals whereas smaller molecules can enter the pore system so that the reaction can take place throughout the whole crystal.⁶⁶ Here, we use the ketyl radicals formed by photoexcitation of the keto groups of the *Zr-bzpd*c-MOF to start polymerization reactions.



Scheme 2. Schematic mechanism for the photoreaction of the keto group of benzophenone units in the framework of *Zr-bzpd*c-MOF: formation of a ketyl radical which then reacts with a C-H bond-containing molecule (in this study EDOT), resulting in a covalent bond.

The *Zr-bzpd*c-MOF was synthesized as described in the literature using a slightly modified procedure (Section 2.1, ESI†).⁶² This synthesis approach leads to rhombic shaped *Zr-bzpd*c-MOF crystals with only a very low amount of amorphous byproduct (Fig. S1, ESI†). The resulting colorless powder was Soxhlet-extracted with acetone for 24 h and dried under reduced pressure overnight to remove solvent molecules.

For the grafting procedure, *Zr-bzpd*c-MOF crystals were dispersed in neat EDOT in a quartz vessel, purged with argon for one hour and then irradiated under argon purging for a specific time with a UV LED at a wavelength of 365 nm to induce the biradical formation at the keto group of the benzophenone dicarboxylate linkers in the framework. To remove excess EDOT and non-attached oligo/polymers, the products were Soxhlet-extracted with acetone for 24 h and dried under reduced pressure (further details on the synthesis and characterization methods are given in Sections 2.1, 3.1 and 3.2 of the ESI†).

The most obvious and visible result to confirm a successful polymerization of EDOT is the strong color change of the samples after irradiation. With increasing reaction time, the color of the sample changes from colorless to dark brownish (Fig. 1a). The crystallinity of the MOFs, as determined via powder X-ray diffraction, is not affected by the PSM (Fig. 1a). All reflections are present and the intensity ratios are comparable.

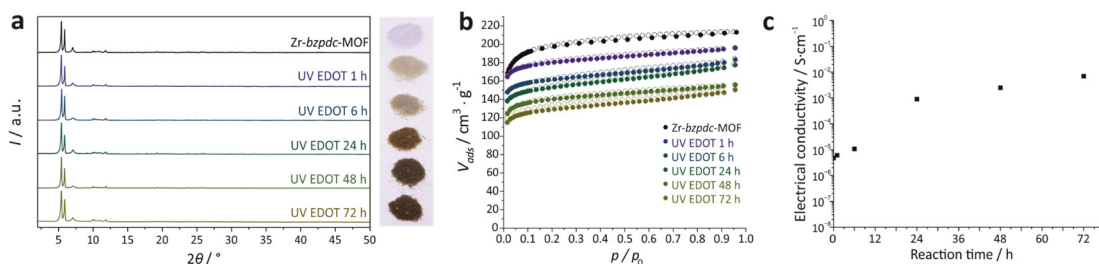


Figure 1. Characterization of Zr-bzpd-MOF and of samples postsynthetically modified using different UV irradiation times. a) PXRD patterns with corresponding pictures of the powders. b) N₂@77 K physisorption isotherms. c) Electrical conductivity values.

The investigation of the postsynthetically modified samples with energy-dispersive X-ray spectroscopy (EDX) showed a sulfur signal associated with the rhombic-shaped MOF crystals after postsynthetic modification with PEDOT (Section 3.3, ESI†). To quantify the amount of EDOT attached on the MOF surface, thermogravimetric and elemental (carbon and sulfur, C-S) analysis were performed. Thermogravimetric analysis (TGA) indicates a mass fraction of up to 2.8% of additional organic species (for the sample UV-irradiated for 72 h) (Section 3.4, ESI†). C-S analysis (Section 3.5, ESI†) gives a sulfur content of 0.76%, corresponding to a somewhat larger additional organic part of 3.4%. On the other hand, results from NMR spectroscopy (Section 3.6, ESI†) on acid-digested samples show that the vast majority of the keto groups – those located in the inner pores of the crystals – has not participated in the reaction, i.e. only the keto groups exposed on the outer surface have reacted. Using the size of the crystals and information from the crystal structure, the number of these exposed keto groups can be calculated. With the results from TGA and C-S analysis and using some assumptions we can estimate that the grafted-from PEDOT chains have lengths of at least ca. 100 EDOT units (for details of the calculations see Section 3.7, ESI†).

We postulate that the polymerization of EDOT proceeds via initiation by surface-standing ketyl radicals and subsequent oxidative polymerization (which is the common polymerization mechanism for EDOT; a corresponding reaction scheme presenting a postulated mechanism is described in Section 4 of the ESI†). Within this mechanism, the ethylene moiety of an EDOT molecule is used for its covalent attachment to the MOF surface. Subsequently, photo-excited benzophenone units of the linkers of the MOF oxidize further EDOT molecules, whereby the keto groups are reduced to alcohols. Usually, iron(III) salts or other oxidizing agents are used for the oxidative polymerization of EDOT.⁶⁷ However, the photo-oxidative potential of irradiated benzophenone is well-known in literature^{68–70} and presents a possible route to oxidative polymerization of EDOT to PEDOT without the necessity for other oxidizing agents (which are not present in our system). The polymerization of EDOT in its neat state without prior attachment to the MOF surface cannot be ruled out.

However, the resulting polymer chains would not be covalently bonded to the MOF crystals and should thus be removed by the extended Soxhlet extraction performed on the samples. Therefore, for the final materials, we propose a covalent attachment of PEDOT chains on the Zr-*bzpd*c-MOF surface, leading to an electrically conductive composite material.

Composites between MOFs and polymers have been described extensively.^{71,72} In our case, the combination of porosity and electrical conductivity is the most exciting aspect of the composite materials described here. Physisorption measurements (Fig. 1b) show a slight decrease in pore volume and surface area which cannot be explained solely by the weight increase due to the mass of the attached polymer (Tab. S1, ESI†). Possibly, PEDOT molecules partially block the pores resulting in a slightly decreased pore volume. The isotherms also show a slight hysteresis which becomes more pronounced with longer irradiation time. Such hysteretic sorption behavior is indicative of the presence of a soft polymer which is deformed during adsorption.^{73,74} It can therefore be taken as an additional indication for a layer of PEDOT molecules at the MOF surface.

The electrical conductivity of the materials was measured using a van der Pauw setup on pressed pellets. The crystallinity of the framework is not affected by the pressure used to obtain the pressed pellets (Section 3.8, ESI†). The results of the electrical conductivity measurements are shown in Fig. 1c. Surprisingly, the non-modified Zr-*bzpd*c-MOF shows an electrical conductivity in a range of about $10^{-6} \text{ S} \cdot \text{cm}^{-1}$. Unexpectedly, this result places the Zr-*bzpd*c-MOF in the small group of intrinsically conducting MOFs. A possible explanation could be the generation of radicals at the keto groups, e.g. by former exposure to light (the actual measurement was performed in the dark under dry argon) or by the application of an electric potential during the measurements (the benzophenone moiety is known to be electrochemically reactive)⁷⁵. A measurable conductivity could then result from radical delocalization within the benzophenone units⁷⁶ and electron hopping between those. In fact, when we first deactivate the radical-forming benzophenone units by reacting them photochemically with ethanol (all benzophenone units within the crystals can be accessed in this way, Fig. S9, ESI†)⁶⁶, there is no measurable conductivity (Section 3.8, ESI†).

The samples irradiated in EDOT show much higher conductivities than the pristine Zr-*bzpd*c-MOF (Tab. S5, ESI†). The electrical conductivity increases during the first 24 h of irradiation by more than two orders of magnitude and then saturates in the range of $10^{-3} \text{ S} \cdot \text{cm}^{-1}$, with the highest value of $0.007 \text{ S} \cdot \text{cm}^{-1}$ observed for samples which had been irradiated for 72 h (Fig. 1c). This value is in the range of semiconducting materials and fits well for various applications, e.g. sensing.

In summary, we have demonstrated the postsynthetic photochemical modification of a MOF by a grafting-from reaction, which does not need any further preparatory steps, but can be carried out directly on the MOF crystals using the surface-standing linker molecules. The resulting composite materials of the Zr-*bzpd*c-MOF with PEDOT show an interesting combination of moderate porosities and good electrical conductivities (Fig. S13, ESI†) so that applications as sensor material or as a biomaterial in neuronal electrodes appear feasible. This work thus reveals great potential for postsynthetic photochemical modifications reactions of the Zr-*bzpd*c-MOF and other MOFs containing photoreactive linkers.

Acknowledgements

We thank Katharina Nolte for thermogravimetric analysis and Claudia Schulze for elemental analysis. Also, we thank the Institute for Organic Chemistry at the Leibniz University Hannover for performing NMR spectroscopy measurements.

Conflicts of interest

There are no conflicts to declare.

References

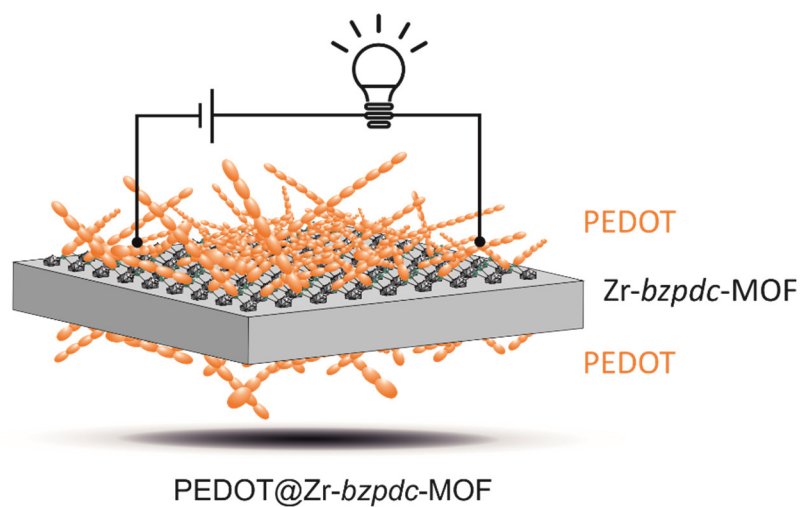
- 1 U. Mueller, M. Schubert, F. Teich, H. Puetter, K. Schierle-Arndt and J. Pastré, *J. Mater. Chem.* **2006**, *16*, 626.
- 2 D. Farrusseng, S. Aguado and C. Pinel, *Angew. Chem. Int. Ed.* **2009**, *48*, 7502.
- 3 J. Lee, O. K. Farha, J. Roberts, K. A. Scheidt, S. T. Nguyen and J. T. Hupp, *Chem. Soc. Rev.* **2009**, *38*, 1450.
- 4 Z. Kang, L. Fan and D. Sun, *J. Mater. Chem. A* **2017**, *5*, 10073.
- 5 B. Li, H.-M. Wen, W. Zhou and B. Chen, *J. Phys. Chem. Lett.* **2014**, *5*, 3468.
- 6 P. Kumar, A. Deep and K.-H. Kim, *Trends Anal. Chem.* **2015**, *73*, 39.
- 7 M. Schulz, A. Gehl, J. Schlenkrich, H. A. Schulze, S. Zimmermann and A. Schaate, *Angew. Chem. Int. Ed.* **2018**, *57*, 12961.
- 8 T. Simon-Yarza, A. Mielcarek, P. Couvreur and C. Serre, *Adv. Mater.* **2018**, *30*, 1870281.
- 9 M. Giménez-Marqués, T. Hidalgo, C. Serre and P. Horcajada, *Coord. Chem. Rev.* **2016**, *307*, 342.
- 10 V. Bon, *Curr. Opin. Green Sustain. Chem.* **2017**, *4*, 44.
- 11 K. K. Tanabe and S. M. Cohen, *Chem. Soc. Rev.* **2011**, *40*, 498.
- 12 T. Islamoglu, S. Goswami, Z. Li, A. J. Howarth, O. K. Farha and J. T. Hupp, *Acc. Chem. Res.* **2017**, *50*, 805.
- 13 P. Roy, A. Schaate, P. Behrens and A. Godt, *Chem. Eur. J.* **2012**, *18*, 6979.

- 14 T. von Zons, L. Brokmann, J. Lippke, T. Preuße, M. Hülsmann, A. Schaate, P. Behrens and A. Godt, *Inorg. Chem.* **2018**, *57*, 3348.
- 15 B. Liu, M. Ma, D. Zacher, A. Bétard, K. Yusenko, N. Metzler-Nolte, C. Wöll and R. A. Fischer, *J. Am. Chem. Soc.* **2011**, *133*, 1734.
- 16 S. M. Cohen, *J. Am. Chem. Soc.* **2017**, *139*, 2855.
- 17 C. Chen, J. Kim, D.-W. Park and W.-S. Ahn, *Mater. Lett.* **2013**, *106*, 344.
- 18 K. Leus, Y.-Y. Liu, M. Meledina, S. Turner, G. van Tendeloo and P. van der Voort, *J. Catal.* **2014**, *316*, 201.
- 19 N. E. Thornburg, Y. Liu, P. Li, J. T. Hupp, O. K. Farha and J. M. Notestein, *Catal. Sci. Technol.* **2016**, *6*, 6480.
- 20 X. Wang, H. Li and X.-J. Hou, *J. Phys. Chem. C* **2012**, *116*, 19814.
- 21 H. Liu, H. Zhu and S. Zhu, *Macromol. Mater. Eng.* **2015**, *300*, 191.
- 22 K. A. McDonald, J. I. Feldblyum, K. Koh, A. G. Wong-Foy and A. J. Matzger, *Chem. Commun.* **2015**, *51*, 11994.
- 23 L. Sun, M. G. Campbell and M. Dincă, *Angew. Chem. Int. Ed.* **2016**, *55*, 3566.
- 24 C.-W. Kung, Y.-S. Li, M.-H. Lee, S.-Y. Wang, W.-H. Chiang and K.-C. Ho, *J. Mater. Chem. A* **2016**, *4*, 10673.
- 25 S. Lin, Y. Pineda-Galvan, W. A. Maza, C. C. Epley, J. Zhu, M. C. Kessinger, Y. Pushkar and A. J. Morris, *ChemSusChem* **2017**, *10*, 514.
- 26 M. G. Campbell and M. Dincă, *Sensors* **2017**, *17*, 1108.
- 27 M. D. Allendorf, A. Schwartzberg, V. Stavila and A. A. Talin, *Chem. Eur. J.* **2011**, *17*, 11372.
- 28 S. K. Bhardwaj, N. Bhardwaj, R. Kaur, J. Mehta, A. L. Sharma, K.-H. Kim and A. Deep, *J. Mater. Chem. A* **2018**, *6*, 14992.
- 29 P. Li and Bo Wang, *Isr. J. Chem.* **2018**, *58*, 1010.
- 30 C. F. Leong, B. Chan, T. B. Faust and D. M. D'Alessandro, *Chem. Sci.* **2014**, *5*, 4724.
- 31 T. C. Narayan, T. Miyakai, S. Seki and M. Dincă, *J. Am. Chem. Soc.* **2012**, *134*, 12932.
- 32 M. G. Campbell, S. F. Liu, T. M. Swager and M. Dincă, *J. Am. Chem. Soc.* **2015**, *137*, 13780.
- 33 M. G. Campbell, D. Sheberla, S. F. Liu, T. M. Swager and M. Dincă, *Angew. Chem. Int. Ed.* **2015**, *54*, 4349–4352.
- 34 M. Hmadeh, Z. Lu, Z. Liu, F. Gándara, H. Furukawa, S. Wan, V. Augustyn, R. Chang, L. Liao, F. Zhou, E. Perre, V. Ozolins, K. Suenaga, X. Duan, B. Dunn, Y. Yamamoto, O. Terasaki and Omar M. Yaghi, *Chem. Mater.* **2012**, *24*, 3511.
- 35 X. Huang, P. Sheng, Z. Tu, F. Zhang, J. Wang, H. Geng, Y. Zou, C.-a. Di, Y. Yi, Y. Sun, W. Xu and D. Zhu, *Nat. Commun.* **2015**, *6*, 7408.

- 36 B. Hoppe, K. D. J. Hindricks, D. P. Warwas, H. A. Schulze, A. Mohmeyer, T. J. Pinkvos, S. Zailskas, M. R. Krey, C. Belke, S. König, M. Fröba, R. J. Haug and P. Behrens, *CrystEngComm* **2018**, *20*, 6458.
- 37 F. Li, X. Zhang, X. Liu and M. Zhao, *ACS Appl. Mater. Interfaces* **2018**, *10*, 15012.
- 38 L. Sun, C. H. Hendon, S. S. Park, Y. Tulchinsky, R. Wan, F. Wang, A. Walsh and M. Dincă, *Chem. Sci.* **2017**, *8*, 4450.
- 39 J. G. Park, M. L. Aubrey, J. Oktawiec, K. Chakarawet, L. E. Darago, F. Grandjean, G. J. Long and Jeffrey R. Long, *J. Am. Chem. Soc.* **2018**, *140*, 8526.
- 40 M. L. Aubrey, B. M. Wiers, S. C. Andrews, T. Sakurai, S. E. Reyes-Lillo, S. M. Hamed, C.-J. Yu, L. E. Darago, J. A. Mason, J.-O. Baeg, F. Grandjean, G. J. Long, S. Seki, J. B. Neaton, P. Yang and J. R. Long, *Nature Mater.* **2018**, *17*, 625.
- 41 A. A. Talin, A. Centrone, A. C. Ford, M. E. Foster, V. Stavila, P. Haney, R. A. Kinney, V. Szalai, F. El Gabaly, H. P. Yoon, F. Léonard and M. D. Allendorf, *Science* **2014**, *343*, 66.
- 42 S. Goswami, D. Ray, K.-I. Otake, C.-W. Kung, S. J. Garibay, T. Islamoglu, A. Atilgan, Y. Cui, C. J. Cramer, O. K. Farha and J. T. Hupp, *Chem. Sci.* **2018**, *9*, 4477.
- 43 C. Lu, T. Ben, S. Xu and S. Qiu, *Angew. Chem. Int. Ed.* **2014**, *53*, 6454.
- 44 H. Shiozawa, B. C. Bayer, H. Peterlik, J. C. Meyer, W. Lang and T. Pichler, *Sci. Rep.* **2017**, *7*, 2439.
- 45 Y. Wang, L. Wang, W. Huang, T. Zhang, X. Hu, J. A. Perman and S. Ma, *J. Mater. Chem. A* **2017**, *5*, 8385.
- 46 T. Wang, M. Farajollahi, S. Henke, T. Zhu, S. R. Bajpe, S. Sun, J. S. Barnard, J. S. Lee, J. D. W. Madden, A. K. Cheetham and S. K. Smoukov, *Mater. Horiz.* **2017**, *4*, 64.
- 47 D. Fu, H. Zhou, X.-M. Zhang, G. Han, Y. Chang and H. Li, *ChemistrySelect* **2016**, *1*, 285.
- 48 T.-Y. Huang, C.-W. Kung, Y.-T. Liao, S.-Y. Kao, M. Cheng, T.-H. Chang, J. Henzie, H. R. Alamri, Z. A. Alothman, Y. Yamauchi, K.-C. Ho and K. C.-W. Wu, *Adv. Sci.* **2017**, *4*, 1700261.
- 49 C.-W. Kung, K. Otake, C. T. Buru, S. Goswami, Y. Cui, J. T. Hupp, A. M. Spokoyny and O. K. Farha, *J. Am. Chem. Soc.* **2018**, *140*, 3871.
- 50 I. Ahmed and S. H. Jhung, *Mater. Today* **2014**, *17*, 136.
- 51 O. Fleker, A. Borenstein, R. Lavi, L. Benisvy, S. Ruthstein and D. Aurbach, *Langmuir* **2016**, *32*, 4935.
- 52 P. Freund, I. Senkowska and S. Kaskel, *ACS Appl. Mater. Interfaces* **2017**, *9*, 43782.
- 53 Y. Mao, G. Li, Y. Guo, Z. Li, C. Liang, X. Peng and Z. Lin, *Nat. Commun.* **2017**, *8*, 14628.

- 54 X. Xu, W. Shi, P. Li, S. Ye, C. Ye, H. Ye, T. Lu, A. Zheng, J. Zhu, L. Xu, M. Zhong and X. Cao, *Chem. Mater.* **2017**, *29*, 6058.
- 55 B. Le Ouay, M. Boudot, T. Kitao, T. Yanagida, S. Kitagawa and T. Uemura, *J. Am. Chem. Soc.* **2016**, *138*, 10088.
- 56 R. Haldar, B. Sen, S. Hurrle, T. Kitao, R. Sankhla, B. Kühl, A. Welle, S. Heissler, G. Brenner-Weiß, P. Thissen, T. Uemura, H. Gliemann, C. Barner-Kowollik and C. Wöll, *Eur. Polym. J.* **2018**, *109*, 162.
- 57 T. C. Wang, I. Hod, C. O. Audu, N. A. Vermeulen, S. T. Nguyen, O. K. Farha and J. T. Hupp, *ACS Appl. Mater. Interfaces* **2017**, *9*, 12584.
- 58 G. Zahn, H. A. Schulze, J. Lippke, S. König, U. Sazama, M. Fröba and P. Behrens, *Microporous Mesoporous Mater.* **2015**, *203*, 186.
- 59 A. Schaate, P. Roy, A. Godt, J. Lippke, F. Waltz, M. Wiebcke and P. Behrens, *Chem. Eur. J.* **2011**, *17*, 6643.
- 60 J. E. Mondloch, M. J. Katz, N. Planas, D. Semrouni, L. Gagliardi, J. T. Hupp and O. K. Farha, *Chem. Commun.* **2014**, *50*, 8944.
- 61 Y. Bai, Y. Dou, L.-H. Xie, W. Rutledge, J.-R. Li and H.-C. Zhou, *Chem. Soc. Rev.* **2016**, *45*, 2327.
- 62 A. Mohmeyer, A. Schaate, B. Brechtken, J. C. Rode, D. P. Warwas, G. Zahn, R. J. Haug and P. Behrens, *Chem. Eur. J.* **2018**, *24*, 12848.
- 63 D. Karaca Balta, Ö. Karahan, D. Avci and N. Arsu, *Prog. Org. Coat.* **2015**, *78*, 200.
- 64 M. A. Winnik and U. Maharaj, *Macromolecules* **1979**, *12*, 902.
- 65 O. Prucker, C. A. Naumann, J. Rühle, W. Knoll and C. W. Frank, *J. Am. Chem. Soc.* **1999**, *121*, 8766.
- 66 A. Mohmeyer, M. Schäfer, A. Schaate, S. Locmelis, and P. Behrens, unpublished results.
- 67 T. Horii, H. Hikawa, M. Katsunuma and H. Okuzaki, *Polymer* **2018**, *140*, 33.
- 68 N. Filipescu and F. L. Minn, *J. Am. Chem. Soc.* **1968**, *90*, 1544.
- 69 B. Qu, Y. Xu, L. Ding and B. Rånby, *J. Polym. Sci. A Polym. Chem.* **2000**, *38*, 999.
- 70 A. Demeter, K. Horváth, K. Böör, L. Molnár, T. Soós and G. Lendvay, *J. Phys. Chem. A* **2013**, *117*, 10196.
- 71 T. Kitao, Y. Zhang, S. Kitagawa, B. Wang and T. Uemura, *Chem. Soc. Rev.* **2017**, *46*, 3108.
- 72 S. Mochizuki, T. Kitao and T. Uemura, *Chem. Commun.* **2018**, *54*, 11843.
- 73 Y. Tsujita, *Prog. Polym. Sci.* **2003**, *28*, 1377.
- 74 J. Weber, M. Antonietti and A. Thomas, *Macromolecules* **2008**, *41*, 2880.
- 75 N. G. Tsierkezos and U. Ritter, *Phys. Chem. Liq.* **2011**, *49*, 729.
- 76 Y. Du, J. Xue, M. Li and D. L. Phillips, *J. Phys. Chem. A* **2009**, *113*, 3344.

Table of content



Photochemical modification of Zr-bzpdC-MOF with PEDOT through direct polymerization of EDOT at the MOF surface gives an electrically conductive material.

3.3 Inside/Outside: Postsynthetic Modification of the Zr-*benzophenonedicarboxylate*-MOF

Authors:

Alexander Mohmeyer,^a Malte Schäfer,^a Andreas Schaate,^{a,b}
Sonja Locmelis,^a Andreas M. Schneider^{a,b} and Peter Behrens^{*a,b}

Manuscript submitted to *Chem. Eur. J.*

Postal Addresses:

^aInstitute for Inorganic Chemistry, Leibniz University Hannover, D-30167
Hannover, Germany

^bCluster of Excellence PhoenixD (Photonics, Optics, and Engineering – Innovation
Across Disciplines), Hannover, Germany

*Corresponding author: peter.behrens@acb.uni-hannover.de
phone: +49 (0)511 762-3697

Preface

This work is focused on a systematical investigation on the postsynthetic modification of *Zr-bzpd*c-MOF starting with a comparison of the reactivity and the obtained products of the reactions of the linker molecule H_2bzpd c, reacted either as a free molecule or when immobilized in the framework. Furthermore, it describes the results of photochemical reactions of the keto groups with simple molecules as water, methanol and ethanol. The reactions with water, which could result in a hydroxylation of the benzene ring of the benzophenone groups, may be especially important for further experiments in aqueous media or samples exposed to light under air humidity.

The second part of this study deals with the photochemical reactions of *Zr-bzpd*c-MOF with series of *n*-alkanes and linear 1-alcohols with diverse chain lengths and the subsequent investigation of effects of the irradiation on the structure, porosity and properties of the modified MOF. By studying the reactivity versus linear alcohols, a clear delineation can be depicted, where shorter alcohol molecules react with photoexcited keto groups throughout the whole crystals whereas longer ones react only with surface-standing keto groups (with 1-butanol representing a borderline case). In case of alkanes from butane to octane, the reaction is always restricted to the outer surface. In consequence, we assume that the PSM takes place either throughout the MOF crystals or only on the surface, depending on the accessibility of the reagents to the pore system, which in turn depends mainly on the size and the polarity of the probe molecules. These results allow designing PSM strategies for this photoreactive MOF in a more specific manner in view of different applications; for example, selective functionalizations of the surface and of the inner part of the crystals appear possible.

The preparation of the composites and the characterization of the samples via X-ray powder diffraction pattern and physisorption with nitrogen and carbon dioxide were carried out by the author. Dr. Sonja Locmelis help and experience were crucial in the reaction with liquid butane. The MOF crystals were further characterized with scanning electron microscopy, which was performed by Thea Heinemeyer. One of the most decisive characterization methods for this study were NMR spectroscopy measurements, performed by the service unit of the Institute for Organic Chemistry at the Leibniz University Hannover. The NMR spectra were interpreted by the author. An idealized structure of the *Zr-bzpd*c-MOF modified with methanol was simulated by Malte Schäfer under the guidance of Dr. Andreas Schneider. Dr. Andreas Schaate and Prof. Dr. Peter Behrens helped in the development of the structural model.

Prof. Dr. Peter Behrens conceived and guided this study. The author of this thesis wrote the manuscript and it was refined in cooperation with Malte Schäfer, Dr. Andreas M. Schneider and Prof. Dr. Peter Behrens.

Inside/Outside: Postsynthetic Modification of the Zr- *benzophenonedicarboxylate*-MOF

Alexander Mohmeyer, Malte Schäfer, Andreas Schaate,
Sonja Locmelis, Andreas M. Schneider and Peter Behrens

Abstract

Abstract: The Zr-based metal-organic framework *Zr-bzpd*c-MOF contains the photoreactive linker molecule benzophenone-4,4'-dicarboxylate (*bzpd*c) which imparts the possibility for photochemical postsynthetic modification. Upon irradiation with UV light, the keto group of the benzophenone moiety will react with nearly every C–H bond-containing molecule. Within this paper, we further explore the photochemical reactivity of the *Zr-bzpd*c-MOF, especially with regard to which restrictions govern internal versus external reactions. We show that apart from reactions with C–H bond-containing molecules, the MOF reacts also with water. By studying the reactivity versus linear alcohols we find a clear delineation in that shorter alcohol molecules (up to butanol as a borderline case) react with photoexcited keto groups throughout the whole crystals whereas longer ones react only with surface-standing keto groups. In addition, we show that with the alkanes *n*-butane to *n*-octane, the reaction is restricted to the outer surface. We hypothesize that the reactivity of the *Zr-bzpd*c-MOF versus different reagents depends on the accessibility of the pore system which in turn depends mainly on the size of the reagents and on their polarity. The possibility to direct the postsynthetic modification of the *Zr-bzpd*c-MOF (selective modification of the whole pore system versus surface modification) gives additional degrees of freedom in the design of this metal-organic framework for shaping and for applications.

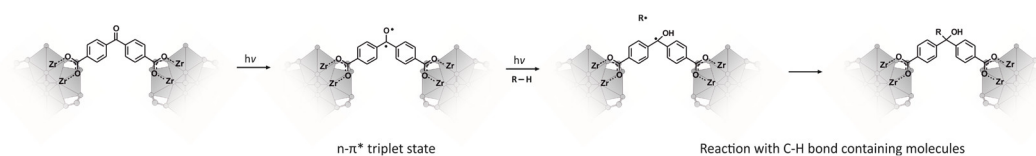
Introduction

Metal-organic frameworks (MOFs) feature an ordered structure with permanent porosity which is of high interest for a variety of applications like catalysis,¹ gas storage and separation,^{2,3} sensing,^{4–6} energy storage and conversion⁷ or biomedicine.^{8,9} To fully exploit this potential, the structure and the properties of a MOF need to be fine-tuned to the specific intended application in order to achieve optimum results. MOFs are well prepared to meet such challenges, as their modular construction from metal oxide nodes and organic linker molecules allows the introduction of various properties by deliberately choosing the metal and the linker

molecule. However, certain specific combinations of properties are difficult to elaborate due to the rather harsh synthesis conditions employed. Especially, some desired functionalities at the organic linker molecules may be too sensitive to withstand the synthesis environment. Therefore, other strategies have been developed to overcome such restrictions imposed by the use of labile or more sophisticated functional groups at the linker molecules during synthesis. One of the most strongly investigated approach to modify and functionalise MOFs is the postsynthetic modification (PSM) of the framework. Several routes like linker exchange, postsynthetic metalation or organic reactions at the linker molecules have been developed.^{10–13}

Especially, the versatility of organic reactions to covalently modify the linker molecules has been widely studied and utilised to introduce different functionalities to the framework after the MOF skeleton has been formed. Such PSM reactions are usually performed on specific functionalities of the organic linker molecules like amino, alkyne, azide or halide groups or by click chemistry. A major requirement to ensure the success of such postsynthetic treatments is the stability of the framework during the PSM.^{10,11,14–16} MOFs with Zr(IV)-based nodes are especially appropriate for PSM due to their high stability towards thermal and chemical stress,^{17,18} making them ideal platforms for introducing different functionalities by chemical transformations and modifications with the aim to adjust the properties of the material with a specific application in mind.^{13,16,19–21}

Recently, we have introduced a novel type of PSM reaction. This makes use of the specific reactivity of the benzophenone moiety. Upon excitation by irradiation with UV light, the ketyl radicals formed react with practically any C-H bond of an organic molecule according to the reaction mechanism schematically shown in Scheme 1.^{22,23}



Scheme 1. Schematic mechanism for the photoreaction of the keto group of benzophenone units in the framework of Zr-*bzpdC*-MOF: irradiation leads to the excitation of the keto group resulting in a biradicaloid triplet state which then reacts with a C-H bond-containing molecule, resulting in the formation of a C-C bond and the reduction of the keto group.²³

We have employed the linker molecule benzophenone-4,4'-dicarboxylic acid (H_2bzpdC) to synthesize the Zr-based metal organic framework Zr-*bzpdC*-MOF.²⁴ The synthesis made use of the modulation method^{25,26} and lead to a compound with formula $\text{Zr}_6\text{O}_4(\text{OH})_6(\text{HCO}_2)_2(\text{bzpdC})_4$. Stock and co-workers have used this linker for the construction of the MOF CAU-8 with the formula $\text{Al}(\text{OH})(\text{O}_2\text{C}-\text{C}_6\text{H}_4-\text{CO}-\text{C}_6\text{H}_4-\text{CO}_2)$ and have studied its photochemical

behavior.^{27,28} The Zr-*bzpd*c-MOF has a two-dimensional layered structure, can be delaminated to thin nanosheets and exhibits a moderate porosity of 650 m² g⁻¹. Its high chemical and thermal stability make it highly suitable for PSM reactions. In a preliminary study, we have converted this MOF in photochemical PSM reactions with decane and PEG and have observed drastically different wetting properties of the products.²⁴ Furthermore, we have initiated photochemical grafting-from polymerisation reactions of EDOT (3,4-ethylenedioxythiophene) to yield nanoporous electrically conducting MOF-PEDOT composites.²⁹ In all cases, the powder X-ray diffraction pattern of the material remained unchanged; accordingly, the modification had only taken place on the surface of the MOF crystals. The central question which then arises is whether the photochemical PSM is in general only possible at the outer surface or whether some characteristics of the organic molecule, like its size or its polarity, decide about whether the reaction takes place only at the surface or throughout the Zr-*bzpd*c-MOF crystal.

In the present study, we systemically investigate the photochemical PSM of the Zr-*bzpd*c-MOF. First, we compare the reactivity and the obtained products of the reactions of the linker molecule H₂*bzpd*c, reacted either as a free molecule or when immobilised in the framework. This part focusses on the reactions with simple molecules, namely methanol and ethanol as well as water. Only few studies have reported on the reactions of benzophenone in aqueous media;³⁰⁻³³ in the present case, these may be especially important, as in the laboratory the MOF samples are exposed to light and air humidity when no special precautions are taken. In the second part of the study, we have reacted the Zr-*bzpd*c-MOF with series of alkanes and alcohols of different chain length. We show that the PSM takes place either throughout the MOF crystals or only on the surface, depending on their polarity and on the chain lengths of the probe molecules. These results allow to design PSM strategies of this photoreactive MOF in view of different applications.

Results and Discussion

Synthesis of Zr-*bzpd*c-MOF

The synthesis of Zr-*bzpd*c-MOF was adapted from our already reported synthesis route²⁴ and leads to rhombic shaped crystals with edge length of about 80–100 μm, as shown in Figure 1. The material was extracted with acetone in a Soxhlet extractor for 24 hours, dried and kept under reduced pressure. Essential properties, like crystallinity and sorption behaviour, are shown in Figure 2 and Figure 3. With a BET area of about 680 m² · g⁻¹ and a total pore volume of about 0.3 cm³ · g⁻¹, the porosity parameters calculated from the data shown are in very good agreement to the published values.²⁴ In order to ensure reproducibility and consistency of our studies, the synthesis approach was scaled up to obtain in one batch a sufficient amount of

Zr-*bzpd*c-MOF for all postsynthetic modification reactions and the application of the various characterisation methods.

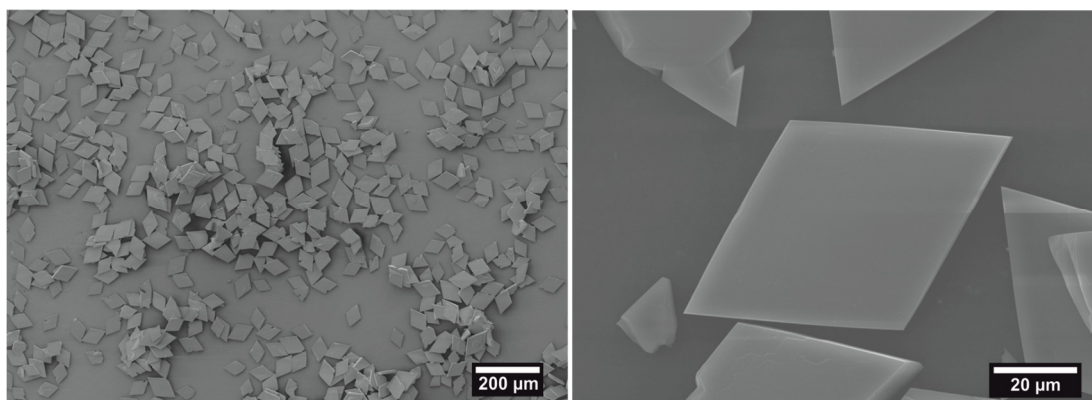
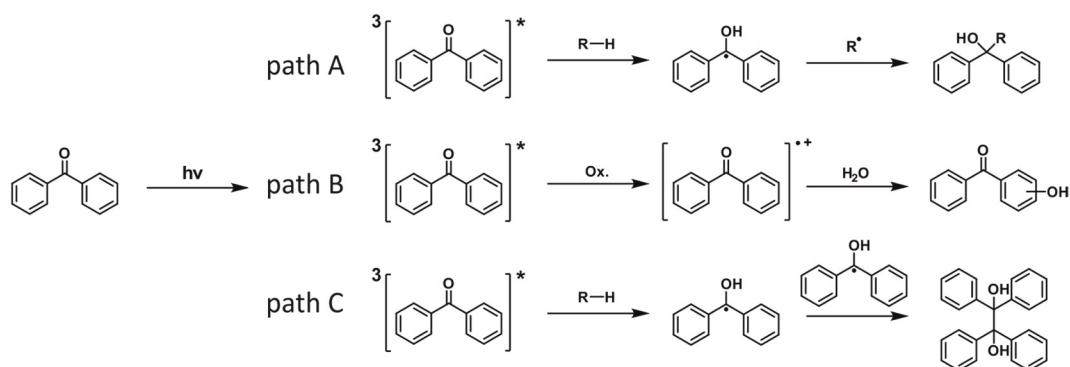


Figure 1. Representative SEM images of rhombic-shaped Zr-*bzpd*c-MOF crystals used for the experiments.

General aspects of the photochemical reactions

For every postsynthetic treatment, the sample was directly dispersed in the neat reactant and purged with argon before irradiation. Irradiated samples are designated by “UV”, followed by the reactant (and possibly other relevant conditions), throughout the paper. A suitable characterisation method to evaluate the PSM of the Zr-*bzpd*c-MOF is solution-state NMR spectroscopy, performed on acid-digested samples. Further characterisation methods applied are powder X-ray diffraction and physisorption experiments.

In principle, photoexcited benzophenone can react in different ways,³¹ as depicted in Scheme 2. Formation of the benzophenone diradical can be followed by the abstraction of an H atom from a substance RH and subsequent addition of R to the former keto carbon atom (path A). However, a radical electron of the photoexcited benzophenone can also become delocalized over a neighbouring aromatic ring, as exemplarily shown in path B for the reaction with water (see below) which leads to a hydroxylation of the benzene ring (path B).^{30,34} Both path A and path B could also occur with benzophenone moieties which are part of the framework. Another often observed reaction of photoexcited benzophenones is the formation of a benzopinacol via dimerisation (path C), typical for example for the reaction with 2-propanol; a similar reaction should be possible with methanol.³⁵ However, this does not appear to be possible in the MOF structure, due to the large distances between the keto groups (smallest distance of about 4.8 Å) and the geometric constraints of the framework.



Scheme 2. Possible reaction paths of a photoexcited benzophenone unit. Path A: Addition of R at the former keto carbon atom, formation of an alcohol. Path B: Addition of R at an aromatic ring, formation of an alcohol. Path C: Formation of benzopinacol.

Photochemical reactions in water

We first studied photochemical reactions in water. The reactivity towards water is of special concern, because as part of the MOF framework, all the benzophenone moieties are exposed, and even air humidity might lead to a reaction under light exposure. Actually, there are only very few studies in the literature for the reaction of benzophenone moieties in aqueous media.³⁰⁻³³ For the studies of the photochemical reactivity towards water, we used the *Zr-bzpdC*-MOF and, for comparison, the free linker molecule *H₂bzpdC* to obtain fundamental insights into possible differences in photoreactivity.

We investigated the photochemical reactivity of *Zr-bzpdC*-MOF in water at a pH of 7 and for comparison, of the free linker molecule *H₂bzpdC* in water of pH 7 and pH 10. The pH values were adjusted with sodium hydroxide and a pH meter. The MOF was of course present as a dispersion; the free diacid formed a dispersion at pH 7 and was dissolved at the higher pH value. The most obvious effect of the photochemical reaction is a colour change from colourless to dark yellow upon irradiation. This was observed for irradiated *Zr-bzpdC*-MOF and for *H₂bzpdC* under basic conditions. For *H₂bzpdC* irradiated in water at a neutral pH value, no colour change could be observed which can be ascribed to the insolubility of the free acid and the inaccessibility of the molecules.

More detailed results concerning the photochemical reaction can be obtained by NMR spectroscopic investigations on solutions. For this purpose, the MOF samples were digested in DMSO-*d*₆ with hydrofluoric acid whereas the irradiated benzophenone dicarboxylic acid samples were dissolved in DMSO-*d*₆. The crucial regions of the NMR spectra of irradiated samples of *H₂bzpdC* and *Zr-bzpdC*-MOF are shown in Figure 2 (full spectra are shown in the Supporting Information, Section 1.1, Figures S1–S10).

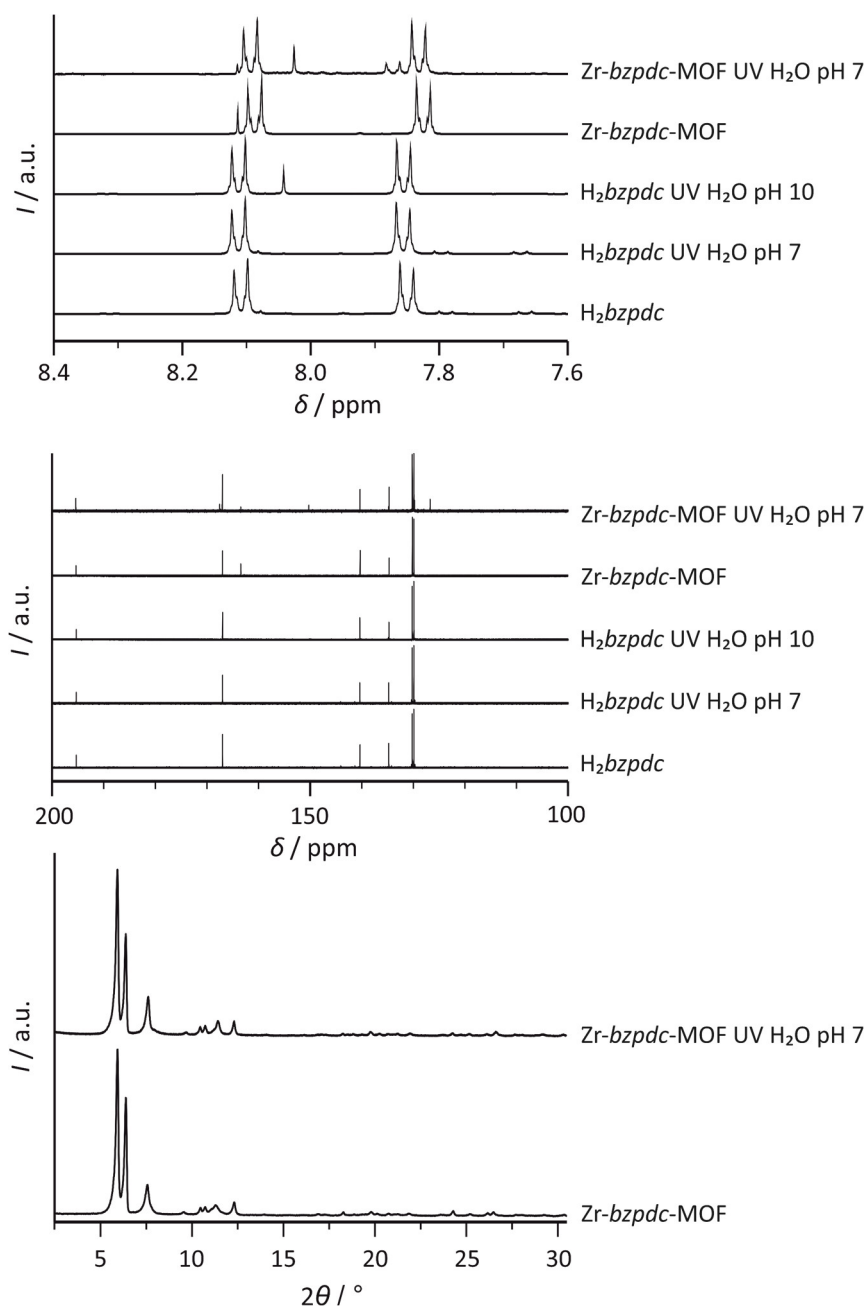


Figure 2. Characterization of the free diacid H_2bzpdC and of the $Zr-bzpdC$ -MOF before and after the irradiation in water (irradiation duration of 72 hours). Selected ranges of 1H (top) and ^{13}C (middle) NMR spectra, taken on dissolved (H_2bzpdC) and acid-digested samples ($Zr-bzpdC$ -MOF), respectively; bottom: PXRD patterns of the $Zr-bzpdC$ -MOF before and after the irradiation in water.

PXRD patterns of the pristine $Zr-bzpdC$ -MOF and the irradiated sample in water (Figure 2) show a comparable crystallinity and there are no indications for major changes in the crystal structure.

1H NMR spectra in Figure 2 show the characteristic multiplet of the aromatic hydrogen atoms of the benzophenone moieties. The additional signal at about

8.11 ppm for dissolved Zr-*bzpd*c-MOF samples belongs to the formic acid molecules which are an integral part of the MOF structure.

After irradiation of H₂*bzpd*c under basic conditions and Zr-*bzpd*c-MOF in water at pH 7 an additional proton signal appears at 8.03–8.04 ppm (Figure 2) in the ¹H NMR spectra, indicating the formation of an *o*-hydroxybenzophenone moiety. That the reaction occurs according to path B and not to path A (see Scheme 2) is supported by the ¹³C NMR spectra, where the signal at about 195 ppm, characteristic of the keto carbon atoms, remains mainly unchanged. The differences and the additional signals in the area of 160 – 170 ppm could be assigned to the aromatic carbon atoms that are affected by the hydroxylation. Based on the ¹H NMR spectra, a comparison of the intensities of the additional signals to the signals of those of the other aromatic protons allows the estimation that about 70% of the linker molecules have become hydroxylated in case of H₂*bzpd*c and about 50% in case of Zr-*bzpd*c-MOF, respectively. For the MOF samples, physisorption measurements were performed (Figure 3).

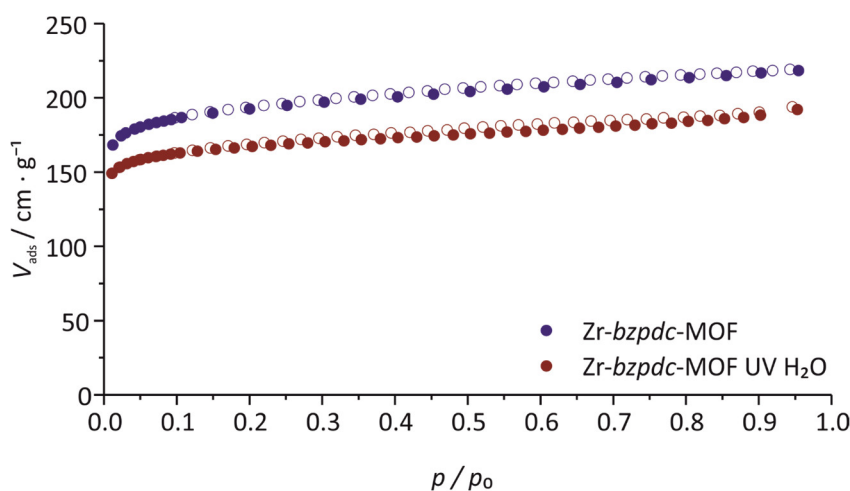


Figure 3. Nitrogen physisorption measurements at 77 K of the pristine Zr-*bzpd*c-MOF and of a sample irradiated in water.

The photochemical PSM affects the pore system of the MOF only to a minor degree, with only slightly decreased values for the BET area and pore volume (see Supporting Information, Section 1.2).

With the proposed reaction according to path B in Scheme 2, where hydroxylation occurs at the phenylene moieties and not at the keto carbon atom, the hybridisation at the central C atom remains *sp*² and, correspondingly, the general geometry of the linker does not change significantly. Thus, the general structure of the framework is not affected by the PSM reaction, which explains that only minor changes occur in the powder XRD pattern. Also, the addition of small OH groups does not significantly

affect the pore system, so that also the physisorption properties after the reaction with water are similar.

The PSM of Zr-*bzpd*c-MOF with water leads to a postsynthetic modification of the linker molecules while preserving its crystallinity and its porosity. It is apparently a suitable and very simple method to introduce hydroxy groups to the framework which should greatly increase the hydrophilicity with regard to the parent Zr-*bzpd*c-MOF.

Photochemical reactions in methanol and ethanol

The photochemical potential of benzophenone groups to bind to molecules containing C-H bonds has been well known for many decades.^{23,34,36-38} The Zr-*bzpd*c-MOF possesses high chemical and good thermal stability, basic prerequisites for successful post-synthetic reactions. According to its crystal structure, all benzophenone moieties present throughout the framework are accessible via the pore system; in addition, the rhombic-shaped crystals present benzophenone groups on their predominant basal surfaces.²⁴ The Zr-*bzpd*c-MOF exhibits moderate permanent porosity consisting of corrugated channels with a minimum free pore diameter of 6.5 Å (visualized in the Supporting Information, Section 1.3, Figure S13). In initial studies, we had shown the general possibility to perform PSM reactions on Zr-*bzpd*c-MOF crystals. As reactants we had used polyethylene glycol and decane (and could in this way change the wetting behaviour of the MOF crystals)²⁴ or EDOT (and could in this way prepare electrically conducting composites).²⁹ However, in these reactions only the benzophenone groups on the outer surface had reacted. Obviously, the reactants mentioned cannot enter the pore system and therefore could not approach the inner keto groups.

Therefore, we studied in depth the corresponding reactions with smaller C-H-bond containing molecules, namely methanol and ethanol, again comparing the reactivity of the Zr-*bzpd*c-MOF and the free acid H₂*bzpd*c. For this purpose, the materials were dispersed in the corresponding alcohol and irradiated under argon atmosphere for 120 hours. H₂*bzpd*c itself is only slightly soluble in methanol and ethanol. However, during irradiation the free acid dissolved completely in methanol but still not in ethanol. Methanol and ethanol were removed under reduced pressure at room temperature. Afterwards, the samples were characterised via powder X-ray diffraction and NMR spectroscopy (Figure 4).

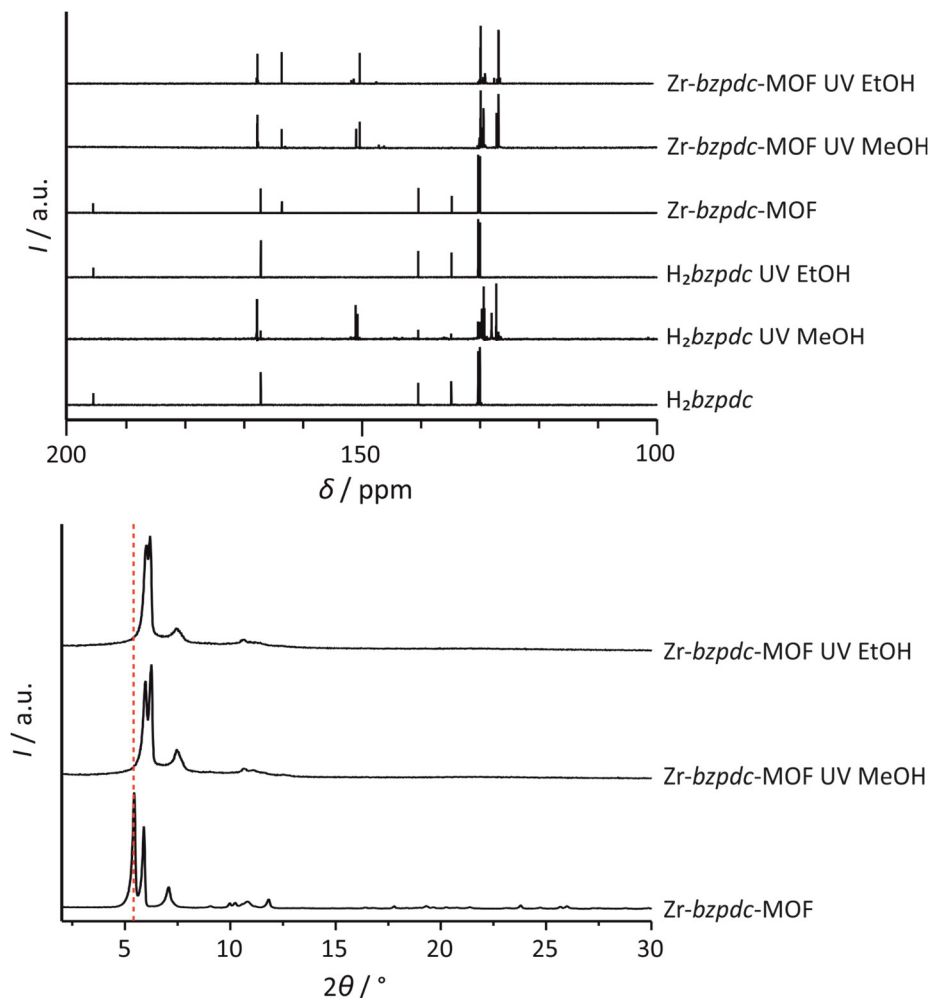
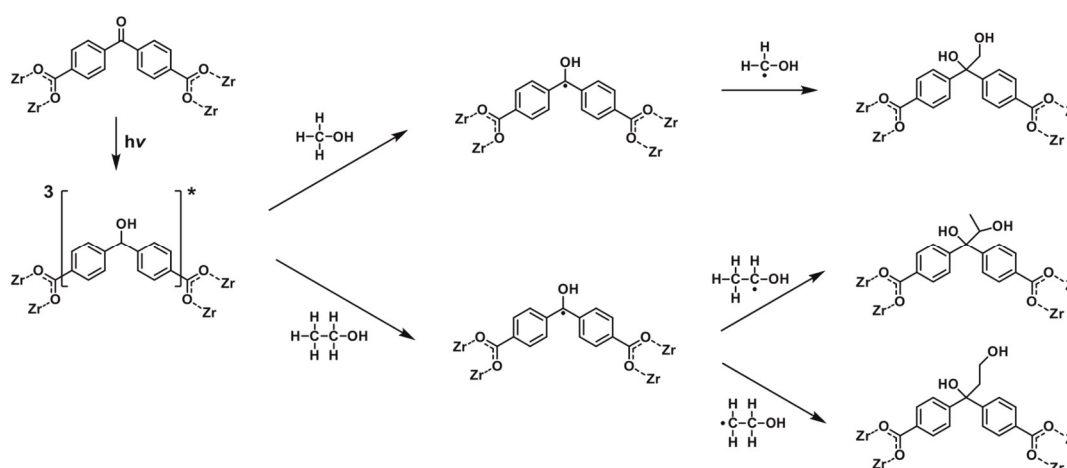


Figure 4. Characterisation of the free acid H_2bzpdc and of $Zr-bzpdc$ -MOF samples (which were acid-digested for NMR preparation) after irradiation in methanol and ethanol, respectively (duration of irradiation: 120 hours). Top: solution-phase ^{13}C NMR spectra; bottom: PXRD patterns (the position of the first reflection of the pristine $Zr-bzpdc$ -MOF is marked with a dotted red line).

Considering the reaction of the free acid in methanol, the ^{13}C NMR spectrum of the product (Figure 4 top) shows that the signal of the keto carbon atom signal at about 195 ppm is missing, indicating a successful and complete reaction of methanol with H_2bzpdc . A detailed inspection of the 1H NMR spectra (see Supporting Information, Section 1.4, Figure S14) does not allow to assign the signals present to one specific product.

On the contrary, the irradiation of the free acid in ethanol does not lead to a reaction as all the ^{13}C NMR signals of the original molecule are still present (see Supporting Information, Section 1.4, Figure S15). This can be explained by the insolubility of H_2bzpdc in ethanol so that there is no access to the keto groups occluded within the dispersed particles. Furthermore, the NMR spectra show that a possible presence of water in the alcohols does not notably influence the reaction of the keto groups with the alcohols.

The Zr-*bzpd*c-MOF shows a successful and complete reaction after irradiation with both alcohols. The ^{13}C NMR spectra in Figure 4 prove a practically complete conversion of the keto groups of the MOF after irradiation by the absence of the keto carbon signal in the corresponding ^{13}C NMR spectra at about 195 ppm (Figure 4 top). This points to a conversion according to path A. The corresponding reactions are shown in Scheme 3. Note that the reaction with ethanol can lead to two different products depending on which of the two carbon atoms of the ethanol molecule becomes attached to the former keto carbon atom. In addition, the signal of the carbon atoms of the benzene rings in alpha position to the keto group experience an upfield shift from 140 ppm to about 150 ppm; this is a strong hint of the reduction of the keto group to an alcohol during the reaction with methanol or ethanol and of a concomitant change of the hybridisation of the keto carbon atom from sp^2 to sp^3 . Also, the signals for the aliphatic carbon atoms of methanol and ethanol, respectively, can be observed in the corresponding ^{13}C NMR spectra at 70–80 ppm (see Supporting Information, Section 1.4, Figure S16–19). Notwithstanding, as in the case of the reaction product of the free acid with methanol, the signals present cannot be assigned to a specific product.



Scheme 3. Reactions of a photoexcited benzophenone linker in Zr-*bzpd*c-MOF with methanol (top branch) and ethanol (bottom branch). Note that two different products are possible for the PSM with ethanol.

Powder X-ray diffraction patterns of the reacted MOFs are shown in Figure 4 (bottom). These indicate a structural change of the framework. This is in contrast to the PXRD patterns obtained from samples which had been reacted with water (see above) and with larger molecules like decane and polyethylene glycol²⁴ as well as with 3,4-ethylenedioxythiophene.²⁹ In these cases, no differences in the PXRD pattern were observed with regard to the parent Zr-*bzpd*c-MOF which is taken as evidence that only surface-standing keto groups had participated in the photochemical reaction. The changes in the PXRD patterns of the samples which

were reacted with methanol or ethanol can be rationalised when it is assumed that the photochemical reaction has taken place throughout the MOF crystals. In the course of such reactions, (at least the major part of) the keto carbon atoms change their hybridisation from sp^2 to sp^3 , leading to a framework with the same linkages and topology as the parent framework, but with different dimensions due to the change in linker geometry. However, due to the different possibilities for the reaction, where addition of the hydroxyalkyl group can occur at different sites of the benzophenone moiety and – in the case of ethanol – at different carbon atoms of the alcohol, these novel MOFs will not have a uniform structure which could be described by a single unit cell (see below).

These results lead to the hypothesis that the molecule size is a major factor in determining whether the postsynthetic addition reaction takes place only at the outer surface of or throughout the crystals. Therefore, we carried out photochemical PSM reactions with primary linear alcohols of chain length C_1 to C_8 (methanol to octanol), including methanol and ethanol which were studied here in depth. Along with the size of the molecules, their polarity and hydrophilicity also change. Therefore, in order to also test the possible influence of polarity of the reactant, reactions with linear alkanes (butane to octane) were included in the study.

Photochemical reactions with alcohols and alkanes of different chain lengths

To test whether the size and/or the polarity of reactant molecules is a major factor in determining the extent of the postsynthetic addition (surface only/pervasive), we carried out photochemical PSM reactions of the Zr-*bzpac*-MOF with linear alcohols of chain length C_1 to C_8 (methanol to octanol) as well as with linear alkanes (butane to octane). In the first part, we focus on the reactions with primary alcohols, thereby including the results described for the PSM reactions with methanol and ethanol in the preceding section.

To investigate whether the PSM reaction with a certain alcohol was successful, the samples were characterised via powder X-ray diffraction and NMR spectra of the acid-digested reaction products. PXRD patterns are shown in Figure 5 (bottom) and selected ranges of the obtained ^{13}C NMR spectra are displayed in Figure 5 (top) (full NMR spectra are provided in the Supporting Information, Section 1.4, Figure S14 – S27). The intensity of the signal of the keto carbon atom is most informative.

After the reaction carried out in 1-propanol, no keto carbon signal is observed anymore; instead, signals for aliphatic carbon atoms at around 70-80 ppm are found. This result is comparable to the situation with methanol and ethanol. On the contrary, in the case of the reaction products obtained with 1-pentanol and also 1-octanol, the keto carbon signal is still present, indicating that the keto groups have not reacted or have done so only to a very small extent. After the irradiation in

1-butanol, the keto carbon signal in the ^{13}C NMR spectrum of the reaction product is very small, indicating that the reaction with this alcohol was also nearly complete. Thus, the PSM with 1-butanol appears to be a borderline case: Irradiation in smaller alcohols lead to a full reaction of the keto groups whereas larger alcohol molecules probably only react at the keto groups located at the outer surface of the MOF crystals.

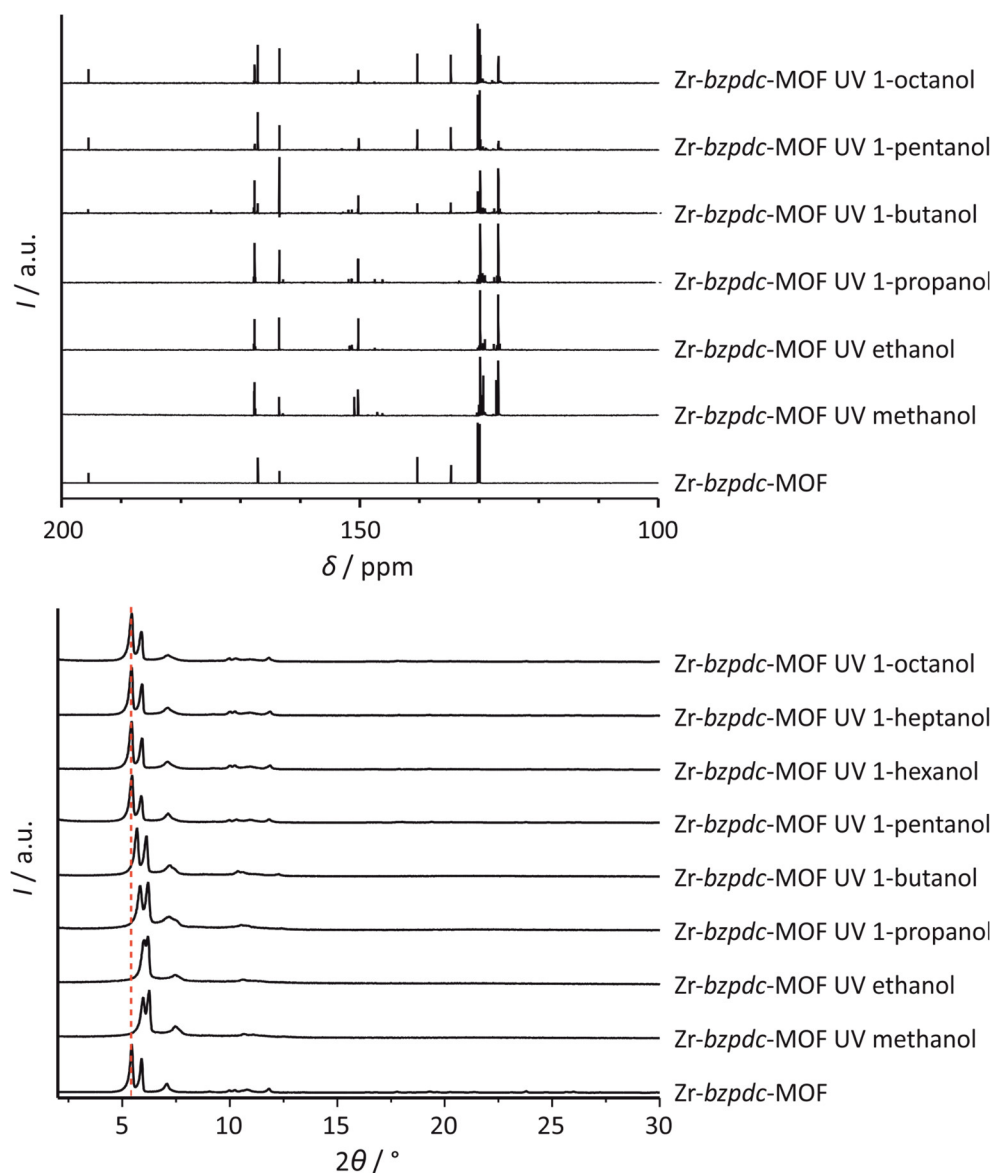


Figure 5. Characterisation of the pristine Zr-*bzpdC*-MOF and Zr-*bzpdC*-MOF samples after irradiation in different alcohols (duration of irradiation: 120 hours). Top: Solution-phase ^{13}C NMR spectra; samples were acid-digested for NMR preparation. Bottom: PXRD patterns (the position of first reflection of Zr-*bzpdC*-MOF is marked with a dotted red line).

This delineation also becomes apparent in the powder X-ray diffraction patterns (Figure 5, bottom). The PXRD patterns of the samples which were irradiated with

long-chain alcohols (pentanol to octanol) show no changes in comparison to that measured on the pristine *Zr-bzpd*c-MOF. In contrast, for those samples which were postsynthetically modified with small alcohols (methanol to butanol), changes can be observed: the first reflections are shifted to slightly higher 2θ values, the reflection pattern at larger 2θ values changes, and in general a minor decrease in crystallinity is indicated by weaker and broader reflections in this range.

The shift of the two first, most intense reflections (110 and 200) to higher 2θ values can be rationalised by the changes in the linker geometry. Each linker molecule connects two IBUs in the structure of the *Zr-bzpd*c-MOF. In course of the photochemical PSM reaction, the hybridization of the initial keto carbon atom changes from sp^2 to sp^3 by the photochemical reaction (Figure 6a). Correspondingly, the bond angles at this carbon atom change from 120° to 109.5° which in turn should result in a shrinkage of the distance between two IBUs on certain lattice planes, provided that the topology of the framework remains the same and that every keto group (or most of them) is affected (Figure 6a). Concomitantly, changes occur in the unit cell dimensions (see Supporting Information, Section 1.5, Table S2).

This is shown in Figure 6a-c for the product of the reaction with methanol. Note that this is the only case where a homogenous structure of the product can be expected (when all keto groups have reacted) and where a uniform unit cell can be determined. In all other cases, different C atoms of the alcohol may become connected to the keto C atom (compare the case of ethanol depicted in Scheme 3), leading to different situations at different transformed keto C atoms. Therefore, we carried out simulations of the structure resulting after the PSM reaction with methanol.

The *a* and especially the *b* axis shrink (Figure 6b), explaining the shift of the first two reflections to higher 2θ values (Figure 5 bottom). The hydroxymethylene residues introduced at the former keto carbon atom through the PSM require additional space between the layers of the structure, thereby leading to an expansion of the structure along the *c* axis (Figure 6c). On the contrary, the bulk structure is not affected when the reaction occurs only at the surface, as illustrated in Figure 6d.

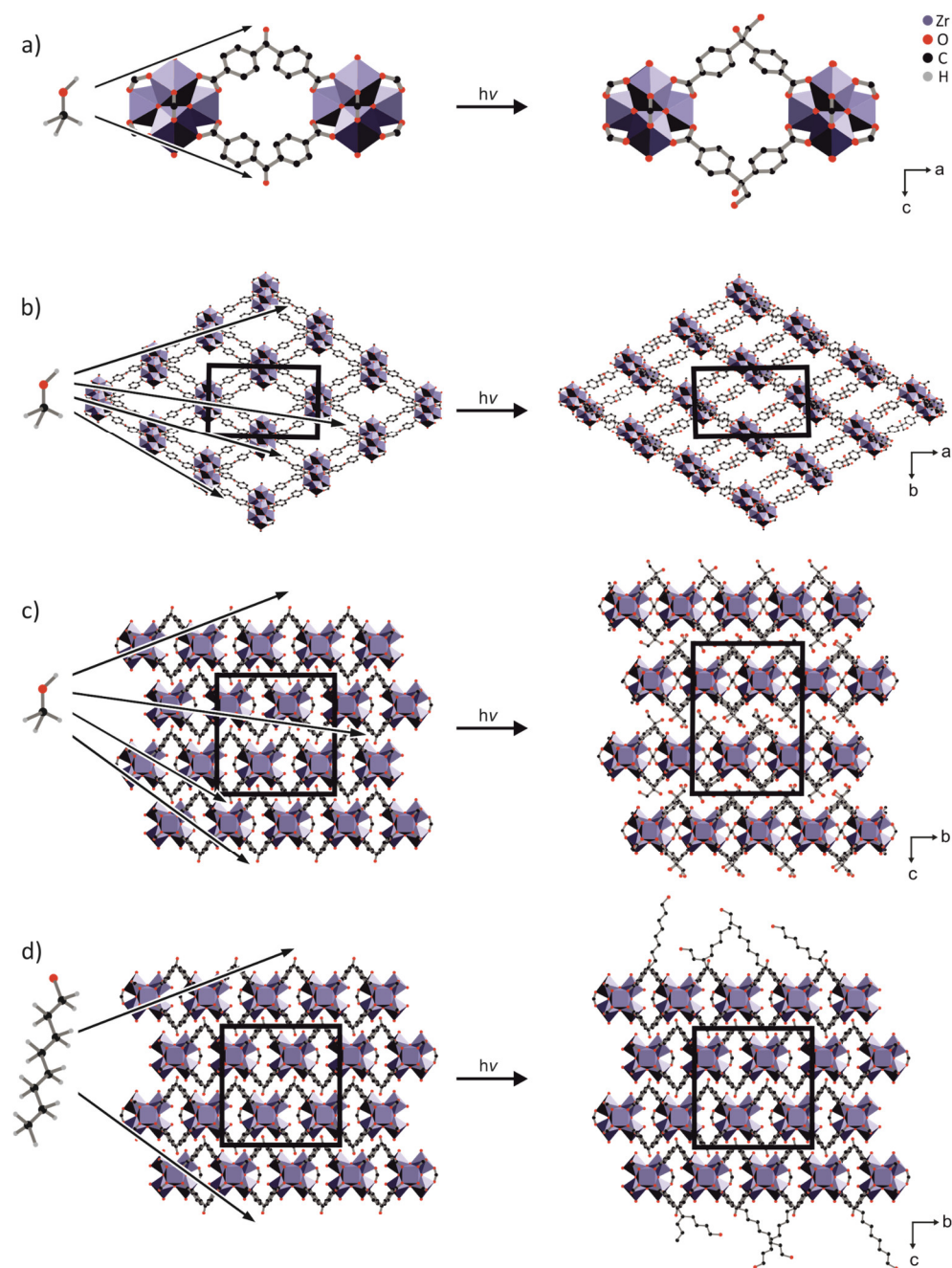


Figure 6. Schematic representation of different reactions occurring during irradiation of the Zr-*bzpdC*-MOF, depending upon the chain lengths of C-H bond-containing molecules (alcohols are shown here as examples). a)-c) Small alcohol molecules (methanol is shown here as example) can diffuse through the whole pore system and the PSM reaction can occur with every photoexcited benzophenone group leading to considerable structural changes: a) at the keto carbon atom, the hybridisation changes from sp^2 to sp^3 ; b) the change in bond angles leads to a shrinkage of the unit cell in the *a-b* plane; c) the additional space required by the hydroxymethylene residues leads to an elongation along the *c* axis. d) Long-chain alcohols (octanol is shown here as an illustrative example) cannot penetrate deeply into the framework; only benzophenone moieties at or near to the surface react, the structure and the unit cell within the interior of the crystals is not affected.

The irradiated samples were further investigated by physisorption measurements with nitrogen at 77 K and carbon dioxide at 273 K. A compilation of the resulting isotherms of the N₂@77 K measurements is shown in Figure 7 (as many of the isotherms closely overlap, the individual sorption curves are shown in the Supporting Information, Section 1.2, Figure S11; values for BET area and pore volume derived from the nitrogen sorption isotherms are given in the Supporting Information, Section 1.2, Table S1). In comparison to the pristine Zr-*bzpd*c-MOF with a BET area of 680 m²·g⁻¹, the samples modified with long-chain alcohols (1-pentanol to 1-octanol) only show about half of this value (ca. 350 m²·g⁻¹). Similar values for the nitrogen BET area were observed in our former studies after the irradiation in PEG (250 m²·g⁻¹),²⁴ decane (350 m²·g⁻¹)²⁴ and EDOT (520–630 m²·g⁻¹).²⁹ The decreased amounts of gas volume adsorbed by these samples indicate a partial pore blocking of the pore systems due to PSM occurring only at the outer surface with long chain alcohols. When the PSM occurs not only at the surface, but throughout the crystals, as is the case with the alcohols methanol up to butanol, the porosity is very low. From the flat N₂ isotherms depicted in Figure 7, BET areas of about 20 m²·g⁻¹ are determined, i.e. nitrogen molecules cannot enter anymore the former pore system.

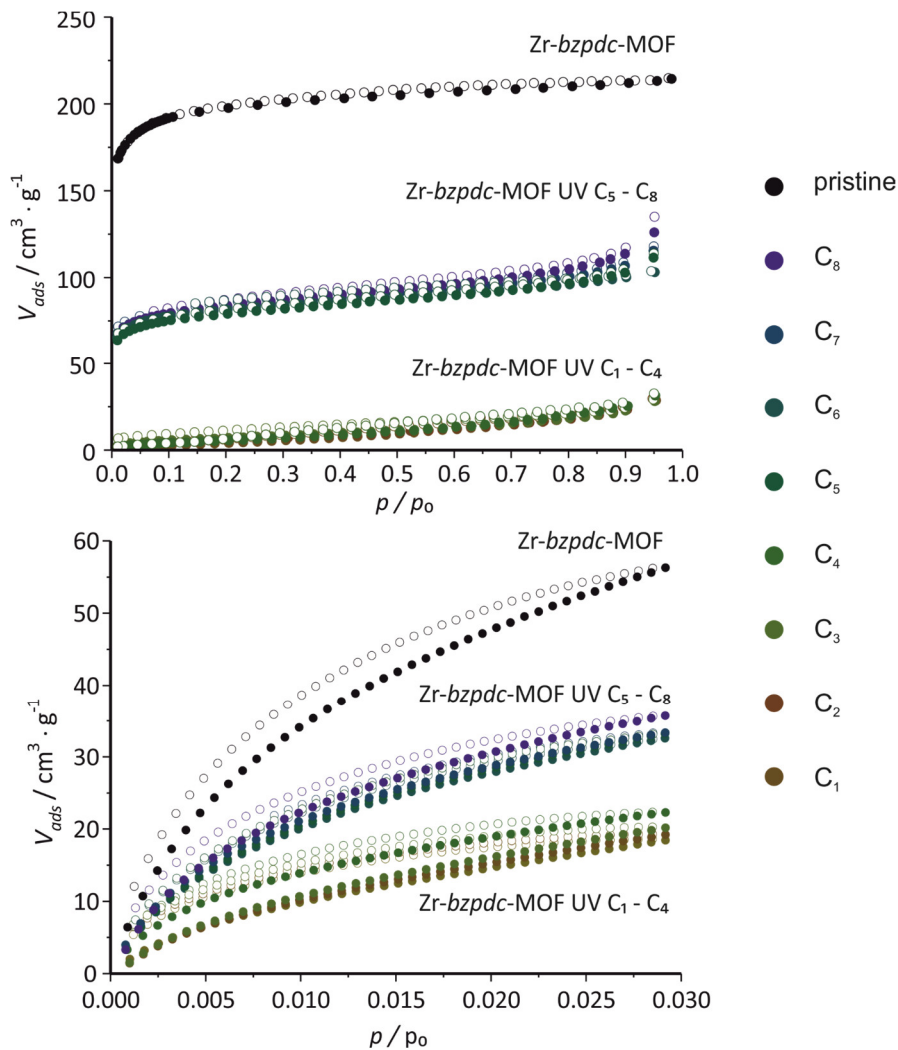


Figure 7. Physisorption isotherms of the pristine *Zr-bzpdC*-MOF and of *Zr-bzpdC*-MOF samples irradiated in primary alcohols with different chain lengths (C₁-C₈ denotes methanol to 1-octanol). Top: Physisorption isotherms obtained with N_2 @77 K; bottom: physisorption isotherms obtained with CO_2 @273 K.

Whereas the nitrogen physisorption isotherms of the samples treated postsynthetically with methanol, ethanol, propanol and butanol thus indicate the formation of essentially nonporous products, this statement is negated by physisorption experiments with carbon dioxide at 273 K. Because of the high temperature and the high relative pressures ($p/p_0 \approx 3 \cdot 10^{-2}$) for this experiment, diffusion is much faster and therefore it is possible to resolve ultra-small micropores (below 0.7 nm). Although the general trend in adsorbed volume of carbon dioxide is similar as for nitrogen (Figure 7 bottom), the samples treated postsynthetically with short-chain alcohols still exhibit a moderate free pore volume which is not measurable with nitrogen at 77 K, possibly due to diffusion hindrance. Based on these results, the pores of the samples should be below ca. 4 Å diameter. When, with

alcohols with more than four carbon atoms the PSM occurs only at or near the surface, a larger accessible porosity results. Like in the case of nitrogen sorption, this porosity is considerably smaller than for the pristine *Zr-bzpd*c-MOF.

A dependence of the amenability of the *Zr-bzpd*c-MOF to the photochemical modification on the chain lengths of the alcohols is thus clearly apparent. Although judging from their largest dimension (diameter of the methylene chain of the alcohols: 4.8 Å), all alcohol molecules should be able to enter the pore system of the *Zr-bzpd*c-MOF (minimum free pore diameter: 6.5 Å), the corrugated channel structure could strongly impede the diffusion of longer-chain alcohols (C₅ to C₈) into the interior of the crystal whereas small-chain alcohols (C₁ to C₄) can diffuse through the whole pore system. Another possibly important aspect is that with chain length of the alcohols, their hydrophobic character increases, which could lead to a decreased diffusion into the pore structure of the rather hydrophilic *Zr-bzpd*c-MOF.²⁴ Therefore, we furthermore tested the PSM reaction with more hydrophobic alkanes, starting with butane and increasing the chain length up to octane. For butane, the reaction was carried out in the liquid phase in a closed ampoule; reactions with even smaller alkanes were precluded due to the high vapour pressures of methane, ethane and propane at room temperature. The characterisation of acid-digested samples with solution NMR spectroscopy was not possible due to insoluble residues still present after the acid treatment of *Zr-bzpd*c-MOF samples irradiated in the different alkanes. The PXRDs pattern of the samples after the PSM reaction are compared to that of *Zr-bzpd*c-MOF in Figure 8.

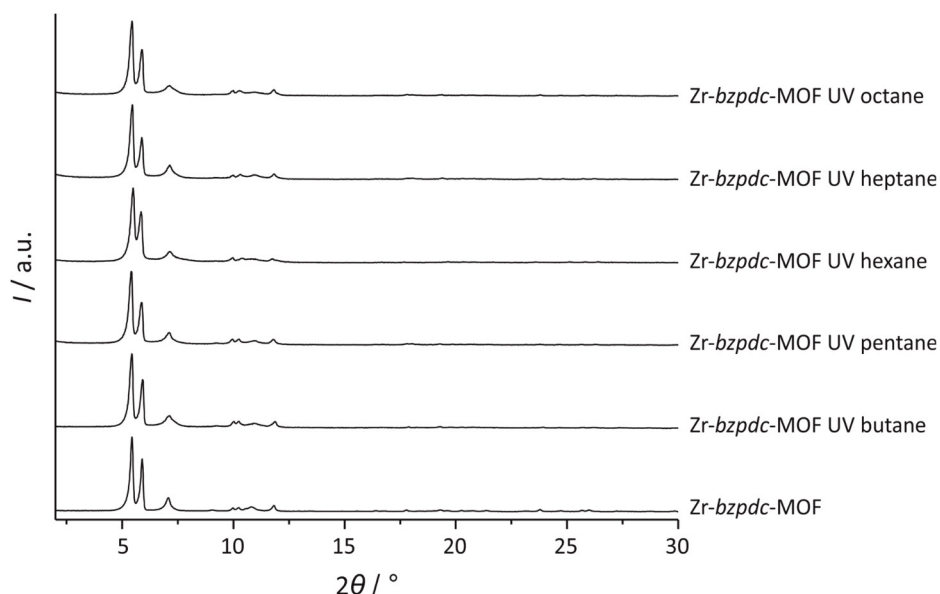


Figure 8. PXRD patterns of pristine *Zr-bzpd*c-MOF and of *Zr-bzpd*c-MOF samples irradiated in different alkanes.

In case of the samples postsynthetically modified with alkanes, no changes can be observed in the X-ray diffraction patterns. Even for butane, the reflection positions and intensities are comparable to those of *Zr-bzpd*c-MOF. The PXRD results are corroborated by physisorption measurements, carried out with nitrogen at 77 K and carbon dioxide at 273 K, shown in Figure 9 (as many of the isotherms closely overlap, the individual sorption curves are shown in the Supporting Information, Section 1.2, Figure S12; values for BET area and pore volume derived from the nitrogen sorption isotherms are given in the Supporting Information, Section 1.2, Table S1).

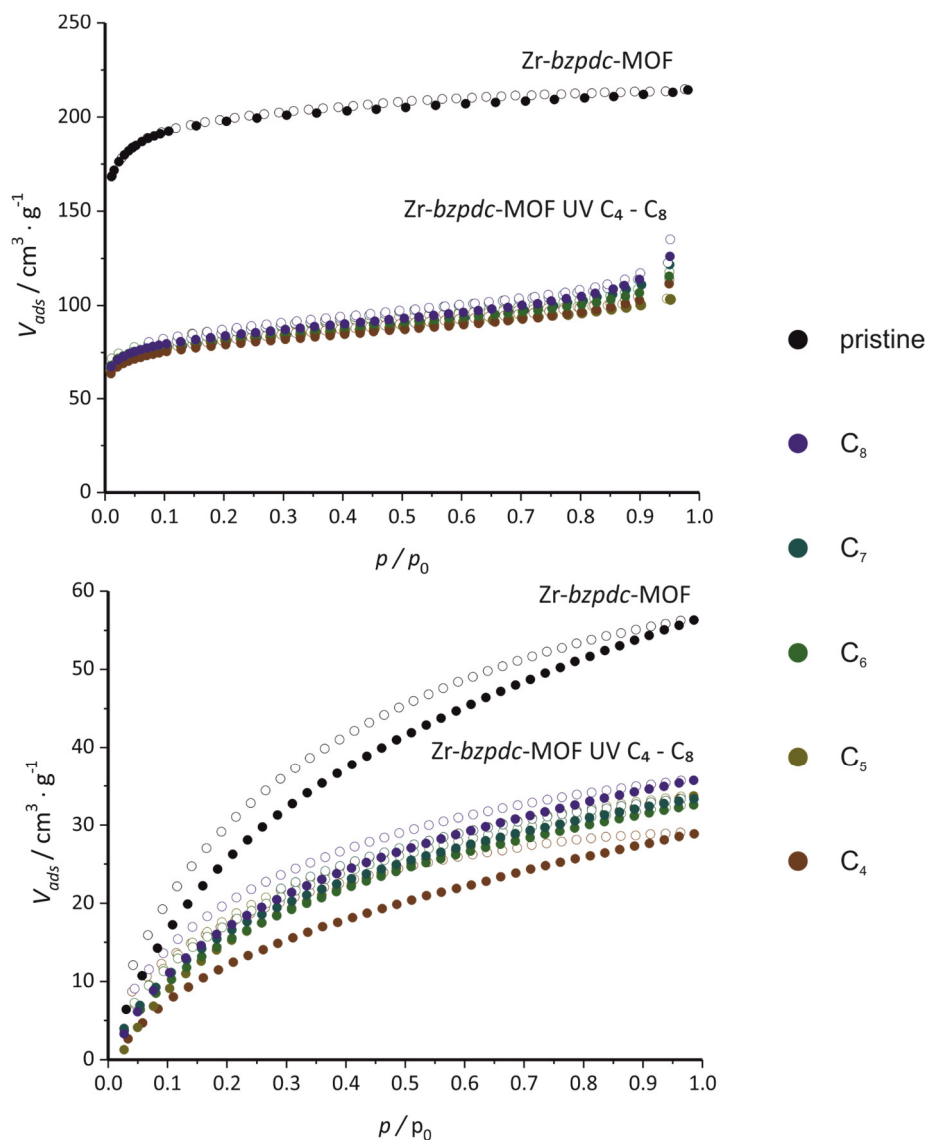


Figure 9. Physisorption isotherms of the pristine *Zr-bzpd*-MOF and of *Zr-bzpd*-MOF samples irradiated in linear alkanes with different chain lengths (C_4 - C_8 denotes *n*-butane to *n*-octane). Top: Physisorption isotherms obtained with N_2 @77 K; bottom: physisorption isotherms obtained with CO_2 @273 K.

Nitrogen physisorption isotherms show a considerable decrease in adsorbed volume for all postsynthetically modified samples. The pore volumes and BET areas are in the range of about $350 \text{ m}^2 \cdot \text{g}^{-1}$, comparable to the values obtained on samples after reaction with long chain alcohols. A similar conclusion can also be drawn from the carbon dioxide isotherms.

The results show that also with butane – and in contrast to butanol – the PSM occurs only at the outer surface of the crystals, i.e. no complete pervasion of the crystals occurs. This is a hint that in addition to molecular size also the polarity of the molecule may be important for the penetration of molecules into the framework and, accordingly, for the extent to which PSM occurs.

Conclusions

The possibility for photochemical postsynthetic modification of the recently introduced *Zr-bzpd*c-MOF is a special characteristic of this porous coordination polymer, as it can be carried out directly after synthesis and work-up and does not need any further preparations. We have already shown that the photochemical reactivity of the benzophenone linker can be employed to adapt the surface properties of the MOF crystals²⁴ and to generate interesting composite materials by direct grafting-from polymerisation reactions.²⁹ Therefore, it is worthwhile to further our understanding of this reaction. We do this here by elucidating the question with which reactants a complete PSM extending throughout the crystal occurs and with which molecules the reaction is restricted to the surface. In this respect, we have shown that with small alcohol molecules (C_1 to C_4 alcohols), the PSM pervades the whole crystals whereas alcohol molecules with longer aliphatic chains (C_5 to C_8 alcohols) react only at the outer surface. The polarity of the molecule probably also plays a role, as with the C_4 alkane butane, the reaction occurs only at the outer surface.

Retrospectively, it is of interest to note the differences between the products of the PSM obtained after irradiation in PEG and decane which we had described in our original paper on the *Zr-bzpd*c-MOF.²⁴ According to PXRD, the reactions only occurred at the outer surface. After the PSM in decane, nitrogen physisorption measurements reveal a BET area of $350 \text{ m}^2 \cdot \text{g}^{-1}$,²⁴ agreeing very well the values obtained after PSM in C_5 to C_8 alcohols and C_4 to C_8 alkanes. With PEG, however, a value of only $250 \text{ m}^2 \cdot \text{g}^{-1}$ is obtained. This indicates that the very hydrophilic PEG molecules might have entered the pore system to some degree before they were restrained from further diffusion by their polymeric nature, and thus substantiates the idea that polarity of the reagent is an important factor in the selection between reactants which can react throughout the pore system and those which only react at the surface.

The concept of selective functionalisation of a MOF – either only at the surface or throughout the whole crystals – is of general interest for various applications like gas separation, optics, electronics or for the generation of composite materials. In case of the Zr-*bzpd*c-MOF, this can be accomplished photochemically directly after synthesis and work-up. The selectivity of the functionalisation is closely coupled to the crystal structure of this MOF, namely on the one hand the exposure of reactive benzophenone moieties at the surface, on the other hand the peculiarities of the pore system, namely rather small apertures and corrugated channels as well as high hydrophilicity. In another *bzpd*c-based MOF, namely CAU-8 (Al-*bzpd*c-MOF), photochemical PSM reactions are also possible, but these always occur throughout the pore system.^{27,28} In this respect, the synthesis of *bzpd*c-based MOFs with other metals appears interesting, perhaps offering further selectivities with which the attractive reactivity of the benzophenone-containing linker can be exploited.

Experimental Section

Materials. Zirconium(IV)-oxychloride octahydrate, formic acid, *N,N*-dimethylformamide (DMF), *n*-butane were purchased from Linde Group, pentane, hexane, heptane, octane, methanol, ethanol, 1-butanol, 1-pentanol, 1-hexanol, 1-heptanol, 1-octanol were purchased from Merck Munich and benzophenone-4,4'-dicarboxylic acid from abcr chemicals Karlsruhe. All chemicals were used without further purification.

Instrumentation. Powder X-ray diffraction (PXRD) measurements were performed at room temperature using a STOE STADI-P transmission diffractometer equipped with curved Ge(111) monochromator with CuK_{α1} radiation ($\lambda = 1.540594 \text{ \AA}$) and a linear position-sensitive detector. The samples were fixed between X-ray amorphous foils. Scanning electron microscopy was carried out with a JEOL JSM-6700F (2 keV). The samples were prepared by the use of ethanolic dispersions dried on a graphite pad under reduced pressure. The resulting images were edited with the software ImageJ 1.49v. Liquid-phase ¹H and ¹³C NMR spectra were measured on a Bruker instrument at 400 MHz and were analysed with ACD NMR Processor 12. Sorption isotherms were measured at an Autosorb 1 (Ar) and Autosorb 3 (N₂, CO₂) instrument from Quantachrome and were evaluated with the software ASiQwin 2.0 (Quantachrome). Measurements were performed with nitrogen at 77 K and with carbon dioxide at 273 K. From nitrogen sorption isotherms, BET areas of the microporous samples were determined with the micropore BET assistant of the accompanying software and total pore volumes were determined at a relative pressure value of about 0.95. UV irradiation experiments were performed with a high-power UV LED Spot epiSPOT by Laser 2000 with a wavelength of 365 nm and 176 mW optical power.

Synthesis of $(\text{Zr}_6\text{O}_4(\text{OH})_6(\text{HCO}_2)_2(\text{bzpdc})_4)$. For reproducibility and consistency, all postsynthetic modification reactions were carried out on *Zr-bzpd*c-MOF single crystals synthesized in a one-batch-serves-all approach by a route slightly modified from the already published recipe.²⁴ Solvothermal synthesis of *Zr-bzpd*c-MOF was carried out in Teflon-sealed screw cap glass vessels using a modulation approach.^{25,39} Favourable conditions to obtain single crystal samples without impurities are as follows: 3.22 g (10 mmol) $\text{ZrOCl}_2 \cdot 8 \text{H}_2\text{O}$ were dissolved in 200 mL DMF. After adding 56.59 mL formic acid (150 molar equivalents (eq) based on amount of Zr^{4+}) and 5.40 g (20 mmol) H_2bzpdc the clear solution was transferred in a 500 mL Teflon-sealed glass vessel and was kept at 120 °C for 2 weeks in a circulating air oven. After the reaction, the solution was cooled down to room temperature and the resulting solid was centrifuged and washed once with 100 mL of DMF and two times with 50 mL acetone and then dried under reduced pressure. For further investigations the sample was activated via Soxhlet-extraction with acetone for 24 hours in the dark. The white powder was kept under reduced pressure until further usage.

Postsynthetic modification. The photochemical reactions were performed using a UV-LED with a wavelength of 365 nm and a radiant flux of about 100 mW cm⁻². A MOF sample of about 100 mg was placed in a quartz cuvette and ca. 3 mL of the neat reactant were added. The reaction batch was flushed for 30 minutes with and kept under argon while irradiating the samples under stirring. The irradiation time was set to 120 hours for alkanes and alcohols. For investigations in aqueous media the irradiation times were 72 hours. After irradiation, the samples were extracted for 24 hours with methanol (Soxhlet extractor) and dried under reduced pressure. For the postsynthetic modification with butane, the MOF was sealed with 5 mL liquid butane in a quartz vial with a stir bar. After irradiation for 120 hours under stirring, unbound molecules were removed under reduced pressure. This sample was used for further investigations without Soxhlet extraction.

Preparation for solution-phase NMR spectroscopy. For liquid-state NMR experiments, 50 mg of the MOF were dispersed in DMSO-d₆. Under vigorous stirring 20 μL aqueous HF (40%) were added and stirred for 18 hours. After complete dissolution of the *Zr-bzpd*c-MOF, an excess of CaCl_2 was added to the clear solution. The supernatant was used for ¹H and ¹³C BB NMR investigations. The spectra were analyzed with ACD/NMR Processor Academic Edition v12.01.

Structural modelling. To investigate structural changes of the MOF by the PSM with methanol, the program suite Materials Studio from Dassault Systèmes BIOVIA was used. First, the crystal structure of pristine *Zr-bzpd*c-MOF was subjected to an energy minimisation employing the UFF (Universal Force Field) within the Forcite program.⁴⁰⁻⁴² The minimisation employed the Ewald summation method for electrostatic interactions. For this kind of interaction as well as for the atom-based

van der Waals interactions the cut off was set to 15 Å. In the first step of the minimisation procedure, only atom coordinates were relaxed while the cell parameters were retained. In the second step, both the unit cell parameters and the atoms were allowed to relax. In order to find the global minimum, this structure was employed for a Quenched Dynamics procedure leading to 10000 energy-minimised structures. The parameters are given in the table below.

Table 1. Parameters for the Quenched Dynamics employed to the model structures.

Parameter	Value
Ensemble	<i>NPT</i>
Temperature	1000 K
Thermo- and barostat	Berendsen
Decay constant	0.1 ps
Time step	1 fs
Total simulation time	20 ns
Frame output every	2000 steps
Final frames	10000

Our model for the sample after PSM with methanol is based on the reaction according to path A. The sp^2 keto carbon atoms of the benzophenone units were transformed to sp^3 C atoms. Instead of the double-bonded oxygen atoms, hydroxy groups and hydroxymethylene groups were placed at these carbon atoms. By doing so, this carbon atom is connected to the corresponding alkyl residue. This structural model then underwent similar procedures as described above for the pristine Zr-*bzpd*-MOF.

Acknowledgements

This work was in part funded by the Deutsche Forschungsgemeinschaft (DFG, German Research Foundation) under Germany's Excellence Strategy within the Cluster of Excellence PhoenixD (EXC 2122, Project ID 390833453). We thank Thea Heinemeyer for preparing the electron microscopic images. M.S. is grateful for a fellowship from the PhD programme "hannover school of nanotechnology–sensors"

of the LNQE, funded by the State of Lower Saxony. In addition, we thank the Institut für Organische Chemie at the Leibniz University Hannover for performing NMR spectroscopy measurements.

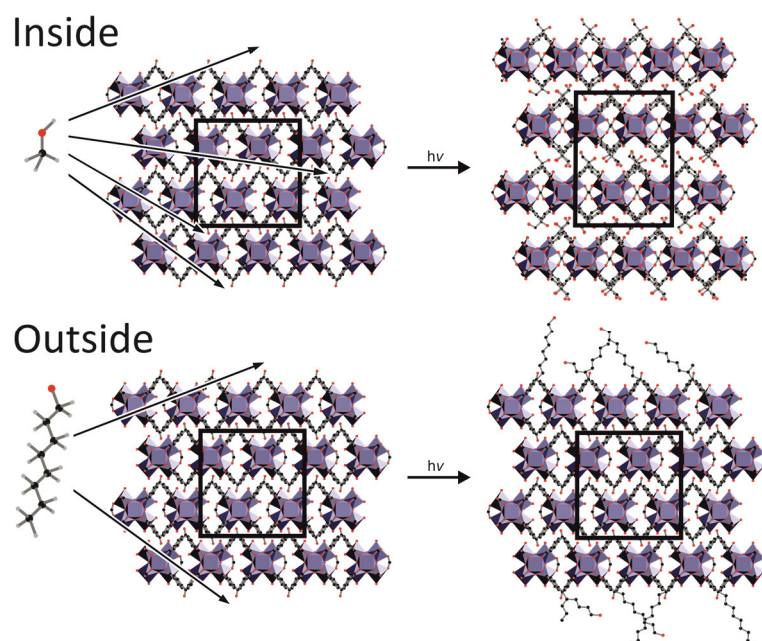
Keywords: Zr-based MOF • modulation • postsynthetic modification • benzophenone • photochemistry

References

- 1 J. Lee, O. K. Farha, J. Roberts, K. A. Scheidt, S. T. Nguyen and J. T. Hupp, *Chem. Soc. Rev.* **2009**, *38*, 1450–1459.
- 2 B. Li, H.-M. Wen, W. Zhou and B. Chen, *J. Phys. Chem. Lett.* **2014**, *5*, 3468–3479.
- 3 J.-R. Li, J. Sculley and H.-C. Zhou, *Chem. Rev.* **2012**, *112*, 869–932.
- 4 P. Kumar, A. Deep and K.-H. Kim, *Trends Anal. Chem.* **2015**, *73*, 39–53.
- 5 L. E. Kreno, K. Leong, O. K. Farha, M. Allendorf, R. P. van Duyne and J. T. Hupp, *Chem. Rev.* **2012**, *112*, 1105–1125.
- 6 M. Schulz, A. Gehl, J. Schlenkrich, H. A. Schulze, S. Zimmermann and A. Schaate, *Angew. Chem. Int. Ed.* **2018**, *57*, 12961–12965.
- 7 Z. Liang, C. Qu, W. Guo, R. Zou and Q. Xu, *Adv. Mater.* **2018**, *30*, e1702891.
- 8 P. Horcajada, R. Gref, T. Baati, P. K. Allan, G. Maurin, P. Couvreur, G. Férey, R. E. Morris and C. Serre, *Chem. Rev.* **2012**, *112*, 1232–1268.
- 9 T. Simon-Yarza, A. Mielcarek, P. Couvreur and C. Serre, *Adv. Mater.* **2018**, *30*, 1870281.
- 10 S. M. Cohen, *J. Am. Chem. Soc.* **2017**, *139*, 2855–2863.
- 11 K. K. Tanabe and S. M. Cohen, *Chem. Soc. Rev.* **2011**, *40*, 498–519.
- 12 P. Roy, A. Schaate, P. Behrens and A. Godt, *Chem. Eur. J.* **2012**, *18*, 6979–6985.
- 13 T. von Zons, L. Brokmann, J. Lippke, T. Preuße, M. Hülsmann, A. Schaate, P. Behrens and A. Godt, *Inorg. Chem.* **2018**, *57*, 3348–3359.
- 14 P. Deria, J. E. Mondloch, O. Karagiari, W. Bury, J. T. Hupp and O. K. Farha, *Chem. Soc. Rev.* **2014**, *43*, 5896–5912.
- 15 W. Morris, C. J. Doonan and O. M. Yaghi, *Inorg. Chem.* **2011**, *50*, 6853–6855.
- 16 R. J. Marshall and R. S. Forgan, *Eur. J. Inorg. Chem.* **2016**, *2016*, 4310–4331.
- 17 J. E. Mondloch, M. J. Katz, N. Planas, D. Semrouni, L. Gagliardi, J. T. Hupp and O. K. Farha, *Chem. Commun.* **2014**, *50*, 8944–8946.
- 18 Y. Bai, Y. Dou, L.-H. Xie, W. Rutledge, J.-R. Li and H.-C. Zhou, *Chem. Soc. Rev.* **2016**, *45*, 2327–2367.
- 19 J. Hynek, S. Ondrušová, D. Bůžek, P. Kovář, J. Rathouský and J. Demel, *Chem. Commun.* **2017**, *53*, 8557–8560.
- 20 H. Amer Hamzah, T. S. Crickmore, D. Rixson and A. D. Burrows, *Dalton Trans.* **2018**, *47*, 14491–14496.

- 21 Y. Zhang, B. Gui, R. Chen, G. Hu, Y. Meng, D. Yuan, M. Zeller and C. Wang, *Inorg. Chem.* **2018**, *57*, 2288–2295.
- 22 T. Konry, A. Novoa, Y. Shemer-Avni, N. Hanuka, S. Cosnier, A. Lepellec and R. S. Marks, *Anal. Chem.* **2005**, *77*, 1771–1779.
- 23 O. Prucker, C. A. Naumann, J. Rühle, W. Knoll and C. W. Frank, *J. Am. Chem. Soc.* **1999**, *121*, 8766–8770.
- 24 A. Mohmeyer, A. Schaate, B. Brechtken, J. C. Rode, D. P. Warwas, G. Zahn, R. J. Haug and P. Behrens, *Chem. Eur. J.* **2018**, *24*, 12848–12855.
- 25 A. Schaate, P. Roy, A. Godt, J. Lippke, F. Waltz, M. Wiebcke and P. Behrens, *Chem. Eur. J.* **2011**, *17*, 6643–6651.
- 26 G. Wißmann, A. Schaate, S. Lilienthal, I. Bremer, A. M. Schneider and P. Behrens, *Microporous Mesoporous Mater.* **2012**, *152*, 64–70.
- 27 H. Reinsch, M. Krüger, J. Marrot, and N. Stock. *Inorg. Chem.* **2013**, *52*, 1854–1859.
- 28 H. G. Baldovi, M. Krüger, H. Reinsch, M. Alvaro, N. Stock and H. Garcia, *J. Mater. Chem. C* **2015**, *3*, 3607–3613.
- 29 A. Mohmeyer, A. Schaate, B. Hoppe, H. A. Schulze, T. Heinemeyer and P. Behrens, *Chem. Commun.* **2019**, *55*, 3367–3370.
- 30 M. Ramseier, P. Senn and J. Wirz, *J. Phys. Chem. A* **2003**, *107*, 3305–3315.
- 31 S. Hashimoto, M. Yasuda and M. Mouri, *Nippon Kagaku Kaishi* **1978**, 79–81.
- 32 X. Zhang, J. Ma and D. L. Phillips, *J. Phys. Chem. Lett.* **2016**, *7*, 4860–4864.
- 33 M. Basu, S. Sarkar, S. Pande, S. Jana, A. K. Sinha, S. Sarkar, M. Pradhan, A. Palb and T. Pal, *Chem. Commun.* **2009**, *46*, 7191–7193.
- 34 Y. Du, J. Xue, M. Li and D. L. Phillips, *J. Phys. Chem. A* **2009**, *113*, 3344–3352.
- 35 Nicolae Filipescu and Fredrick L. Minn. *J. Am. Chem. Soc.* **1968**, *90*, 1544–1547.
- 36 M. A. Winnik and U. Maharaj, *Macromolecules* **1979**, *12*, 902–905.
- 37 B. Qu, Y. Xu, L. Ding and B. Ranby, *J. Polym. Sci. A Polym. Chem.* **2000**, *38*, 999–1005.
- 38 J. N. Pitts, R. L. Letsinger, R. P. Taylor, J. M. Patterson, G. Recktenwald and R. B. Martin, *J. Am. Chem. Soc.* **1959**, *81*, 1068–1077.
- 39 G. Zahn, H. A. Schulze, J. Lippke, S. König, U. Sazama, M. Fröba and P. Behrens, *Microporous Mesoporous Mater.* **2015**, *203*, 186–194.
- 40 Materials Studio 2018; Dassault Système BIOVIA, San Diego, CA. **2017**.
- 41 M. A. Addicoat, N. Vankova, I. F. Akter, T. Heine, *J. Chem. Theory Comput.* **2014**, *10*, 880–981.
- 42 D. Coupry, M. A. Addicoat, T. Heine, *J. Chem. Theory Comput.* **2016**, *12*, 5215–5225.

Table of content



Inside/Outside: The photochemical postsynthetic modification of the Zr-*benzophenone-dicarboxylate*-MOF can be directed to occur only on the surface or throughout the whole crystals, providing additional possibilities to selectively introduce novel functionalities and tailor the properties of this MOF. Major control parameters are size and polarity of the modifying reagent.

4 Conclusion and outlook

This work gives an insight into one of the hallmarks of metal-organic frameworks compared to other classes of materials – the postsynthetic adaption of properties – which is in this work based on a photochemical reactive motif of the organic ligand. The aim of this work was the generation of a novel porous coordination polymer, and also an application-oriented adjustment of its properties, based on the V-shaped photoreactive linker molecule benzophenone-4,4'-dicarboxylate (*bzpd*c²⁻). To achieve an appropriate fundament for the postsynthetic modification concerning chemical, mechanical and thermal stability, a zirconium-based system was used resulting in rhombic-shaped crystals. The new *Zr-bzpd*c-MOF crystallizes in an orthorhombic crystal system. It is one of the less common examples of a two-dimensional porous metal-organic framework and also one of the few MOFs exhibiting intrinsic electrical conductivity. The photoreactive keto groups of the benzophenone moieties point away from the surface of the largest faces of the rhombic crystals, providing easily accessible sites for postsynthetic photochemical surface modifications to regulate the surface properties and to impart novel functionalities. The interior benzophenone linker groups can only be accessed via the rather narrow pores. This work shows that these sites can be addressed selectively. The work presented here represents a comprehensive concept study for only one novel metal-organic framework, ranging from the fundamental synthetic studies and the general characterization up to shaping strategies and application-oriented postsynthetic modifications to pave the way for various applications with a photochemical-based method applicable either in solvents and also in solid state.

In the first part of the thesis, the synthetic requirements to produce the porous crystalline *Zr-bzpd*c-MOF were investigated and the resulting MOF was systematically characterized. The approach used to synthesize the metal-organic framework is the modulated synthesis procedure, consisting in the addition of monocarboxylic acids to the synthesis solution and in many cases the only way to obtain crystalline Zr-based metal-organic frameworks in a reliable manner. Specifically, for the *Zr-bzpd*c-MOF, the only option to synthesize a crystalline material was the modulation with formic acid; adding other monocarboxylic acids like acetic acid, propionic acid and benzoic acid to the reaction mixture resulted only in amorphous products. In addition to the concentration of the modulator formic acid, the reaction temperature and the reaction time are important parameters in the synthesis of the novel *Zr-bzpd*c-MOF. Only the addition of high amounts of formic acid as modulator (>100 eq related to Zr⁴⁺ ions) resulted in highly crystalline material. With 100 eq formic acid in the synthesis solution, it was possible to obtain

rhombic single crystals which appear to consist of stacked two-dimensional layers. These crystals were suitable to generate a structure model from single-crystal X-ray diffraction data. Higher amounts of formic acid led to smaller and more isometric crystals with a clearly distinct morphology. Other approaches to modulate the synthesis led to amorphous products, except for the modulation with a mixture of formic acid and sodium formate, which resulted in another porous phase signified by a dissimilar powder X-ray diffraction pattern, a different (rod-like) morphology, lower porosity and lower thermal stability compared to the *Zr-bzpd*c-MOF.

The structure of the novel *Zr-bzpd*c-MOF consists of Zr_6O_4 clusters, which are coordinated by eight linker molecules and two formate molecules. The clusters are bridged over two linker molecules building up a rhombic shaped two-dimensional framework. ABAB stacking of the individual MOF layers results in one-dimensional corrugated pore channels with a minimum free pore diameter of 6.5 Å. The calculated X-ray powder diffraction pattern fit very well to the experimental data. Argon physisorption measurements give a specific surface area of about 650 m²·g⁻¹.

The MOF shows a good thermal stability up to 250 °C and also an appropriate chemical stability which was tested against different aqueous solutions. This allows for further investigations of this MOF and also for possible usage in realistic setups. Based on the two-dimensional structure, the first aim was the generation of delaminated thin sheets of *Zr-bzpd*c-MOF. The access to such sheets could open the way to interesting applications like membranes, dielectrics or two-dimensional heterostructures. The possibility of delamination was examined with an ultrasonication-based approach applied to a dispersion of the MOF crystals in 2-propanol. Measurements of the thicknesses of the resulting layers were performed by atomic force microscopy. The results revealed extended sheets with a thickness of only few nanometers down to monolayers. It has to be stated, however, that the yield of layers is quite low; correspondingly, these can be used for fundamental studies of their properties and for basic studies in shaping. The second interesting feature presented in the study is the intrinsic photochemical reactivity of the benzophenone group at the linker molecules, which was demonstrated with two C–H bond containing molecules. *Zr-bzpd*c-MOF crystals were dispersed in the neat substances, namely the hydrophilic polymer PEG300 (polyethylene glycol 300) and the hydrophobic alkane decane and irradiated under inert conditions. The solvents cannot enter the pore system and thus become attached via covalent bonds at the surface of the MOF crystals. In this way, the surface properties of the MOF crystals (e.g. dispersibility in different solvents) can be changed drastically. The photochemical reaction did not result in any changes in the PXRD patterns proving that the MOF did not undergo any structural transformation or amorphization during the treatment and is basically stable under the reaction conditions, giving

further proof for a surface-only reaction and substantiating that the MOF. The porosity of the modified samples is still moderate with values of about $350 \text{ m}^2\cdot\text{g}^{-1}$; NMR spectra indicate, that only a small amount of the keto groups was affected by the postsynthetic modification reaction. These two facts, combined with the absence of changes in the X-ray diffraction patterns, prove that (predominantly) the outer surface of the MOF crystals was postsynthetically modified. Both features, delamination and postsynthetic modifiability are helpful tools in the shaping of MOFs and the adjustments of its properties for diverse applications.

The highly interesting and promising initial results with regard to the photochemical postsynthetic modification at the linker molecules were extended and exploited in the further work of this special MOF, firstly in a more application-oriented, secondly with a more fundamental approach.

The first study concerns the photochemical reactivity of *Zr-bzpd*c-MOF with the monomer 3,4-ethylenedioxythiophene (EDOT). In addition to the expected attachment of this monomer to the surface of the MOF crystals, an unexpected polymerization to PEDOT took place. Thus, a composite material consisting of MOF crystals decorated with PEDOT chains resulted. Such grafting-from reactions starting at the surface of a MOF crystal are rare, and to the best of our knowledge no such polymerization reaction has been reported to date where after MOF synthesis no further provisions have to be undertaken to prepare the MOF for the reaction.

Within the field of electrically conducting MOFs, this material combines good electrical conductivity with a still moderate porosity, as it is predominantly the outer surface of the MOF crystals which becomes postsynthetically modified. The electrical conductivity of the composite increases during the first 24 h of irradiation by more than two orders of magnitude and then saturates in the range of $10^{-3} \text{ S}\cdot\text{cm}^{-1}$, resulting in a semiconducting material appropriate for various applications, e.g. sensing.

The third study deals with the further understanding of the postsynthetic modification of the *Zr-bzpd*c-MOF. It deals with the question what the prerequisites are for the PSM reaction to occur only at the surface or whether it is also possible to have PSM reactions pervading throughout the whole MOF crystals. It is found that the PSM of *Zr-bzpd*c-MOF crystals with small polar molecules like water and alcohols from methanol up to 1-propanol pervades the whole crystals. The reaction then has a strong impact on the bulk structure, with characteristic shifts of certain peaks in the PXRD pattern which are shifted to higher 2θ values. Physisorption measurements show that PSMs with alcohols from methanol up to 1-propanol result in non-porous materials. The ratio of keto groups which have reacted through PSM can be determined with NMR spectroscopy on acid-digested samples. For the alcohol molecules methanol up to propanol practically every keto group of the material is

affected by PSM. The PSM of Zr-*bzpd*c-MOF with butanol is a borderline case, where a slight shift of the reflections in the PXRD pattern is observable, indicating the PSM has pervaded the whole crystals, but ^{13}C NMR spectra exhibit a small signal for unreacted keto groups; PSM reactions with alcohol molecules with longer aliphatic chains, 1-pentanol up to 1-octanol, leave the majority of keto groups unaffected. Presumably only the outer surface (or a few outer layers, depending on the penetration depths of the different alcohols) of the Zr-*bzpd*c-MOF crystals can react with these larger molecules. Physisorption measurements assist these findings, as they are indicative of moderately porous materials with BET areas of about $350\text{ m}^2\cdot\text{g}^{-1}$. In a comparable manner, linear alkane molecules (butane up to octane) react with Zr-*bzpd*c-MOF only at the outer surface. The difference in behavior between butane (surface-only PSM) and butanol (bulk PSM) indicates that the polarity of the molecule may also play a role, when the idea that the more polar butanol molecules diffuse more easily into the hydrophilic MOF crystals than the nonpolar butane molecules.

In our view, the spatial selectivity of the functionalization by photochemical PSM of the Zr-*bzpd*c-MOF depends mainly on the size of the reagents and on their polarity. Note that on behalf of their size, all tested molecules should in principle be able to pass through the pore system. However, the channels of the pore system are one-dimensional (allowing for easy blocking) and strongly corrugated (impeding the diffusion with increasing chain length of the molecule). In this respect, the time allowed for diffusion becomes important. This is 30 minutes after the MOF has been placed in the neat phase of the reactant and before the UV irradiation is switched on. Thereafter, diffusion of reactants will be handicapped further by molecules which have undergone the photochemical reaction and are then covalently bound to the framework, possibly blocking the pores. As noted above, the polarity of the reactant molecules will also play a role in whether they are able to penetrate the framework in the given time. Interestingly, with the Al-based MOF CAU-8 (Al-*bzpd*c-MOF), photochemical PSMs can also be carried out. However, based on the crystal structure, there are no keto groups available at the surface; these are all pointing into the pore system. This is why a selective functionalization of this MOF is not possible in a straightforward manner. The concept of selective functionalization of a MOF, either at the surface or throughout the whole crystals, is of general interest for various applications like gas separation, optics and electronics or to generate composite materials.

The different studies presented in this work reveal a great potential for postsynthetic, photochemical modifications reactions of the Zr-*bzpd*c-MOF and other MOFs containing photoreactive linkers. The investigated Zr-*bzpd*c-MOF itself shows promising properties, with the two-dimensional structure offering possibilities to

appropriate shaping of the material for electronics and also for the generation of membranes. For this purpose, also the ability to tailor the pore metrics by postsynthetic modification reactions could be a promising feature. The possibility for postsynthetic modification of this MOF based on a photochemical approach which is also applicable in liquids could be a universal tool to decorate the MOF with diverse molecules in a simple process, thereby being able to differentiate between pervading modifications throughout the crystals and/or only the surface in a sophisticated way. Noteworthy, the benzophenone photoaddition is universally applicable to most organic compounds containing a C-H bond, thus allowing for nearly any desired surface modification. Other further investigations could deal with the decoration of the MOF surface by a covalent linkage with biocompatible, thermo- or pH-responsive molecules and therefore the construction of a switchable material to regulate the accessibility of the pore system, appropriate to generate drug delivery systems for biomedical applications with precise adjustable properties and release functionalities. Another promising approach is the generation of MOFs with benzophenonedicarboxylate as linker molecules based on other metals, perhaps offering further selectivities with which the attractive reactivity of the benzophenone-containing linker can be exploited. Especially iron is an appropriate candidate to increase the intrinsic electrical conductivity by installing conductive centers directly in the pristine MOF. Compared to already known intrinsic conductive MOFs consisting of linker molecules with extended systems of conjugated π -bonds and predominantly chemically non-reactive linker molecules, the present approach could end up with an electrically conductive material with a high adjustability of the properties based on the photochemical reactivity of the linker molecules allowing nearly any desired surface modification. A most exciting prospect relies on the fact that benzophenone moieties are used as photoinitiators for UV-polymerizable polymers; also, benzophenones act as initiators for two-photon reactions where the high energy necessary for photoexcitation is collected from two photons with lower energies (i.e., visible red light). This offers the prospect to write structures with micron or even submicron range resolution into MOF crystals, using laser direct writing (LDW) or two-photon polymerization (2PP) processes, or corresponding spatially defined reactions with single molecules.

5 Supplementary Information

5.1 Delamination and Photochemical Modification of a Novel Two-Dimensional Zr-Based Metal–Organic Framework

Contents

S1.	General synthesis and parameter variation	119
S1.1	Variation of reaction time and modulation with formic acid	119
S1.2	Variation of temperature/reaction time	119
S1.3	Concentration	121
S1.4	Modulation	122
S2.	Crystal structure, composition and properties	126
S2.1	Crystal structure investigation	126
S2.2	Determination of composition by TGA and ^1H NMR spectroscopy	129
S2.3	Physisorption	132
S2.4	Chemical stability	133
S3.	Delamination	134
S3.1	TEM and SEM images	134
S4.	Postsynthetic modification	135
S4.1	NMR spectroscopy	135
S5.	References	136

S1. General synthesis and parameter variation

S1.1 Variation of reaction time and modulation with formic acid

The synthesis system for the *Zr-bzpd*c-MOF was thoroughly investigated; various synthesis parameters were systematically varied.

Different reaction times and variation of the amount of formic acid as modulator show clearly that reaction times of more than 24 hours and a modulator amount of more than 90 eq are necessary to synthesize a crystalline sample of the *Zr-bzpd*c-MOF. Fig. S1 shows the PXRD patterns of the substances obtained with different reaction times and different amounts of modulator.

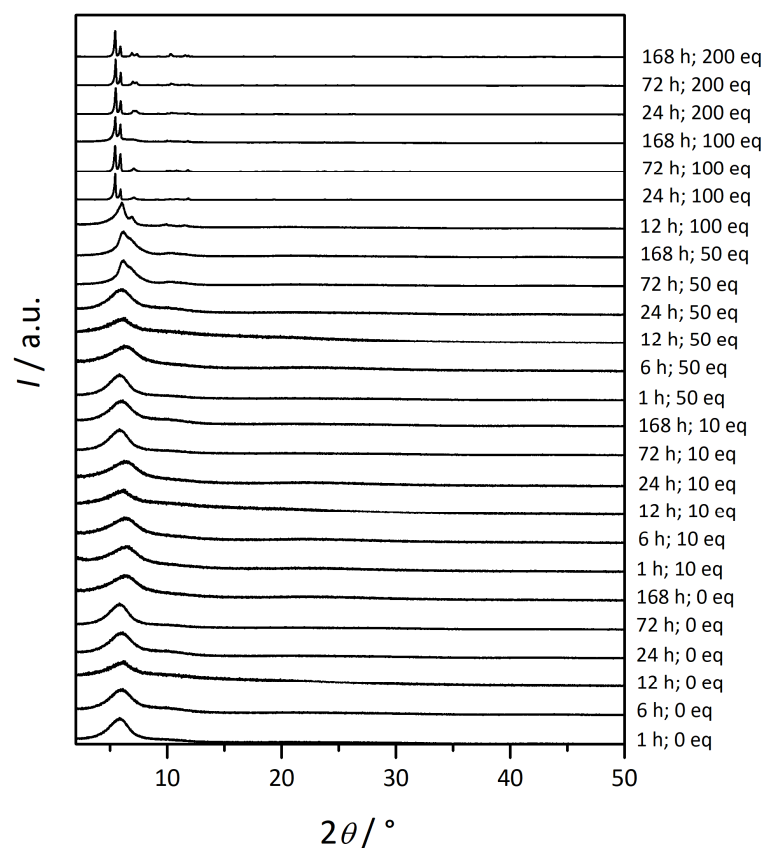


Figure S1. PXRD patterns of products obtained in syntheses where the reaction time and the amount of formic acid as modulator were varied. The results form the basis for the construction of the scheme in Figure 2 of the manuscript. Syntheses were performed at a temperature of 120 °C. For each synthesis 0.517 mmol $\text{ZrOCl}_2 \cdot 8 \text{H}_2\text{O}$ and 0.517 mmol H_2bzpd c were dissolved in 20 mL DMF.

S1.2 Variation of temperature/reaction time

Detailed investigations were conducted to evaluate the influence of the temperature and the reaction time for the modulated synthesis with 100 eq formic acid. PXRD patterns of samples obtained are shown in Figure S2. It can be clearly observed that crystalline *Zr-bzpd*c-MOF can only be synthesized within a small temperature window from 110 to 120 °C.

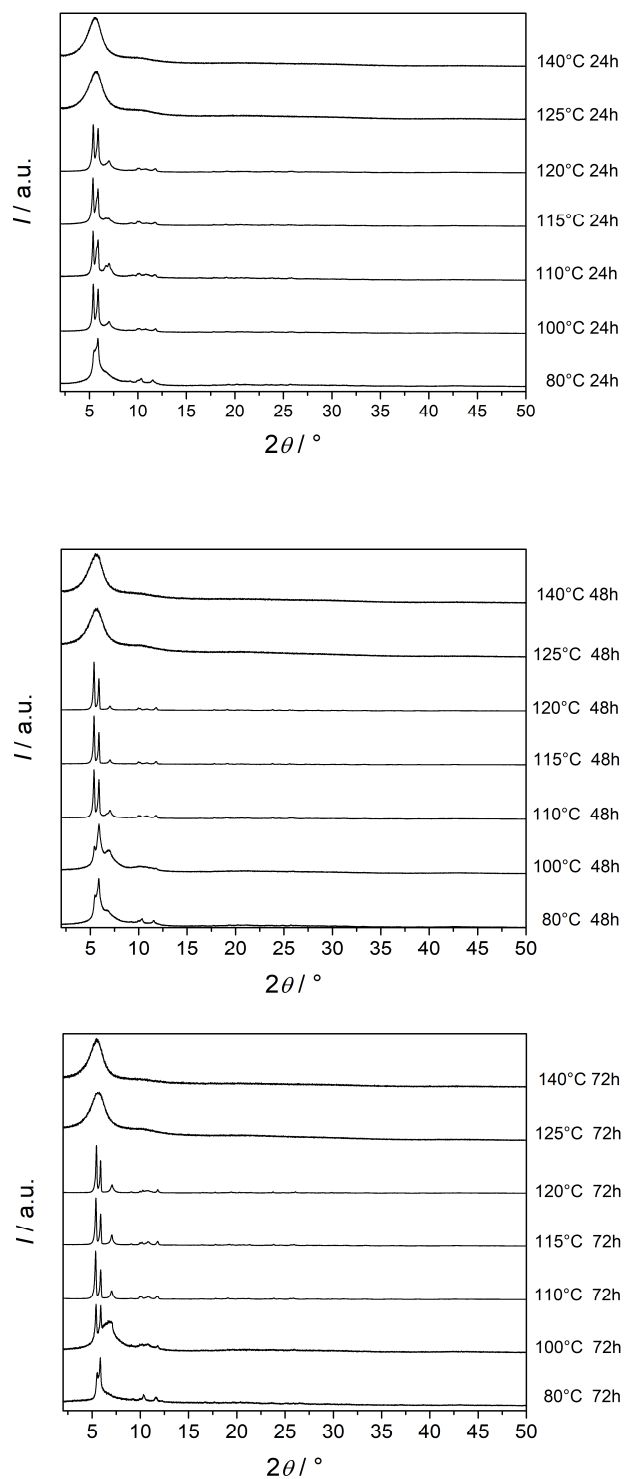


Figure S2. PXRD patterns of the products of syntheses with different reaction times (24 h, 48 h, 72 h) at different temperatures between 80 °C – 140 °C. For each synthesis 0.517 mmol $\text{ZrOCl}_2 \cdot 8 \text{H}_2\text{O}$ and 0.517 mmol H_2bzpd and 51.7 mmol formic acid were dissolved in 20 mL DMF.

S1.3 Concentration

Detailed investigations were performed with regard to the concentration of the reaction solution. While keeping the ratio of $\text{ZrOCl}_2 \cdot 8 \text{H}_2\text{O}$, H_2bzpdc and formic acid constant, their concentration in the reaction mixture was varied. As solvent 20 mL DMF were used.

At low concentrations of reactant (1/2x, 1/5x), no crystalline material was formed. At high concentrations of reactants (5x, 10x), different crystalline materials were obtained. The product of the synthesis with fivefold increased concentration is an unknown phase containing impurities of the unreacted precursor H_2bzpdc . The PXRD of the synthesis product obtained with tenfold concentrations corresponds to that of the *Zr-formate* MOF, published by W. Liang *et al.*⁵ The data reveal that also the concentration window to obtain crystalline *Zr-bzpdc*-MOF is very limited.

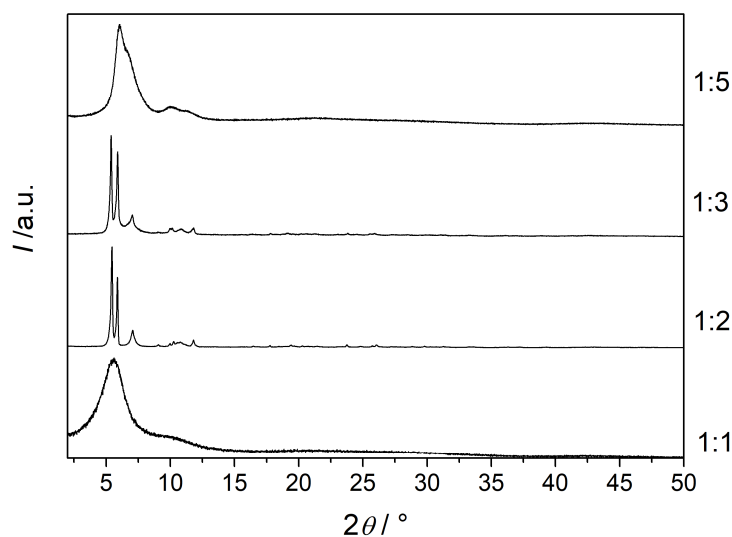


Figure S3. PXRD patterns of syntheses carried out with different concentrations of $\text{ZrOCl}_2 \cdot 8 \text{H}_2\text{O}$, H_2bzpdc and formic acid in the same molar ratio of 1:1:100 eq and a constant amount of DMF (20 mL). Standard procedure: 0.517 mmol $\text{ZrOCl}_2 \cdot 8 \text{H}_2\text{O}$ and 0.517 mmol H_2bzpdc and 51.7 mmol formic acid dissolved in 20 mL DMF. Reaction time: 72 h; Temperature: 120 °C.

S1.4 Modulation

Formic acid

Detailed investigations were carried out with regard to the concentration of the modulator formic acid in the synthesis solution. By increasing the amount of formic acid to more than 70 eq, a crystalline Zr-*bzpd*c-MOF can be obtained. Products synthesized with more than 180 eq of formic acid show a splitting of the reflection at ca. 7°. As shown in the manuscript the morphology of the product is also changing, from rhombic to more isometric crystals.

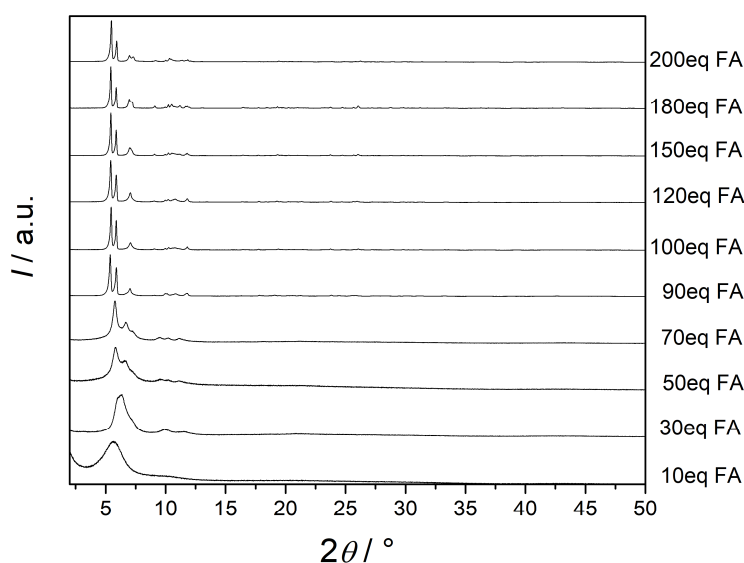


Figure S4. PXRD patterns of products of syntheses with different amounts of formic acid added to the synthesis. For each synthesis 0.517 mmol $\text{ZrOCl}_2 \cdot 8 \text{H}_2\text{O}$ and 0.517 mmol H_2bzpd c and a defined amount of formic acid were dissolved in 20 mL DMF and kept for 72 hours at 120 °C in an oven.

Acetic acid, propionic acid and benzoic acid

The PXRD pattern for the modulated synthesis with acetic acid (10, 50, 100, 200 eq), propionic acid (10, 50, 100, 200 eq) and benzoic acid (10, 30, 100 eq) are not shown because all syntheses yielded amorphous products.

Formic acid/sodium formate

Using a mixture of formic acid and sodium formate as modulator leads to another porous phase, signified by its powder X-ray diffraction pattern (Figure S5, upper diffractogram), by a different morphology (Figure S6) and lower thermal stability (Figure S7).

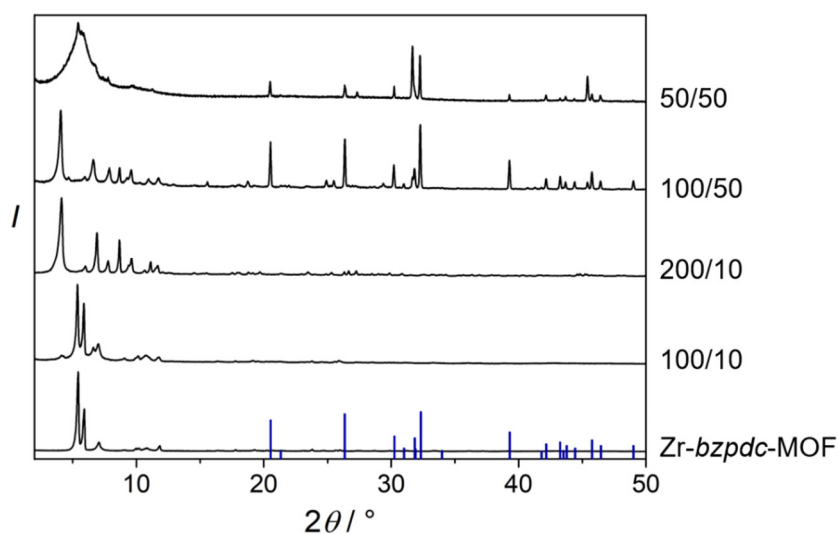


Figure S5. PXRD pattern for products obtained by modulation with different equivalents of formic acid/sodium formate compared to Zr^{4+} ions.. Reflection positions are indicated for sodium formate (blue lines). The syntheses solutions were kept in an oven at 120 °C for 72 hours.

SEM images show a rod-like morphology with a length of the rods of 10-50 μm and a thickness of about 1-5 μm (Fig. S6). The PXRD pattern, in particular with its first reflection at small 2θ values, and the morphology of the crystals of this new phase indicate that it could be a porous metal-organic framework.

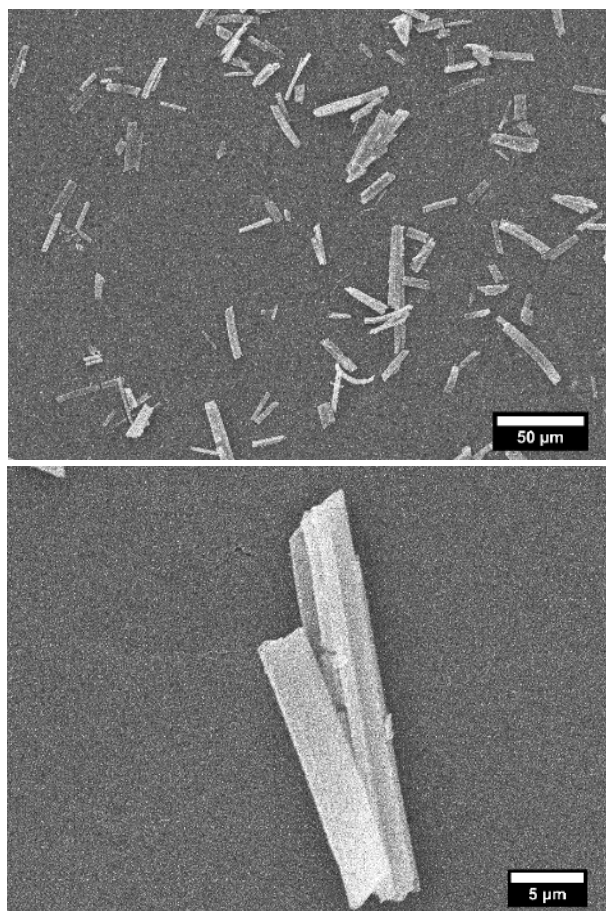


Figure S6. SEM images of the product synthesized with a combination of formic acid and sodium formate (200:10) show rod-like crystals with micrometer dimensions.

To further investigate the properties of the new phase, physisorption and thermogravimetric analysis were performed (Figure S7). The crystalline product shows a microporous adsorption behaviour and a BET area of about $500 \text{ m}^2 \cdot \text{g}^{-1}$. The thermal stability of this second phase is much less than that of the *Zr-bzpd*-MOF. It decomposes at about $150 \text{ }^\circ\text{C}$. Due to the insufficient thermal stability, no further investigations were conducted on this phase.

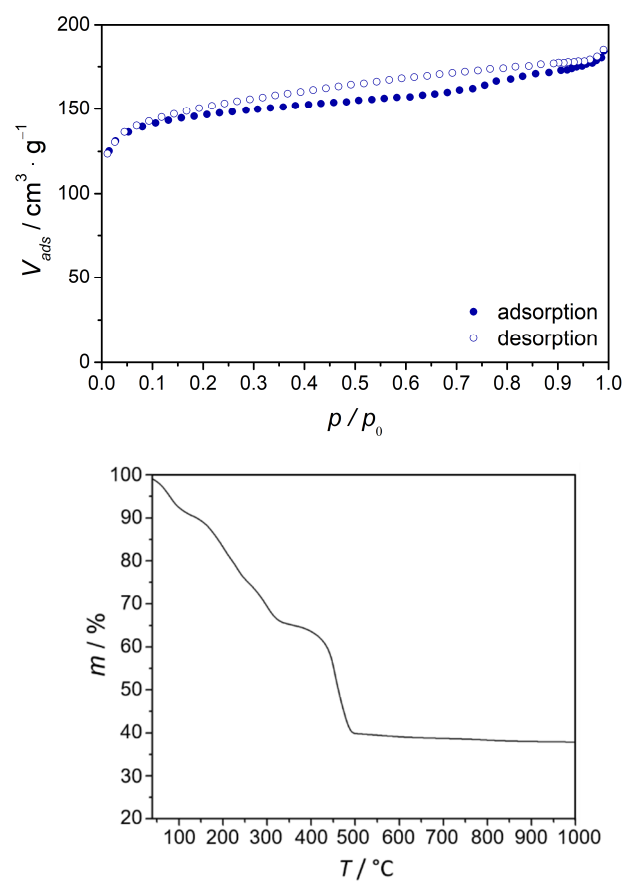


Figure S7. Physisorption measurement (N_2 @77 K) and thermogravimetric analysis (heating rate: $5 \text{ K} \cdot \text{min}^{-1}$) of the product synthesized with a combination of formic acid and sodium formate (200:10).

S2. Crystal structure, composition and properties

S2.1 Crystal structure investigation

As can be seen in SEM images (Figure 4a), the majority of crystals exhibit a highly anisotropic morphology of rhombic platelets with small height. Several suitable single crystals were investigated by single-crystal X-ray diffraction; the collected data were of nearly the same quality or, in some cases, worse than those which led to the results described here. To improve the size of the crystals, several syntheses were performed with increasing reaction times (up to one month) and different concentrations around those of the standard procedure. These attempts were not successful, and further ~~other~~ attempts were hampered by the small synthesis windows for the Zr-*bzpd*c-MOF. The high-resolution SEM picture in Figure S8 points to another problem: The “leafy” appearance indicates the possibility of stacking disorder of the individual MOF layers. This disorder and the small height of the crystals prevented us to obtain better results from the crystal structure determination.

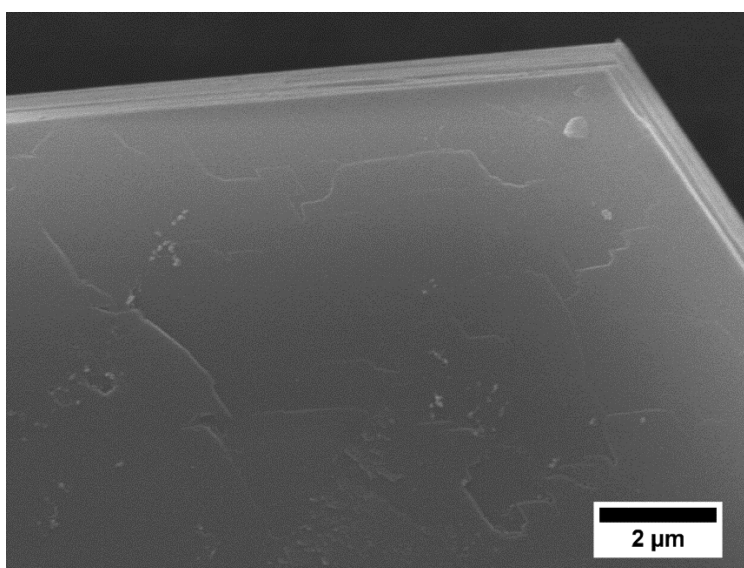


Figure S8. SEM image showing an edge of a Zr-*bzpd*c-MOF crystal similar to the ones used for single-crystal X-ray diffraction experiments.

A crystal with dimensions of $0.120 \times 0.080 \times 0.005 \text{ mm}^3$ was picked and mounted on a goniometer head. Single crystal X-ray diffraction studies were carried out with a Bruker KAPPA APEX II CCD diffractometer equipped with a graphite crystal monochromator situated in the incident beam, which produces $\text{CuK}\alpha$ radiation ($\lambda = 1.54178 \text{ \AA}$). Data collection was carried out at $-40 \text{ }^\circ\text{C}$. Because of the small third dimension of the crystal, no reflections at higher diffraction angles were obtained. The SAINT program was used for integration of the diffraction profiles² and

adsorption corrections were applied by using the SADABS routine.³ The structure was solved by direct methods using WinGX⁴ with SHELXS.⁵ The most stable structural model was found in space group *Cmcm*. Data related to the structural investigation are given in Table S1.

While the atom positions could be refined without problems, the thermal displacement factors of the atoms could only be refined isotropically, most likely because of the insufficient data at high diffraction angles. Nevertheless, a structural model was obtained, the calculated X-ray powder diffraction pattern of which fits very well to the experimental data. The hydrogen atoms were added theoretically, riding on the concerned atoms. The atom positions from the crystal structure model are summarized in Table S2.

Table S1. Data related to the structural investigation of Zr-*bzpd*c-MOF.

Crystal size / mm	0.12 x 0.08 x 0.005
Crystal system	orthorhombic
Space group	<i>Cmcm</i> (63)
Lattice parameters	a=29.8710(17) Å b=19.2467(11) Å c=19.4041(12) Å
Cell volume	11155.77 Å ³
No. of reflections	8531
Observed data	1044
Parameters	114
Unique Reflections	2305
R(int)	0.1426
R1	0.1970
wR2	0.5381
GooF	1.756

Table S2. Table of atomic coordinates for the structural model of Zr-*bzpd*c-MOF.

Symbol	Element	<i>x</i> / <i>a</i>	<i>y</i> / <i>b</i>	<i>z</i> / <i>c</i>	<i>U</i>_{iso} / Å²
ZR1	Zr	0.4176	0.6142	0.7500	0.0578
ZR2	Zr	0.5000	0.5227	0.8404	0.0569
ZR3	Zr	0.5000	0.7069	0.8396	0.0661
O1	O	0.4586	0.6144	0.8416	0.0678
O2	O	0.4584	0.7045	0.7500	0.0943
O3	O	0.4563	0.5225	0.7500	0.0713
O4	O	0.3814	0.5478	0.6825	0.0503
O5	O	0.3779	0.6818	0.8206	0.0771
O6	O	0.5000	0.8198	0.8058	0.0834
O7	O	0.5000	0.7090	0.9526	0.0952
O8	O	0.5678	0.7489	0.8764	0.0864
O9	O	0.5000	0.5192	0.9551	0.0817
O10	O	0.5000	0.4081	0.8249	0.0903
O11	O	0.4322	0.4848	0.8777	0.0659
O12	O	0.2478	0.3703	0.4288	0.0924
C1	C	0.3921	0.4978	0.6397	0.0720
C2	C	0.3550	0.4638	0.5981	0.0515
C3	C	0.3652	0.4266	0.5396	0.0822
C4	C	0.3273	0.3986	0.5080	0.1236
C5	C	0.2825	0.4036	0.5298	0.0532
C6	C	0.2768	0.4362	0.5923	0.0841
C7	C	0.3100	0.4698	0.6236	0.0883
C8	C	0.2498	0.3711	0.4906	0.0680
C9	C	0.2905	0.8366	0.9696	0.0776
C10	C	0.2803	0.7983	0.9136	0.0780
C11	C	0.3124	0.7647	0.8790	0.0728
C12	C	0.3604	0.7657	0.9033	0.0754
C13	C	0.3664	0.8037	0.9599	0.0764
C14	C	0.3350	0.8382	0.9917	0.1218
C15	C	0.3933	0.7237	0.8614	0.0822
C16	C	0.5000	0.8400	0.7500	0.0673
H3	H	0.3944	0.4207	0.5228	
H4	H	0.3324	0.3733	0.4673	

H6	H	0.2486	0.4346	0.6137
H7	H	0.3040	0.4974	0.6624
H10	H	0.2504	0.7953	0.8987
H11	H	0.3049	0.7400	0.8389
H13	H	0.3955	0.8058	0.9783
H14	H	0.3425	0.8649	1.0306
H16	H	0.5000	0.8889	0.7500

S2.2 Determination of composition by TGA and ^1H NMR spectroscopy

Thermogravimetric analysis

The analysis of the TGA data shows that the weight percentages derived from the experimental data deviate by about 5% related to an IBU saturated with hydroxyl groups. After replacing two formate molecules for hydroxyl groups in the chemical formula, the theoretical value fits well to the experimental values. This indicates a partial coordination of the IBU with formate molecules.

Table S3. Table of thermogravimetric analysis data of Zr-*bzpd*c-MOF; experimental data are given as “uncorrected” and “corrected” (by subtraction of the mass loss ascribed to guest molecules); calculated values are given for different chemical formulae.

mass loss	experimental	corrected	$\text{Zr}_6\text{O}_4(\text{OH})_8(\text{bzpd})_4$	$\text{Zr}_6\text{O}_4(\text{OH})_6(\text{HCO}_2)_2(\text{bzpd})_4$
linker	48.9%	62.5%	60.8%	62.8%
residue	29.3%	37.5%	39.2%	37.2%

The comparison of the PXRD pattern of the Zr-*bzpd*c-MOF performed at room temperature with the PXRD obtained at 300 °C (Figure S9) shows slight shifts of the first two reflections and the presence of only three reflections at 300 °C of the (*hk*0) family indicates a loss of defined three-dimensional stacking of the two-dimensional layers.

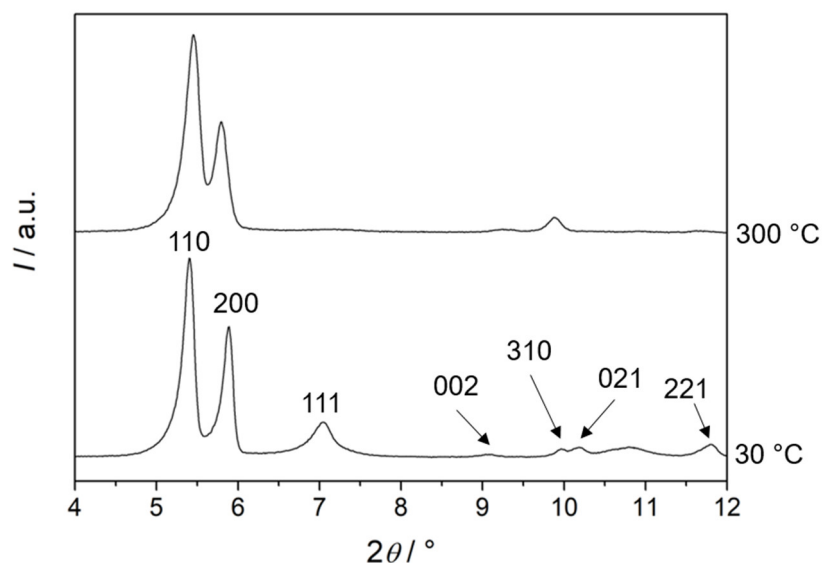


Figure S9. PXRD pattern with indices of *Zr-bzpdC*-MOF measured at 30 °C compared to the PXRD measured at 300 °C.

NMR Spectroscopy

For liquid-state NMR experiments 50 mg of the MOF were dispersed in [D₆]DMSO. Under vigorous stirring 30 μ L aqueous HF (40%) were added and stirred for 18 hours. After complete dissolution of the *Zr-bzpdC*-MOF, an excess of CaCl₂ was added to the clear solution. The supernatant was used for ¹H and ¹³C BB NMR investigations.

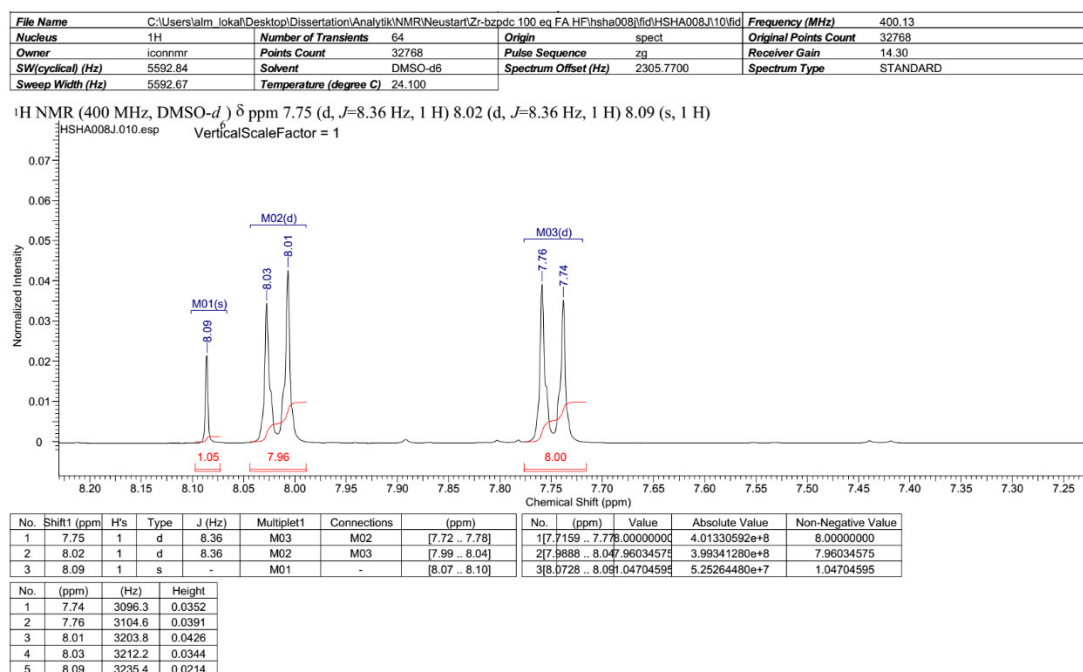


Figure S10. ¹H NMR investigation of dissolved *Zr-bzpdC*-MOF to determine the organic compounds and their ratio in the framework. 400 MHz, [D₆]DMSO, 25 °C, TMS: δ = 8.07 (s, 1 H, formic acid), 7.71 – 8.02 ppm (m, 16 H, H₂*bzpdC*).

The analysis of the ^1H NMR spectrum (Fig. S10) shows the signal for the formate proton at 8.7 ppm and the aromatic protons of the benzophenone dicarboxylate at 7.7 – 8 ppm. The integration reveals that the ratio of formate molecules compared to linker molecules is 1:1.995.

The combination of TGA and data from ^1H NMR spectroscopy on the dissolved MOF leads to a formula $\text{Zr}_6\text{O}_4(\text{OH})_6(\text{HCO}_2)_2(\text{bzpdc})_4$. Here, the twelve coordination sites of the IBU of the Zr-*bzpd*c-MOF are saturated by eight linker molecules, two hydroxyl groups and two formate molecules.

S2.3 Physisorption

For physisorption measurements 50 mg of the samples were outgassed in vacuum at 50 °C for 24 h prior to the sorption measurement. Surface areas were estimated by applying the Brunauer–Emmett–Teller (BET) equation. To determine the BET surface area the “Micropore BET Assistant” implemented in the ASiQwin 2.0 software from Quantachrome was used. The total pore volumes were estimated by single-point method at $p/p_0 = 0.95$. Nitrogen sorption isotherms were measured at 77 K on a Quantachrome Autosorb-3MP instrument and the argon sorption isotherms at 87 K on a Quantachrome Autosorb-1 instrument. The logarithmic scale of the Ar-isotherm for Zr-*bzpd*c-MOF and NLDFT calculation for pore size distribution is shown in Fig. S11.

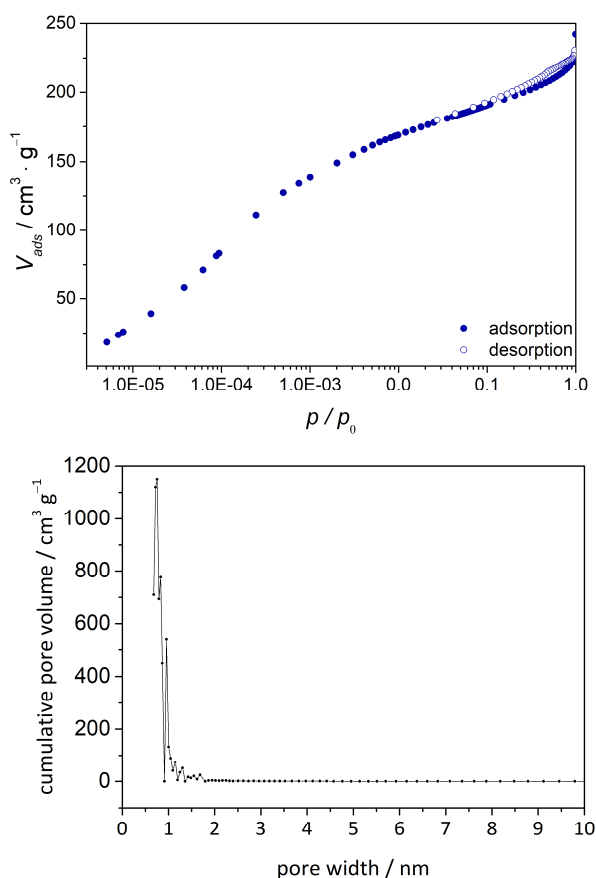


Figure S11. Left: logarithmic scale of the physisorption measurement of Zr-*bzpd*c-MOF with argon at 87 K; right: pore size distribution calculated with Kernel: “Ar at 87 K_zeolites/silica (cylinder. Pores, NLDFT equ.).

The logarithmic scale of the isotherm shows a slight increase at $1\text{E-}4$ relative pressure that indicates an ordered pore system with a defined pore diameter of less than 1 nm. The pore size distribution indicates the presence of an ordered pore system, but it is not possible to resolve such small pores out of this data.

S2.4 Chemical stability

Many Zr-based MOFs exhibit a high hydrolytic stability. Corresponding investigations on the Zr-*bzpd*c-MOF were carried out by dispersing 30 mg of the MOF in 1 mL of aqueous solutions of NaOH and HCl, respectively, which were adjusted to pH values in the range from 1 to 13. The suspensions were then vortexed with a VWR Digital Vortex Mixer for 24 h at speed 900. Afterwards the samples were freeze dried and characterized via PXRD (Fig. S12).

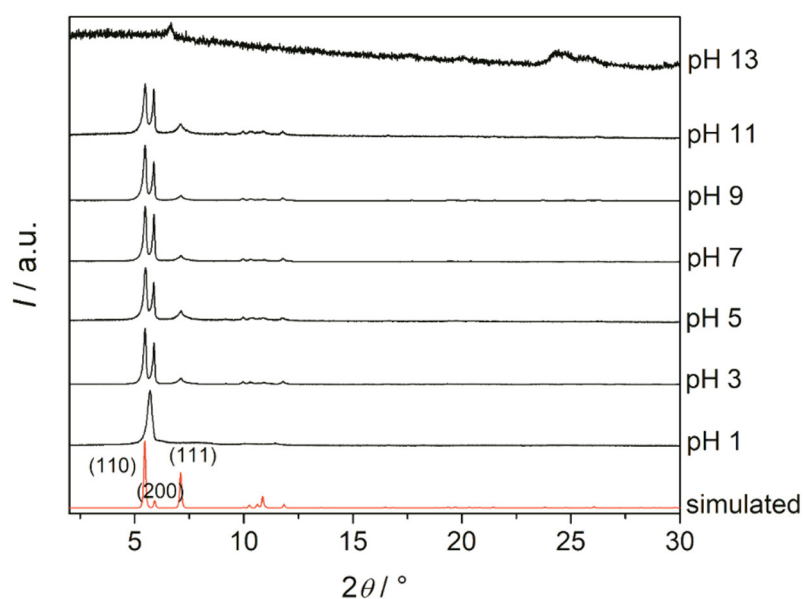


Figure S12. PXRD pattern of Zr-*bzpd*c-MOF treated with aqueous solutions with different pH values compared to the simulated XRD.

The PXRD pattern show characteristic reflections of Zr-*bzpd*c-MOF in a pH range of pH 3 to pH 11. Vortexing at pH 1 induced a loss of crystallinity, vortexing at pH 13 led to destruction of the framework. The Zr-*bzpd*c-MOF thus shows a good stability under basic and acidic conditions.

S3. Delamination

S3.1 TEM and SEM images

Fig. S13 shows larger versions of the TEM and SEM images displayed in Fig. 8 of the manuscript.

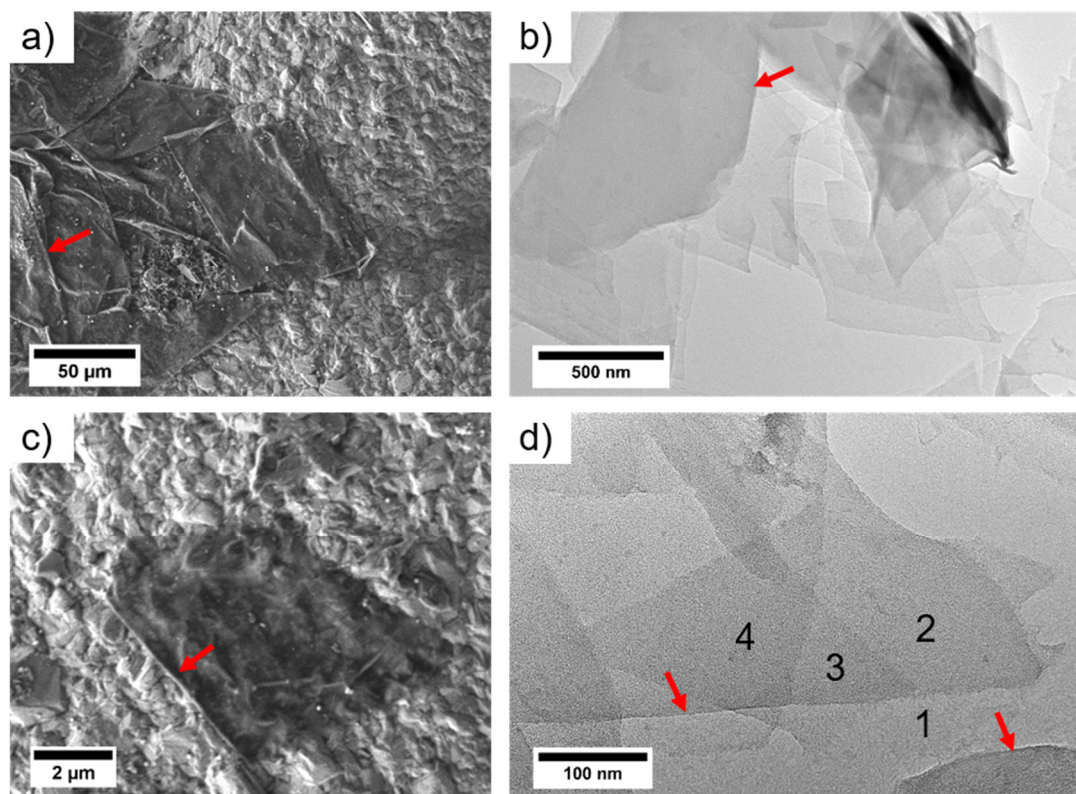


Figure S13. Enlarged versions of the TEM and SEM images displayed in Fig. 8 of the manuscript. a) and c): SEM images show delaminated Zr-*bzpdC*-MOF sheets that behave like wrapping paper. Also the substrate is visible through the particle (c), which indicates a thickness of just a few nm. b) and d): TEM image of delaminated Zr-*bzpdC*-MOF show rhombic shaped sheets with nearly uniform thickness.

S4. Postsynthetic modification

S4.1 NMR spectroscopy

The postsynthetically modified samples were dissolved in [D₆]DMSO with hydrofluoric acid with the same procedure as described above (Section 2.2). The spectra are shown in Figs. S14 and S15.

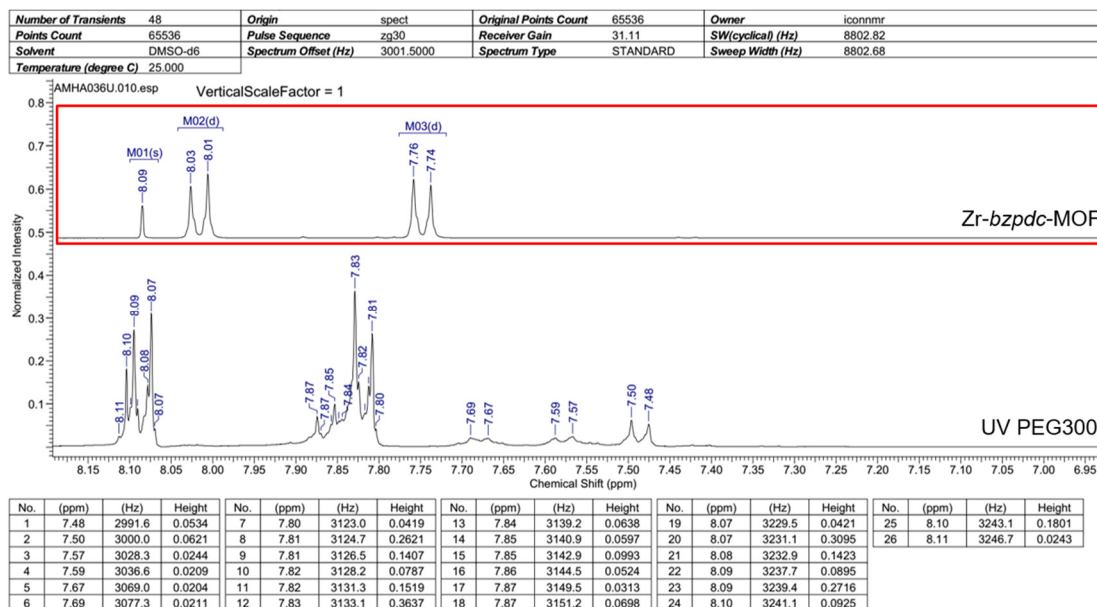


Figure S14. ¹H NMR spectrum of the sample treated with UV light in PEG300. 400 MHz, [D₆]DMSO, 25°C, TMS compared to ¹H NMR signals of untreated, dissolved Zr-bzpd-MOF (red box).

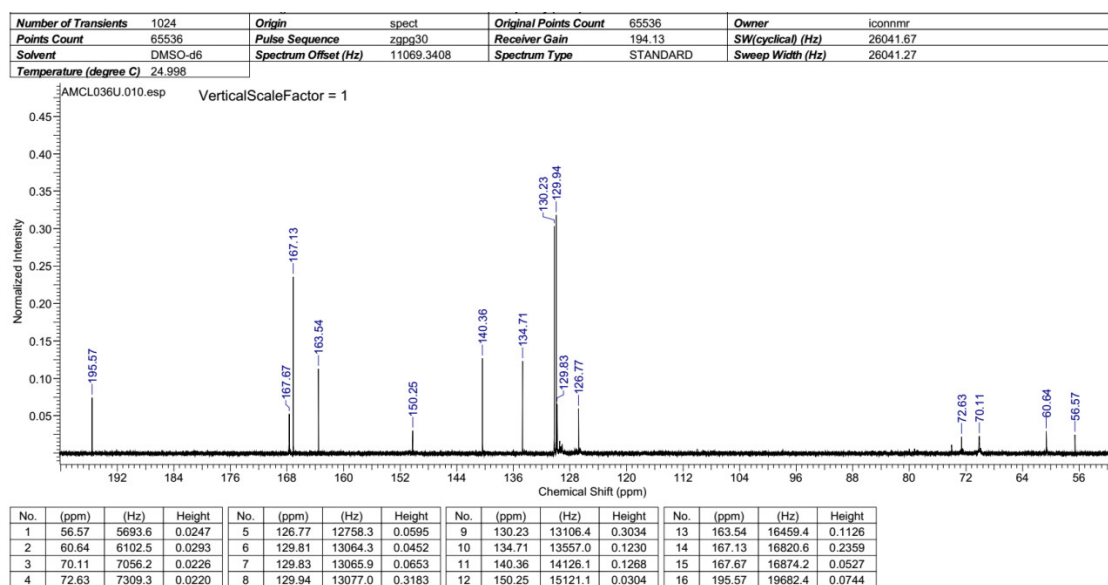


Figure S15. ¹³C-BB NMR spectrum of the sample treated with UV light in PEG300. 400 MHz, [D₆]DMSO, 25°C, TMS.

The chemical shifts of the signals in the NMR spectra of the postsynthetically modified sample differ from those observed on the untreated sample due to slightly

different amounts of hydrofluoric acid in the solution, which influences the chemical shifts. The ^1H NMR spectra show a different coupling behavior at 7.7 – 8.3 ppm compared to the linker molecule of untreated Zr-*bzpd*c-MOF (Fig. S10). Also, the presence of signals for PEG300 (7.4 – 7.7 ppm) indicates a successful postsynthetic modification of the MOF. The signal of the keto carbon atom should not be affected by the postsynthetic modification due to the fact that only the keto groups at the surface have reacted. The ^{13}C NMR spectrum (Fig. S14) substantiates this by the presence of the peak for the carbon atom of the keto group (195.57 ppm).

S5. References

- 1 Liang, W., Babarao, R., Murphy M. J., D'Alessandro D. M., *Dalton Trans.* **2015**, 28, 1516.
- 2 SAINT Integration Engine, version 7.68A, Bruker AXS, Inc.
- 3 Sheldrick, G. M. (2008) SADABS – Area Detector Adsorption and Other Corrections, version 2.03, Bruker AXS, Inc., **2008**.
- 4 Farrugia, L. J. (2012), *J. Appl. Cryst.* **2012**, 45, 849.
- 5 Sheldrick, G. M. (2008) *Acta Cryst.* A64, 112.

5.2 Direct grafting-from of PEDOT from a photoreactive Zr-based MOF – A novel route to electrically conductive composite materials

Contents

S1.	Materials and Instrumentation	138
S1.1	Materials	138
S1.2	Instrumentation	138
S2.	Experimental section	139
S2.1	Synthesis of Zr- <i>bzpd</i> c-MOF	139
S2.2	Postsynthetic modification with 3,4-ethylenedioxythiophene (EDOT) and ethanol	139
S2.3	Preparation for NMR spectroscopy	139
S2.4	Conductivity measurements	140
S3.	Additional results	141
S3.1	SEM images of Zr- <i>bzpd</i> c-MOF crystals	141
S3.2	Physisorption results	142
S3.3	Energy-dispersive X-ray spectroscopy	142
S3.4	Thermogravimetric analysis	148
S3.5	Elemental analysis	150
S3.6	Solution-state NMR investigations	151
S3.7	Theoretical Calculations	155
S3.8	Conductivity measurements	156
S4.	Postulated reaction mechanism	158
S5.	References	160

S1. Materials and Instrumentation

S1.1 Materials

Zirconium(IV)-oxychloride octahydrate, formic acid, *N,N*-dimethylformamide (DMF) and 3,4-ethylenedioxythiophene were purchased from Sigma Aldrich. Ethanol and acetone were purchased from VWR and benzophenone-4,4'-dicarboxylic acid from abcr Chemicals. All chemicals were used without further purification.

S1.2 Instrumentation

X-ray powder diffraction measurements were performed at room temperature using a STOE STADI-P transmission diffractometers equipped with curved Ge(111) monochromators with $\text{CuK}\alpha_1$ radiation ($\lambda = 1.540594 \text{ \AA}$) and a linear position-sensitive detector. The samples were fixed between X-ray amorphous foils.

Scanning electron microscopy and electron-dispersive X-ray spectroscopy were carried out on a JEOL JSM-6700F (2 keV). Solution-state ^1H and ^{13}C NMR spectra were measured on a BRUKER instrument at 400 MHz and were analysed with ACD NMR Processor 12. Physisorption isotherms were measured on an Autosorb 3 instrument from Quantachrome Instruments and were evaluated with the software ASiQwin 2.0 by Quantachrome Instruments. BET areas of the microporous samples were determined with the micropore BET assistant of the accompanying software. TGA data were obtained on a NETZSCH STA 409PC/PG instrument with a heating rate of $10 \text{ K}\cdot\text{min}^{-1}$ with a gas flow of 80% argon and 20% oxygen. Elemental analysis for carbon and sulfur (C-S analysis) was performed with an ELTRA C/S Analyzer and the UNI Software from ELTRA GmbH was used for evaluation. UV irradiation experiments were performed with a high power LED UV Spot from Laser 2000 with a wavelength of 365 nm. Van der Pauw experiments of the electrical conductivity were performed in a glovebox under Ar atmosphere. Conductivity measurements were performed using a self-made 4-point-probe setup with a Keithley 2100 multimeter (Beaverton, USA).

S2. Experimental section

S2.1 Synthesis of Zr-*bzpd*c-MOF

Solvothermal synthesis of Zr-*bzpd*c-MOF was carried out in Teflon-sealed screw cap glass vessels. Favorable conditions for the synthesis of a product without amorphous impurities are as follows: 3.22 g (10 mmol) $\text{ZrOCl}_2 \cdot 8 \text{H}_2\text{O}$ were dissolved in 200 mL DMF. After adding 56.59 mL formic acid (1.5 mol, 150 molar equivalents (eq) based on the amount of Zr^{4+}) and 8.11 g (30 mmol, 3 eq) H_2bzpd c, the clear solution was transferred in a 500 mL Teflon-sealed glass vessel and was kept at 120 °C for 2 weeks in a circulating air oven. After the reaction, the solution was cooled down to room temperature and the resulting solid was obtained by decanting, washed once with 100 mL of DMF and two times with 50 mL methanol and afterwards dried under reduced pressure. For further investigations the sample was activated via Soxhlet-extraction with acetone for 24 hours. The white powder was kept under reduced pressure until further usage. The resulting Zr-*bzpd*c-MOF crystals have a rhombic shape and a size of about 100 μm (Figure S1). The yield of the synthesis is about 50%.

S.2.2 Postsynthetic modification with 3,4-ethylenedioxythiophene (EDOT) and ethanol

For the postsynthetic modification (PSM) with EDOT, 100 mg Zr-*bzpd*c-MOF was dispersed in 2 mL neat EDOT and purged with Ar for 1 hour. Afterwards the dispersion was irradiated under Ar purging for a specific time (between 1 h – 72 h). After isolation of the product, it was washed two times with acetone and then Soxhlet-extracted with acetone for 48 hours. The samples were dried under reduced pressure overnight.

For comparison, a sample in which all the keto groups had reacted was prepared using the PSM with ethanol. The same procedure with 72 hours irradiation under argon purging was applied to Zr-*bzpd*c-MOF in ethanol. A ^{13}C NMR spectrum verified the complete reaction of the keto groups by the absence of a keto carbon signal at about 195 ppm (Figure S9).

S.2.3 Preparation for NMR spectroscopy

For solution-state NMR experiments, 50 mg of the MOF were dispersed in $[\text{D}_6]\text{DMSO}$. Under vigorous stirring 20 μL aqueous HF (40%) were added and stirred for 18 hours. After complete dissolution of the Zr-*bzpd*c-MOF, an excess of CaCl_2 was added to the clear solution. The supernatant was used for ^1H and ^{13}C BB NMR investigations.

S.2.4 Conductivity measurements

The Soxhlet-extracted and dried samples (activated in vacuum for at least 24 hours) were pressed into pellets (diameter of 8 mm, thickness between 0.7 – 0.9 mm) by using a hydraulic press for 1 minute at a weight of one ton (≈ 2000 bar). Van der Pauw measurements were performed in a glove box under inert atmosphere in the dark ($O_2 < 0.5$ ppm, $H_2O < 0.5$ ppm). Conductivity measurements were performed using a self-made 4-point-probe setup with a Keithley 2100 multimeter (Beaverton, USA). The van der Pauw method excludes the resistances of contacts and wires so that only the resistance of the material is observed.¹

S3. Additional results

S3.1 SEM images of Zr-*bzpd*c-MOF crystals

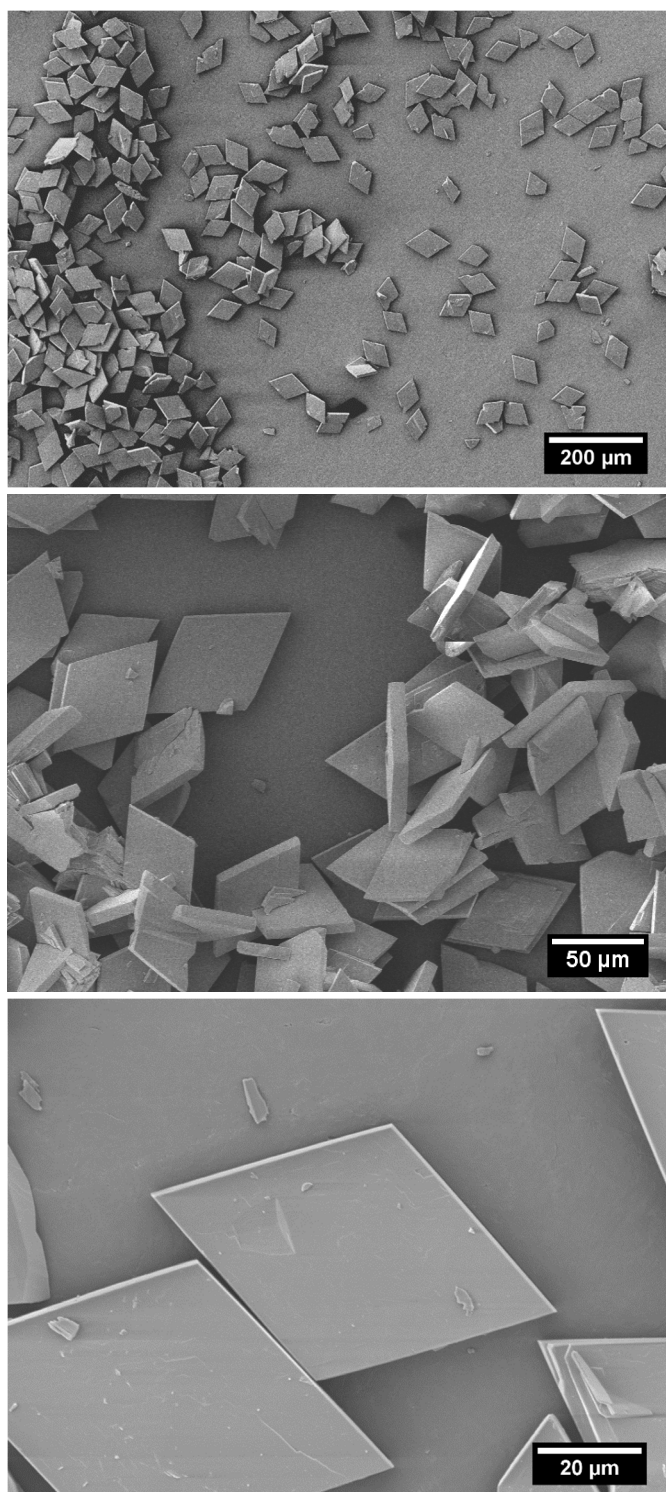


Figure S1. SEM images of single crystals of Zr-*bzpd*-MOF.

S.3.2 Physisorption results

Results of physisorption measurements ($N_2@77K$) are shown in Table S1.

Table S1. Calculated BET areas and total pore volumes for *Zr-bzpd*c-MOF and postsynthetically modified samples with PEDOT.

Sample	BET area / $m^2 \cdot g^{-1}$	Total pore volume / $cm^3 \cdot g^{-1}$
<i>Zr-bzpd</i> c-MOF	670	0.40
UV EDOT 1 h	630	0.37
UV EDOT 6 h	600	0.34
UV EDOT 24 h	570	0.30
UV EDOT 48 h	540	0.26
UV EDOT 72 h	520	0.23

S.3.3 Energy-dispersive X-ray spectroscopy

Energy-dispersive X-ray spectroscopy is used to display qualitatively the presence of EDOT/PEDOT molecules at the *Zr-bzpd*c-MOF surface through the sulfur signal at about 2.3 keV compared to the zirconium signals at 0.15 keV and 2.05 keV. The results are shown in the following figures for the *Zr-bzpd*c-MOF as-synthesized (Figure S2) and the irradiated samples with 24 h (Figure S3), 48 h (Figure S4) and 72 h (Figure S5) hours of UV light exposure in EDOT, respectively.

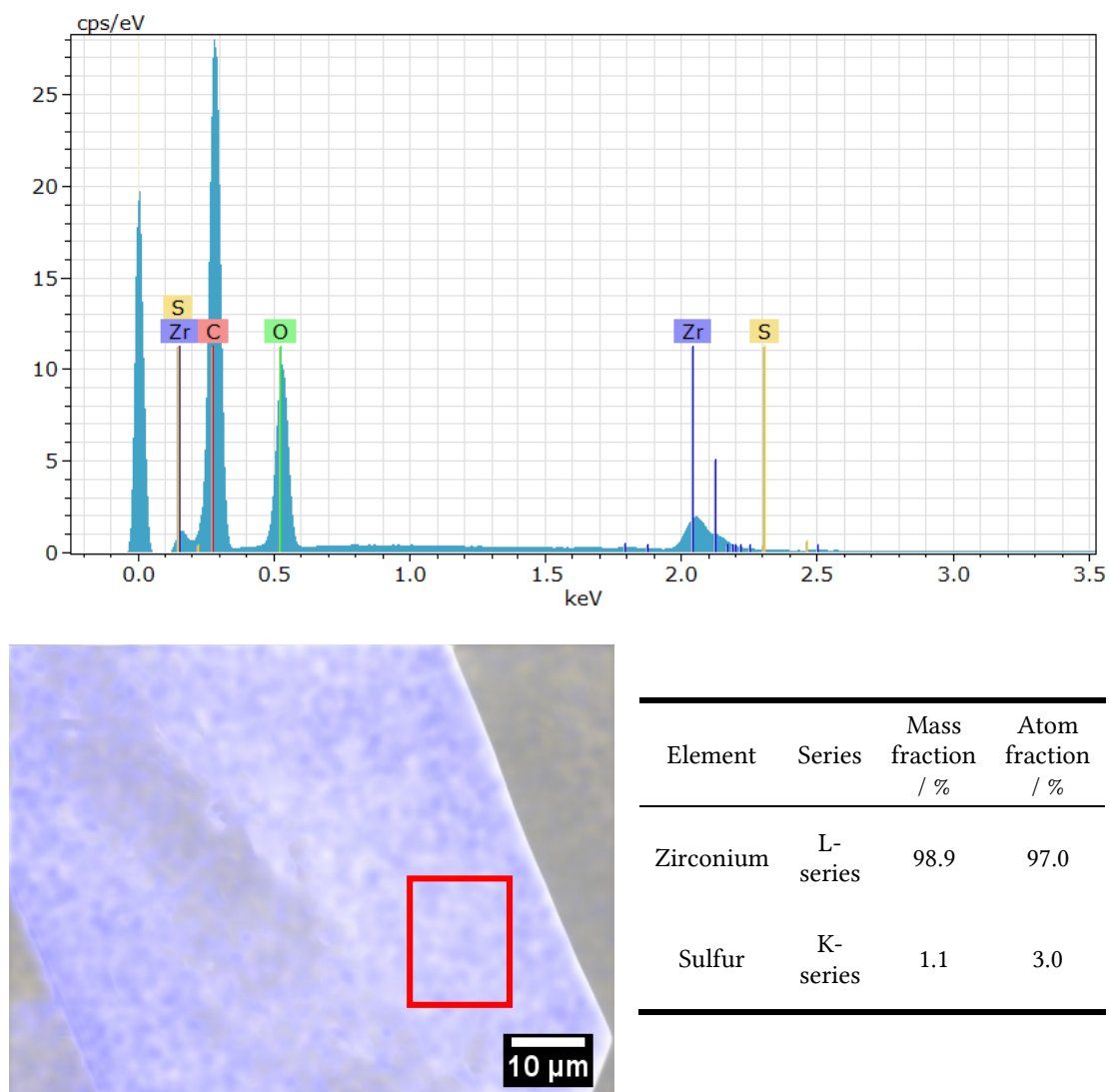


Figure S2. EDXS analysis of *Zr-bzpdC*-MOF as synthesized. Top: EDX spectrum with element assignments. Bottom: Image of measured crystal and the elemental analysis for zirconium and sulfur.

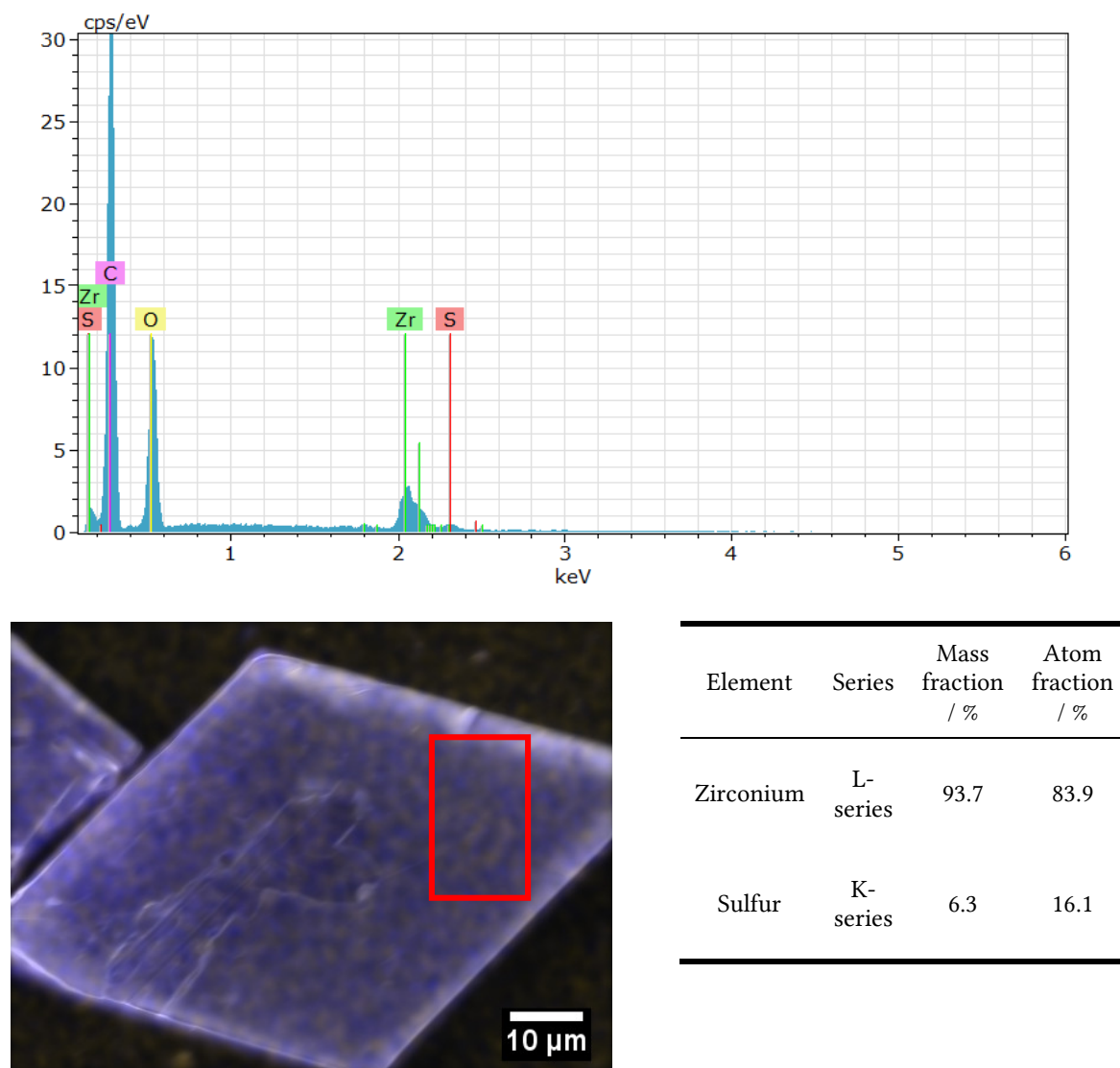


Figure S3. EDXS analysis of irradiated sample for 24 hours. Top: EDX spectrum with element assignments. Bottom: Image of measured crystal and the elemental analysis for zirconium and sulfur.

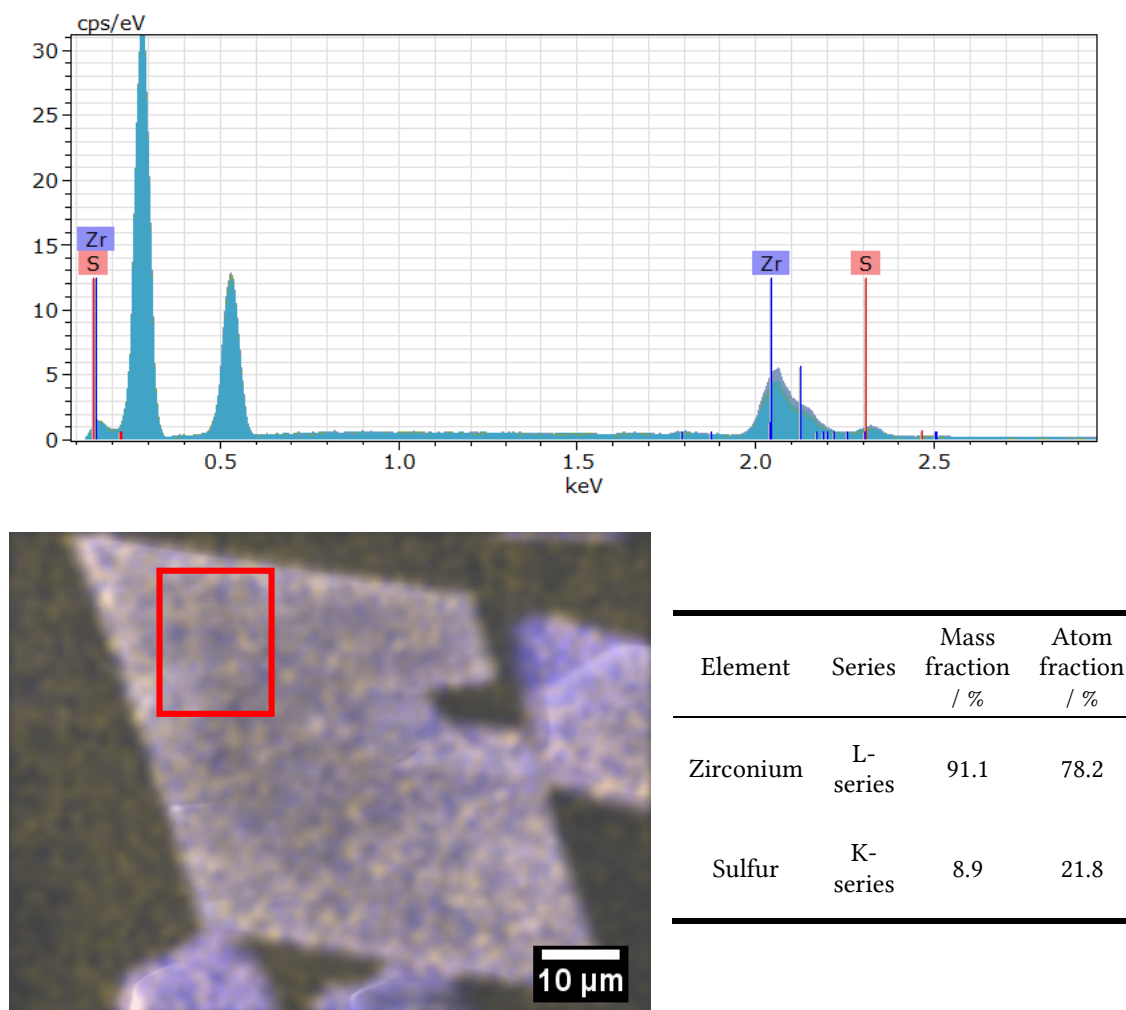


Figure S4. EDXS analysis of irradiated sample for 48 hours. Top: EDX spectrum with element assignments. Bottom: Image of measured crystal and the elemental analysis for zirconium and sulfur.

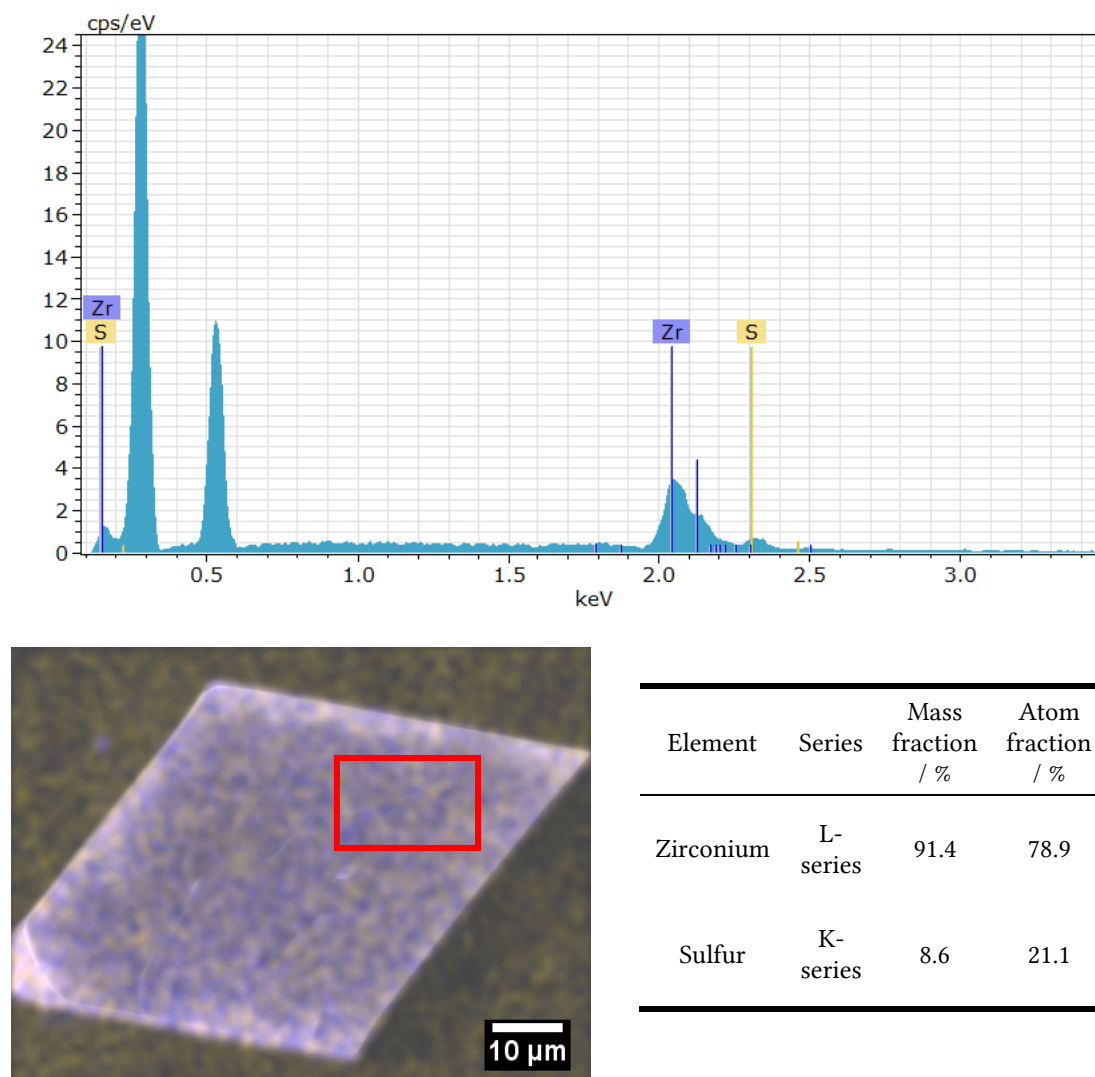


Figure S5. EDXS analysis of irradiated sample for 72 hours. Top: EDX spectrum with element assignments. Bottom: Image of measured crystal and the elemental analysis for zirconium and sulfur.

Quantitative data regarding the contents of Zr and S as derived from the EDX results are given in Table S2. Without further calibration, we take these results to qualitatively underline the presence of EDOT/PEDOT in the samples whereby the amount of the sulfur-containing species appears to increase with longer irradiation times.

Table S2. Mass fractions of zirconium and sulfur as calculated from EDXS data.

Sample	Zr / %	Sulfur / %
Zr- <i>bzpd</i> c-MOF	98.9	1.1
UV EDOT 24 h	93.7	6.3
UV EDOT 48 h	91.1	8.9
UV EDOT 72 h	91.4	8.6

S3.4 Thermogravimetric analysis

Thermogravimetric analysis curves of Zr-*bzpd*c-MOF and for a sample of Zr-*bzpd*c-MOF postsynthetically modified with EDOT for 72 hours are shown in Figures S6 and S7, respectively.

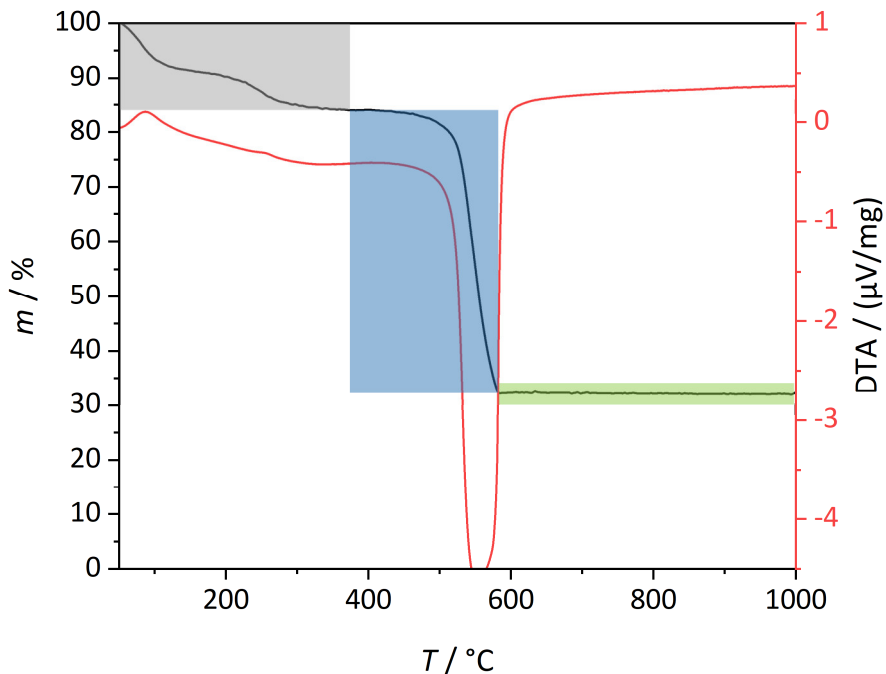


Figure S6. TGA and DTA curves for Zr-*bzpd*c-MOF. (grey: desorption of guest molecules; blue: combined removal of linker molecules and EDOT molecules; green: inorganic residue (ZrO₂))

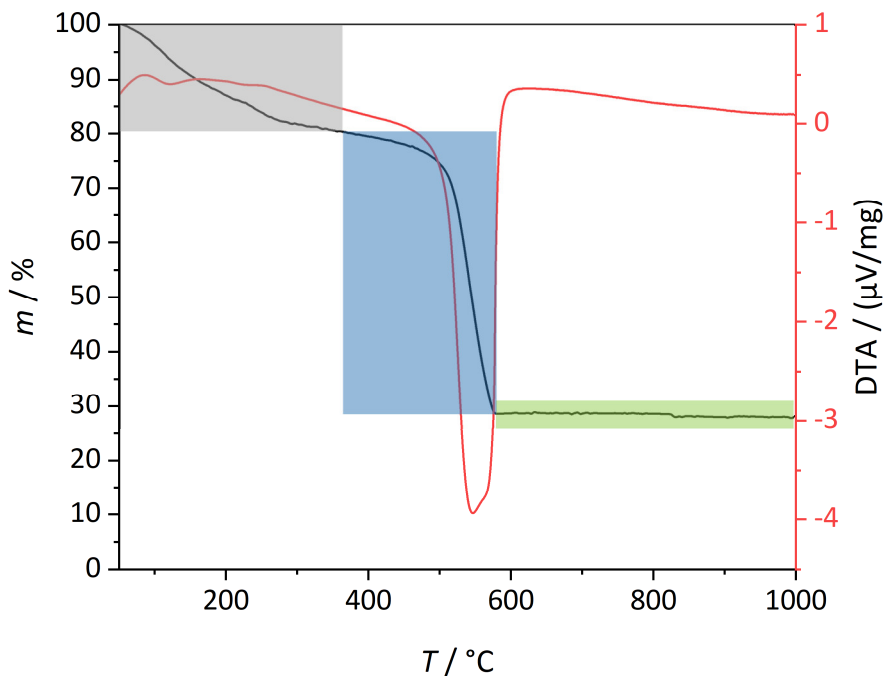


Figure S7. TGA and DTA curves for a sample of Zr-*bzpd*c-MOF postsynthetically modified with EDOT for 72 hours. (grey: desorption of guest molecules; blue: combined removal of linker molecules and EDOT molecules; green: inorganic residue (ZrO₂))

Comparing the amount of the organic contents of Zr-*bzpd*c-MOF to that of postsynthetically modified Zr-*bzpd*c-MOF shows an excess for the latter of about 2.8% of organic molecules which can be ascribed to the presence of EDOT/PEDOT molecules (Table S3). The amount of EDOT/PEDOT is calculated by comparing the “corrected” amounts with the “theoretical” amounts of the organics and the residue originating from the same amount of ZrO₂. Under the assumption that only the keto groups on the outer surface of the MOF crystals react in the photochemical reaction, an approximate average chain length of the PEDOT chains can be calculated (see Section 3.7).

Table S3. Evaluation of the thermogravimetric measurements. Mass fractions derived from thermogravimetric analysis curves of Zr-*bzpd*c-MOF and of Zr-*bzpd*c-MOF postsynthetically modified with EDOT for 72 hours; data are given as “experimental” and “corrected” (after subtraction of the mass loss ascribed to guest molecules).

Zr- <i>bzpd</i> c-MOF	Experimental	Corrected	Theoretical composition for Zr- <i>bzpd</i> c-MOF ²
Guest removal	-17.8%	-	-
Decomposition of organics	-51.3%	-62.4%	-62.8%
Residue (ZrO ₂)	30.9%	37.6%	37.2%

UV EDOT 72 h	Experimental	Corrected	Theoretical composition for Zr- <i>bzpd</i> c-MOF ²
Guest removal	-19.6%	-	-
Decomposition of organics	-51.3%	-63.8%	-62.8%
Residue (ZrO ₂)	29.1%	36.2%	37.2%

S3.5 Elemental analysis

The carbon and sulfur contents were determined via C-S analysis. The results are shown in Table S4. The amount of 0.76% sulfur corresponds to about 3.4% EDOT.

Table S4. Mass fractions of carbon and sulfur as determined via C-S analysis of Zr-*bzpd*c-MOF and of a sample of Zr-*bzpd*c-MOF postsynthetically modified with EDOT for 72 hours.

Sample	Carbon / %	Sulfur / %
Zr- <i>bzpd</i> c-MOF	42.94 (15)	0.03 (02)
UV EDOT 72 h	43.80 (12)	0.76 (02)

S3.6 Solution-state NMR investigations

NMR spectra of acid-digested Zr-*bzpd*c-MOF show the presence of formic acid in the framework and signals for the benzophenone groups (Figure S8). This is comparable to results already published.² The singlet at about 8.09 ppm represents the formate molecules. The signals for the aromatic protons of benzophenone-4,4'-dicarboxylic acid are contained in the multiplet at 7.79 ppm – 8.08 ppm.

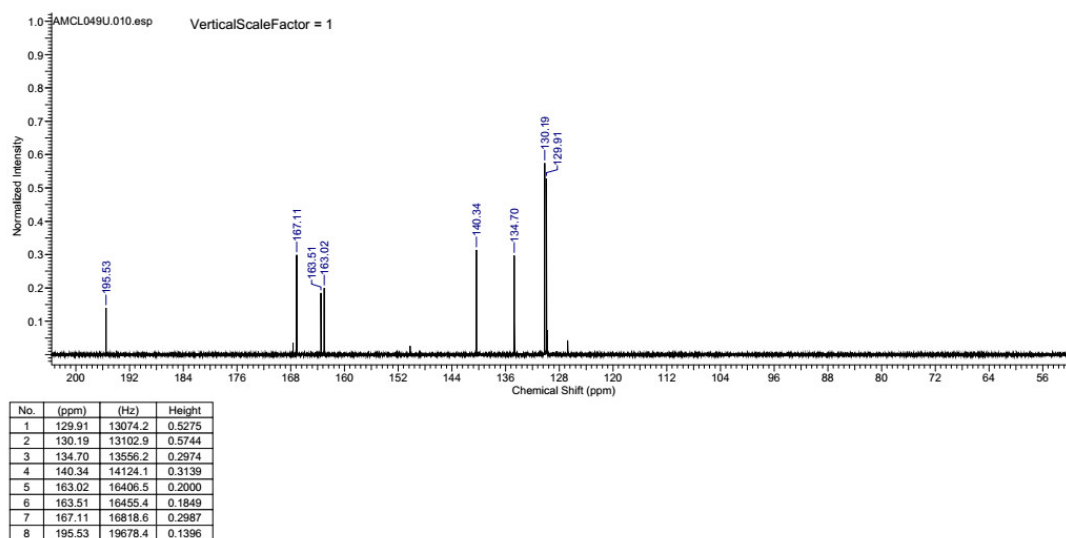
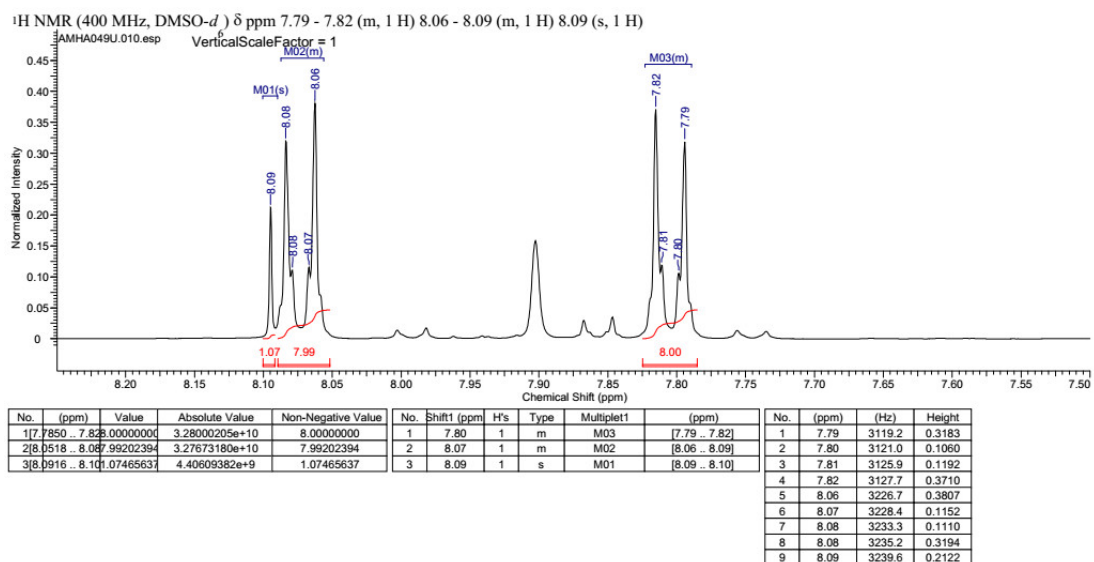


Figure S8. ¹H and ¹³C NMR spectra of acid-digested sample of Zr-*bzpd*c-MOF.

For further investigations the keto carbon signal of about 195 ppm is the most important one. The ^{13}C NMR spectrum of the sample postsynthetically modified with ethanol (Figure S9) shows, when compared to the untreated sample, no signal for the keto carbon atom. This indicates a complete reaction of the keto groups with ethanol molecules, leading to the formation of a C–C bond and a hydroxyl group. The ^1H NMR spectrum correspondingly shows a quartet at about 3.45 ppm (methylene group) and a triplet at about 1.05 ppm (methyl group). As no benzophenone groups are present in this sample anymore, the mechanism proposed in the manuscript to explain the conductivity of the pristine Zr-*bzpd*c-MOF is not effective anymore. Correspondingly, no electrical conductivity is measured on this sample.

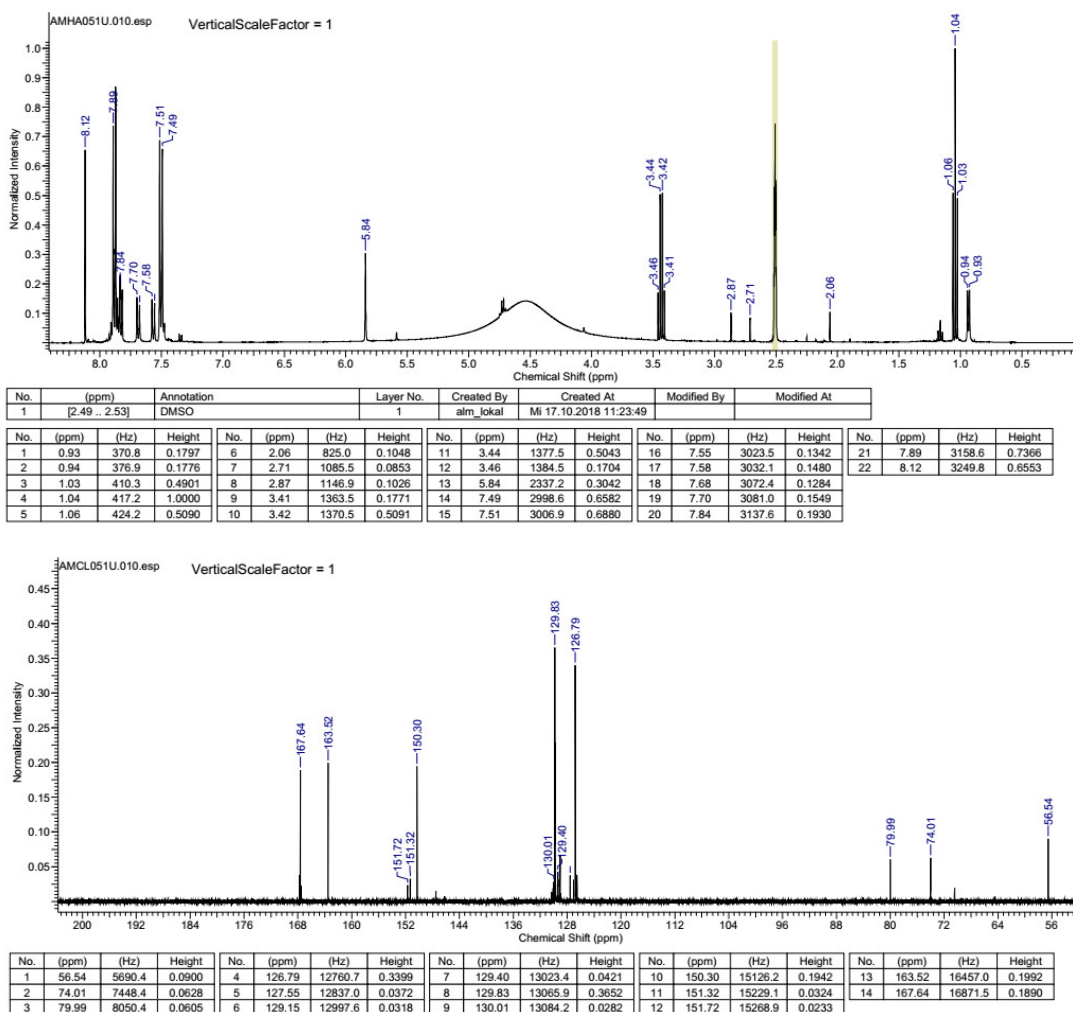


Figure S9. ^1H and ^{13}C NMR spectra of acid-digested Zr-*bzpd*-MOF postsynthetically modified with ethanol.

For a Zr-*bzpd*c-MOF sample postsynthetically modified with EDOT (irradiation for 72 hours) which was dissolved after synthesis, ^1H and ^{13}C NMR spectra are shown in Figure S10. In the ^1H NMR spectrum, signals for thiophene units should appear at about 6.5 ppm. A multiplet with a very low intensity can be observed at this position; however, this signal cannot be quantified. The ^1H NMR spectrum can thus only show the presence of a very small quantity of EDOT units in the dissolved postsynthetically modified sample. We ascribe the fact that no signals are observed for oligo-/polymer chains of PEDOT to the insolubility of PEDOT chains which can then not be detected with solution-state NMR spectroscopy. The presence of the keto carbon signal in the ^{13}C NMR spectrum shows that only a small amount of the keto groups has reacted with EDOT molecules. This is line with the assumption that only surface-standing keto groups have reacted.

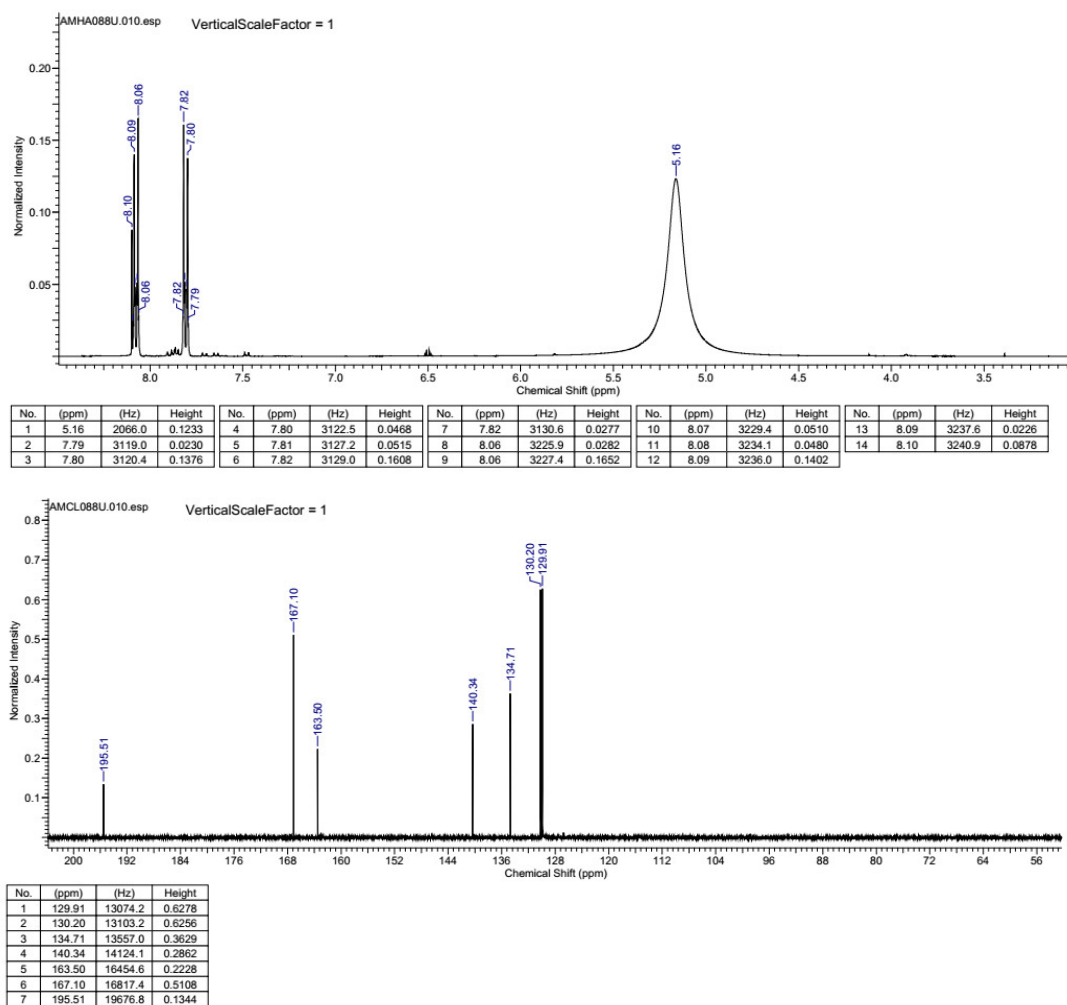


Figure S10. ^1H and ^{13}C NMR spectra of acid-digested sample of Zr-*bzpdC*-MOF postsynthetically modified with EDOT for 72 hours.

S3.7 Theoretical Calculations

Based on the fact that

- according to the crystal structure of Zr-*bzpd*c-MOF, keto groups accessible for the PSM are present on the basal planes

and using

- the dimensions of the crystals
- the (theoretical) density of the Zr-*bzpd*c-MOF

as well as

- the contents (mass fractions) of EDOT/PEDOT as derived from TGA and C-S analysis (2.8% and 3.4%, respectively)

we can estimate the lower boundary of the average chain lengths of PEDOT molecules attached to the MOF surface if we make the following additional assumption:

- every surface-standing keto group has initiated the polymerization of a PEDOT chain

This assumption implies that growing polymer chains do not sterically hinder the access of still unreacted surface-standing keto groups and that chain initiation dominates over chain propagation. The distance between surface-standing keto groups is ca. 11 Å; therefore, steric hindrance from grown polymer chains may not be such a strong issue. On the other hand, often chain propagation dominates over chain initiation. With these restrictions in mind, we carried out the following calculations which provide us with an estimate of the lower boundary of the PEDOT chain lengths.

We determined the average size of the basal rhombic planes of the crystals to 4346 μm^2 (average rhombus size: 82 μm x 53 μm , determined with ImageJ on about 30 crystals in Figure S1). The average thickness of the crystals varies more strongly between 5 – 10 μm . For the calculations we use a thickness of 7.5 μm to determine a volume of $1.6298 \cdot 10^{-8}$ cm^3 per crystal. With the theoretical density of 1.16 $\text{g} \cdot \text{cm}^{-3}$ the mass of one crystal is about $1.89 \cdot 10^{-8}$ g. Referring again to the crystal structure model for the Zr-*bzpd*c-MOF, the number of surface-standing keto groups accessible for the photochemical reaction is about $3.0 \cdot 10^9$ per crystal. The total amount of keto groups is about $2.34 \cdot 10^{13}$ per crystal. A crystal of Zr-*bzpd*c-MOF has about 0.01% keto groups at the outer surface.

1 g of such rhombic shaped Zr-*bzpd*c-MOF crystals thus offers $1.6 \cdot 10^{17}$ keto groups for reaction. The mass of EDOT/PEDOT bound by to this amount of MOF is 28 mg or 34 mg, respectively, depending on the determination method (TG vs. C-S analysis). Distributing this mass of EDOT/PEDOT over $1.6 \cdot 10^{17}$ keto groups, we obtain average chain lengths of about 70 monomer units from the TGA result and of about 90 monomer units from the result of the C-S analysis, respectively. Due to the uncertainties mentioned above, we state with due caution that the grafted-from PEDOT chains have lengths of at least ca. 100 EDOT units.

S3.8 Conductivity measurements

Electrical conductivities were measured on pressed pellets. In order to verify that the press procedure did not affect the crystallinity of the samples, PXRD diagrams were measured afterwards (Figure S11).

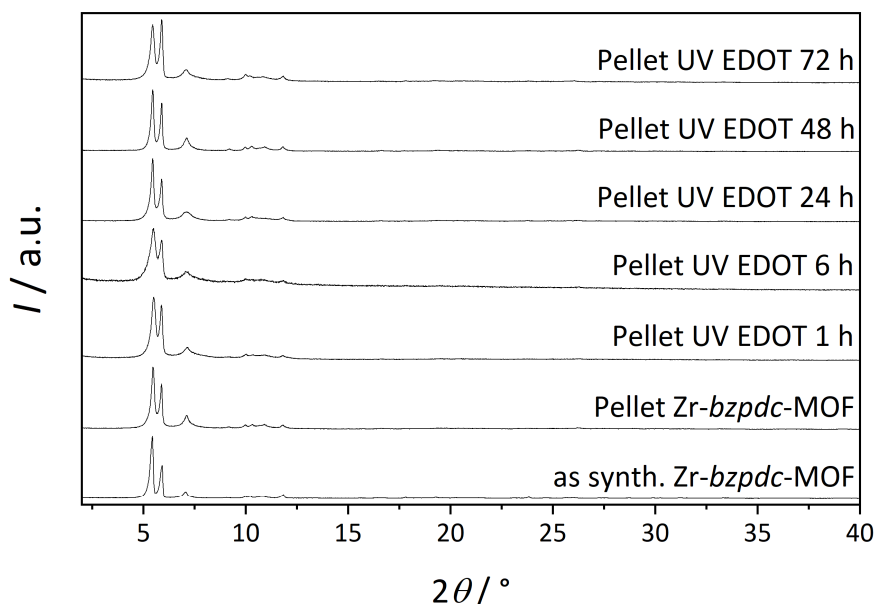


Figure S11. PXRD patterns of pressed pellets after conductivity measurements.

Photographs of pressed pellets with four ohmic contacts (Figure S12) and results from electrical conductivity measurement (Table S5) show the influence of the photochemical polymerization reaction on the color of the samples and on their electrical conductivity.

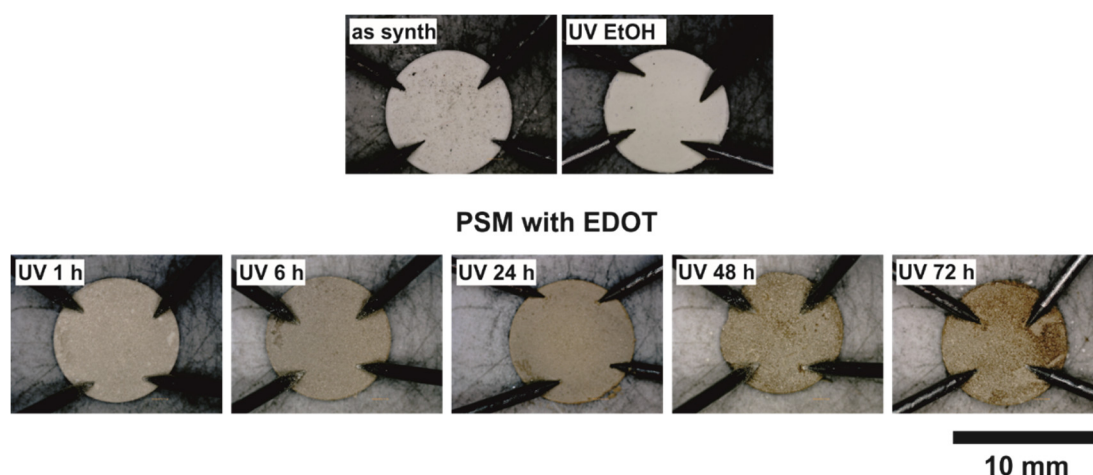


Figure S12. Photographs of the contacted pressed pellets of the samples.

Table S5. Results of electrical conductivity measurements of *Zr-bzpdC*-MOF and postsynthetically modified samples.

Sample	Pellet thickness / nm	Conductivity / S·cm ⁻¹
<i>Zr-bzpdC</i> -MOF	0.78	$5.37 \cdot 10^{-6}$
UV EtOH 72 h	0.77	immeasurably low
UV EDOT 1 h	0.80	$6.05 \cdot 10^{-6}$
UV EDOT 6 h	0.83	$1.07 \cdot 10^{-5}$
UV EDOT 24 h	0.77	$8.96 \cdot 10^{-4}$
UV EDOT 48 h	0.74	$2.48 \cdot 10^{-3}$
UV EDOT 72 h	0.75	$6.93 \cdot 10^{-3}$

To visualize the properties of the hybrid materials after different reaction times, we plot the BET area versus the electrical conductivity (Figure S13). The postsynthetic polymerization of EDOT at the MOF surface leads to a slight decrease in porosity. The graph shows impressively that after a reaction time of more than 24 hours the porosity remains about the same (around $500 \text{ m}^2 \text{ g}^{-1}$) whereas the electrical conductivity increases with longer reaction time.

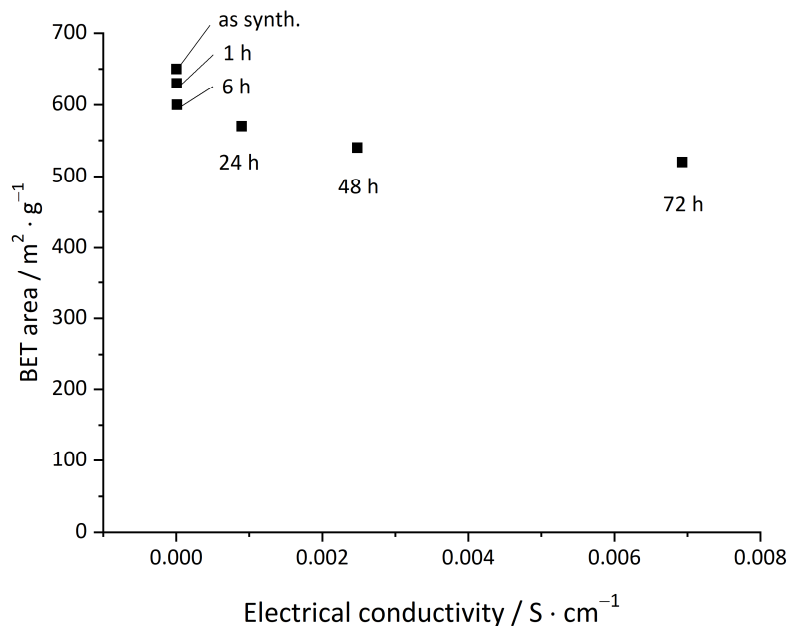
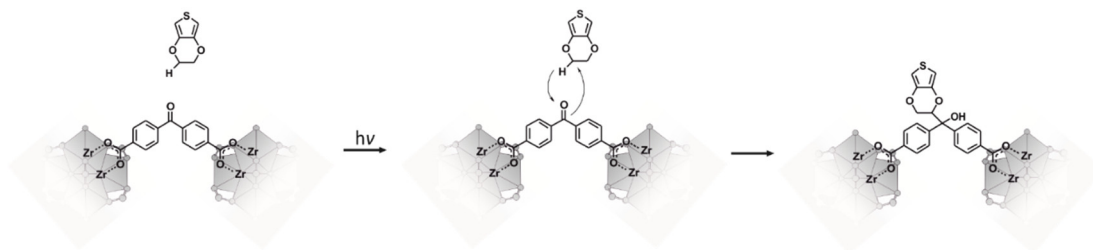


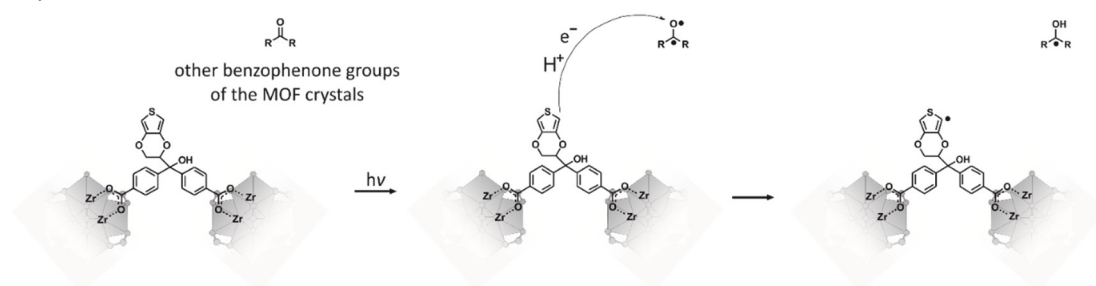
Figure S13. Plot of the BET area versus the electrical conductivity for *Zr-bzpdC*-MOF and postsynthetically modified samples. The reaction times for the postsynthetic reaction are indicated.

S4. Postulated reaction mechanism

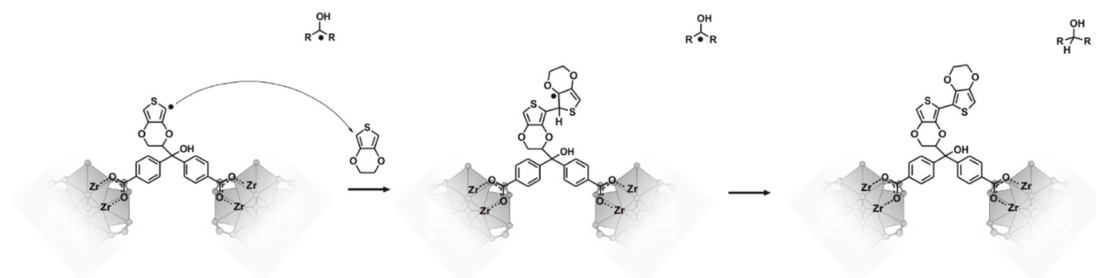
For the polymerization of EDOT at the surface keto groups of the *Zr-bzpdC*-MOF through irradiation, we postulate the reaction mechanism detailed below. In the first step, we postulate that a photoexcited keto group reacts with a C-H bond of the ethylene group of EDOT, resulting in a covalent bond between the linker molecule and the EDOT unit (of course, this initial reaction could also occur at the thiophene part). This mechanism is well known for the photoreactive benzophenone group (see Scheme 1 of the main paper).³⁻⁵ In general, the following steps could also occur in solution, leading to oligo-/polymers not attached to the MOF surface. However, the following extensive Soxhlet extraction should remove all molecules which are not covalently attached to the MOF. Therefore, we postulate the presence of a covalent bond between the MOF crystals and those PEDOT chains which have not been removed by the extraction.



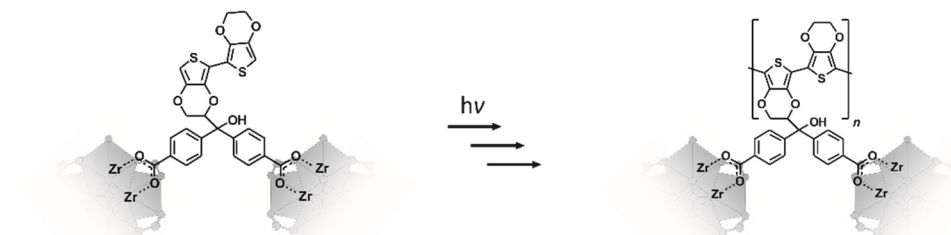
For the second step, we propose the oxidative formation of a radical at the attached EDOT moiety. The only oxidizing agent present in the reaction system is the benzophenone unit of the linker, and in fact, the photo-oxidative potential of irradiated benzophenone has been described in literature,⁶⁻⁸ and the corresponding electron transfer is of course part of the photochemical addition reaction. The shortest distance between two neighbouring keto groups of the MOF crystals is 4.8 Å.



This radical can then attack another EDOT molecule in the third step resulting in a dimer radical. This then loses a hydrogen atom to the ketyl radical, so that on the surface of the MOF crystals the linker molecules actually contain diphenylmethanol groups. The formation of the alcohol group is a consequence of the reduction of the keto group.



The polymerization can then continue under further oxidative radical formation, accompanied by reduction of surface-standing keto groups of the framework.



S5. References

- 1 A. A. Ramadan, R. D. Gould and A. Ashour, *Thin Solid Films* **1994**, 239, 272.
- 2 A. Mohmeyer, A. Schaate, B. Brechtken, J. C. Rode, D. P. Warwas, G. Zahn, R. J. Haug and P. Behrens, *Chem. Eur. J.* **2018**, 24, 12848.

- 3 D. Karaca Balta, Ö. Karahan, D. Avcı and N. Arsu, *Prog. Org. Coat.* **2015**, *78*, 200.
- 4 M. A. Winnik and U. Maharaj, *Macromolecules* **1979**, *12*, 902.
- 5 O. Prucker, C. A. Naumann, J. Rühle, W. Knoll and C. W. Frank, *J. Am. Chem. Soc.* **1999**, *121*, 8766.
- 6 N. Filipescu and F. L. Minn, *J. Am. Chem. Soc.* **1968**, *90*, 1544.
- 7 B. Qu, Y. Xu, L. Ding and B. Rnby, *J. Polym. Sci. A Polym. Chem.* **2000**, *38*, 999.
- 8 A. Demeter, K. Horváth, K. Böör, L. Molnár, T. Soós and G. Lendvay, *J. Phys. Chem. A* **2013**, *117*, 10196.

5.3 Inside/Outside: Postsynthetic Modification of the Zr-*benzophenonedicarboxylate*-MOF

Contents

S1. Additional results	162
S1.1 NMR investigations - PSM of H ₂ <i>bzpd</i> c and Zr- <i>bzpd</i> c-MOF in aqueous media	162
S1.2 Physisorption	169
S1.3 Voronoi network	175
S1.4 NMR investigations - PSM of Zr- <i>bzpd</i> c-MOF and H ₂ <i>bzpd</i> c with alcohols	176
S1.5 Simulation	185
S2. References	185

S1 Additional results

S1.1 NMR investigations - PSM of $H_2bzipdc$ and $Zr-bzipdc$ -MOF in aqueous media

Figures S1 – S10 show solution phase NMR spectra of $H_2bzipdc$ and of acid-digested samples of $Zr-bzipdc$ -MOF, both before and after irradiation in water or basic solution, respectively. In the 1H NMR spectra taken on the samples which had successfully undergone PSM with water, namely $H_2bzipdc$ under basic conditions and $Zr-bzipdc$ -MOF in water, an additional signal at about 8.03–8.04 ppm indicates the presence of a hydroxyl group at an aromatic carbon atom of the benzophenone moiety. The signals for the aromatic protons of benzophenone-4,4'-dicarboxylic acid are contained in the 1H NMR spectra of all samples in the multiplet at 7.81 ppm – 8.10 ppm. In the ^{13}C NMR spectra of all samples, the signal of the keto carbon atom at 195 ppm is most important. It vanishes or is strongly reduced in intensity upon successful PSM.

Pristine $H_2bzipdc$

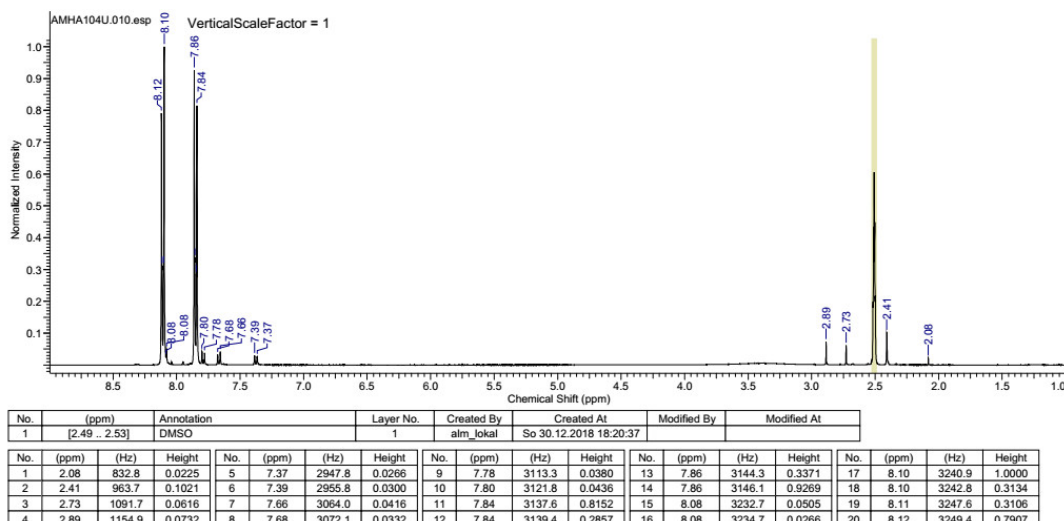


Figure S1. 1H NMR spectrum of pristine $H_2bzipdc$.

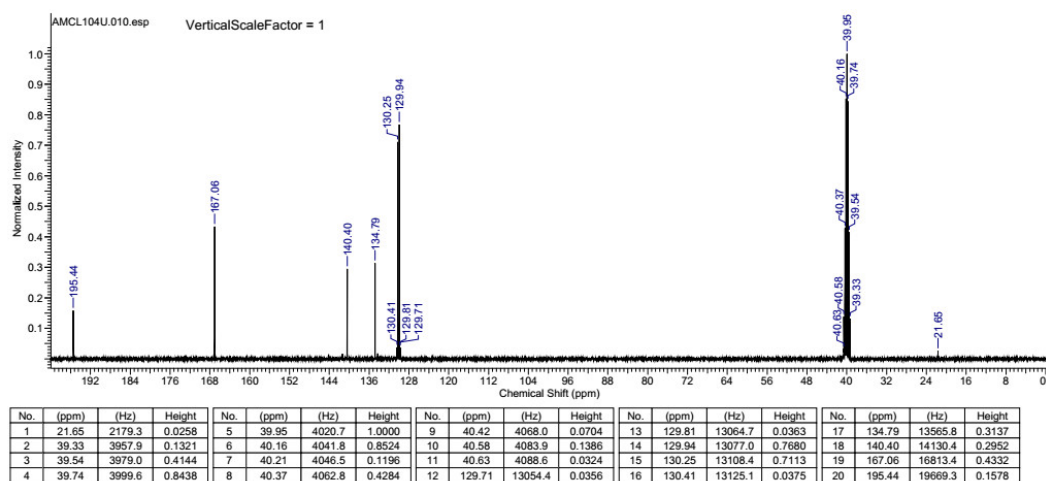


Figure S2. ^{13}C NMR spectrum of pristine H_2bzpdC .

H_2bzpdC after irradiation in water at pH 7

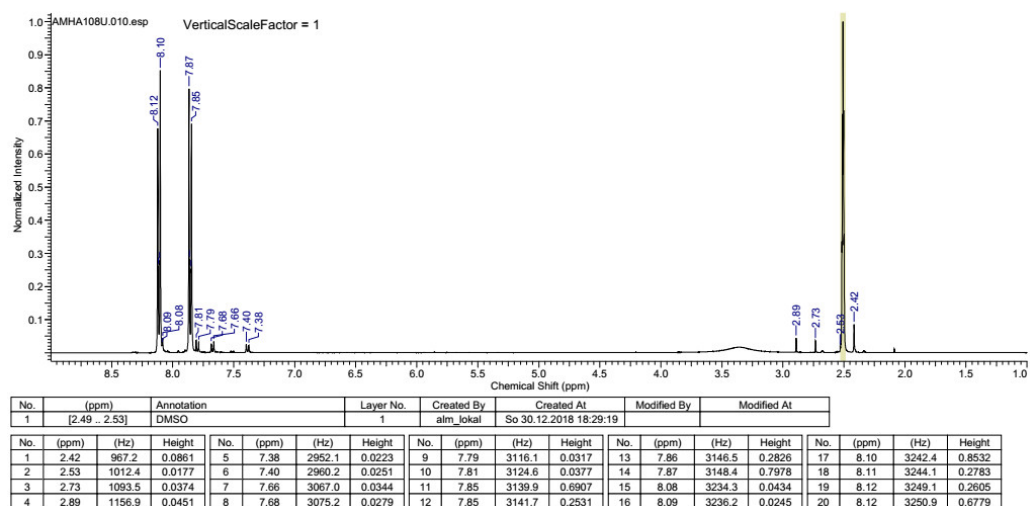


Figure S3. ^1H NMR spectrum of H_2bzpdC after irradiation in water, carried out at a pH value of about 7.

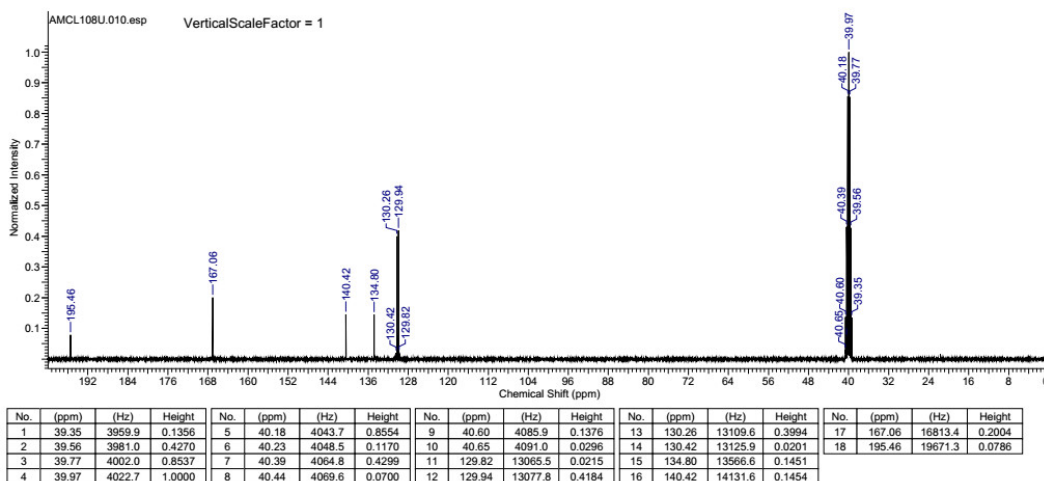


Figure S4. ¹³C NMR spectrum of H₂bzpdc after irradiation in water, carried out at a pH value of about 7.

H₂bzpdc after irradiation in water at pH 10

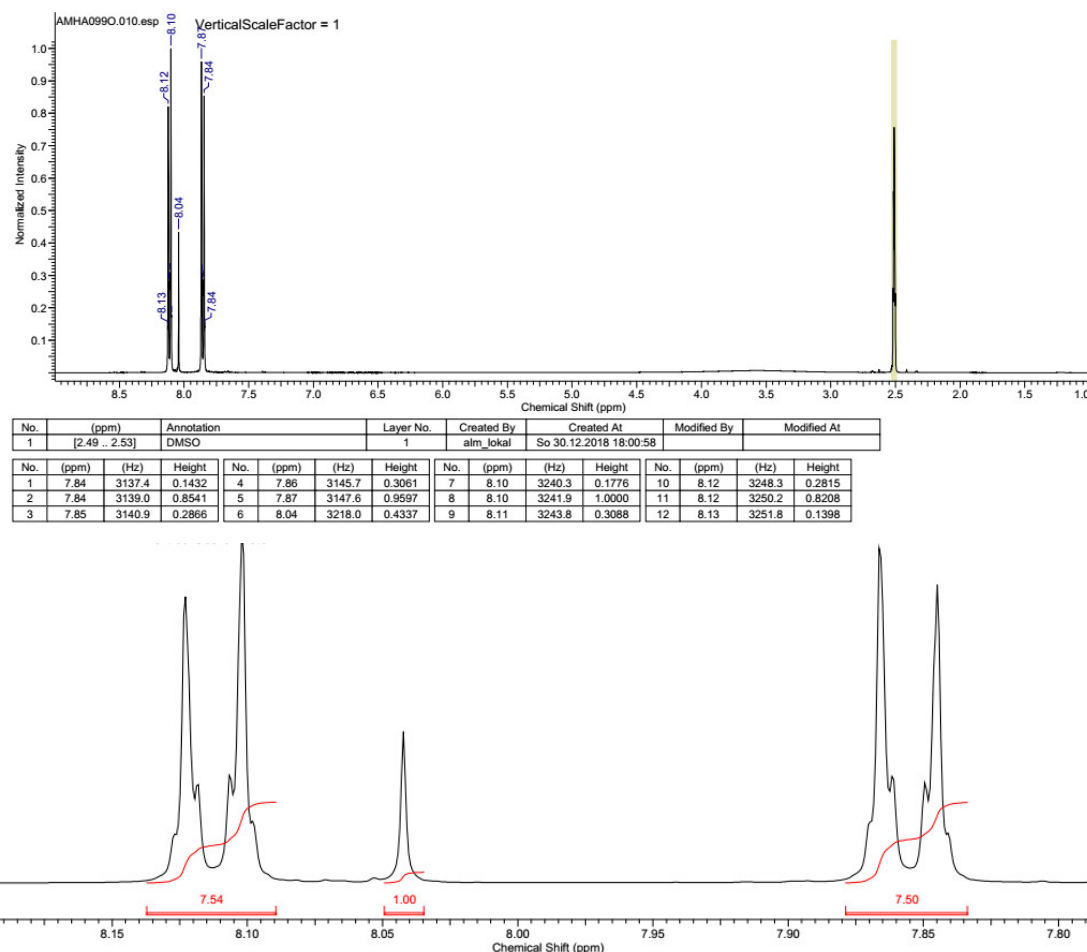


Figure S5. Top: ¹H NMR spectrum of H₂bzpdc after irradiation in water at a pH value of about 10 (adjusted with NaOH). Bottom: Integrated peak areas for the determination of the ratio of reacted linker molecules (about 50%).

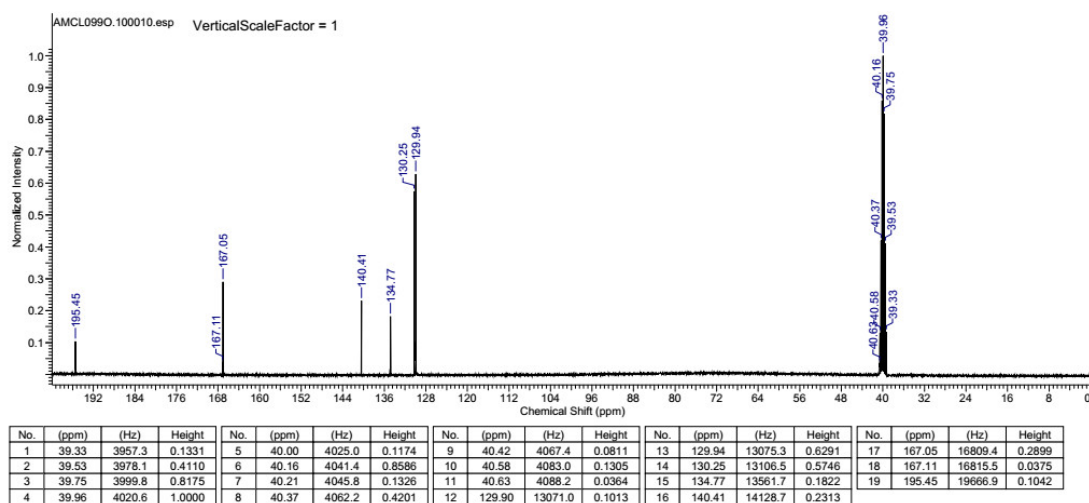


Figure S6. ^{13}C NMR spectrum of H_2bzpdc after irradiation in water, carried out at a pH value of about 10 (adjusted with NaOH).

Pristine Zr-*bzpd*c-MOF

The ^1H NMR spectrum of acid-digested pristine Zr-*bzpd*c-MOF shows the presence of formate ions (singlet at 8.11 ppm) which are part of the structure of the MOF.¹ The signals for the aromatic protons of benzophenone-4,4'-dicarboxylic acid are contained in the multiplet at 7.81 ppm – 8.10 ppm.

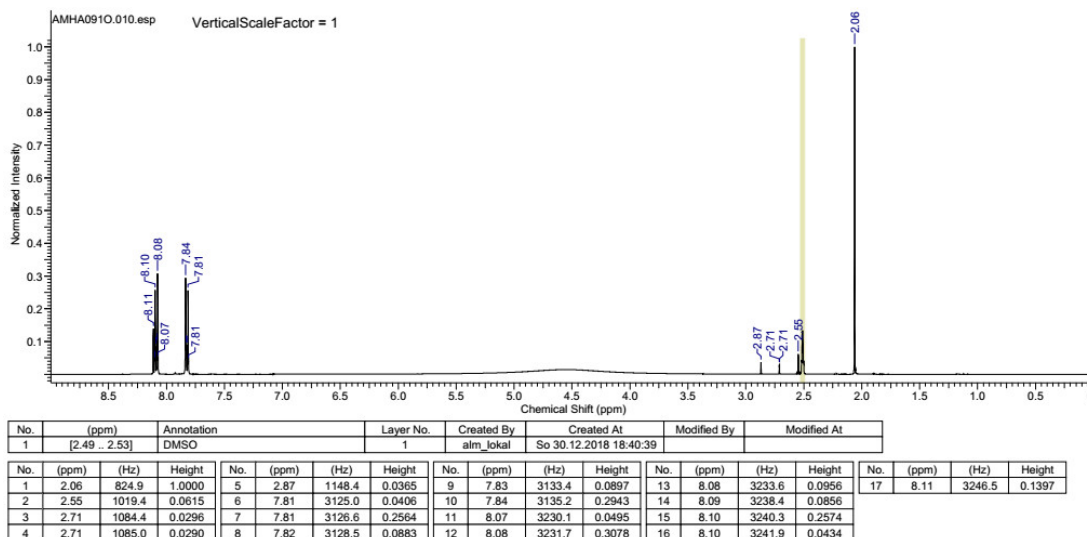


Figure S7. ^1H NMR spectrum of acid-digested Zr-*bzpd*-MOF.

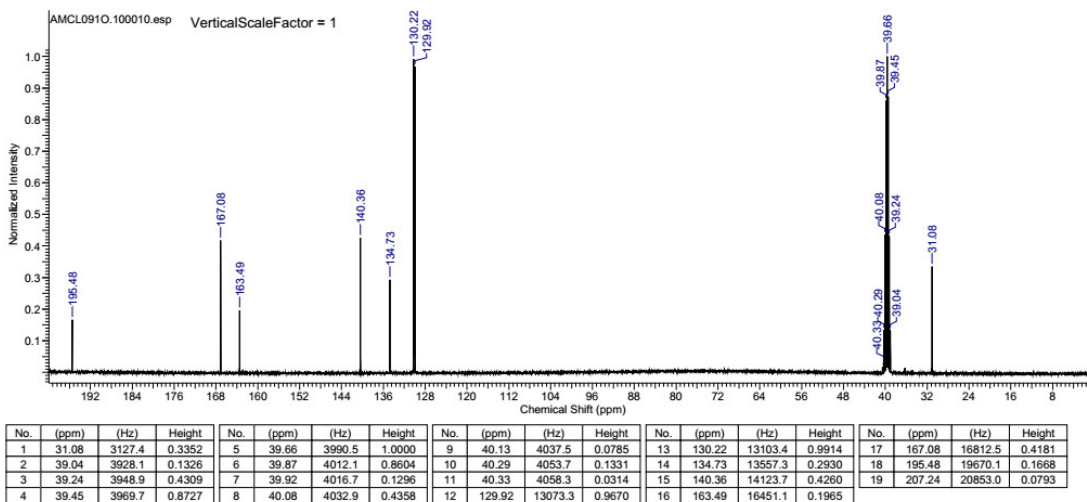


Figure S8. ^{13}C NMR spectrum of acid-digested Zr-*bzpd*-MOF.

Zr-*bzpd*c-MOF after irradiation in water at pH 7

The ^1H NMR spectrum of the irradiated MOF sample exhibits a signal at 8.03 ppm, corresponding to a hydroxyl group at an aromatic carbon atom of the benzophenone moiety. The signal at 4.91 ppm is the proton signal of water; the water in the solution stems from the aqueous hydrofluoric acid used in the digestion procedure of the MOF.

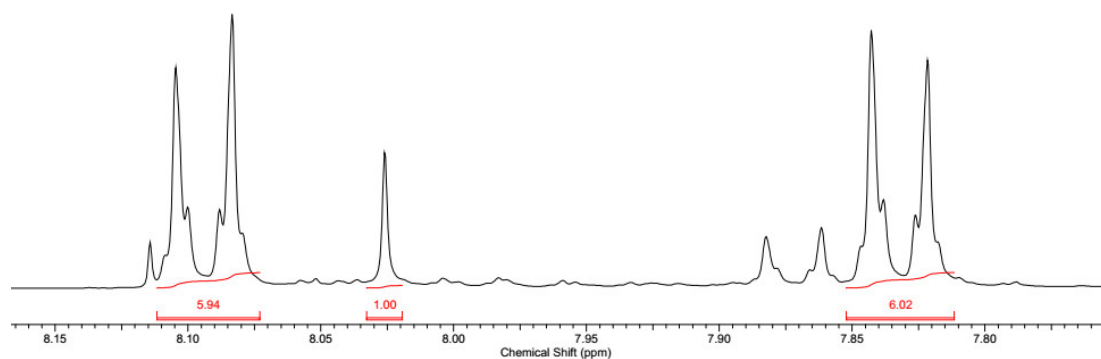
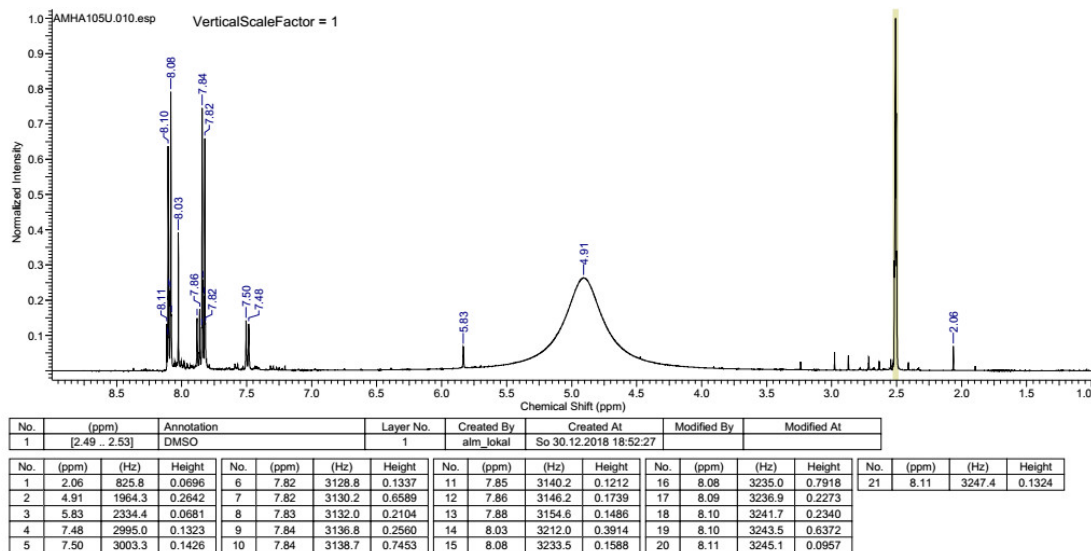


Figure S9. Top: ^1H NMR spectrum of acid-digested Zr-*bzpd*c-MOF after irradiation in water. Bottom: Integrated peak areas for the determination of the ratio of reacted linker molecules (about 70%).

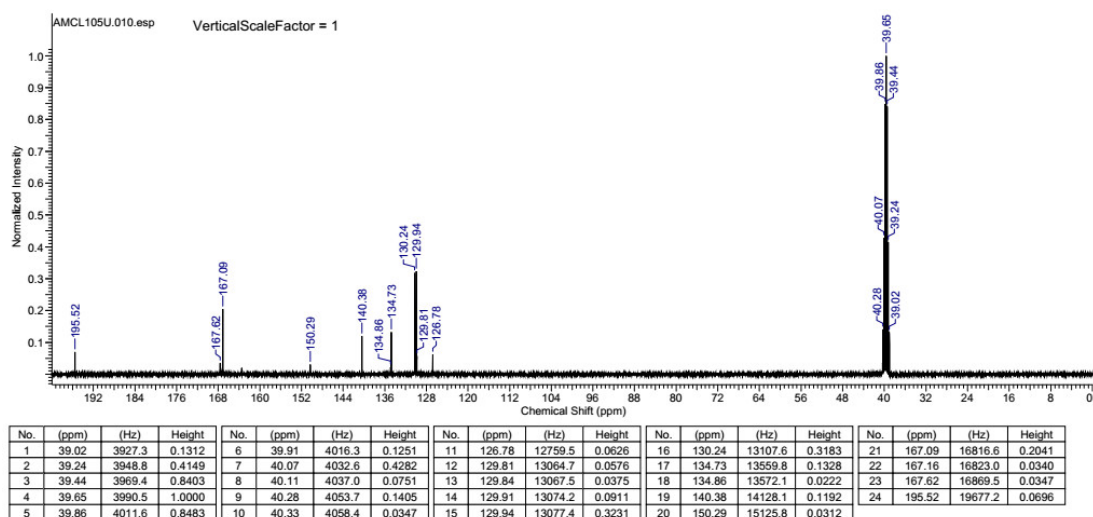


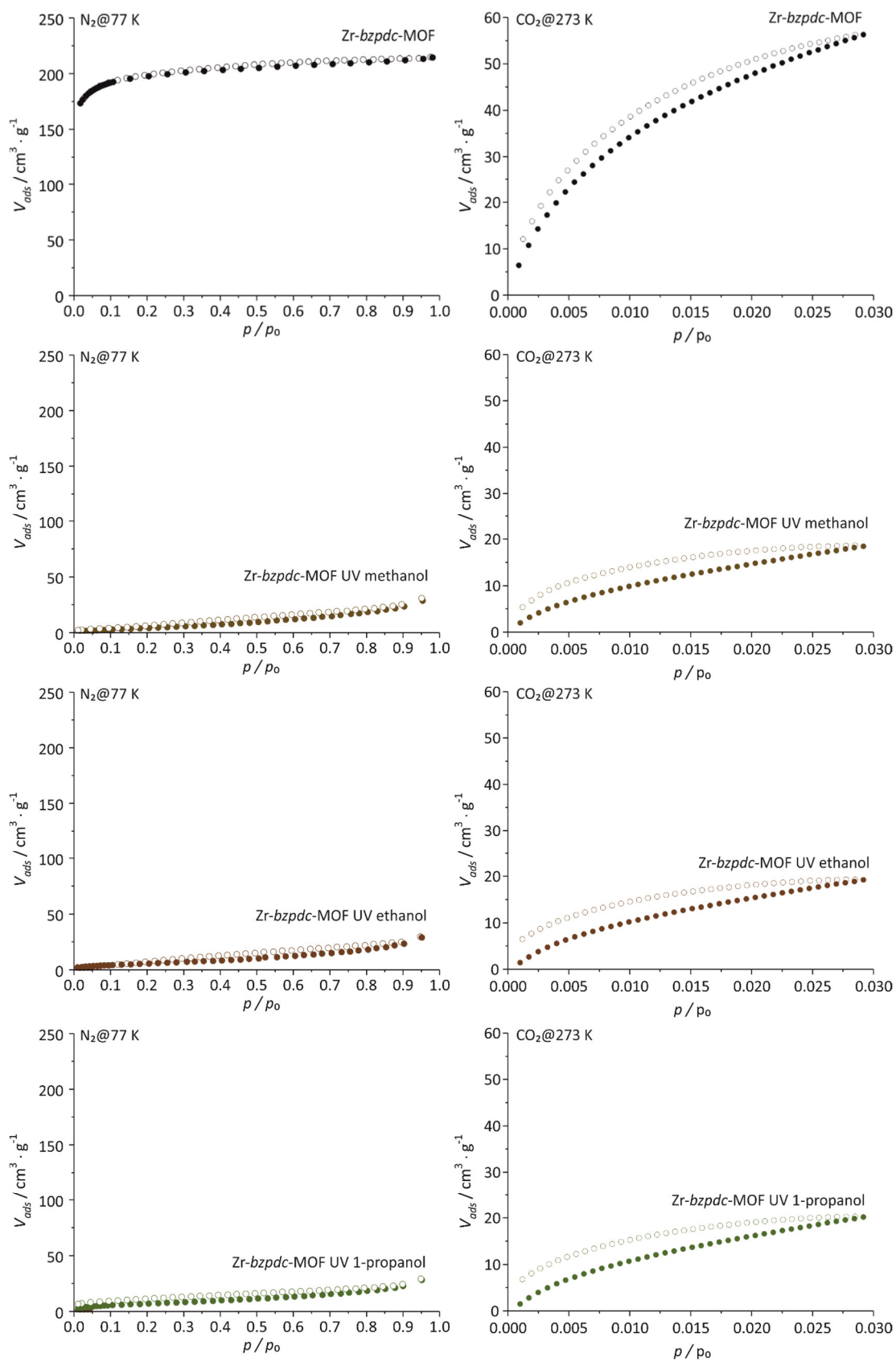
Figure S10. ^{13}C NMR spectrum of acid-digested Zr-*bzpdC*-MOF after irradiation in water.

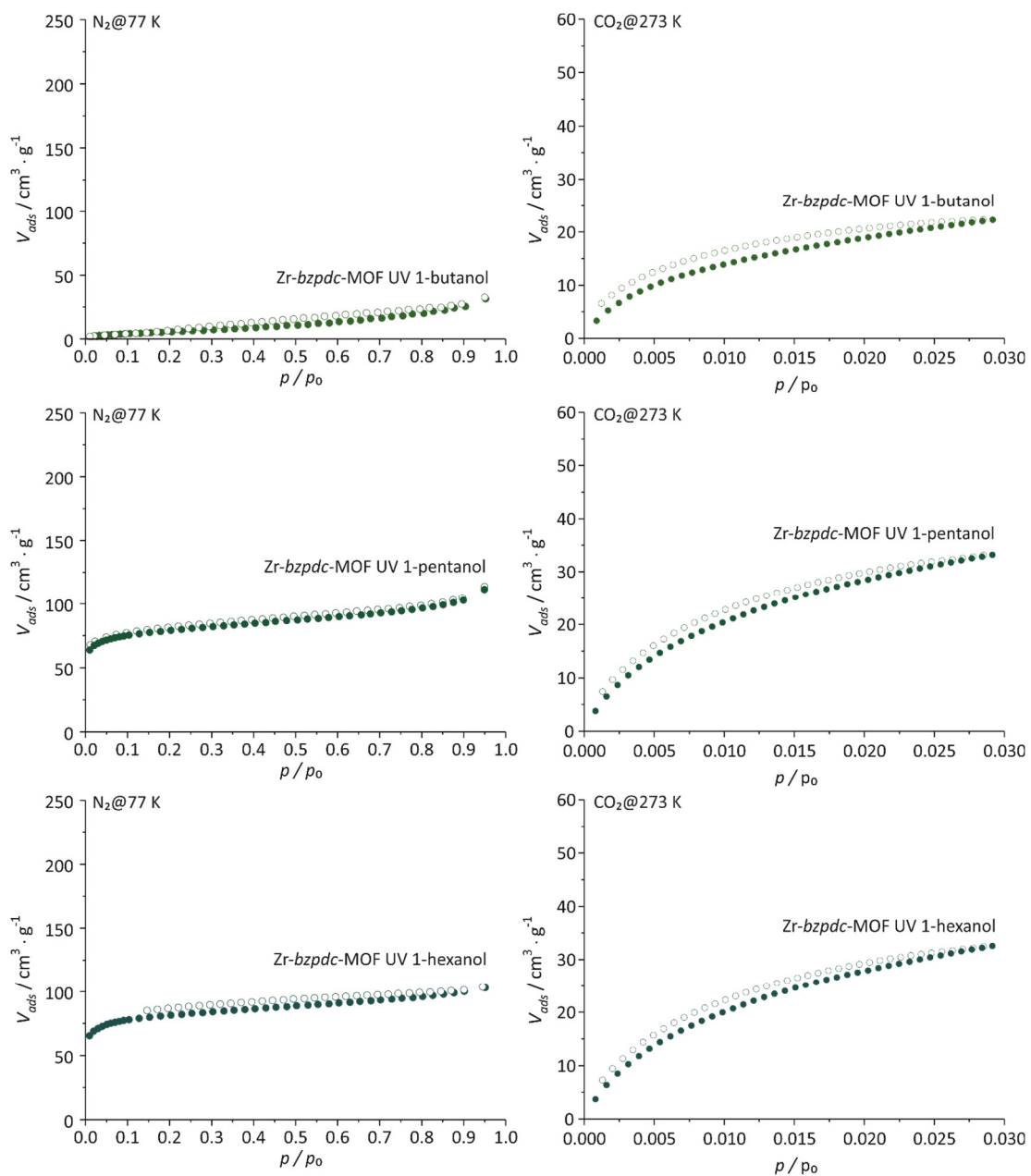
S1.2 Physisorption measurements

Results of physisorption measurements ($N_2@77K$) for Zr-*bzpd*c-MOF and Zr-*bzpd*c-MOF irradiated in the corresponding liquids are given in Table S1; the individual isotherms ($N_2@77K$ and $CO_2@273K$) for the samples modified with alcohols (Figure S11) and alkanes (Figure S12) are also shown.

Table S1. BET areas and total pore volumes calculated from $N_2@77K$ physisorption data for Zr-*bzpd*c-MOF and Zr-*bzpd*c-MOF irradiated in different liquids.

Sample	BET area / $m^2 \cdot g^{-1}$	Total pore volume / $cm^3 \cdot g^{-1}$
pristine Zr- <i>bzpd</i> c-MOF	670	0.40
Zr- <i>bzpd</i> c-MOF UV H_2O	520	0.32
Zr- <i>bzpd</i> c-MOF UV methanol	20	0.04
Zr- <i>bzpd</i> c-MOF UV ethanol	20	0.04
Zr- <i>bzpd</i> c-MOF UV propanol	20	0.04
Zr- <i>bzpd</i> c-MOF UV butanol	320	0.14
Zr- <i>bzpd</i> c-MOF UV pentanol	330	0.15
Zr- <i>bzpd</i> c-MOF UV hexanol	330	0.15
Zr- <i>bzpd</i> c-MOF UV heptanol	350	0.16
Zr- <i>bzpd</i> c-MOF UV octanol	350	0.16
Zr- <i>bzpd</i> c-MOF UV butane	330	0.15
Zr- <i>bzpd</i> c-MOF UV pentane	340	0.15
Zr- <i>bzpd</i> c-MOF UV hexane	350	0.15
Zr- <i>bzpd</i> c-MOF UV heptane	350	0.16
Zr- <i>bzpd</i> c-MOF UV octane	340	0.16





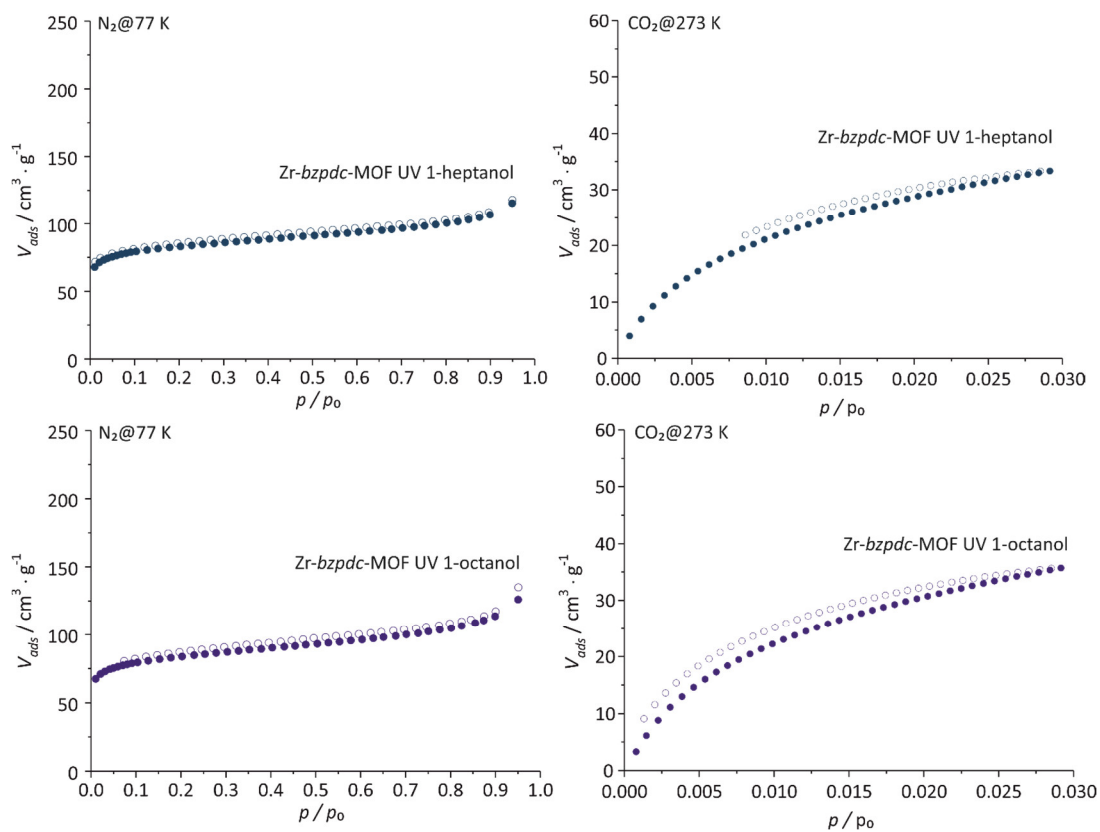
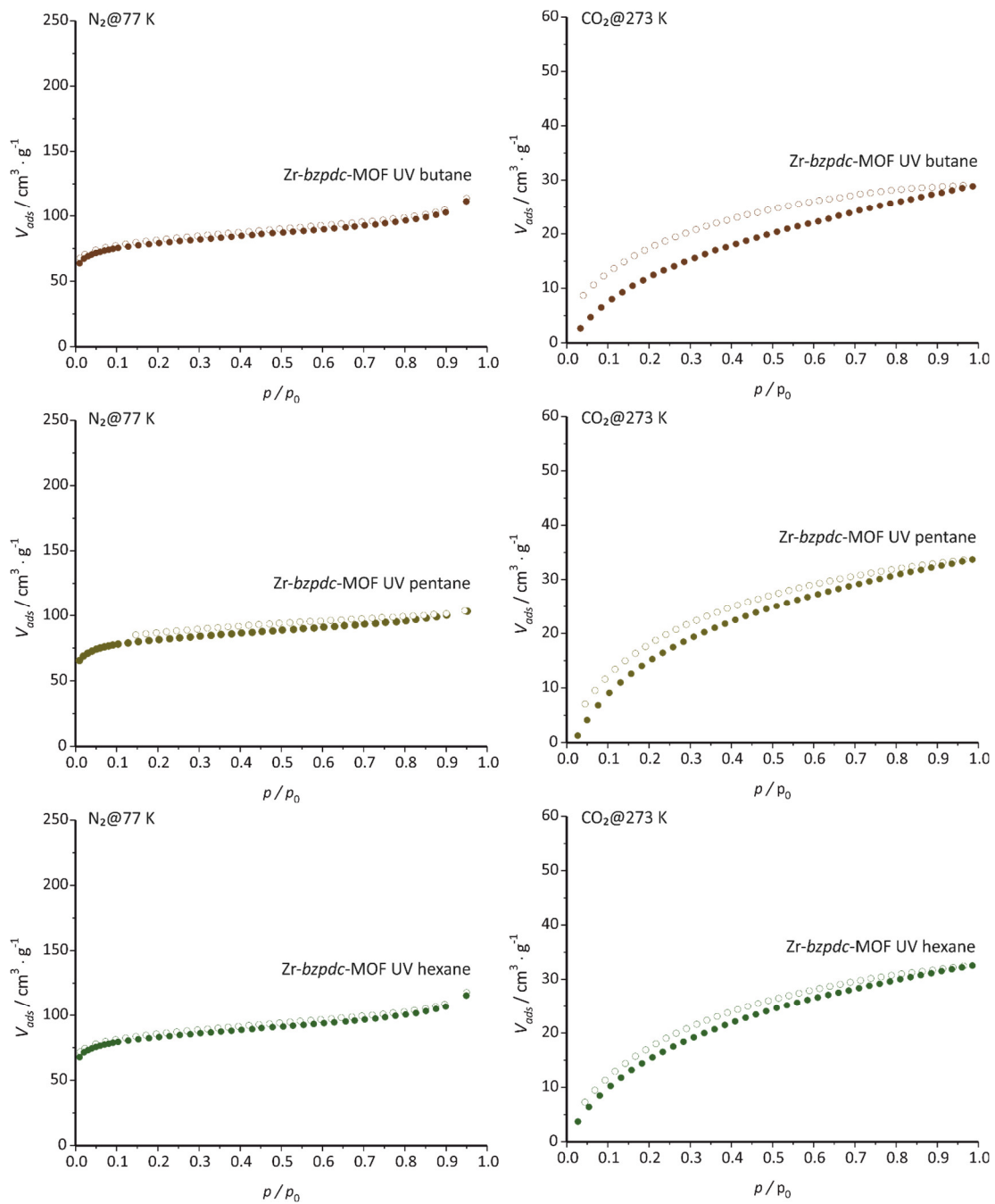


Figure S11. Physisorption isotherms for *Zr-bzpdC*-MOF and *Zr-bzpdC*-MOF samples irradiated in the corresponding alcohol.



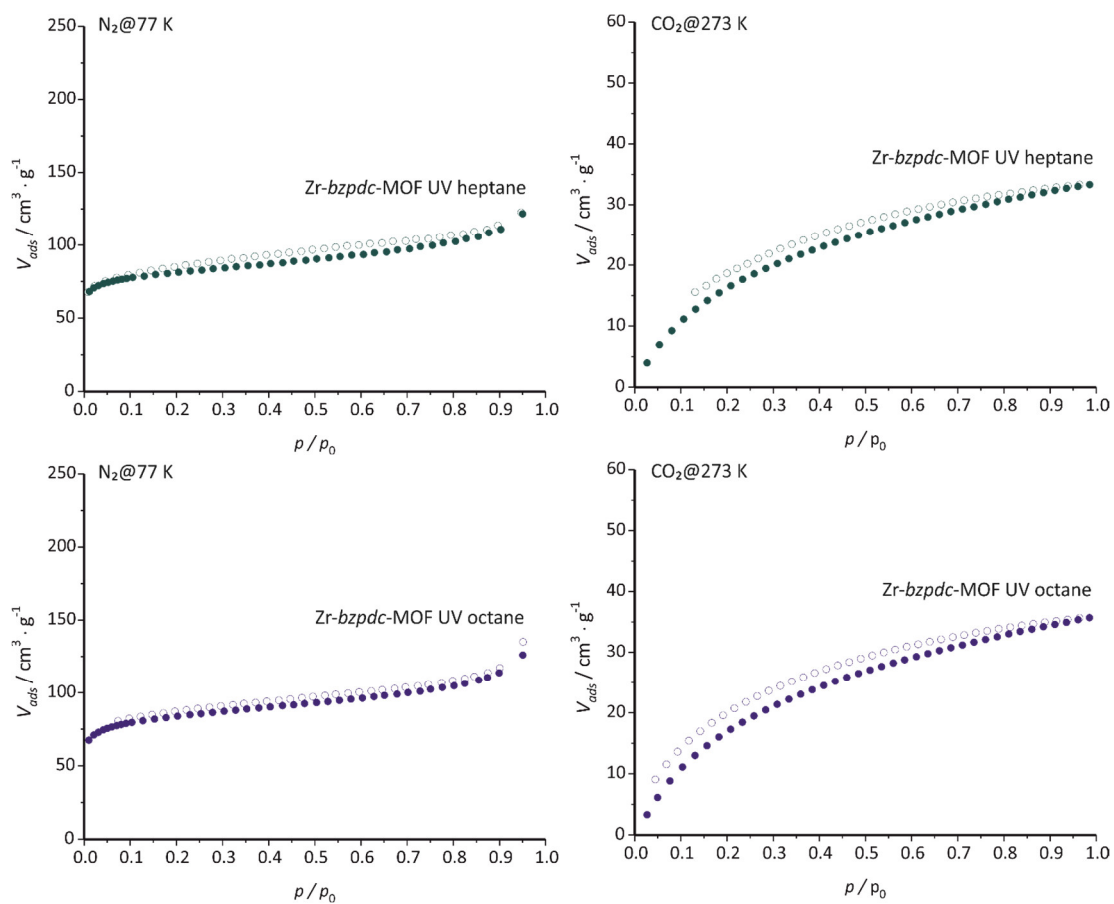


Figure S12. Physisorption isotherms for Zr-bzpdC-MOF and Zr-bzpdC-MOF samples irradiated in the corresponding alkane.

S1.3 Pore system of *Zr-bzpd*c-MOF

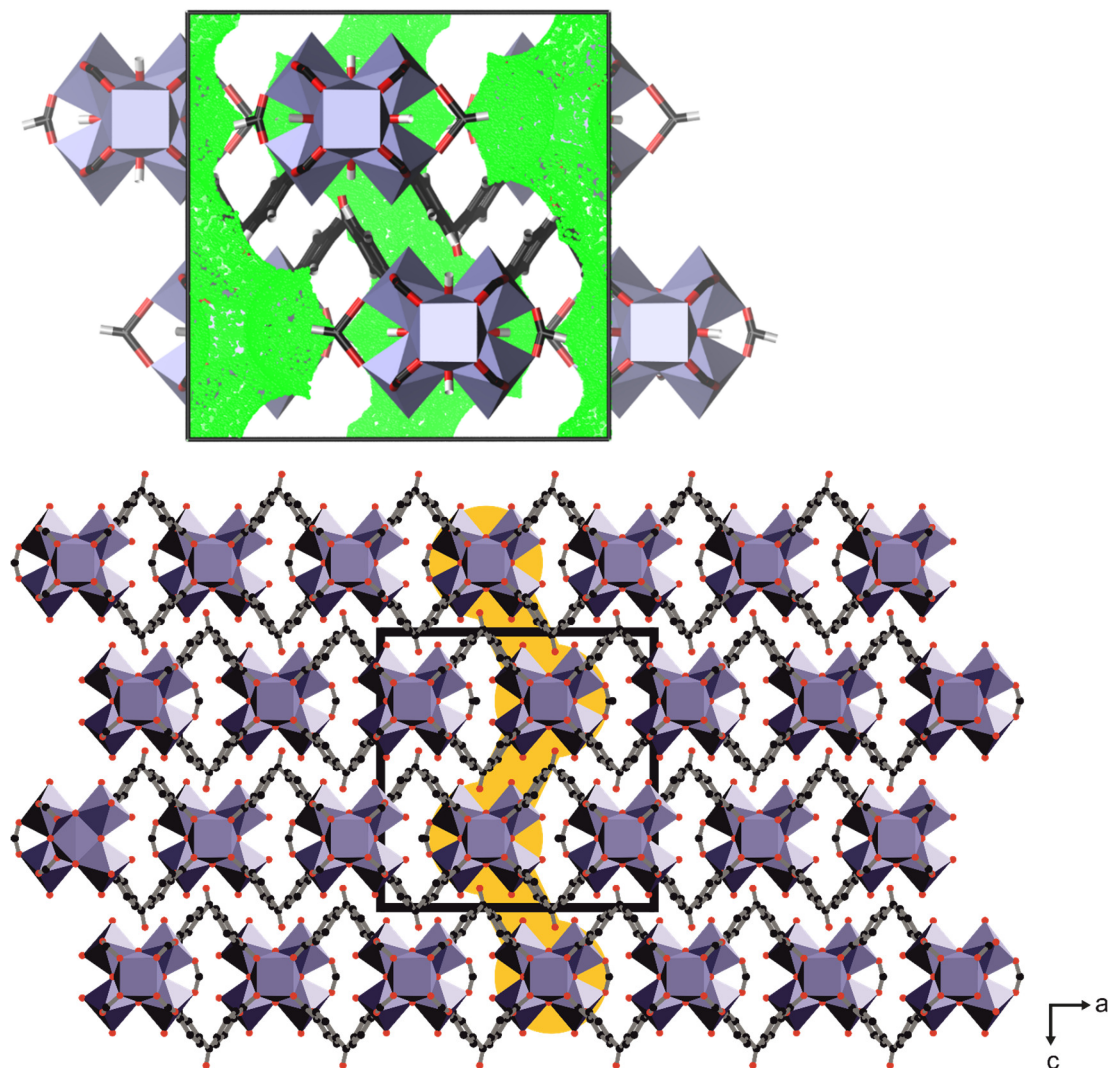


Figure S13. Representations of the pore system of the *Zr-bzpd*-MOF¹ along the *a* axis; top: visualized as a Voronoi network (Zeo++)² using the program Voro++;³ bottom: Schematic depiction of the pore system within the structure of the *Zr-bzpd*-MOF.

S1.4 NMR investigations - PSM of Zr-*bzpd*c-MOF and H₂*bzpd*c with alcohols

The following Figures S14 – S27 show the NMR spectra of Zr-*bzpd*c-MOF and H₂*bzpd*c after irradiation in different alcohols. For the postsynthetic modification with methanol, ethanol and propanol, no keto carbon signal is observable at 195 ppm in the ¹³C NMR spectra, indicating a complete reaction of the keto moieties with the alcohols. The characteristic region of the ¹³C NMR spectra is also shown in Figure 5 of the manuscript.

H₂*bzpd*c after irradiation in methanol

The ¹H NMR spectrum of H₂*bzpd*c irradiated in methanol (Figure S14) shows similar signals as the acid-digested Zr-*bzpd*c-MOF irradiated in methanol (Figure S16), like the singlet at about 4.01 ppm for the methylene unit of the hydroxymethyl group bonded to the former keto carbon atom. This proves a successful PSM reaction with methanol. Correspondingly, in the ¹³C NMR spectrum (manuscript, Figure 4) no signal for the keto carbon atom at 195 ppm is observed anymore indicating a complete reaction of every keto group similar to the results in the rigid metal-organic framework.

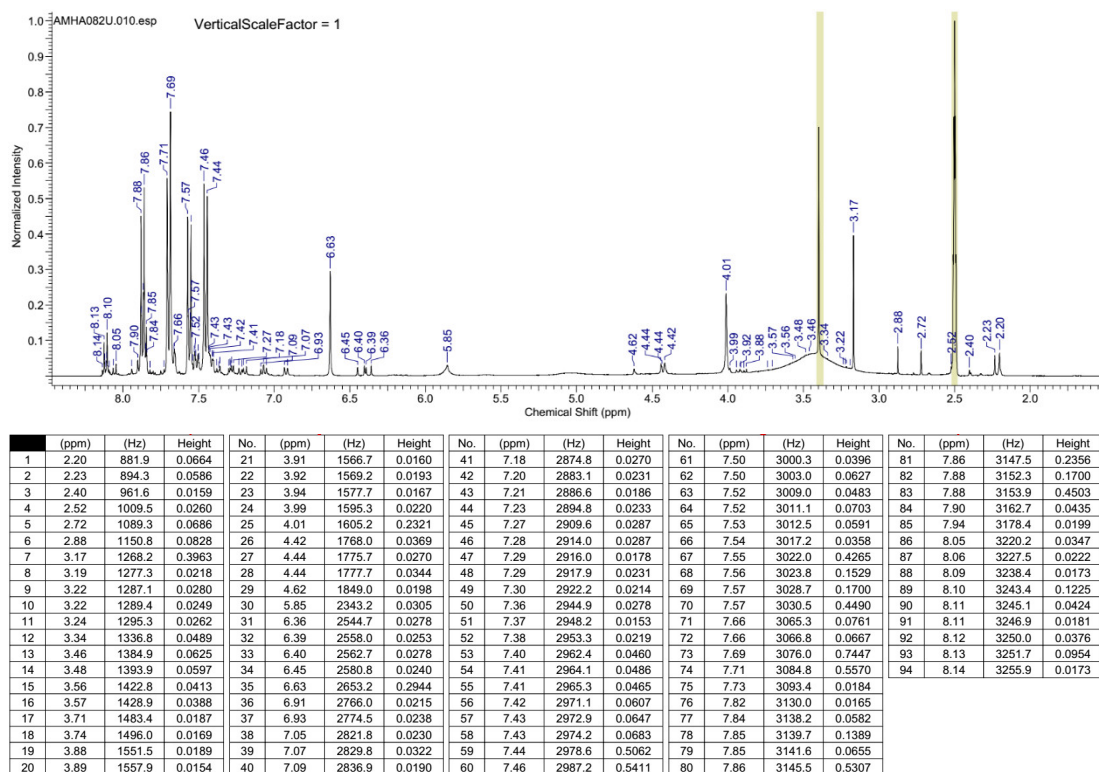


Figure S14. ¹H NMR spectrum of H₂*bzpd*c after irradiation in methanol.

$H_2bzipdc$ after irradiation in ethanol

The 1H NMR spectrum of $H_2bzipdc$ after irradiation in ethanol (Figure S15) is that of pristine $H_2bzipdc$ (Figure S1); no reaction occurred due to the low solubility of $H_2bzipdc$ in ethanol and inaccessibility of the keto groups in the organic crystals.

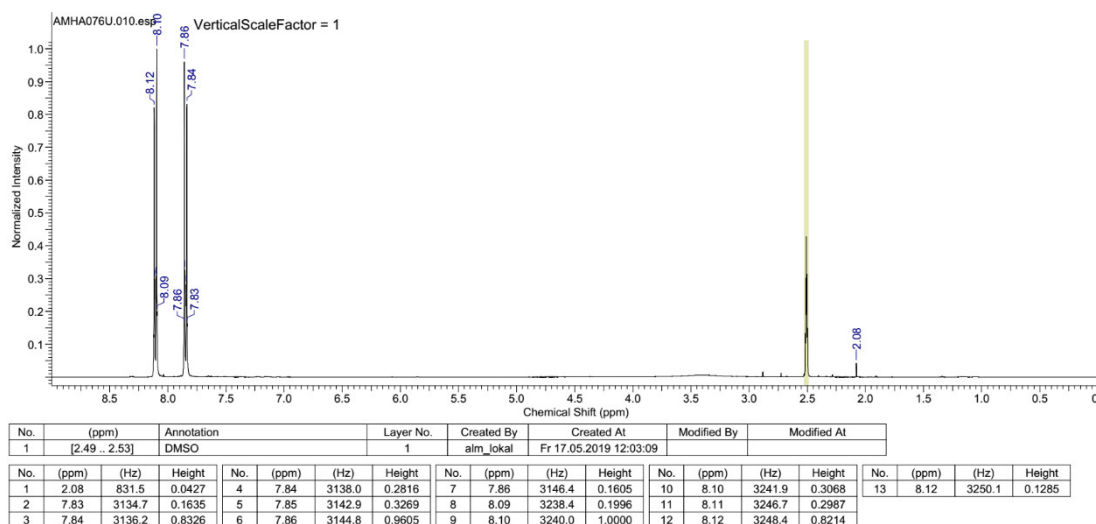


Figure S15. 1H NMR spectrum of $H_2bzipdc$ after irradiation in ethanol.

Zr-*bzpd*c-MOF after irradiation in methanol

The ^1H NMR spectrum of the acid-digested Zr-*bzpd*c-MOF which was irradiated in methanol (Figure S16) shows a singlet at about 4.01 ppm for the methylene unit of the hydroxymethyl group bonded to the former keto carbon atom as a result of the successful PSM reaction with methanol. Correspondingly, in the ^{13}C NMR spectrum (Figure S17) no signal for the keto carbon atom at 195 ppm is observed anymore.

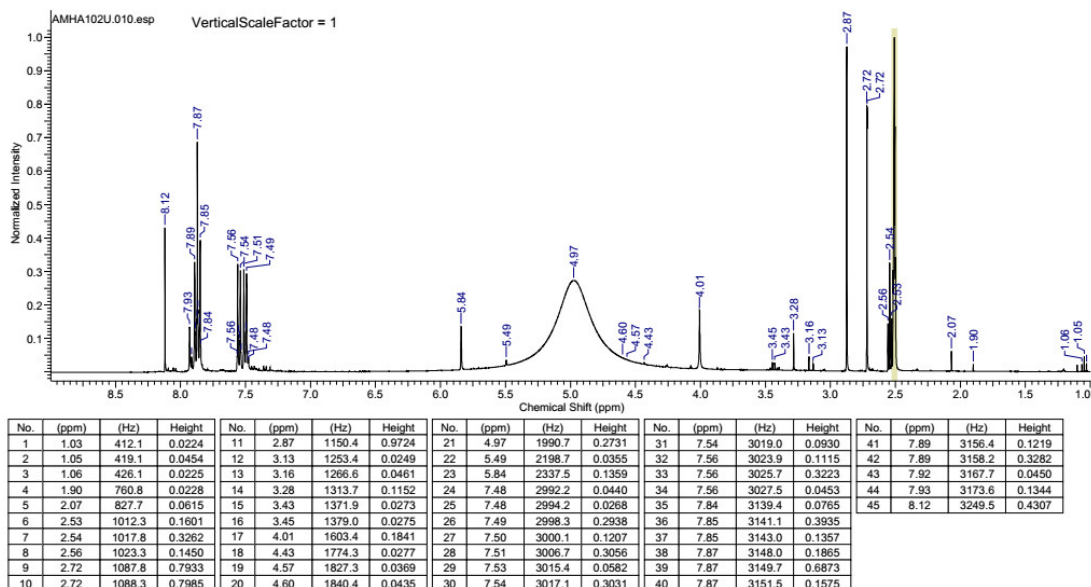


Figure S16. ^1H NMR spectrum of acid-digested Zr-*bzpd*c-MOF after irradiation in methanol.

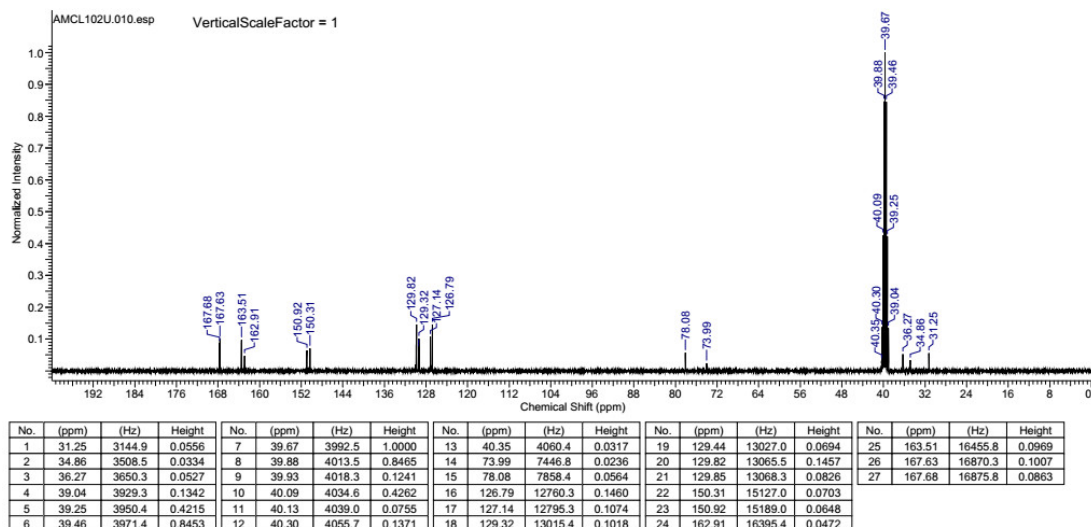


Figure S17. ^{13}C NMR spectrum of acid-digested Zr-*bzpd*c-MOF after irradiation in methanol.

Zr-*bzpd*c-MOF after irradiation in ethanol

The ^1H NMR spectrum of the acid-digested Zr-*bzpd*c-MOF which was irradiated in ethanol (Figure S18) shows a quartet at about 3.45 ppm (methylene group) and a triplet at about 1.05 ppm (methyl group), both belonging to the residue derived from ethanol which has become attached to the former keto carbon atom as a result of the successful PSM reaction with ethanol. Correspondingly, in the ^{13}C NMR spectrum (Figure S19) no signal for the keto carbon atom at 195 ppm is observed anymore.

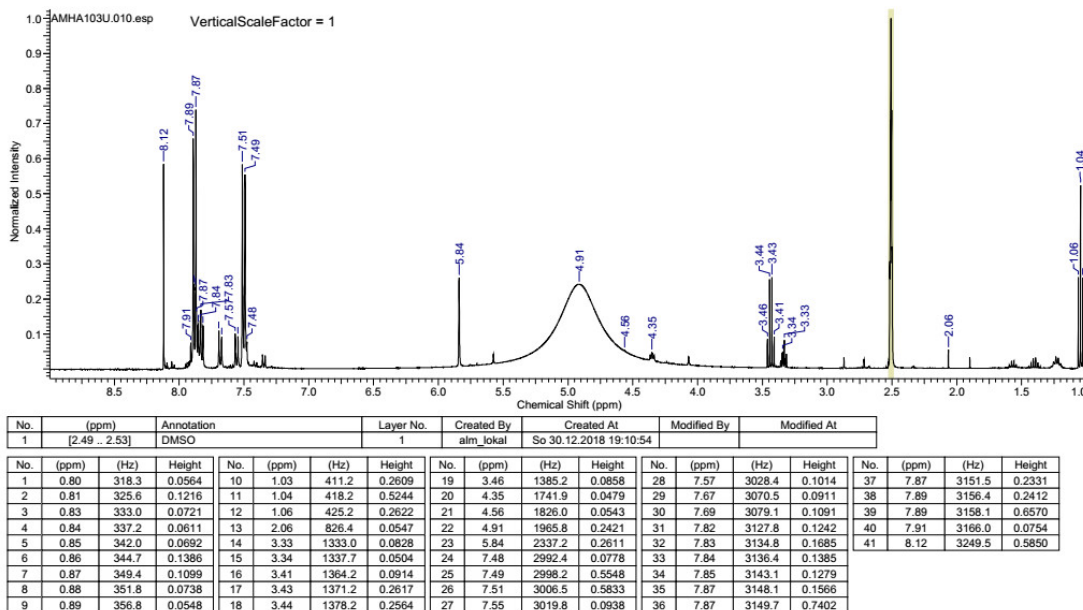


Figure S18. ^1H NMR spectrum of acid-digested Zr-*bzpd*c-MOF after irradiation in ethanol.

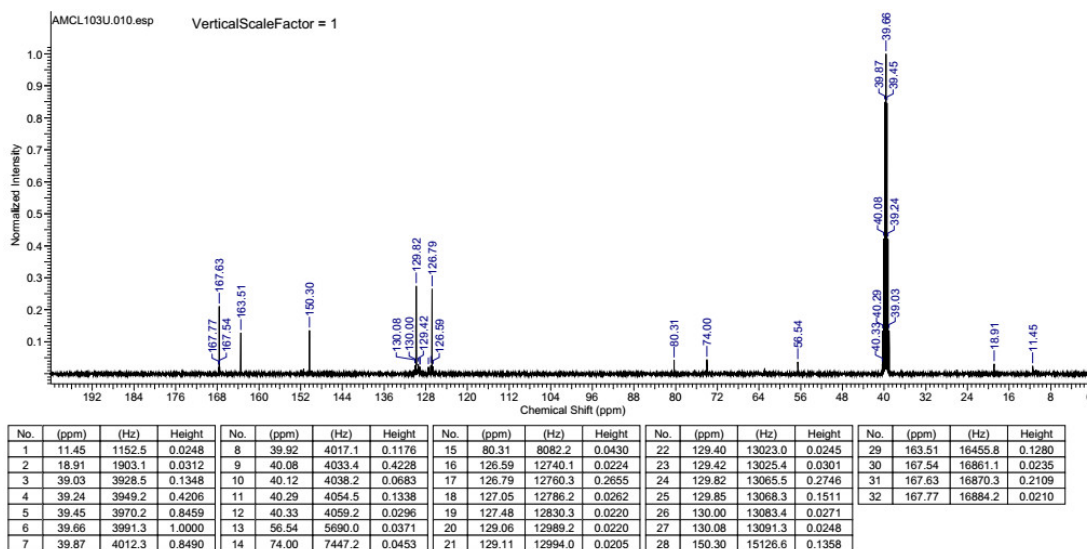


Figure S19. ^{13}C NMR spectrum of acid-digested Zr-*bzpd*c-MOF after irradiation in ethanol.

Zr-*bzpd*c-MOF after irradiation in 1-propanol

The ^1H NMR spectrum of the acid-digested Zr-*bzpd*c-MOF which was irradiated in 1-propanol (Figure S20) shows a quartet at about 3.33 ppm (methylene group), a multiplet at about 0.81 ppm and 0.87 ppm (probably triplets from methyl groups) and a sextet at 1.4 ppm (methylene group). This indicates a successful PSM of the keto groups with different C-H bonds of the alkyl chain of 1-propanol, leading to different reaction products. Accordingly, in the ^{13}C NMR spectrum (Figure S21), no signal for the keto carbon atom (195 ppm) is observed anymore.

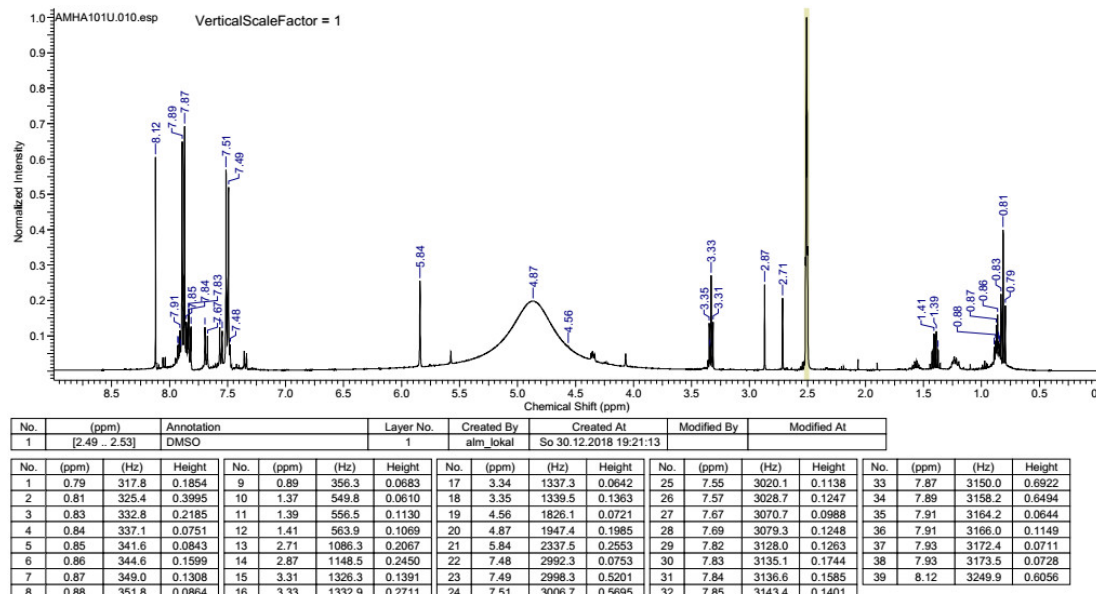


Figure S20. ^1H NMR spectrum of acid-digested Zr-*bzpd*c-MOF after irradiation in 1-propanol.

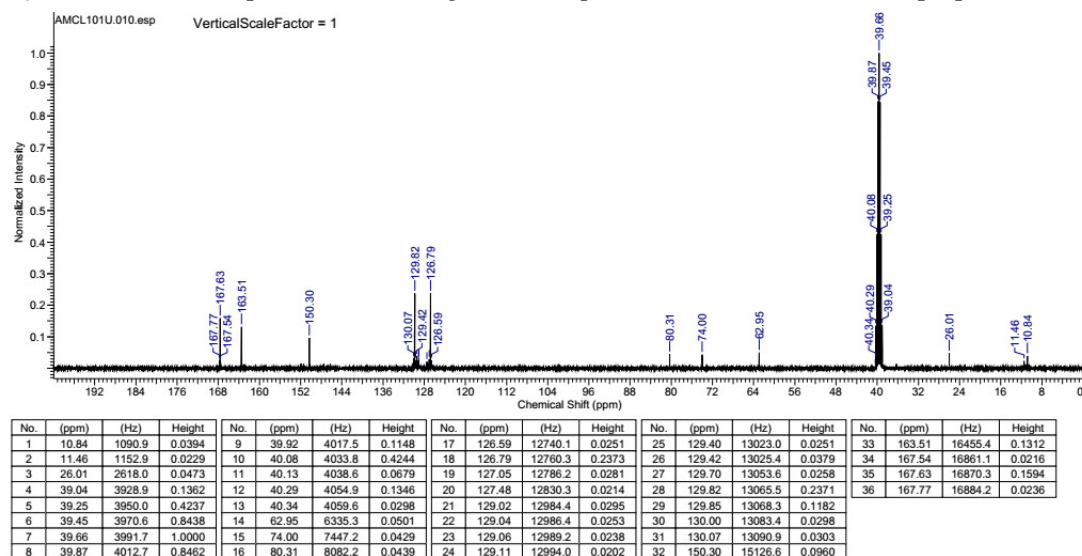


Figure S21. ^{13}C NMR spectrum of acid-digested Zr-*bzpd*c-MOF after irradiation in 1-propanol.

Zr-*bzpd*c-MOF after irradiation in 1-butanol

The ^1H NMR spectrum of the acid-digested Zr-*bzpd*c-MOF which was irradiated in 1-butanol (Figure S22) shows multiplets at about 0.8 ppm and 1.0 – 1.5 ppm for methyl and methylene groups. This indicates a successful PSM of the keto groups with different C–H bonds of the alkyl chain of 1-butanol, leading to different reaction products. However, the signals are considerably less intense, indicating a lower conversion of the PSM reaction. Correspondingly, an – albeit very weak – signal of the keto carbon can still be observed in the ^{13}C NMR spectrum (Figure S23), indicating that a majority of the keto groups has reacted with 1-butanol. The reaction with 1-butanol therefore represents a borderline case.

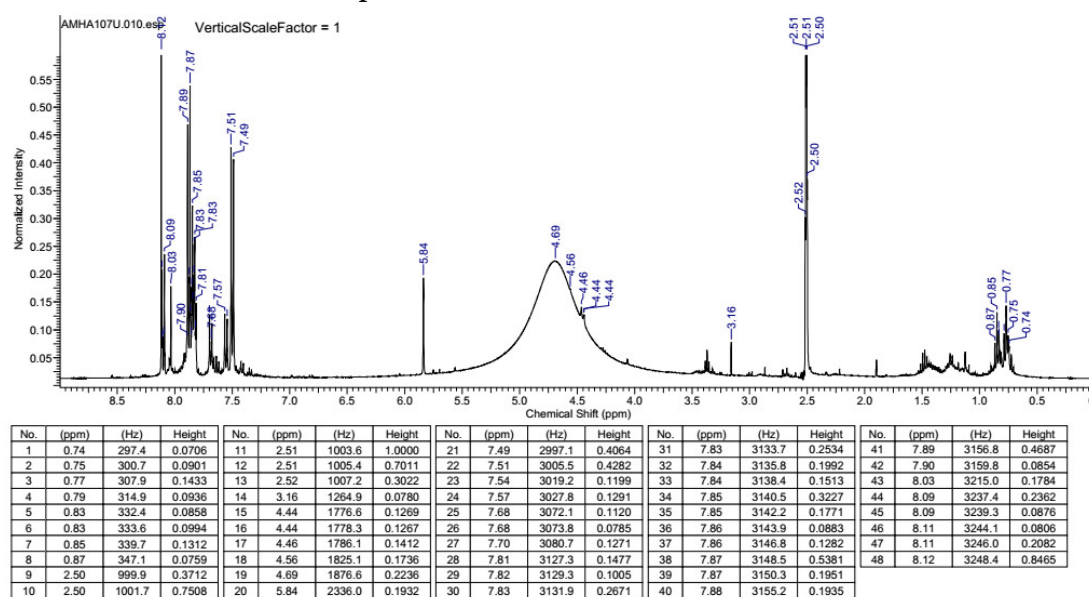


Figure S22. ^1H NMR spectrum of acid-digested Zr-*bzpd*-MOF after irradiation in 1-butanol.

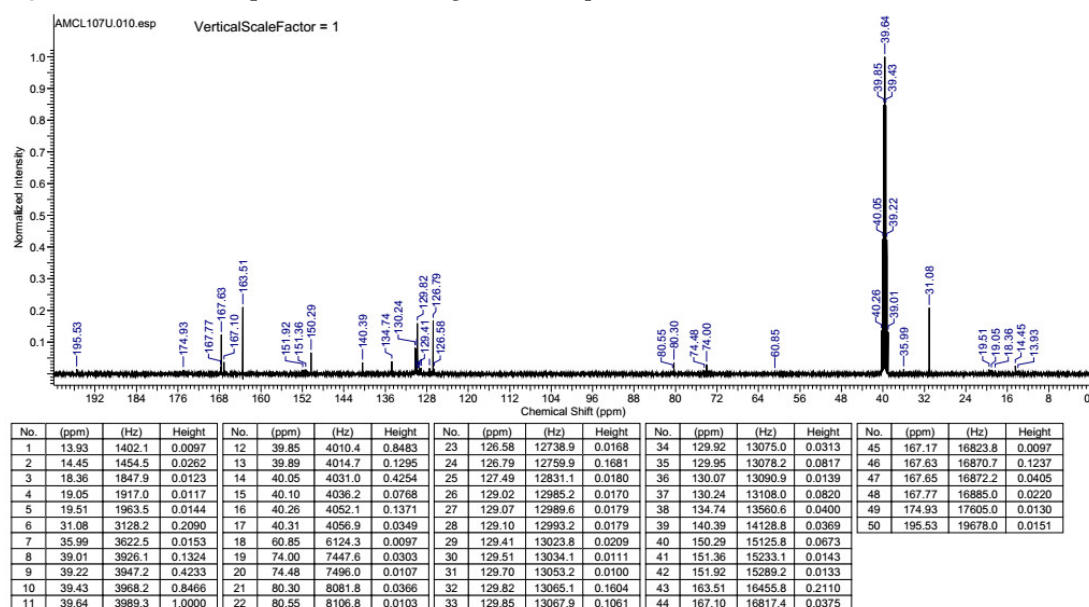


Figure S23. ^{13}C NMR spectrum of acid-digested Zr-*bzpd*-MOF after irradiation in 1-butanol.

Zr-*bzpd*c-MOF after irradiation in 1-pentanol

The ^1H NMR spectrum of the acid-digested Zr-*bzpd*c-MOF which was irradiated in 1-pentanol (Figure S24) shows weak multiplets at about 3.43 ppm (methylene group) and overlapping multiplets in the region from 1.09 ppm up to 1.3 ppm (probably triplets for methyl groups). PSM reactions of the keto groups with different C–H bonds of the alkyl chain of 1-pentanol could lead to different reaction products. The weak intensity of these signals, however, indicates that a reaction of pentanol with keto groups has occurred only to a very limited extent.

In the ^{13}C NMR spectrum (Figure S25), the keto carbon signal at 195 ppm can still be observed with nearly the same intensity as in the spectrum of the acid-digested pristine Zr-*bzpd*c-MOF. With the indications from ^1H NMR spectroscopy that some reaction products have formed, we conclude that only a small number of the keto groups has reacted. Experience from former investigations, where the surface/wetting properties of the MOF could be changed substantially by PSM,¹ leads us to presume that this small part is located at or near the surface.

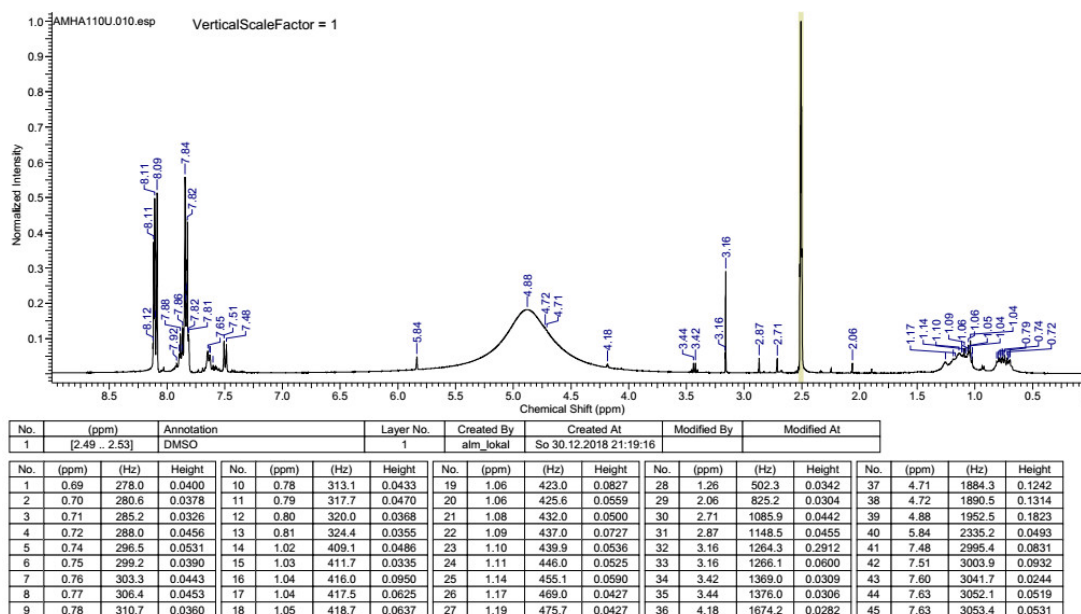


Figure S24. ^1H NMR spectrum of acid-digested Zr-*bzpd*c-MOF after irradiation in 1-pentanol.

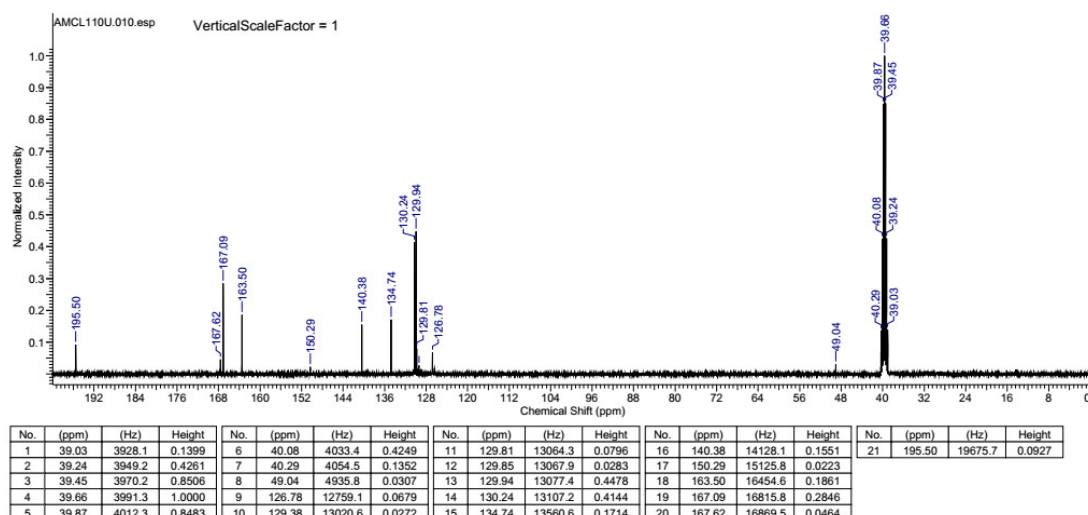


Figure S25. ^{13}C NMR spectrum of acid-digested Zr-*bzpdC*-MOF after irradiation in 1-pentanol.

Zr-*bzpdC*-MOF after irradiation in 1-octanol

The ^1H NMR spectrum of UV irradiated samples with 1-octanol (Figure S26) shows a quartet at about 3.43 ppm (methylene group) and overlapping multiplets at about 0.79 ppm and 1.09 ppm up to 1.4 ppm (probably triplets for methyl groups). PSM reactions of the keto groups with different C–H bonds of the alkyl chain of 1-octanol could lead to different reaction products. The weak intensity of these signals, however, indicates that a reaction of 1-octanol with keto groups has occurred only to a very limited extent.

In the ^{13}C NMR spectrum (Figure S27), the keto carbon signal at 195 ppm can still be observed with nearly the same intensity as in the spectrum of the acid-digested pristine Zr-*bzpdC*-MOF. With the indications from ^1H NMR spectroscopy that some reaction products have formed, we conclude that only a small number of the keto groups has reacted. Experience from former investigations, where the surface/wetting properties of the MOF could be changed substantially by PSM,¹ leads us to presume that this small part is located at or near the surface.

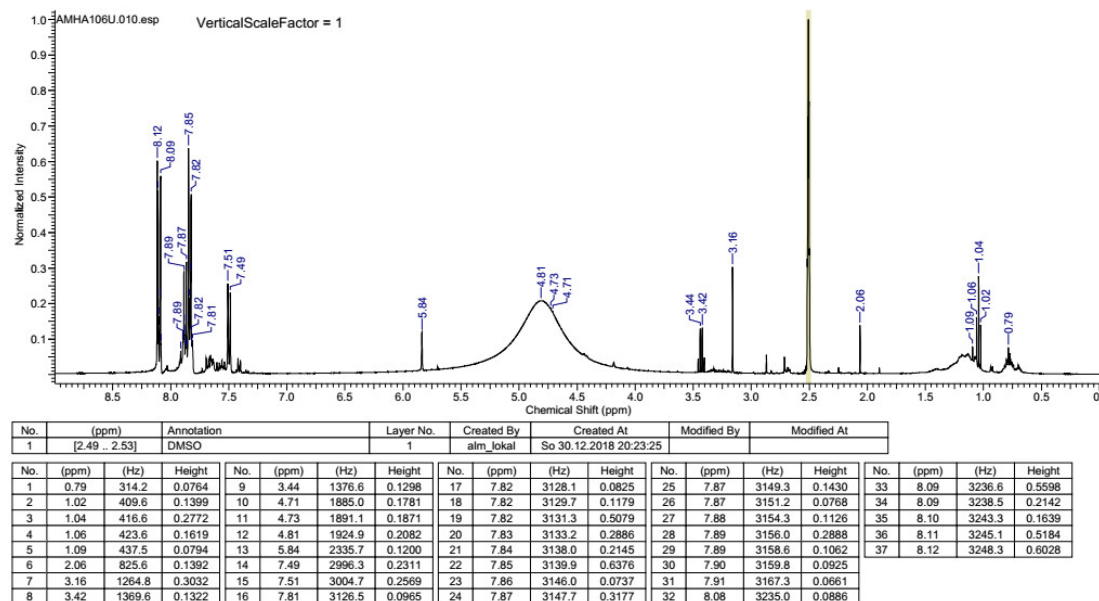


Figure S26. ^1H NMR spectrum of acid-digested Zr-*bzpdC*-MOF after irradiation in 1-octanol.

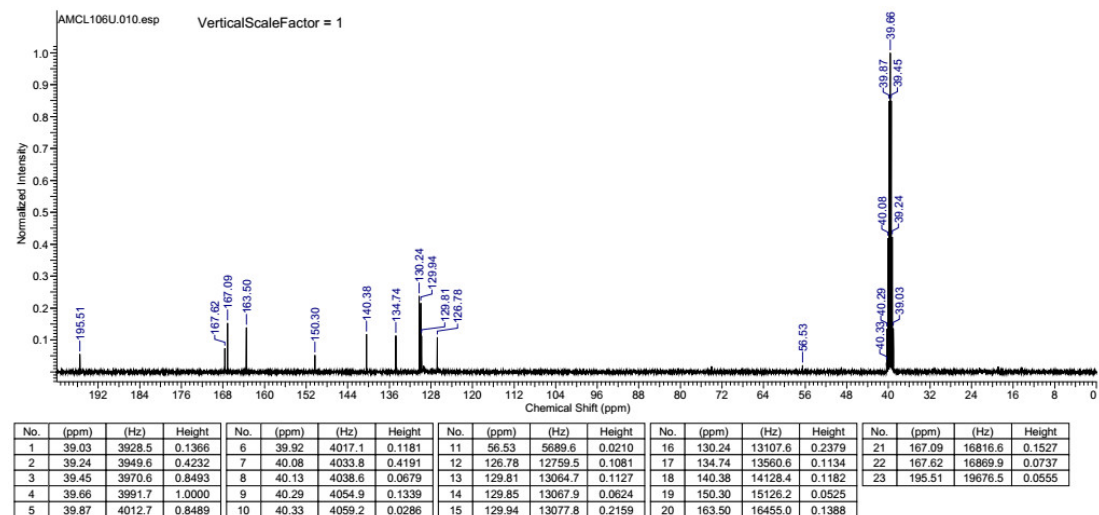


Figure S27. ^{13}C NMR spectrum of acid-digested Zr-*bzpdC*-MOF after irradiation in 1-octanol.

S1.5 Simulation

Table S2. Lattice parameters derived from the simulation of pristine Zr-*bzpd*c-MOF and of a Zr-*bzpd*c-MOF where every keto group has reacted with methanol.

sample	$a / \text{\AA}$	$b / \text{\AA}$	$c / \text{\AA}$	$\alpha / ^\circ$	$\beta / ^\circ$	$\gamma / ^\circ$	$V / \text{\AA}^3$
Zr- <i>bzpd</i> c-MOF	29.86	19.25	19.40	90.00	90.00	90.00	11155.77
UV methanol	29.15	17.70	24.22	89.10	90.41	88.96	12497.42

S2. References

- 1 A. Mohmeyer, A. Schaate, B. Brechtken, J. C. Rode, D. P. Warwas, G. Zahn, R. J. Haug and P. Behrens, *Chem. Eur. J.* **2018**, *24*, 12848–12855.
- 2 T.F. Willems, C.H. Rycroft, M. Kazi, J.C. Meza, and M. Haranczyk, *Microporous Mesoporous Mater.* **2012**, *49*, 134–141.
- 3 C. H. Rycroft, *Chaos* **2009**, *19*, 41111.

6 List of publications

Articles

Title: “Nanosafety: Validating Metal-Organic Framework Nanoparticles for Their Nanosafety in Diverse Biomedical Applications“

S. Wuttke, A. Zimpe, T. Bein, S. Braig, K. Stoiber, A. Vollmar, D. Müller, K. Haastert-Talini, J. Schaeske, M. Stiesch, G. Zahn, A. Mohmeyer, P. Behrens, O. Eickelberg, D. A. Bölükbas, S. Meiners, *Adv. Healthcare Mater.* **2017**, *6*, 1600818.

Title: “Azobenzene Guest Molecules as Light-Switchable CO₂ Valves in an Ultrathin UiO-67 Membrane”

A. Knebel, L. Sundermann, A. Mohmeyer, I. Strauß, S. Friebe, P. Behrens, J. Caro, *Chem. Mater.* **2017**, *29*, 7, 3111-3117.

Title: “Delamination and Photochemical Modification of a Novel Two-Dimensional Zr-Based Metal–Organic Framework”

A. Mohmeyer, A. Schaate, B. Brechtken, J. C. Rode, D. P. Warwas, G. Zahn, R. J. Haug, P. Behrens, *Chem. Eur. J.* **2018**, *24*, 12848–12855.

Title: “Graphene-like metal-organic frameworks: Morphology control, optimization of thin film electrical conductivity and fast sensing applications”

B. Hoppe, K. Hindricks, D. P. Warwas, H. A. Schulze, A. Mohmeyer, T. J. Pinkvos, S. Zailskas, M. R. Krey, C. Belke, S. König, M. Fröba, R. J. Haug, P. Behrens, *CrystEngComm* **2018**, *20*, 6458-6471.

Title: “Direct grafting-from of PEDOT from a photoreactive Zr-based MOF – A novel route to electrically conductive composite materials”

A. Mohmeyer, A. Schaate, B. Hoppe, H. A. Schulze, T. Heinemeyer, P. Behrens, *Chem. Commun.* **2019**, *55*, 3367-3370.

Title: “Role of Structural Defects in the Adsorption and Separation of C₃ Hydrocarbons in Zr-Fumarate-MOF (MOF-801)”

P. Iacomi, F. Formalik, J. Marreiros, J. Shang, J. Rogacka, A. Mohmeyer, P. Behrens, R. Ameloot, B. Kuchta, P. L. Llewellyn, *Chem. Mater.* **2019**, *31*, 8413-8423.

Title: “Inside/Outside: Postsynthetic Modification of the Zr-*benzophenone-dicarboxylate*-MOF”

A. Mohmeyer, M. Schäfer, A. Schaate, S. Locmelis, A. M. Schneider, P. Behrens, submitted to *Chem. Eur. J.* **2019**.

Oral presentations

2nd EuroMOF, Delft, Netherlands, October 2017

Title: “Postsynthetic Modification and Delamination of a Novel Two-Dimensional Zr-based MOF with Photoreactive Surface”

A. Mohmeyer, A. Schaate, P. Behrens

Poster presentations

1st EuroMOF, Potsdam, Germany, October 2015

“Synthesis and Structural Study of a Keto-Functionalized Zr-Based Metal-Organic Framework”

A. Mohmeyer, A. Schaate, G. Zahn, P. Behrens

28. Deutsche Zeolith-Tagung, Gießen, Germany, March 2016

„A new keto-functionalized Zr-based metal-organic framework and its unique properties”

A. Mohmeyer, A. Schaate, P. Behrens

LNQE Nanoday 2016, Hannover, Germany, September 2016

„A new keto-functionalized Zr-based metal-organic framework and its unique properties”

A. Mohmeyer, A. Schaate, P. Behrens

29. Deutsche Zeolith-Tagung, Frankfurt am Main, Germany, March 2017

“A Novel Two-Dimensional MOF with Photoreactive Groups: Delamination and Postsynthetic Modification”

A. Mohmeyer, A. Schaate, D. P. Warwas, G. Zahn, P. Behrens

LNQE Nanoday 2017, Hannover, Germany, September 2017

“A Novel Two-Dimensional MOF with Photoreactive Groups: Delamination and Postsynthetic Modification”

A. Mohmeyer, A. Schaate, J. C. Rode, R. J. Haug, P. Behrens

30. Deutsche Zeolith-Tagung, Kiel, Germany, February 2018

“Metal-Organic Frameworks with Bioactive Polyphenolate Linker Molecules for Biomedical Applications”

A. Mohmeyer, F. Schneider, P. Behrens

CPM-8, Delray Beach, USA, May 2018

“A Novel Two-Dimensional Zr-based MOF with Photoreactive Surface and its Different Physisorption Behaviour Through Postsynthetic Modification”

A. Mohmeyer, A. Schaate, J. C. Rode, M. Schäfer, A. M. Schneider, R. J. Haug, P. Behrens

LNQE Nanoday 2018, Hannover, Germany, September 2018

“Grafting-from a Two-Dimensional Zr-based MOF with Photoreactive Surface through Polymerization of EDOT – A Novel Electrically Conductive Hybrid Material”

A. Mohmeyer, A. Schaate, B. Brechtken, J. C. Rode, R. J. Haug, P. Behrens

7 Curriculum vitae

Name	Alexander Mohmeyer
Date of birth	June 09, 1990
Place of birth	Alfeld (Leine)
Nationality	German
10/2015 – 08/2019	Dissertation at the Institute for Inorganic Chemistry, Gottfried Wilhelm Leibniz Universität Hannover in the group of Prof. Dr. Peter Behrens Title: “Synthesis, Characterization and Postsynthetic Modification of a Novel Two-Dimensional Zr-based Metal-Organic Framework”
10/2013 – 09/2015	Master of Science at the Institute for Inorganic Chemistry, Gottfried Wilhelm Leibniz Universität Hannover in the group of Prof. Dr. Peter Behrens Title: “Decoration of Metal-Organic Frameworks Compounds for Biomedical Applications”
10/2010 – 09/2013	Bachelor of Science at the Institute for Inorganic Chemistry, Gottfried Wilhelm Leibniz Universität Hannover in the group of Prof. Dr. Peter Behrens Title: “Morphology-Controlled Synthesis of Bismuth Compounds”
06/2009	Abitur (A-Levels) at the Gymnasium Alfeld in Alfeld (Leine)